Solution and Adsorption Characterization of Novel Water-Soluble Ionic Block Copolymers for Stabilization of Magnetite Nanoparticles

Beth Lynn Caba

Dissertation submitted to the Faculty of the Virginia Polytechnic and State University in partial fulfillment of the requirements for the degree of

Doctor of Philosophy
In
Macromolecular Science and Engineering

Dr. Richey M. Davis, Chairman
Dr. Aaron S. Goldstein
Dr. Judy S. Riffle
Dr. John Y. Walz, Jr.
Dr. Garth L. Wilkes

April 30, 2007
Blacksburg, Virginia

Keywords:

triblock copolymer, charged micelle, magnetite, nanoparticle, self-assembly, segment density profile, poly(ethylene oxide), core, corona, adsorption, brush extension, steric stabilization, drug delivery, contrast agent

Solution and Adsorption Characterization of Novel Water-Soluble Ionic Block Copolymers for Stabilization of Magnetite Nanoparticles

Beth Lynn Caba

ABSTRACT

There is a need for multifunctional polymer-particle complexes for use in biomedical applications such as for drug delivery or as MRI contrast agents where composition and stability are essential for the complexes to function. This work outlines a general methodology for rationally designing complexes stabilized with polymer brush layers using adapted star polymer models for brush extension and pair potential. Block copolymer micelles were first utilized for experimental validation by using the brush extension model to predict the size and the interaction model to predict the second virial coefficient, A_2. Subsequently, the models were used to predict the size and colloidal stability of magnetite-polymer complexes using the modified Deryaguin-Verwey-Landau-Overbeek theory.

Novel hydrophilic triblock copolymers comprised of poly(ethylene oxide) tailblocks and a carboxylic acid containing polyurethane center block were examined by static and dynamic light scattering (SLS and DLS), small angle neutron scattering (SANS), and densiometry. Under conditions when the charge is suppressed such as at low pH and/or high ionic strength, the polymer chains self-assemble into micelles, whereas unimers alone are present under conditions where charge effects are important, such as high pH and low ionic strength.

A model for effective interaction between star polymers was used to obtain an expression for the second virial coefficient (A_2) for micelles in solution. The values of A_2 obtained using this method were compared with experimentally determined values for star polymers and micelles. In doing so, not only was a new means of calculating A_2 a priori introduced, but the applicability of star polymer expressions to micellar systems was

established. Through the analogy of micelles to sterically stabilized nanoparticles, this model was applied to water-soluble block copolymers adsorbed on magnetite nanoparticles for the purpose of tailoring a steric stabilizing brush layer. The sizes of the magnetite-polymer complexes were predicted using the star polymer model employed for the micelle study with an added layer to account for the anchor block. Colloidal stability was predicted from extended DLVO theory using the pair interaction. This work will lead to a better understanding of how to design ion-containing block copolymers for steric stabilization of metal oxide nanoparticles.

For my father:

LCDR Donald L. Patton

Love an Engineer

ACKNOWLEDGEMENTS

I have had the good fortune to work with **Dr. Richey Davis**, whose unfailing enthusiasm, creativity, and good nature have made the experience a joy. I would also like to thank the members of my committee, past and present, for support and input: **Dr. William Ducker**, **Dr. Aaron Goldstein**, **Dr. Judy Riffle**, **Dr. Kevin Van Cott**, **Dr. John Walz**, and **Dr. Garth Wilkes**.

I am appreciative to many of Dr. Riffle's students, without whose creative efforts in synthesis and characterization of polymers and nanoparticles, this research would not have been possible. They include **Anita Carmichael-Baranauskas**, **Jon Goff**, **Dr. Linda Harris**, **Phil Huffstetler**, **Thompson Mefford**, **Nikorn Pothayee**, **Shane Thompson**, and **Dr. Qian Zhang**. The SANS experiments at NIST could not have been accomplished without the generous on-site assistance of **Dr. Paul Butler** and **Dr. Min Lin** and the subsequent modeling efforts of **Dr. Elliot Gilbert**, **Dr. Robert Woodward**, and **Matt Carroll**.

I thank **Dr. Jody Krsmanovic and Dr. Matt Guzy** for introducing me to many laboratory techniques and **Dr. Doug Henderson** for extensive training and assistance. I also thank my colleague **Nurxat Nueraji**, with whom I conducted the biopanning experiments, and **Dr. Spencer Clark** and **Min Mao** for many helpful discussions.

I would like to thank **Riley Chan** for his ability to fix just about anything and **Angie Flynn**, **Diane Cannaday**, and **Chris Moore** for assistance with countless matters.

To my labmates, **Akhilesh Garg** and **William Miles**, I owe a debt of gratitude for encouragement, experimental input, and companionship.

I am grateful for a supportive family: my parents, **Donald and Lucy Patton**, my sister, **Lora Solada**, and my husband, **Dr. Aaron Caba**.

I also thank the following for financial support: NSF Grant #BES-0086876, NSF Grant #DGE-0114346, NSF Grant #DMR-0312046, NSF Grant #DMR-0602932, the Eastman Chemical Company Fellowship in Polymer Science, the OmNova Signature Award, Procter and Gamble, and Luna Innovations.

Table of Contents

1 Introduction 1
1.1 Significance and Motivation 1
1.2 Specific Research Objectives 1
1.3 Overview of Chapters 3
1.4 References 6
2 Literature Review 7
2.1 Block Copolymers in Solution 8
2.1.1 Micelle Formation 9
2.1.1.1 Uncharged Copolymers 11
2.1.1.2 Charged Copolymers 12
2.1.2 Prediction of Micelle Size Using a Star Polymer Model 13
2.1.3 The Second Virial Coefficient 15
2.1.4 Micelle-Micelle Separation 16
2.2 Polymer Adsorption 16
2.2.1 Adsorption Configuration 17
2.2.2 Theoretical Models for Adsorption 17
2.2.2.1 Exact Enumeration 17
2.2.2.2 Self-Consistent Field (SCF) Lattice Model 18
2.2.2.3 Diffusion Equation 20
2.2.2.4 Scaling Theory 21
2.2.3 Adsorption of Charged Homopolymers 22
2.2.4 Block Copolymers 23
2.2.4.1 Non-Selective Solvent 23
2.2.4.2 Selective Solvent 25
2.3 Colloidal Stabilization with Adsorbed Polymer 26
2.3.1 Adsorption Isotherms 26
2.3.1.1 Gibbs Adsorption Isotherm 26
2.3.1.2 Langmuir Isotherm 27
2.3.1.3 Frumkin Adsorption Isotherm 28
2.3.2 DVLO Theory of Stabilization 28
2.3.2.1 Electrostatic Potential 29
2.3.2.2 Van der Waals Potential 31
2.3.2.3 Steric Potential 33
2.3.2.4 Magnetic Potential 39
2.3.3 Flocculation 40
2.3.3.1 Bridging Flocculation 40
2.3.3.2 Charge Neutralization Flocculation 41
2.3.3.3 Depletion Flocculation 42
2.4 Colloidal Rheology 43
2.4.1 Hard Sphere Model 43
2.4.2 Charged Sphere Model 44
2.4.3 Stabilized Sphere Model 45
2.5 Polymers in Nanomedicine 46

2.5.1 Polymers for Targeted Delivery 46
2.5.2 Magnetic Resonance Imaging (MRI) 50
2.6 Biopolymers 53
2.6.1 Structure of Polypeptides 53
2.6.2 Artificial Amino Acids 53
2.6.3 Transfer of Genetic Information 54
2.6.4 Deliberate Design 54
2.6.5 Combinatorial Libraries 54
2.6.6 Environmental Applications 56
2.6.7 Processing Applications 59
2.6.8 Recombinant DNA Technology for Synthesis of Biopolymers 60
2.6.9 Polymerase Chain Reaction 61
2.6.10 Purification 61
2.7 Key Experimental Techniques 61
2.7.1 Light Scattering 61
2.7.1.1 Static Light Scattering 63
2.7.1.2 Dynamic Light Scattering 66
2.7.2 Zeta Potential 68
2.7.3 Densiometry 69
2.7.4 Small Angle Neutron Scattering (SANS) 70
2.8 References 74
3 Solution properties and characterization of water-soluble triblock copolymers 91
3.1 Abstract 91
3.2 Keywords 91
3.3 Introduction 91
3.4 Materials and Methods 94
3.4.1 Chemicals 94
3.4.2 Dynamic Light Scattering 95
3.4.3 Static Light Scattering 98
3.4.4 Refractive Index Increment 99
3.4.5 Sample Preparation for Light Scattering 99
3.5 Results and Discussion 101
3.5.1 Refractive index increment 101
3.5.2 DLS for determination of hydrodynamic radius 103
3.5.3 SLS for determination of aggregation number and second virial coefficient: an example 104
3.5.4 Effect of Copolymer Composition on Micellization 106
3.5.5 Effect of Temperature on Micelle Size 110
3.5.6 Effect of Temperature on Aggregation Number 113
3.5.7 Comparison with the Density Distribution Prediction 115
3.5.8 Volume Fraction Profile 118
3.5.9 A Visual Comparison of Size 119
3.6 Conclusions 120
3.7 References 121
4 A SANS study of controlled aggregation of polyurethane-containing PEO block copolymers in water 129

4.1 Abstract 129
4.2 Keywords 129
4.3 Introduction 129
4.4 Materials and Methods 132
4.4.1 Chemicals 132
4.4.2 Small Angle Neutron Scattering 133
4.4.3 Light Scattering 135
4.4.4 Densiometry 139
4.5 Results and Discussion 140
4.5.1 Light scattering 140
4.5.2 Partial Specific Volumes 140
4.5.3 Small Angle Neutron Scattering (SANS) 143
4.5.4 Data Reduction 145
4.5.5 Solvent Selection 145
4.5.6 Data Analysis 146
4.5.7 Model Fits 148
4.5.8 Comparison with the Density Distribution Prediction 153
4.6 Conclusions 154
4.7 References 155
5 Pair Interactions Between Micelles: Prediction of the Second Virial Coefficient for Micelles Using a Star Model 160
5.1 Abstract 160
5.2 Keywords 160
5.3 Introduction 160
5.4 Materials and Methods 163
5.4.1 Chemicals 163
5.4.2 Light Scattering 165
5.4.3 Densiometry 169
5.5 Results and Discussion 170
5.5.1 Estimation of Micelle Size with the Density Distribution Prediction 170
5.5.2 Extension of the Star Polymer Interaction Model to Determine A_2 172
5.5.3 Micelle-micelle separation 183
5.6 Conclusions 183
5.7 References 184
6 Adsorption of Brush-Forming Copolymers on Magnetite Nanoparticles 189
6.1 Abstract 189
6.2 Keywords 189
6.3 Introduction 189
6.4 Materials and Methods 193
6.4.1 Chemicals 193
6.4.2 Light Scattering 196
6.4.3 Zeta Potential 197
6.4.4 Densiometry 198
6.4.5 Transmission Electron Microscopy 198
6.4.6 Thermal Gravimetric Analysis 200
6.5 Results and Discussion 201

6.5.1 Estimation of R_m with the Density Distribution Prediction 201
6.5.2 Extension of the DD Model to Include an Anchor Layer 203
6.5.3 Colloidal Stability 205
6.5.4 Self-diffusion of water in a PEO brush 220
6.6 Conclusions 222
6.7 References 223
7 EDC-Mediated Crosslinking of Copolymer Micelles 230
7.1 Abstract 230
7.2 Keywords 230
7.3 Introduction 230
7.4 Materials and Methods 232
7.4.1 Chemicals 232
7.4.2 Separation Methods 234
7.4.3 Crosslinking Reaction 234
7.4.4 Cisplatin Encapsulation 237
7.4.5 Platinum assay for determination of cisplatin concentration 237
7.4.6 Absorbance for determination of lidocaine concentration 238
7.4.7 Dynamic Light Scattering 239
7.4.8 Zeta Potential 240
7.5 Results and Discussion 240
7.5.1 Self-Assembly in the Absence of Crosslinking 240
7.5.2 Crosslinking Reactions 241
7.5.3 Cisplatin encapsulation 247
7.5.4 Lidocaine loading 249
7.6 Summary 251
7.7 References 252
8 Combinatorial Search for Dodecapeptides for Adsorption on Alumina 255
8.1 Abstract 255
8.2 Keywords 255
8.3 Introduction 255
8.4 Materials and Methods 257
8.4.1 Chemicals 257
8.4.2 Substrate 257
8.4.2.1 10XM9 Salts, 1M $MgCl_2$, and Ampicillin 258
8.4.2.2 IMC Medium 258
8.4.2.3 RM Medium 258
8.4.2.4 RMG Plates 259
8.4.3 Biopanning 259
8.4.3.1 Overview 259
8.4.3.2 Growth 261
8.4.3.3 Adsorption and Selection 262
8.4.3.4 Isolation 263
8.4.3.5 Plasmid Isolation 263
8.4.3.6 Sequencing 265
8.4.4 Zeta potential 266
8.5 Results and Discussion 267

8.5.1 Round 3 results 267
8.5.2 Selectivity 268
8.5.3 Ionic strength of the IMC Media and Resulting Debye Length..... 269
8.5.4 Effect of IMC buffer on Substrate 270
8.6 Summary 271
8.7 References 272
9 Summary 274
9.1 Conclusions 274
9.2 Future Work 277
9.2.1 Micelles 277
9.2.2 Magnetite-polymer complexes 277
9.2.3 Crosslinked micelles for drug delivery 279
9.2.4 Combinatorial search for custom anchor blocks 279
9.3 References 279
Appendix: Propagation of Errors 281

List of Figures

Figure 2-1. Structures formed by aggregation: a micelle and a bilayer. 9

Figure 2-2. Schematic representation of the micelle showing the density distribution model[61] parameters. 14

Figure 2-3. Electrical double layer on a charged surface..... 30

Figure 2-4. Pair potential for an example system with 2000 g/mol PEO grafted to a sphere with R_c = 5 nm and f = 10, 20, 50, 100, and 200. The transition from a soft to hard interaction potential may be observed. 39

Figure 2-5. General schematic of shear thinning behavior. 43

Figure 2-6. Approach to creating crosslinked micelles for drug delivery 48

Figure 2-7. EDC crosslinking reaction of two carboxylate groups with ethylenediamine. An isourea by-product is formed. 49

Figure 2-8. EDC crosslinking reaction of two carboxylate groups with ethylenediamine in the presence of NHS. 50

Figure 2-9. Longitudinal magnetization. 51

Figure 2-10. Transverse magnetization..... 52

Figure 2-11. Light scattering experimental setup. 62

Figure 2-12. Example Zimm plot. The slope of the θ=0 line is the mean square radius of gyration; the slope of the c=0 line is the second virial coefficient. The y-intercept is the inverse of the weight-average molecular weight. Open circles are experimental data. Filled circles are extrapolated points. 65

Figure 2-13. Illustration of a block copolymer micelle with nomenclature of the SANS model. R is the hard-sphere radius of the core. $2R_g$ is the thickness of the corona. 72

Figure 3-1. Structure of a representative triblock copolymer with PEO tail blocks and a polyurethane center block that contains carboxylic acid groups. 95

Figure 3-2. dn/dc for polymers in 0.1M NaCl at pH 2. 102

Figure 3-3. dn/dc for polymers in 0.1M NaCl at pH 4. 102

Figure 3-4. dn/dc for polymers in 0.1M NaCl at pH 6. 103

Figure 3-5. An example of a typical Debye plot. This is for micelles of 1930-3.1-1930 in 0.1M NaCl at pH 2 and 25°C as measured on the CGS-3. 105

Figure 3-6. Hydrodynamic radius (DLS) and aggregation number (SLS) for 15k-3-15k copolymer at pH 2 and 0.1M NaCl. No micellization or temperature dependence was observed. 107

Figure 3-7. Titration data for the block copolymers with 0.1M NaCl in water. NaOH added was measured volumetrically using standardized 0.1M NaOH which was titrated to check concentration. Moles of COO- in the polymer expected are based on number of polyurethane repeat units previously measured by titration by Harris et al.[57] 110

Figure 3-8. Hydrodynamic radius measured for 4845-2.5-4845 at 0.1M NaCl. 111

Figure 3-9. Hydrodynamic radius measured for 4845-4.7-4845 at 0.1M NaCl. 111

Figure 3-10. Hydrodynamic radius measured for 1930-3.1-1930 at 0.1M NaCl. 112

Figure 3-11. Aggregation number as a function of temperature and pH for 4845-2.5-4845 at 0.1M NaCl..... 114

Figure 3-12. Aggregation number as a function of temperature and pH for 4845-4.7-4845 at 0.1M NaCl..... 114

Figure 3-13. Aggregation number as a function of temperature and pH for 1930-3.1-1930 at 0.1M NaCl..... 115

Figure 3-14. Schematic representation of the micelle showing the density distribution model[60] parameters. 116

Figure 3-15. The hydrodynamic radius measured by DLS (25°C, pH 2, 0.1M NaCl) is compared to a prediction based on the density distribution model by Vagberg et al.[60] . 117

Figure 3-16. Volume fraction profiles for 1930-3.1-1930, 4845-2.5-4845, and 4845-4.7-4845 in 0.1M NaCl at 25C based on Vagberg's approach. Micelles with higher aggregation numbers form denser brushes, and those with longer PEO chains have the corona extending further into solution. 119

Figure 3-17. A visual representation of relative micelle sizes. The size of the center shown reflects the end-to-end distance if the center block were extended as far as possible without breaking or bending bonds. The number in the center of each is the aggregation number measured by SLS. The total size of the micelle is the hydrodynamic diameter as measured by DLS..... 120

Figure 4-1. Structure of a representative triblock copolymer with PEO tail blocks and a polyurethane center block that contains carboxylic acid groups. 132

Figure 4-2. Density measurements for PEO homopolymer in D_2O at pH 2 with 0.1M NaCl. 141

Figure 4-3. Density measurements for triblock copolymers in D_2O at pH 2 with 0.1M NaCl. 142

Figure 4-4. Illustration of a block copolymer micelle with nomenclature of the SANS model. R is the hard-sphere radius of the core. $2R_g$ is the thickness of the corona. 146

Figure 4-5. SANS data and global fits to a triblock copolymer micellar model for 1930-3.1-1930. The H_2O solvent data has been omitted from the graph for clarity. 149

Figure 4-6. SANS data and global fits to a triblock copolymer micellar model for4850-2.5-4850. 150

Figure 4-7. SANS data and global fits to a triblock copolymer micellar model for 4850-4.7-4850. 150

Figure 4-8. Schematic representation of the micelle showing the density distribution model[48] parameters. 153

Figure 4-9. Comparison of the density distribution[48] prediction for micelle radius with measured hydrodynamic radius (DLS) and total radius by SANS. All measurements were in D_2O at pD 2. 154

Figure 5-1. Structure of a representative triblock copolymer with PEO tail blocks and a polyurethane center block that contains carboxylic acid groups. 163

Figure 5-2. Example of a Debye plot for 4850-2.5-4850 polymer in D_2O with 0.1M NaCl and a pD of 2. 168

Figure 5-3. Schematic representation of the micelle showing the density distribution model[15] parameters. 170

Figure 5-4. Pair potential for an example system with 2000 g/mol PEO grafted to a sphere with R_c = 5 nm and f = 10, 20, 50, 100, and 200. The transition from a soft to hard interaction potential with increasing f may be observed. 173

Figure 5-5. Volume fraction profile for an example system with 2000 g/mol PEO grafted to a sphere with R_c = 5 nm and f = 10, 20, 50, 100, and 200. 174

Figure 5-6. Mass fraction profiles for 1930-3.1-1930, 4850-2.5-4850, and 4850-4.7-4850 in 0.1M NaCl at 25C based on Vagberg's approach. Micelles with higher aggregation numbers form denser brushes, and those with longer PEO chains have the corona extending further into solution. 178

Figure 5-7. Mass fraction profiles for PEO-PPO-PEO micelles in water at 25°C. 180

Figure 5-8. Mass fraction profiles for PEO-PS copolymers in cyclopentane at 25°C... 181

Figure 6-1. Structure of the pentablock stabilizer with PEO-PPO tail blocks and polyurethane center block containing carboxylic acid groups. 194

Figure 6-2. Structure of the PEO-g-PEI stabilizer. For these polymers, m can be either 1 or 2. 195

Figure 6-3. Adsorption of carboxylic acid onto magnetite. 195

Figure 6-4. Transmission electron microscopy (TEM) image of the magnetite used in this study. TEM was performed by Thompson Mefford. 199

Figure 6-5. Particle size distribution for the magnetite used in this study. TEM and analysis was performed by Thompson Mefford. 200

Figure 6-6. TGA scan for the urethane pentablock on magnetite. 201

Figure 6-7. Schematic representation of the complex showing the density distribution model[45] parameters. 202

Figure 6-8. Parameters of the density distribution model[45] extended to include an anchor layer. 203

Figure 6-9. Geometry for the Likos-Lowen[62] star polymer model. 211

Figure 6-10. Example plot showing the effect of increasing the number of corona chains per particle, f on steric repulsion. The dimensionless center-to-center distance is r/σ. These example calculations assume f = 10, 20, 50, 100, and 200. R_c was 5 nm, ν was 0.583, and the attached chains were 2000 g/mol PEO. The value of σ was calculated as $1.3*R_g$, and R_g for the complex was calculated using the moment of inertia approach described earlier in the chapter, and as such varies with f. 214

Figure 6-11. Steric potential by the Likos and Lowen expression for a core radius of 3.8 nm. 215

Figure 6-12. Example plot showing the effect of increasing the number of corona chains per particle,,f on volume fraction in the corona. The center-to-center distance is r. These example calculations assume f = 10, 20, 50, 100, and 200. R_c was 5 nm, ν was 0.583, and the attached chains were 2000 g/mol PEO. The value of σ was calculated as $1.3*R_g$, and R_g for the complex was calculated using the moment of inertia approach described earlier in the chapter, and as such varies with f. 216

Figure 6-13. Volume fraction in the PEO corona for the polymer-magnetite complexes for R_c = 3.8 nm. The starting point for each sample depends on the thickness R_c+t_a.... 216

Figure 6-14. DLVO interaction potential for 3kPEO-0.6kPEI (m=2) in deionized water with R_c = 3.8 nm. The magnetization used was measured by Nikorn Pothayee using a 7 Tesla Quantum Design MPMS SQUID magnetometer (345,000 A/m). 217

Figure 6-15. A hypothetical DLVO prediction for magnetite (R_c = 3.8 nm) with adsorbed 3kPEO-0.6kPEI (m=2) in PBS based on the assumption that no desorption occurs in PBS. The magnetization used was (345,000 A/m). 218

Figure 6-16. Titration of magnetite in water with 0.1M H_2SO_4 under a nitrogen purge. 220

Figure 6-17. Simple polynomial fit relating the self-diffusion coefficient of water and the weight fraction of PEO. Data is from Borodin et al.[90] 221

Figure 7-1. Approach to creating crosslinked micelles for drug delivery 232

Figure 7-2. Structure of a representative triblock copolymer with PEO tail block and polyurethane center block containing carboxylic acid groups. 233

Figure 7-3. EDC crosslinking reaction of two carboxylate groups with ethylenediamine. An isourea by-product is formed. 235

Figure 7-4. EDC-mediated crosslinking reaction of two carboxylate groups with ethylenediamine in the presence of NHS. 236

Figure 7-5. Reaction of ODPE with cisplatin to form a light blue solution. 237

Figure 7-6. Calibration curve for platinum assay. Cisplatin concentration is in the original solution. 238

Figure 7-7. Calibration curve for lidocaine in water 239

Figure 7-8. Dichloromethane swelling the micelle core. 242

Figure 7-9. Effect of DCM to water ratio on micelle size for 4845-5-4845 polymer in water. The hydrodynamic diameter is an intensity-weighted average. 243

Figure 7-10. Hydrodynamic diameter of a 4845-5-4845 micelle swollen with DCM. The pH was approximately 4 and the initial concentration of polymer was 7.5 mg/mL. 244

Figure 7-11. pH dependence of hydrodynamic diameter for crosslinked micelles. No electrolyte beyond the titrants was added. The error bars are one standard deviation. .. 246

Figure 7-12. Titration of crosslinked micelles with 0.1M H_2SO_4. The error bars are one standard deviation. 247

Figure 7-13. Lidocaine was used as a test drug for encorporation into a crosslinked micelle. 249

Figure 8-1. Flowchart for third round of biopanning. Six panning steps were performed. 260

List of Tables

Table 3-1. Properties of triblock copolymers. 95

Table 3-2. Angular dependence of qR_H for the largest copolymer micelle. 105

Table 3-3. Comparison of unimer size measured by DLS to: (a) an experimental correlation (Eq. 3-15)[69] and (b) wormlike chain prediction (Eq. 3-18).[71] 109

Table 4-1. Properties of triblock copolymers. 133

Table 4-2. Summary of static and dynamic light scattering data on polymers in D_2O and H_2O, both with 0.1M NaCl and pH or pD 2. 140

Table 4-3. Summary of densiometry on the triblock copolymers with 0.1M NaCl, pD or pH 2. 143

Table 4-4. Scattering length densities for polymers and solvents. 146

Table 4-5. Summary of fitting of SANS data for in 0.1M NaCl, equivalent pH 2. 152

Table 5-1. Properties of triblock copolymers. 164

Table 5-2 Summary of densiometry on the triblock copolymers with 0.1M NaCl, pD 2. 172

Table 5-3. Comparison of experimental A_2 to star and hard sphere values for novel polyurethane-containing hydrophilic triblock copolymers at 25°C, pD 2, 0.1M NaCl in D_2O. R_H was determined by DLS, R_g is from a Guinier analysis on SANS data, and f is from SLS. 176

Table 5-4. Comparison of experimental A_2 to star and hard sphere values for studies on PEO-PPO-PEO in water and PEO-PS in cyclopentane. 179

Table 5-5. Prediction of R_g and A_2 for star polymers. 182

Table 5-6. Volume fraction and micelle-micelle separation for the triblock copolymers. 183

Table 6-1. Properties of the polymeric stabilizers. 195

Table 6-2. Complex size measured by DLS and predicted using the Density Distribution model.[a] 204

Table 6-3. Zeta potential and stability observations for the complexes. 207

Table 6-4. Estimation of R_g and σ. 213

Table 6-5. Estimated diffusion parameters in the complexes. 222

Table 7-1. Properties of triblock copolymers. 233

Table 7-2. Recipe for 1L of PBS. 233

Table 8-1. Bound sequences. 267

Table 8-2. Classification of bound sequences..... 267

Table 8-3. Relationship between selectivity, number of panning steps, and number of unique sequences remaining. 269

Table 8-4. XPS performed by N. Nueraji on alumina plate (c-plane) before beginning experiment and after 6 panning steps. In each instance, the plate had been rinsed with deionized water before the measurement. Surface contamination by the growth medium is evident. 271

1 Introduction

1.1 Significance and Motivation

There is a need for multifunctional polymer-particle complexes for use in biomedical applications such as for drug delivery or as MRI contrast agents where composition and stability are essential for the complexes to function. Control of both the size and interactions between complexes, particularly under physiological conditions, is required. Multifunctional polymer-particle complexes require a steric stabilizing layer of a polymer, which is typically poly(ethylene oxide) (PEO) to prevent nonspecific protein adsorption which would trigger an undesirable immune response. For metal oxide and metal nanoparticles in aqueous media, this requires a stabilizing polymer layer thickness comparable in thickness to the particle due to the especially strong attractive VdW forces. This, in turn, requires modeling steric particle interactions in terms other than the commonly used force laws based on polymer brushes on a flat surface, i.e. the Deryaguin approximation cannot be used for the steric effects. Before the present work, there had been no demonstration of a methodology for designing these complexes using validated models for the structure for and interactions between complexes. This work outlines such a methodology and demonstrates its use in several model nanoparticle systems.

1.2 Specific Research Objectives

The overall objective of this research was to develop an approach to deliberately design polymer-particle complexes that would be of a specified size, stable in vivo, and would possess the necessary structure for the application (such as for MRI contrast or drug delivery). In order to accomplish this general objective, several specific research objectives were necessary:

1. <u>Analyze the structure of a micelle system in terms of models developed for star polymers.</u>

A new class of novel hydrophilic triblock copolymers which form micelles in aqueous solution was examined by static and dynamic light scattering (SLS and DLS), small angle

neutron scattering (SANS), and densiometry. The polymers were symmetric A-B-A block copolymers having two poly(ethylene oxide) tailblocks and a carboxylic acid containing polyurethane center block. This unique combination leads to an interesting balance between hydrogen bonding, hydrophobicity and charge effects in solution. Under conditions when the charge is suppressed such as at low pH and/or high ionic strength, the polymer chains self-assemble into micelles, whereas unimers alone are present under conditions where charge effects are important, such as high pH and low ionic strength. The results helped validate use of the density distribution model by Vagberg,[1] which was based on star polymers.

2. Validate the use of a star polymer model in describing the interactions between micelles.

The model for effective interaction between star polymers developed by Likos et al.[2-4] was used to obtain an expression for the second virial coefficient (A_2) for micelles in solution. The values of A_2 obtained using this method were compared with experimentally determined values for PEO-PPO-PEO micelles[5] and novel polyurethane-containing hydrophilic triblock copolymer micelles.[6] In doing so, not only was a new means of calculating A_2 a priori introduced, but the applicability of the expression introduced by Likos et al. for star polymers to micellar systems was established. Through the analogy of micelles to sterically stabilized nanoparticles, this study demonstrated that this model can be used to model steric interactions for the latter class of materials.

3. Experimentally characterize polymer-magnetite complexes in terms of size and stability.

Adsorption of several water-soluble block copolymers on magnetite nanoparticles was examined for the purpose of tailoring a steric stabilizing brush layer. These magnetite complexes are being developed for use as drug delivery vehicles and MRI contrast agents. The copolymers included a poly(ethylene oxide) (PEO) chain with three carboxylic acid groups on one end, several block copolymers of PEO and poly(ethyleneimine) (PEI), and a symmetric pentablock copolymer having PEO, poly(propylene oxide) (PPO), and a carboxylic acid-containing urethane block. The

complexes were examined using light scattering and zeta potential, and observations on stability were made.

4. Using the adaptations to the star polymer models for structure and interaction as described in earlier specific objectives, describe the interaction of two polymer-coated particles with extended DLVO theory.

The sizes of the magnetite-polymer complexes were predicted using a star polymer model and compared to sizes measured by dynamic light scattering. Colloidal stability in water and phosphate buffered saline was predicted using an extended DLVO theory. The volume fraction in the PEO corona was calculated with the blob model and related to the mobility of water in the corona.

1.3 Overview of Chapters

Chapter 2 is a literature review providing an overview of relevant topics including basic theoretical background and a review of current research. The six primary topics covered in the review are: (1) polymers in solution, (2) polymers at interfaces, (3) colloidal stability, (4) polymer complexes in nanomedicine, (5) combinatorial biochemistry techniques to design polypeptides, and (6) introductory information on the main experimental techniques used.

In **Chapter 3**, an aqueous solution study of unique self-assembling triblock copolymers with ionic, hydrophobic cores is introduced. These triblock copolymers consist of a symmetric PEO block at either end with a carboxylic acid containing, but relatively hydrophobic, polyurethane center block.[6] Self-assembly with an ionic block in the center without the presence of multi-valent counterions is unique, and a balance of hydrogen bonding, hydrophobicity, and electrostatic repulsion is achieved in the micellization process. At low pH and/or high salt, self-assembly into micelles occurs. The predominant tool used in this study was static and dynamic light scattering, which allowed measurement of size (hydrodynamic radius), molecular weight, and second virial coefficient of the micelles. These measurements were critical in subsequent work. The

density distribution model by Vagberg[1] is also introduced in this chapter as a tool to examine brush extension in the corona.

The work in the previous chapter is extended in **Chapter 4** by using small angle neutron scattering (SANS) to probe the internal structure of the micelles in water and D_2O. The same polymers were examined at conditions where micellization occurs. Areas of interest in this study included the relative sizes of core and corona, the degree of hydration of the core, and the interpenetration of PEO chains into the core. A triblock model consisting of a homogeneous core with a corona of non-interacting Gaussian chains was developed from an existing diblock model by Pedersen et al.[7-9]

Chapter 5 is focused on development of a method to predict the second virial coefficient, A_2, for a polymer micelle. A_2 is a useful means of describing the interaction between entities in solution, but can be somewhat challenging to measure. The model for the effective pair potential between star polymers developed by Likos et al.[2-4] was used as the basis for this expression for A_2 for micelles in solution. A comparison was made with experimental measurements from the literature as well as the polyurethane triblocks examined in this dissertation. This is an important contribution, as it is an a priori method for calculating A_2 of not only micelles, but also sterically stabilized nanoparticles.

In **Chapter 6**, adsorption of block copolymers on magnetite and subsequent stabilization in water and phosphate buffered saline (PBS) is described. This is an ongoing collaborative effort between the students of Professor Judy Riffle and Professor Richey Davis with the objective of developing magnetite-based MRI contrast agents with greatly increased relaxivities, resulting in enhanced contrast. The copolymers studied were poly(ethyleneoxide)-*g*-poly(ethyleneimine), poly(ethylene oxide) with three carboxylate groups grafted to one end of the chain, and a symmetric pentablock consisting of poly(ethylene oxide), poly(propylene oxide), and a novel carboxylic acid-containing urethane center block. The polymers bind strongly to the surface of magnetite and form a thick brush layer which sterically stabilizes the complexes. Size and zeta potential on

the particles before and after adsorption were measured. The model for the effective interaction between star polymers developed by Likos et al.[2-4] was used to predict colloidal stability in conjunction with extended DLVO theory. In addition, Vagberg's density distribution model was expanded to include a surface layer of adsorbed anchor block. This allowed a description of the PEO segment densities in the brush layer.

The urethane triblock copolymers of the first three chapters are revisited in **Chapter 7**, which describes initial attempts to use EDC-mediated crosslinking to create crosslinked micelles capable of delivery a drug payload after the work of Bronich et al.[10] Due to the partial hydrophobicity of the center block, these copolymers have the unique advantage that they self-assemble without needing a divalent counter-ion. The size of the micelles in solution is in a size range (20-30 nm hydrodynamic diameter) that is advantageous for in vivo use.

Chapter 8 is independent of the rest of the dissertation and describes work to use a biopanning technique to develop anchor blocks capable of selectively adsorbing on alumina. The combinatorial library employed was the FliTrx™ Random Peptide Display Library from Invitrogen, which contains *E. coli* bacteria with the capability to display 10^9 dodecapeptides exposed on flagella and constrained by a thioredoxin loop. Due to this forced accessibility, it is possible to select for strongly adsorbing peptide sequences.

Conclusions from the work are described in **Chapter 9**. In addition, some thoughts for future studies are provided.

Note: This dissertation is structured as a series of papers for individual publication. Therefore there is some overlap between the chapters, particularly in the introductory sections of each. In some instances, limited amounts of data from one chapter have been included in another when necessary to aid the reader in understanding the work.

1.4 References

1. Vagberg, L.J.M., Cogan, K.A., and Gast, A.P., Light-Scattering Study of Starlike Polymeric Micelles. *Macromolecules*, **1991**. 24(7): p. 1670-1677.

2. Jusufi, A., Watzlawek, M., and Lowen, H., Effective interaction between star polymers. *Macromolecules*, **1999**. 32(13): p. 4470-4473.

3. Likos, C.N., et al., Star polymers viewed as ultrasoft colloidal particles. *Physical Review Letters*, **1998**. 80(20): p. 4450-4453.

4. Likos, C.N., Soft matter with soft particles. *Soft Matter*, **2006**. 2(6): p. 478-498.

5. Nolan, S.L., et al., Light scattering study on the effect of polymer composition on the structural properties of PEO-PPO-PEO micelles. *Journal of Colloid and Interface Science*, **1997**. 191(2): p. 291-302.

6. Harris, L.A., et al., Magnetite nanoparticle dispersions stabilized with triblock copolymers. *Chemistry of Materials*, **2003**. 15(6): p. 1367-1377.

7. Pedersen, J.S., Structure factors effects in small-angle scattering from block copolymer micelles and star polymers. *Journal of Chemical Physics*, **2001**. 114(6): p. 2839-2846.

8. Pedersen, J.S. and Gerstenberg, M.C., The structure of P85 Pluronic block copolymer micelles determined by small-angle neutron scattering. *Colloids and Surfaces a-Physicochemical and Engineering Aspects*, **2003**. 213(2-3): p. 175-187.

9. Pedersen, J.S., et al., A Small-Angle Neutron and X-ray Contrast Variation Scattering Study of the Structure of Block Copolymer Micelles: Corona Shape and Excluded Volume Interactions. *Macromolecules*, **2003**. 36: p. 416-433.

10. Bronich, T.K., et al., Polymer Micelle with Cross-Linked Ionic Core. *Journal of the American Chemical Society*, **2005**. 127: p. 8236-8237.

2 Literature Review

This literature review has two objectives. It will cover the basic theoretical background necessary to the undertaking of the objectives outlined in the first section of this dissertation. In addition, it will provide a review of both relevant current research in the literature and certain past work essential to the development of key theories.

There are six main topics covered in this review. These are: (1) polymers in solution, (2) adsorption of polymers on surfaces, (3) colloidal stability, (4) applications for polymer complexes in nanomedicine, (5) use of combinatorial biochemistry for design of polymers, and (6) an introduction to the main experimental techniques used in this dissertation. The section on polymers in solution will focus on how block copolymers self-assemble in solution to form micelles and aggregates. A description of some simple aggregation kinetics models will be provided. In addition, the use of a star polymer model to describe brush extension in the micelle will be introduced. The section on polymers at interfaces will focus on adsorption of block copolymers on surfaces in aqueous systems. The basics of adsorption isotherms will be covered. Several models for brush extension on flat and curved surfaces will be discussed. The section on colloidal stability will concentrate on an extended DLVO theory which includes contributions from electrostatic, van der Waals, magnetic and steric potential. Particular emphasis will be placed on the description of steric interaction with a model based on star polymers. The section on polymer complexes in nanomedicine will provide a review of advances in the use of self-assembled polymers in medical applications. The two foci will be use of self-assembled micelles for targeted drug or gene delivery and the use of superparamagnetic iron oxide nanoparticles (SPIONs) for either specific delivery or as MRI contrast agents. The section on combinatorial biochemistry will include some basic background on biosynthesis of polymers, and then will describe the use of combinatorial design techniques in libraries of bacteria. Some medical and environmental applications will be described. The final section provides an introduction to the key experimental techniques employed in this work. This is meant only to supply an overview of how each

technique works and what it may be used for. Specific experimental details are given in each appropriate chapter.

2.1 Block Copolymers in Solution

Micelles which self-assemble from block copolymers are useful in a number of applications, such as emulsification, stabilization, drug delivery, and gene therapy.[1-3] There is a large body of literature describing studies of micellar systems where the micellar cores consist of nonionic, insoluble polymer chains, such as poly(ethylene oxide)-poly(propylene oxide)-poly(ethylene oxide) (PEO-PPO-PEO) triblocks[1, 4-11] poly(ethylene oxide)-poly(butylene oxide) (PEO-PBO) diblocks,[5, 12] and polystyrene-polyethylene oxide) (PS-PEO) diblock[13-16] copolymers. However, the literature is much more limited on micelle-forming ionic block copolymers in water, particularly for those in which the ionic block forms the center of the micelle. There are some examples of aggregates composed of diblock copolymers where an ionic block forms a micellar core when neutralized. One such system concerned the pH-sensitive assembly of poly(methacrylic acid)-g-poly(ethylene glycol) (PMA-PEG).[17] At low pH, collapse of the aggregates was observed and was attributed to intramolecular complexes due to hydrogen bonding along the backbone. Another such PMA-PEG system was examined as an aqueous reversible emulsifier.[18, 19] Acid conditions caused hydrogen-bonding between the backbone and grafts to form hydrophobic segments. Li et al.[20] examined the formation of nanoaggregates of PEO-PMA which formed when the PMA block was neutralized using alkaline earth metals. These systems formed a neutralized polyion core with a PEO corona. Such polymers may also be used for stabilizing solutions. For instance, Moeser and Hatton[21, 22] used PEO-PPO-PEO to stabilize magnetite particles in order to extract organics from water.

There are also several examples of micelle-forming amphiphilic block copolymers in aqueous solutions in which an ionic block is the hydrophilic corona block. Matsuoka et al.[23-25] describe micelle formation for several hydrophilic-hydrophobic diblock copolymers in which the corona chains were polysulfonic acids and the core block was poly(diethylsilacyclobutane). These novel copolymers micellized readily in water, yet

did not show surface activity, i.e. did not form a Gibbs monolayer at the air-water interface. The authors hypothesized that this could be partly attributed to strong electrostatic repulsion between tailblock chains causing a destabilization in the monolayer. Examples may also be found[26] of micelles with an ionic core; however, these were in a hydrophobic solvent. Such cases may be used for controlled synthesis of metal nanoparticles.[27] A similar study involved trapping of water in the ionic core of a block copolymer micelle in a hydrocarbon solvent.[28]

2.1.1 Micelle Formation

Self-assembly of amphiphilic molecules can occur spontaneously. It is important to note that these structures are based on non-covalent, non-ionic forces, such as van der Waals, hydrophobicity, hydrogen-bonding, and screened electrostatic interactions. This gives the systems a great deal of mobility and makes them susceptible to changes in condition such as pH or electrolyte concentration.[29]

Aggregation of molecules, such as surfactants, into organized structures is called micellization. The critical micelle concentration (CMC) is the concentration at which stable micelles are formed to a significant degree in a surfactant-containing system. [30] Amphiphilic aggregates can take on a variety of forms, t of which are illustrated in Figure 2-1.

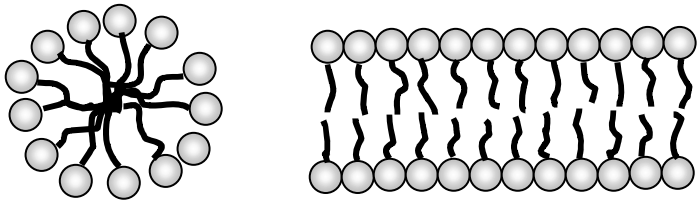

Figure 2-1. Structures formed by aggregation: a micelle and a bilayer.

Critical micelle concentration is readily identified by a variety of experimental methods, largely because the formation of aggregates profoundly impacts the physical properties of the system. These methods include osmotic pressure, turbidity, solubilization, magnetic resonance, surface tension, equivalent conductivity, and self diffusion.[31]

A number of models exist to describe the formation of micelles and to characterize the CMC. One reasonable model is the closed-association model, which depends on an aggregation number, N. This aggregation number is similar in concept to a degree of polymerization, in that N indicates the number of individual molecules that have come together to form the aggregate. The following outlines the development of this model, as described in Evans.[31]

The formation of micelles may be described by adding molecules, S, to a growing aggregate, S_{n-1} in a stepwise fashion according to the following equation:

$$S + S_{n-1} \leftrightarrow S_n$$

Eq. 2-1

This results in the following simple equilibrium equation:

$$K_n = \frac{[S_n]}{[S][S_{n-1}]}$$

Eq. 2-2

This equation specifies n equilibrium constants. As this is difficult to work with, various models have been proposed to simplify the math. The closed-association model assumes the existence of a single aggregation number, allowing simplification to the following:

$$NS \leftrightarrow S_N$$

Eq. 2-3

$$K_N = \frac{[S_N]}{[S]^N}$$

Eq. 2-4

A total surfactant concentration, $[S]_T$, is introduced as follows:

$$[S]_T = N[S_N] + [S] = NK_N[S]^N + [S]$$

Eq. 2-5

This expression may be differentiated to determine the concentration at which additional amphiphilic molecules will first preferentially join aggregates. This is the CMC, as described below:

$$CMC = [S]_{CMC}\left(1 + N^{-1}\right) = \left(N^{2} K_{N}\right)^{-1/N-1}\left(1 + N^{-1}\right)$$

Eq. 2-6

Since the term N^{-1} becomes smaller with increasing N, it is possible to neglect it, yielding:

$$\Delta G = RT\ln(CMC)$$

Eq. 2-7

Addition of polymeric surfactants to stabilize otherwise unstable colloids is a common practice in industrial applications, as will be discussed in more detail later in this review.

2.1.1.1 Uncharged Copolymers

Assembly of uncharged copolymers is frequently driven by differences in solvent quality for the two blocks. For instance, a block copolymer having one hydrophilic and one hydrophobic block will often assemble readily in either aqueous or organic solution. One of the most popular classes of polymers for study of uncharged micelles is the collection of polymers known as Pluronics. These symmetric PEO-PPO-PEO copolymers micellize readily in water into a variety of structures.[4, 8, 9, 32-42]

A particularly clever example of micellization behavior was described by Arotçaréna et al.[43] They used sequential free radical polymerization to make block copolymers having two hydrophilic blocks. The two hydrophilic blocks have different thermal properties, which allow a switching of the direction of the micelles. That is to say, by changing the temperature, the hydrophilicity of each end may be separately manipulated. Therefore, micelles may be in effect turned inside out.

In addition to the CMC, many systems have a critical micellization temperature (CMT) above which micelles will form. For example, Goldmints et al.[44] studied a deuterated PEO_{23}-PPO_{34}-PEO_{23} copolymer which formed micelles at temperatures above 40°C. The aggregation number increased with temperature above the CMT, but the radius of the micelle remained the same. This was attributed to dehydration of the core. The increase in aggregation number without an increase in the overall size is typical for Pluronics

copolymers as summarized by Alexandridis.[5] An increasing aggregation number with temperature was shown by several researchers for L64(PEO_{14}-PPO_{31}-PEO_{14})[42, 45] and F127(PEO_{95}-PPO_{62}-PEO_{95}).[46] This was also shown for P85 (PEO_{27}-PPO_{41}-PEO_{27}) by Brown et al.[47] However, a study on P85 by SANS showed an increase in both the radius and aggregation number between 20 and 50°C[7] as did a study on F68(PEO_{81}-PPO_{31}-PEO_{81}).[48] Some of the differences in observations can depend on the method employed, due to the dehydration of the PPO block with an increase in temperature.

2.1.1.2 Charged Copolymers

A carboxylic acid-containing polymer can also be incorporated into micelles with uncharged polymers containing a hydrophobic section by hydrogen bonding. This was demonstrated in a study by Zeghal and Auvray[49] in which they examined micelles composed of a mixture of Pluronic P105 (PEO_{34}-PPO_{52}-PEO_{34}) and poly(methacrylic acid) (PMA). Using a combination of SANS (with a deuterated polyacid) and NMR, they characterized the structure of the corona and investigated the effect of changing the degree of charge on the PMA and the temperature on the aggregation number and size of the resulting micelles. In this system, PMA was present in both the core and corona of the micelles, but in different ionization states. The PMA in the core was neutral; the PMA in the corona was ionized. They found that as the number of available hydroxyl groups increased, so did the number of PMA chains in the micelle. This being an electrostatic effect, it was dependent on pH but not temperature. The number of Pluronic chains in the micelle, however, was dependent on both pH and temperature, as micellization was driven by both hydrophobic interaction of the PPO chains and hydrogen bonding of the PMA with PPO.

There are examples in the literature of diblock copolymers containing an ionic block which forms a micellar core, but the ionic block must be neutralized. For instance, work by Li et al.[20] described nanoaggregates of poly(ethylene oxide)-b-poly(methacrylate) where the ionic block was neutralized using alkaline earth metals. This resulted in a neutralized polyion core with a PEO corona. Also, Bronich et al.[50] describe the use of a divalent metal ion (Ca^{2+}) to cause poly(ethylene oxide)-b-polymethacrylate polymers to form into micelles, despite the charges on the polymethacrylate block. Block ionic

complexes can also be formed by combining poly(ethylene oxide)-b-poly(sodium methacrylate) with surfactants such as hexadecyltrimethylammonium bromide.[51] This complexation has also been demonstrated with poly(ethylene oxide)-b-poly(methacrylate) and cetyltrimethylammonium chloride[52] or chitosan.[53]

There are also examples in the literature of self-assembly of hydrogen-bonding graft copolymers in water. One such system concerned the pH-sensitive assembly of poly(methacrylic acid)-g-poly(ethylene glycol).[17] At low pH, collapse of the aggregates was observed and was thought to be the result of intramolecular complexes due to hydrogen bonding along the backbone. Another such poly(methacrylic acid)-g-poly(ethylene glycol) system was examined as an aqueous reversible emulsifier.[18, 19] Acid conditions caused hydrogen-bonding between the backbone and grafts to form hydrophobic segments.

One additional consideration in describing the aggregation behavior of these copolymers is the possibility of hydrogen bonding between different parts of the copolymer. For instance, hydrogen bonding interactions between homopolymer polyacids and PEO on diblocks have been observed in numerous instances.[54, 55] PMAA and PEO complex under acidic conditions only if the molecular weight of the PEO is at least 2000 g/mol.[56] Investigators have found that hydrogen bonding also occurs between PEO and polyacids when they are present as a block copolymer, rather than as two separate homopolymers.[19, 57-60]

2.1.2 Prediction of Micelle Size Using a Star Polymer Model

Micelle dimensions can be predicted with the density distribution (DD) model, developed by Vagberg et al.[61] This model, based on a model for star polymers by Daoud and Cotton[62] assumes concentric shells with a constant number of blobs. Blob size $\xi(r)$, is a continuous function of distance from the surface. The segment density in the shell varies with distance from the core (Figure 2-2).

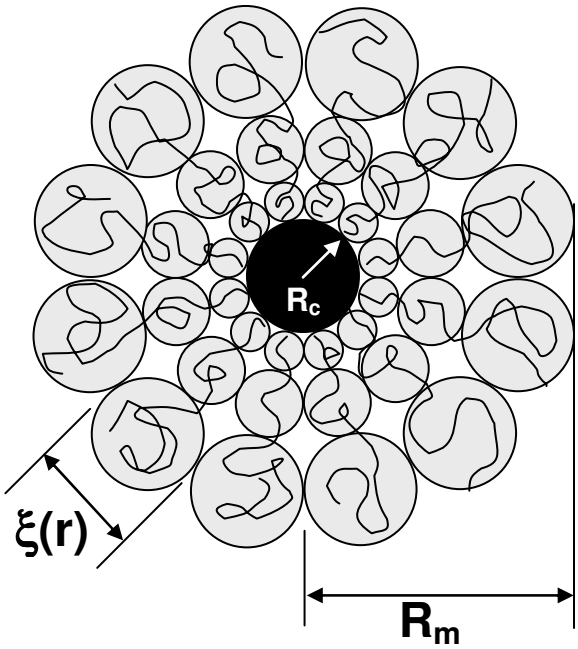

Figure 2-2. Schematic representation of the micelle showing the density distribution model[61] parameters.

The DD model predicts micelle radius, $R_{m,}$, as:

$$R_m = \left[N a_s^{1/\nu} \frac{8 f^{(1-\nu)/2\nu}}{3\nu 4^{1/\nu}} + R_c^{1/\nu} \right]^{\nu}$$

Eq. 2-8

where N is the number of Kuhn segments, ν is the Flory exponent, R_c is the radius of the core, and f is the number of corona chains.

The blob diameter, ξ(r) is given by:

$$\xi(r) = \frac{4r}{f^{1/2}}$$

Eq. 2-9

in which r is the distance from the center.

Several groups have compared the density distribution prediction with experimental measurements of PEO-containing block copolymers or similar systems. Farhina et al.[63] examined the micellization of a series of PS-PEO copolymers in water and cyclopentane by DLS. They found that the model slightly over predicted the brush thickness and partly attributed it to polydispersity and uncertainties in the input parameters to the model.

Harada et al.[64] also found in their study of aqueous mixtures of poly(ethylene glycol)-b-poly(α,β-aspartic acid) and poly(ethylene glycol)-b-poly(L-lysine) that R_m values predicted were slightly larger than R_H values measured by DLS. These findings are both compatible with the original observations by Vagberg et al.[61] who attributed this difference to draining in the corona, causing a decrease in R_H. Conversely, a study by Johnsson et al.[65] using PEG-derivatized lipids found that the predicted values tended to be slightly smaller than experimentally observed. For this study, the core of the radius was estimated using the measured aggregation number and the volume occupied by the components in the core. A study by Fitzgerald et al.[66] on dimeric PEO surfactants also indicated that the predicted thickness of the shell was less than that experimentally fit from SANS data by 7-24% for the spherical micelles.

2.1.3 The Second Virial Coefficient

The second virial coefficient, A_2, arises from interactions between polymer and solvent. A_2 may be described by

$$A_2 = \frac{N_{AV}}{M^2} 2\pi \int_{2a}^{\infty} (1 - \exp(-A_{\text{int}}))r^2 dr$$

Eq. 2-10

in which A_{int} is the pair potential, r is the center-to-center separation of two particles of radius a, M is the molecular weight of the micelle, and N_{AV} is Avogadro's number.

A_2 based on the classical hard-sphere model is given by:

$$A_2 = \frac{16\pi N_{AV} R^3}{3M_2^2}$$

Eq. 2-11

in which N_{AV} is Avogadro's number, R is the radius of the micelle, and M_2 is the molecular weight of the micelle.[67]

A_2 may be measured using light scattering. For instance, A_2 for PEO has been measured by multiple groups, including Yamaguchi et al.[68] and Devanand and Selser.[69] The second virial coefficient may also be measured by osmometry.[70] A_2 can also be characterized for

micelles. For instance, Vagberg et al. used static light scattering to measure A_2 for PEO-PS micelles in cyclopentane.[61] Piscarcik et al. measured A_2 for alkanediyl-α,ω-bis(dimethylalkylammonium bromide) surfactants in water.[71]

Interactions between star polymers in semi-dilute and concentrated solutions has been addressed in a rich body of literature. In particular, Vlassopoulos et al. have examined multiarm star polymers in solution using static and dynamic scattering techniques and have characterized interactions in semi-dilute solutions in terms of a structure factor.[72-77]

2.1.4 Micelle-Micelle Separation

The micelle-micelle separation based on a hard sphere model may be calculated by the relationship

$$\frac{\bar{h}}{d} = \left[\left(\frac{1}{3\pi\phi} + \frac{5}{6} \right)^{1/2} - 1 \right]$$

Eq. 2-12

in which d is the diameter of a micelle, ϕ is the volume fraction of micelles in solution, and $\bar{h}$ is the average separation between micelles.[78]

2.2 Polymer Adsorption

Adsorption is the increased concentration of a solute near an interface. Conversely, a decrease in solute concentration is depletion. Adsorption and depletion are driven by the free energy relationships between the polymer and solvent as opposed to the polymer and surface. The adsorbed amount is essential for description of the behavior of the system. Two means of describing the adsorbed amount are as follows. One may measure the amount of polymer contacting the surface, Γ^a. An alternate means is Γ^{ex}, the amount of the polymer in the interfacial region that is not attributable to the bulk concentration of polymer. These two values become nearly indistinguishable at very low polymer concentrations, and often the adsorption is described only as Γ in this case.[79]

2.2.1 Adsorption Configuration

Polymers may adsorb onto surfaces in three basic configurations: loops, trains, and tails. Trains are adsorbed directly onto the surface; loops and tails extend into the system solvent. Trains lie flat on the surface, loops are attached at two ends, and tails extend into the solution. Block copolymers may be used to direct the adsorption of trains and tails in a particular manner. The bound fraction, p, is a measure of the portion of the polymer that exists as trains.

Polydispersity plays an important role in adsorption. The different molecular weights within a sample cause variations in adsorption behavior. An example from Fleer et al.[79] describes the adsorption behavior of a system containing two monodisperse polymers of different molecular weights. With increasing polymer concentration, three regions may be observed. At low concentration, there is no lack of space forcing a competition, so both molecular weights adsorb. At intermediate concentration, saturation is imminent and the high molecular weight chains preferentially adsorb, displacing low molecular weight chains as necessary. At high concentration, saturation is complete, and the adsorbed amount plateaus.

2.2.2 Theoretical Models for Adsorption

A number of methods have been developed to model and predict adsorption behavior of polymers. Some of these are described within this section. Unless otherwise noted, monodisperse homopolymers are assumed. Some variations from this will be specifically described within the body of the text. Two general categories of models are included. The first includes models which rely on conformational statistics. These examine a small number of chains, but take into account the actual volumes and interactions within the chains. The other group uses a mean-field approach and is computationally challenging.

2.2.2.1 Exact Enumeration

For exact enumeration, the number of segments in the polymer chain and the type of lattice (i.e. tetrahedral) is specified. A computer program determines all possible conformations for the chain, assuming self-avoidance. This leads directly to an approximation of the bound fraction, p, after taking into account an energetic weighting

factor, $e^{-U_a/kT}$, in which U_a is the adsorption energy. The adsorption energy is given by $U_a = m\chi_s kT$, in which m is the number of adsorbed segments and χ_s is the net adsorption energy per segment. Designating the number of possible conformations with m adsorbed segments as N_m, the bound fraction is then given as: [79]

$$p = \frac{1}{r}\frac{\sum_m mN_m e^{m\chi_s}}{\sum_m N_m e^{m\chi_s}}$$

Eq. 2-13

2.2.2.2 Self-Consistent Field (SCF) Lattice Model

A mean-field lattice approach makes use of layers of lattice sites to reduce the number of conformations to something finite and countable. The chains are "built" monomer by monomer. Each subsequent segment has recollection of only the previous segment. This is not, therefore, a self-avoiding walk. The weighting close to the surface is based on a factor e^{χ_s}. In all other locations, the weighting factor is 1. An end segment distribution, G(s,z), is defined in which s is the number of segments and z is the number of the lattice layer. The generalized form is given below. In this equation, $\lambda_o = 1\text{-}2\lambda_1$ and λ_1 is a predefined probability that a chain will cross into the next lattice layer. This is based on the geometry of the lattice chosen.[79]

$$G(z,s+1) = G(z)\{\lambda_1 G(z-1,s) + \lambda_o G(Z,s) + \lambda_1 G(z+1,s)\}$$

Eq. 2-14

Scheutjens and Fleer developed a self-consistent field (SCF) lattice model based on Eq. 2-15 through Eq. 2-21. These equations are used in an iterative fashion to reach a numerical solution. The segment weighing factor, $G_i(z)$, is given by:

$$G_i(z) = e^{\frac{-u_i(z)}{kT}}$$

Eq. 2-15

in which $u_i(z)$ is the segment potential in layer z. All potentials are given relative to the bulk solution.[79] The segment potential is subsequently divided as shown below into an

entropically driven potential, u'(z), and a portion dependent on the interaction of the segments, $u_i^{int}(z)$.

$$u_i(z) = u'(z) + u_i^{int}(z)$$

Eq. 2-16

The weighting factor, G_i, is given by:

$$G_i(z;s+1) = G_i(z)\langle G_i(z;s)\rangle$$

Eq. 2-17

in which s is the number of segments. The term $\langle G_i(z;s)\rangle$ represents an average over the three layers sandwiching s. The volume fraction, φ_i, is:

$$\varphi_i(z,s) = \frac{C_i}{G_i(z)} G_i(z;s) G_i(z;r_i - s + 1)$$

Eq. 2-18

in which C_i is a normalization constant. Assuming a value of unity for r_1, which would represent a monomeric solvent, this results in:

$$\varphi_1(z) = \varphi_1^b G_1(z)$$

Eq. 2-19

in which φ_1^b is the concentration of i in the bulk solution. This expression can be summed to yield:

$$\varphi_i(z) = \sum_{s=1}^{r_i} \varphi_i(z,s)$$

Eq. 2-20

In the Scheutjens-Fleer scheme, full occupancy of the lattice is designated. Therefore, the following equation must hold.

$$\sum_i \varphi_i(z) = 1$$

Eq. 2-21

The Scheutjens-Fleer model assumes a lattice geometry in which the layers are parallel to the surface.[80] It is also discreet and not continuous. A related model was introduced in a paper by Ploehn,[81] in which the lattice in a SCF model was replaced by a continuum. A requirement of a continuum model is that at any point, the volume fractions must sum to one. A continuum model allows the monomer and solvent volumes to differ from one another and allows the description of compressibility.

2.2.2.3 Diffusion Equation

An additional approach to modeling the behavior of polymers adsorbing at surfaces makes use of the behavior of a diffusing particle. This was developed by Edwards[82] and de Gennes.[83] In this case, the same general equation described in mean field lattice theory is rewritten in terms of potentials:

$$G(z,s+1)e^{u(z)/kT} - G(z,s) = \lambda_1$$

Eq. 2-22

By assuming that G(z,s) is continuous with regard to both variables and by replacing u(z) with u(z)Δs, this becomes:

$$\frac{G(z,s+\Delta s)e^{u(z)\Delta s/kT} - G(z,s)}{\Delta s} = \lambda_1 l^2 \frac{1}{\Delta z}\left\{\frac{G(z+\Delta z,\, s) - G(z,s)}{\Delta z} - \frac{G(z,s) - G(z-\Delta z,\, s)}{\Delta z}\right\}$$

Eq. 2-23

which may be further simplified by taking the limit as Δs and Δz approach zero. The resulting differential equation is: [79]

$$\frac{\partial G(z,s)}{\partial s} = \lambda_1 l^2 \frac{\partial^2 G(z,s)}{\partial z^2} - \frac{u(z)}{kT} G(z,s)$$

Eq. 2-24

In the case of a random walk, the last term may be eliminated, since a purely random walk does not include a weighting factor. [79]

2.2.2.4 Scaling Theory

Scaling theory assumes strong repulsion of segments such that polymer chains do not overlap on the surface. In a semi-dilute solution, variations in segment concentration occur as the polymer coils are forced to interpenetrate. This theory makes use of a correlation length, ξ, which may be considered to be an average mesh size of a loose network formed of chains in solution.

The correlation length, ξ_s, is:

$$\frac{\xi_s}{l} = (pv)^{-1/4} \varphi^{-3/4}$$

Eq. 2-25

in which l is the monomer length, p is a chain stiffness parameter, v is an excluded volume parameter, and φ is the volume fraction. [79]

Scaling theory may be used to describe polymer adsorption in the weak regime where χ_S is close to χ_{SC}, which is the critical value of the interaction parameter such that the bound fraction approaches zero as the chain becomes infinitely long. It also assumes irreversible adsorption. A simplification may be used based on the assumption that the correlation length scales with $\varphi^{-3/4}$ for a good solvent. This yields:

$$\frac{\xi}{l} = \varphi^{-3/4}$$

Eq. 2-26

which may be further altered based on work by De Gennes[83] which assumed that the adsorbed layer was "self-similar" meaning that $\xi(z) \approx z$, resulting in:

$$\varphi(z) = \left(\frac{l}{z}\right)^{4/3}$$

Eq. 2-27

De Gennes and Pincus[84] developed a set of equations to describe adsorption behavior. These are shown as the following three equations, in which φ^s is the volume fraction adsorbed at the surface, ξ^b is the correlation length at great distance from the surface, and

D is an extrapolation length which describes a shift between adsorption regions as a function of distance from the surface, z. This parameter, D, and the correlation length in the bulk solution, ξ^b, define three regions. Close to the surface (z<D), the interaction between the polymer segment and the surface dominates. In the middle section (D<z<ξ^b), self-similar behavior applies. As z approaches ξ^b, the volume fraction decays toward the bulk condition.

$$\varphi(z) = \varphi^s \qquad 0 < z < l$$

Eq. 2-28

$$\varphi(z) \approx \varphi^s \left(\frac{l}{z}\right)^{1/3} \qquad l < z < D$$

Eq. 2-29

$$\varphi(z) \approx \varphi^s \left(\frac{l}{z}\right)^{1/3} \left(\frac{2D}{z+D}\right) \qquad D < z < \xi^b$$

Eq. 2-30

$$\varphi^s \approx \frac{l}{D}$$

Eq. 2-31

2.2.3 Adsorption of Charged Homopolymers

The presence of a charge on a polymer complicates the adsorption behavior. In addition to the steric effects always present, electrostatic interactions come into play. This is further influenced by the presence of a charged surface. The charge of a polymer and a surface, as well as solvent and salt conditions, may be used to manipulate systems.[79] For a charged polymer adsorbing on an uncharged surface, the addition of salt typically promotes adsorption by screening the repulsion between charged polymer segments. For a polymer and surface with the same charge, increasing the salt concentration helps screen both polymer-polymer repulsion and polymer-surface repulsion.

One example of a study of adsorption of charged homopolymers was undertaken by Killmann and Reiner.[85] They used poly-L-lysine and poly-L-glutamic acid on two

substrates: negatively charged hydrophilic and neutral hydrophobic silica surfaces. On the hydrophobic surface, the polypeptides adsorbed into flatter configurations due to electrostatic repulsion between the chains. On the hydrophilic surface poly-L-lysine adsorbed more; the negatively-charged poly-L-glutamic acid adsorbed less. For this surface, the effect of ionic strength was significant in that screening at higher ionic strength allowed more material to adsorb for both adsorbates.

2.2.4 Block Copolymers

Block copolymers consist of two or more repeat units that are segregated by type. Block copolymers can be exceedingly useful in that they can perform as two or more separate, but linked, materials. The behavior of block copolymers is different depending on whether it takes place in a selective or a non-selective solvent. A selective solvent is one in which one of the blocks is insoluble. Conversely, a non-selective solvent is characterized by solubility of all blocks.

2.2.4.1 Non-Selective Solvent

A block copolymer adsorbed from a non-selective solvent will have an anchor layer swollen with solvent and a layer consisting of the tails. The relative lengths of the anchor and tail blocks are important. When the tail blocks are longer, the repulsion between the tails is stronger, and surface coverage may be less. When the anchor block is longer, there is less repulsion between the tails. As such, the interface can become saturated with anchor blocks. As described by Marques and Joanny[86] the asymmetry ratio, β_n is the ratio between the cross-sectional areas of the anchor and tail blocks. In the non-selective case, the asymmetry ratio is described as in the following equation, in which ν_A is the fraction of anchor segments, N_A is the number of bonds in the anchor block, and N_B is the number of bonds in the tail (buoy) block. This formulation assumes that the monomer size (or cross-sectional area) is the same for both blocks.

$$\beta_n = \left(\frac{N_B}{N_A}\right)^{6/5} = \left(\frac{\nu_A}{1-\nu_A}\right)^{6/5}$$

Eq. 2-32

The anchor regime, in which adsorption behavior is dominated by the anchor properties, occurs when β_n is greater than N_A; the tail regime occurs when β_n is less than N_A. Two useful values are the surface chain density, σ, and the chain layer thickness, δ. They are described in the Marques-Joanny theory by the following equations for the tail dominated regime.

$$\sigma \propto \left(\frac{N_A}{N_B}\right)^{6/5} = \left(\frac{\nu_A}{1-\nu_A}\right)^{6/5}$$

Eq. 2-33

$$\delta \propto N_A^{2/5} N_B^{3/5} = N\nu_A^{2/5}(1-\nu_A)^{3/5}$$

Eq. 2-34

In the anchor dominated regime, the equations are as follows. The layer thickness, δ, varies linearly with N_B.

$$\sigma \propto \frac{1}{N_A} = \frac{1}{N\nu_A}$$

Eq. 2-35

$$\sigma \propto \frac{N_B}{N_A^{1/3}} = \frac{1-\nu_A}{\nu_A^{1/3}} N^{2/3}$$

Eq. 2-36

$$\delta \sim \sigma^{1/3} N_B$$

Eq. 2-37

The adsorbed amount for a non-selective solvent is described by the following equation, in which α is a numerical constant.

$$\theta^a \approx \theta_{hA}^a \left(1 + \alpha \frac{N_B}{N_A}\right)$$

Eq. 2-38

2.2.4.2 Selective Solvent

A block copolymer adsorbed from a selective solvent has a thin adsorbed layer of the anchor block. In the solution, the anchor block will come together, forming solvent-excluding micelles. On the surface, the anchor block forms a melt phase, wetting the surface. This is known as the Van der Waals brush regime as described by Marques et al.[87] The asymmetry ratio, β_s, is the ratio of the effective anchor area to the effective cross-sectional area per chain of the tail block. This is given by the following equation, in which N_A is the number of backbone bonds in the anchor block, N_T is the number of backbone bonds in the tail block, and ν_A is the fraction of anchor segments.

$$\beta_s \equiv \frac{N_B^{6/5}}{N_A} = \frac{(1-\nu_A)^{6/5}}{\nu_A}$$

Eq. 2-39

Within the Van der Waals regime, the number of grafted chains per unit area, σ, and the layer thickness, δ, are given by the following equation.

$$\sigma \propto N_A^{-1/2} N_B^{-1/4} = N^{-3/4} \nu_A^{-1/2} (1-\nu_A)^{-1/4}$$

Eq. 2-40

$$\delta \propto N_A^{-1/6} N_B = N^{5/6} \nu_A^{-1/6} (1-\nu_A)$$

Eq. 2-41

Prediction of the adsorbed amount of a diblock copolymer from a selective solvent is complicated because the polymer may form micelles in solution if it is above the critical micelle concentration (CMC). Adsorption then requires the breaking up of micelles. In addition, the micelles themselves may adsorb onto the surface.[79]

Rudolph et al.[88] studied the behavior of amphiphilic diblock copolymers on aluminum oxide surfaces in various solvents. They found solvent quality to be of significance. Using adsorption experiments and surface plasmon resonance, they examined the impact of varying the solvent ratio. Their solvent system was ethanol with a mixture of trichloroethylene-toluene. The diblock polymers consisted of methacrylic acid (MAA) as the anchor block and methyl methacrylate (MMA) as the tail block. Nonpolar toluene

is a preferential solvent for MMA; Polar ethanol is a preferential solvent for MAA. Polymer was initially adsorbed onto the alumina in a trichloroethylene-ethane solvent. Loosely bound polymer was rinsed off with pure solvent. After this, the adsorbed polymer was introduced to various solvent mixtures containing increasing amount of trichloroethylene or ethanol cosolvent, and SPR was used to determine the layer thickness. The addition of trichloroethylene or toluene, both of which are good solvents for the MMA stabilizer block caused an increase in adsorbed layer thickness. This may be explained as an expansion of the tailblock coils.

2.3 Colloidal Stabilization with Adsorbed Polymer

2.3.1 Adsorption Isotherms

Adsorption isotherms are commonly used to describe the deposition of surfactants or polymers on surfaces. A typical plot is of the amount of polymer adsorbed versus equilibrium concentration, often on a logarithmic scale. Regardless of the isotherm model chosen, it remains true that if an increase in equilibrium concentration results in a decrease in surface energy, then adsorption must have occurred. In general, these theories are useful for small molecules, surfactants, and globular proteins, but not for polymers, as polymers adsorb in loops, trains, and tails.

2.3.1.1 Gibbs Adsorption Isotherm

The Gibbs adsorption isotherm may be used to describe the amount of solute adsorbed on a surface in terms of the chemical potential of the solvent and the measured surface tension. This method treats the interface between two bulk states as though it is abrupt, creating an interface with surface area, but no volume.[31]

The Gibbs adsorption equation is:

$$\Gamma = \frac{n_i^{\sigma}}{A}$$

Eq. 2-42

in which n_i^{σ} is the number of moles in the system and A is the surface area. The adsorbed amount is related to the surface tension, γ by:

$$d\gamma = \sum_i \Gamma_i d\mu_i$$

Eq. 2-43

in which μ_i is the chemical potential of the solute. For a binary system such as a solvent (1) and a solute (2), if the position of the surface is chosen such that the surface excess of the solvent is zero, this reduces to:

$$\Gamma_{2,1} = \frac{d\gamma}{d\mu_2}$$

Eq. 2-44

For a monovalent electrolyte, the relationship is:

$$\Gamma_{2,1} = -\frac{1}{2RT}\frac{d\gamma}{d\ln\left(\frac{c}{c_o}\right)}$$

Eq. 2-45

in which c is the concentration in the bulk solution and c_o is the initial concentration.

2.3.1.2 Langmuir Isotherm

The Langmuir isotherm is frequently used to describe adsorption, and assumes no interaction between adsorbate molecules. It is advantageous in that unlike the Gibbs model, it does not require the experimental measurement of surface tension. This model is based on a number of assumptions, including a homogeneous surface, a lack of interactions between adsorbed solute, and a requirement for formation of a monolayer. [31] The fraction of surface sites occupied by the surfactant, θ, is:

$$\theta = \frac{K\left(\frac{c}{c^o}\right)}{1 + K\left(\frac{c}{c^o}\right)}$$

Eq. 2-46

in which c is the concentration of the adsorbate in the bulk phase, c^o is the initial concentration, and K is the equilibrium constant. This may be derived by either kinetic or

thermodynamic arguments. At high solution concentrations, adsorption increases. Also, increasing the binding constant causes additional coverage.

2.3.1.3 Frumkin Adsorption Isotherm

The Langmuir adsorption isotherm assumes no interaction between the molecules of the adsorbate. In cases such as the brush-forming block copolymers considered in this research, this is not the case. One model that may be used to account for this effect is the Frumkin adsorption isotherm.[89] This model introduces an attraction constant, A, defined as:

$$A = \frac{Z_A w_{AA}}{RT}$$

Eq. 2-47

in which Z_A is a coordination number describing possible interactions with neighboring molecules and w_{AA} is the individual interaction between adsorbed molecules. A negative value for A indicates that attraction is occurring between the adsorbed molecules. A positive value indicates a repulsive interaction. The resulting model for the isotherm is:

$$\theta = \frac{K \, c/c^o \exp(-A\theta)}{1 + K \, c/c^o \exp(-A\theta)}$$

Eq. 2-48

2.3.2 DVLO Theory of Stabilization

According to the classical Derjaguin-Landau-Verwey-Overbeek (DLVO) theory, stabilization depends on the combination of electrostatic and van der Waals (vdW) interactions between surfaces. The curve describing the total interaction potential, Φ, can be used to predict stability. At very close ranges the vdW forces will dominate, resulting in coagulation. However a repulsive barrier of $\Phi/kT >> 1$ caused by electrostatic or steric forces can lead to kinetic stability, which is often sufficient for stabilization. In addition, it is possible to have a secondary minimum, which would provide a relatively low energy state and encourage kinetic stabilization.[90] As the particles approach, they become trapped in the secondary minimum and are loosely flocculated. However, if the

energy well is shallow, the flocculated system may be readily redispersed with the application of agitation. By contrast, particles that reach the primary minimum typically cannot be readily redispersed.

The general expression for interaction potential, Φ, is the sum of the interaction potentials:

$$\Phi = \Phi_{ES} + \Phi_{vdW} + \Phi_{M} + \Phi_{S}$$

Eq. 2-49

in which the subscript ES is electrostatic, vdW is van der Waals, M is magnetic, and S is steric (adsorbed polymer). All potential curves will be reported in this manuscript as a ratio of potential (Φ) to thermal energy (kT) for ease of interpretation.

2.3.2.1 Electrostatic Potential

The behavior near a charged surface may be described in terms of an electrical double layer. A model in common use was developed by Stern in which the charged surface attracts a layer of counter-ions by electrostatic and van der Waals forces. This is referred to as the Stern layer. Beyond this layer lies a diffuse layer (Gouy-Chapman double layer) comprised of a gradient of charge distribution. The gradient includes a large initial decrease in counter-ion concentration, due to shielding by the Stern layer.[30] This is illustrated in Figure 2-3.

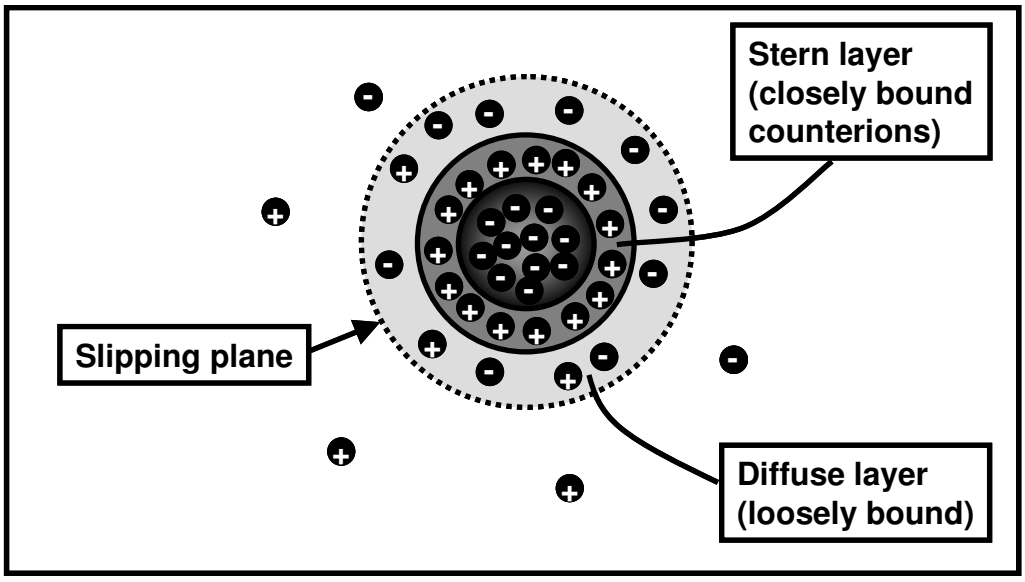

Figure 2-3. Electrical double layer on a charged surface.

Zeta potential, ζ, describes the electrical potential at a slipping plane within the diffuse layer. Zeta potential decreases with increased ionic strength. The Debye-Hückel radius, κ^{-1}, is commonly used to describe the range of the electrostatic double layer. It is highly dependent on the ionic strength of the system, as a higher concentration of electrolytes will cause the Stern layer to perform more effectively in charge shielding. The ionic strength may be calculated as:

$$I = \frac{1}{2}\sum_i c_i (z_i)^2$$

Eq. 2-50

in which I is the ionic strength, c is the concentration in mol/L, and z is the charge.[91] Likewise, the Debye length may be calculated by:

$$\kappa^2 = \frac{4\pi}{\varepsilon\ kT}\sum_i n_i^o (z_i)^2 (e_o)^2 \quad \Rightarrow \quad \kappa^{-1} = \left(\frac{\varepsilon\ kT}{4\pi} \frac{1}{\sum_i n_i^o (z_i)^2 (e_o)^2} \right)^{1/2}$$

Eq. 2-51

in which n_i^o is the concentration and e_o is the charge on an electron.

Electrostatic effects occur in colloidal systems having charged groups on the surface of the particles. For stabilization to occur, repulsive forces are required. Based on an diffuse electrical double layer, as described in a previous section, a potential,Φ_{ES} , may be described. A constant potential expression is useful for curved surfaces having a thick electrical double layer ($\kappa a<5$) and surface potentials of approximately 25 mV or less.[29]

$$\Phi_{ES} = 2\pi a \varepsilon \varepsilon_o \psi_o^2 e^{-\kappa(r-2a)}$$

Eq. 2-52

In this equation, ε is the dielectric constant of the medium (water), ε_o is the permittivity of free space, ψ_o is the surface potential, and κ is the inverse Debye length. For a thin electrical double layer ($\kappa a >10$) the equivalent expression is:

$$\Phi_{ES} = 2\pi a \varepsilon \varepsilon_o \psi_o^2 \ln\left(1 + e^{-k(r-2a)}\right)$$

Eq. 2-53

Electrostatic interactions are particularly susceptible to electrolyte concentration and pH. Quesada-Perez et al. used turbidity as a technique to examine electrostatic interactions between negatively charged colloidal particles in low salt suspensions.[92] Using DLVO potential, the effective charge of the colloid was fitted. Tran et al. studied the effect of salt concentration on stability of SiO_2 particles with a grafted polyelectrolyte layer.[93] Brushes were created by grafting trichlorosilane-terminated polystyrene chains directly onto silica. The chains were subsequently sulfonated to create negatively charged polyelectrolytes. As the polyelectrolytes were covalently bound to the surface, the electrostatic interaction between chains could be readily studied as a function of the thickness of the grafted brush layer. The authors observed that the brush was highly extended in water due to repulsion interactions between the negatively charged chains. However, electrostatic screening by addition of salt to the system caused alterations in the layer thickness. Increase in ionic strength caused a decrease in the layer thickness.

2.3.2.2 Van der Waals Potential

Van der Waals forces act on all molecules. They are weaker than Coloumbic forces, but their omnipresence makes them essential to understanding colloidal behavior. There are three origins of van der Waals forces: rotation of permanent dipoles (Keesom), an

induced dipole caused by proximity to a permanent dipole (Debye), and an induced dipole caused by the electronic polarizability of a neighboring molecule (London). The last origin is very important because it is present in all molecules, including neutral molecules containing no fixed dipole. The attraction caused by London dispersion forces on a molecular scale is described based on a Bohr model by:

$$w(r) = -\frac{(a_o e)^2 \alpha_o}{(4\pi \varepsilon_o)^2 r^6}$$

Eq. 2-54

in which α_o is the electronic polarizability, a_o is the Bohr radius, ε_o is the permittivity of free space, and r is the separation.[30]

For a colloidal system containing spherical particles in a medium, the Hamaker constant may be used to calculate the attractive van der Waals forces. The Hamaker constant depends only on material properties and may be directly calculated using Lifshitz theory. The Lifshitz theory does not depend on additivity, instead describing the system in terms of continuous media and using only bulk properties. It is common to find tabulated values of Hamaker constants.

The vdW contribution to the interaction potential for a pair of spherical particles may be described with a Derajaguin approximation using Eq. 2-55 as:

$$\Phi_{vdW} = -\frac{1}{6} A_{eff} \left(\frac{2a^2}{r^2 - 4a^2} + \frac{2a^2}{r^2} + \ln\left(\frac{r^2 - 4a^2}{r^2} \right) \right)$$

Eq. 2-55

in which a is the particle radius and r is the center-to-center separation of two particles. A_{eff} is the effective retarded Hamaker constant, calculated from:

$$A_{eff} = A_{\nu=0} + A_{\nu>0} = \frac{3}{4} kT \left(\frac{\bar{\varepsilon}(0) - \varepsilon(0)}{\bar{\varepsilon}(0) + \varepsilon(0)} \right)^2 + \frac{3\hbar\omega}{16\sqrt{2}} \frac{\left(\bar{n}_o^2 - n_o^2 \right)^2}{\left(\bar{n}_o^2 + n_o^2 \right)^{3/2}} F(H)$$

Eq. 2-56

in which, k is the Boltzmann constant, T is the temperature, $\varepsilon(0)$ and $\bar{\varepsilon}(0)$ are the dielectric constants for the medium and the substrate, n_o and $\bar{n}_o$ are the low frequency refractive indices of the medium and substrate, $2\pi\hbar$ is Planck's constant, and ω is the frequency of the dominant relaxation in the ultraviolet range. F(H) accounts for retardation effects, and is unity at the nonretarded limit:

$$F(H) \approx \left(1+\left(\frac{\pi H}{4\sqrt{2}}\right)^{3/2}\right)^{-2/3}$$

Eq. 2-57

H is given by the following equation in which h is the surface to surface separation and c is the speed of light.

$$H = n_o\left(\bar{n}_o^2 + n_o^2\right)^{1/2}\frac{h\omega}{c}$$

Eq. 2-58

One additional correction to the Hamaker constant may be made in order to account for screening by the electrolyte. This is as described in the following equation and has an effect only for the zero frequency portion of the Hamaker constant as determined from Eq. 2-56 evaluated in the limit of zero frequency.[29]

$$A = A_{\nu=0}(2\kappa h)e^{-2\kappa h} + A_{\nu>0}$$

Eq. 2-59

The resulting complete expression is:

$$A_{eff} = \frac{3}{4}kT\left(\frac{\bar{\varepsilon}(0)-\varepsilon(0)}{\bar{\varepsilon}(0)+\varepsilon(0)}\right)^2 e^{-2\kappa h} + \frac{3\hbar\omega}{16\sqrt{2}}\frac{\left(\bar{n}_o^2 - n_o^2\right)^2}{\left(\bar{n}_o^2 + n_o^2\right)^{3/2}}F(H)$$

Eq. 2-60

2.3.2.3 Steric Potential

In the previous section, DLVO theory was discussed to describe the interaction of particles according to a combination of electrostatic and van der Waals forces. If the particles have been altered by adsorbing or grafting molecules onto the surfaces, then

steric forces must also be considered. The steric effect most relevant to this work is repulsion between colloidal particles having a brush layer of polymers adsorbed onto them. Addition of a polymeric stabilizer to a system results in particles coated in some variation on dangling chains. In simple terms, when the particles come into proximity with one another, the chains cause repulsion based on the entropically unfavorable situation that forcing the chains into more tightly configured states would cause.

Polymers are frequently used to stabilize dispersions of colloids.[79, 94] A number of polymeric molecules may be used for steric stabilization of colloids, including both homopolymers and copolymers. However, in light of the focus of this study, this discussion will focus on block copolymers, in particular brush and graft copolymers. Block copolymers are particularly well suited for steric stabilization, as they can provide a high degree of coverage with strong adsorption while still having extended tails which interact favorably with the medium.[95]

Steric stabilization may occur when two surfaces have polymer chains attached at one end and extend into solution. This could in general represent either adsorption of a block copolymer to form a brush or grafting of a copolymer directly onto a surface. In either case, the assumption is that the polymer is firmly attached. If the surfaces approach within a distance of twice the length the polymer chains extend into solution, then some change in conformation of the polymer chains is necessary. The chains may interpenetrate or they may avoid one another. Either way, a change in free energy results.

According to Flory-Krigbaum theory, the free energy of mixing may be described as in the following equation, in which V_1 is the volume of the solvent molecule, χ is the polymer-solvent interaction parameter, k is Boltzmann's constant, and ϕ_2 is the volume fraction of polymer segments.[96]

$$\Delta G_{mix} = \frac{kT}{V_1}\left[(\chi - 1)\phi_2 + \left(\frac{1}{2} - \chi\right)\phi_2^2\right]$$

Eq. 2-61

Steric stabilization occurs as a result of the combination of two effects. First, there is a mixing effect driven by the χ-parameter which may have either an attractive or repulsive force. If stabilization is the goal, the polymer-solvent system would be chosen such that the force was repulsive. In addition, there is what may be considered to be a repulsive elastic contribution which results from pushing the polymer chains into a more confined space.[96]

A study by de Laat and Schoo investigated the effect of block lengths in block copolymer systems on colloidal stability.[97] Blocks of polyvinylmethyl ether (PVME) and poly(vinyloxy-4-butyric acid) (PVOBA) were utilized on a hematite (α-Fe_2O_3) substrate. In addition, the adsorption behavior of each homopolymer was observed. PVME homopolymer did not adsorb onto hematite, while PVOBA homopolymer did. Block copolymers of PVME and PVOBA were adsorbed onto the hematite with the PVOBA acting as an anchor block and the PVME providing the tailblock. The presence of both a charged anchor block and an uncharged tailblock allowed a comparison between the electrostatic and steric stabilization effects by varying the respective length of the blocks. As expected, the hydrodynamic thickness of the adsorbed layer increased with an increase in the length of the PVME block. For relatively short tailblocks, electrostatic stabilization prevailed; however, for long PVME tailblocks, steric stabilization dominated. This was demonstrated by the absence of sensitivity to salt concentration.

Steric stabilization using adsorbed polymer can be particularly efficient when non-adsorbing chains are terminally attached, forming an extended, brush-like layer.[98] There are a number of expressions for steric repulsion. Some of these are designed for polymer brushes adsorbed on flat surfaces, and are reasonably applied to polymer-particle complexes where the radius of curvature of the particle is low relative to the brush dimension. Scaling models employing stepwise density functions were developed by Alexander,[99, 100] de Gennes,[101] and Cantor,[102] while self consistent mean field (SCF) models[103-105] used continuous functions to describe polymer density.

Using a self-consistent field approach, a relationship between surface density, n_p, and chain extension was developed by Russel[90] based on work by Dolan and Edwards[104] for adsorption on a macroscopically flat surface. The relationship between the dimensionless layer thickness, α_o, the dimensionless surface density, ϕ_p, and the ratio between the actual and ideal excluded volume per chain, z is:

$$\alpha_o^3 - \left(1 + \frac{1}{9}\phi_p^2\right)\alpha_o^{-1} = \frac{1}{6}z$$

Eq. 2-62

The dimensionless layer thickness, α_o, is given in terms of the extended layer thickness, L, the number of Kuhn segments, N, and the length of a statistical segment, l, taken from the literature to be 0.6 nm.[90] The dimensionless surface density, ϕ_p, is given in terms of N, n_p, l, and a parameter representing triplet interactions, w. The final parameter, z, is given in terms of N, n_p, l, and the excluded volume parameter, v.

$$\alpha_o = \frac{L}{N^{1/2}l} \qquad \phi_p = \frac{Nn_p w^{1/2}}{l} \qquad z = \frac{N^{3/2}n_p v}{l}$$

Eq. 2-63

For the case of a densely adsorbed brush layer, the steric contribution to the interaction potential may be described based on self-consistent field theory as:[106]

$$\Phi_S = kT\left(\frac{9\pi^5}{32}\right)^{1/3} n\sigma aL\left(\frac{v\sigma}{l}\right)^{2/3}\left(1 - \frac{r-2a}{2L}\right)^4$$

Eq. 2-64

in which, n is the number of statistical segments per chain, σ is the graft density, l is the length of a statistical segment, and v is the product of the excluded volume per statistical segment and l^3. For PEO, l = 0.6 nm and v = 8.42e-3 nm^3 as given by Russel.[90] This expression assumes dense brushes, resulting in compression rather than interpenetration upon impingement. As the brushes impinge, the number of available conformations decreases, causing a repulsive force.

Polymer chains on curved surfaces are less extended at a given adsorption density than their flat counterparts. The curvature of the surfaces provides additional space for the

polymer chains at a given graft density as compared to a flat plate. The resulting density profile was described by Daoud and Cotton.[62] Their model, based on scaling theory, proposed that polymers tethered to a spherical surface assumed the conformation of a string of blobs increasing in size with distance from the surface. This model has been applied to a number of systems to describe aggregation and adsorption behavior of neutral and charged block copolymers.[87, 107, 108] Halperin performed a scaling analysis by applying the star model to polymer micelles in selective solvents.[109]

The Daoud and Cotton model contains an adjustable parameter; the model was therefore extended in two ways. D'Oliveira et al.[110] developed the Discrete Blob (DB) model, which was based on distinct layers and assumed dense packing of blobs on the surface. Based on the premise that the number of blobs in each sublayer was equal to the number of tethered chains, an expression for the diameter of the discretely packed blobs was developed, which allowed prediction of the total layer thickness. The Density Distribution (DD) model by Vagberg et al.[61] described the increasing diameters of the blobs as a continuous function, also allowing direct computation of the brush length. Farinha et al.[63] examined the DB and DD models using PS-PEO block copolymers both in micellar solution and adsorbed onto PS latex spheres and found them to be comparable both with experimental results and one another. Vagberg et al. also extended the star polymer model to include a finite core, R_c. This allowed prediction of micelle size based on aggregation number. This model has been used to describe a number of systems, including dendrimer-star polymers,[77, 111] poly(ethylene oxide) lipid micelles,[65] and polyelectrolyte block copolymer micelles.[112]

The interaction potential between two particles is critical to the stability of the suspension. The interaction potential may in some instances be measured directly using a surface force apparatus (SFA), as pioneered by Ducker.[113] However, there are some geometric limitations to the use of SFA. For smaller radius colloids, it becomes increasingly difficult to make a measurement with typical geometries, such as sphere and plate or crossed cylinders. The ability to predict interaction potentials of small colloids becomes increasingly useful, particularly as the radius of the particle and the thickness of

the polymer brush become similar in dimension (i.e. the brush becomes increasingly curved.)

Several groups have examined the steric interaction for polymer-coated curved surfaces. Lin and Gast employed a self consistent mean field theory with a Derjaguin approximation to describe the interaction potential for chains tethered on colloidal surfaces.[114]

On highly curved surfaces, such as nanoparticles, in which the brush thickness is similar to or even larger than the radius of the particle, flat plate models are not applicable. One approach is to use steric repulsion models based on star polymers, which have a small core and a large corona of extended chains. The Likos[115] expression for the effective pair potential is:

$$A_{\text{int}} = \frac{5}{18} f^{3/2} \begin{cases} -\ln\left(\frac{r}{\sigma} + \frac{1}{1+\frac{\sqrt{f}}{2}} \right); & r \le \sigma \\ \frac{1}{1+\frac{\sqrt{f}}{2}} \left(\frac{\sigma}{r} \right) \exp\left(-\frac{\sqrt{f}}{2\sigma} (r-\sigma) \right); & r > \sigma \end{cases}$$

Eq. 2-65

in which r is the center-to-center separation, f is the number of arms, and $\sigma/2$ is the distance from the center of the core to the center of the outermost blob layer. For this expression, σ is defined as $1.3*R_g$, the radius of gyration of the ensemble.[116] The first portion of the equation (relating to close approaches) is a logarithmic relationship based on Witten and Pincus.[117] This describes the entropic repulsion caused by osmotic pressure when chains from adjacent stars overlap. The exponential longer distance relationship ($r>\sigma$) is based on Yukawa decay (used to describe a screened Coulomb potential[118]) with the decay length set to the diameter of the largest blobs and has been

extensively tested using machine simulation.[119] The two portions of the expression have been shifted to meet smoothly at r=σ.

One key point regarding this approach is that as it is based on star polymers, it is designed for use with highly curved brushes and so translates well to smaller particles or micelles. As the interaction potential is difficult to measure directly, two means of testing the model are by measurement of a structure factor (such as by small angle neutron scattering) or by measurement of the second virial coefficient, A_2 (such as by light scattering).

One significant advantage of the Likos model is that it predicts increasing "hardness" with an increase in the number of star arms, f. This is shown in Figure 2-4.

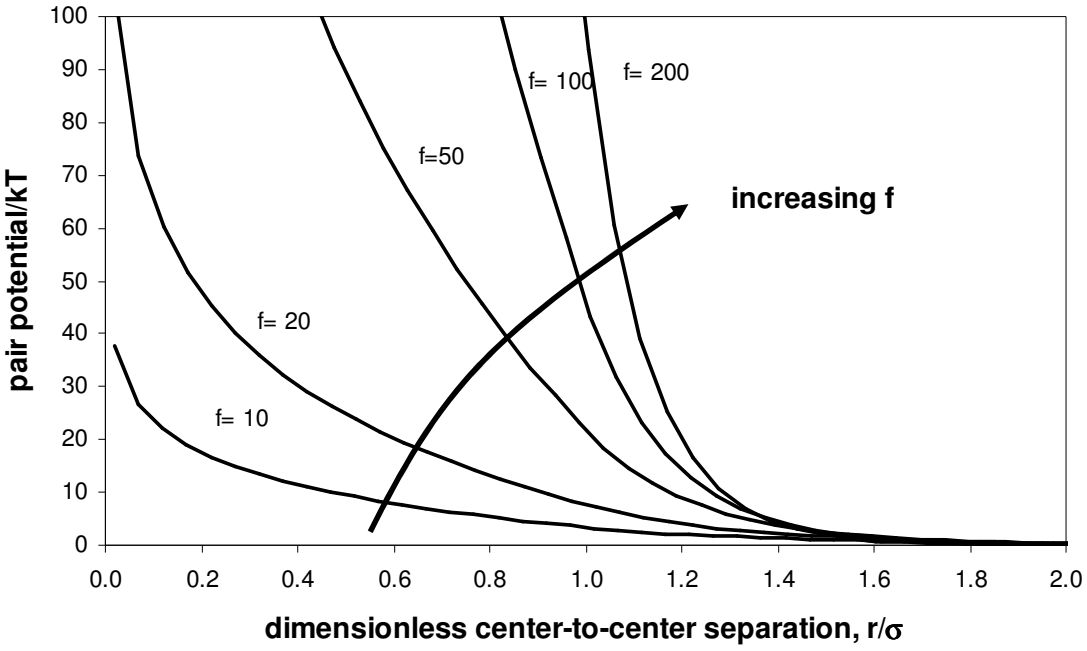

Figure 2-4. Pair potential for an example system with 2000 g/mol PEO grafted to a sphere with R_c = 5 nm and f = 10, 20, 50, 100, and 200. The transition from a soft to hard interaction potential may be observed.

2.3.2.4 Magnetic Potential

For the case of the magnetic substrate, an additional contribution to the interaction potential comes from the magnetic forces. However, the magnetite particles in this study are small enough to fall into the superparamagnetic regime so their magnetic dipoles have

no overall orientation in the absence of an applied magnetic field.[120] For the discussions in this dissertation, the magnetic potential has been neglected except in the presence of an applied magnetic field.

The magnetite potential, Φ_M, between two particles in an applied magnetic field is:

$$V_M = -\frac{8\pi\mu_0 a^3 M^2}{9\left(\frac{h}{a}+2\right)^3}$$

Eq. 2-66

in which M is the magnetization , μ_o is the magnetic permeability of vacuum, h is the surface-to-surface separation of two particles, and a is the radius of the particle.[121] Plaza et al. used this expression to describe stability of nickel ferrite spheres in the presence and absence of a magnetic field.[122] Chin et al used a magnetic pair-dipole model to examine the effect of a magnetic field on aggregation of superparamagnetic magnetite-polystyrene particles and the transition from the secondary to the primary minimum.[123]

2.3.3 Flocculation

Flocculation, also called coalescence or coagulation, occurs when particles aggregate in an unstable dispersion. The conditions necessary for flocculation (or the prevention thereof) have been hinted at so far throughout this paper. This section will examine flocculation in more detail, linking together some of the previous topics on adsorption and colloidal stability. It will focus only on flocculation as related to the presence of polymers in the colloidal system.

2.3.3.1 Bridging Flocculation

One means of deliberately inducing flocculation is by adding polymeric flocculants. A commonly used mechanism is reversible bridging. The premise is relatively straightforward, although quantitative description of the process is challenging. Bridging flocculation occurs when two surfaces, each having extended adsorbed or grafted polymer chains come into close proximity. The free end of a polymer chain or chains on one surface adsorbs onto the other, forming a fragile bridge. In colloidal applications, this leads to aggregates.

A key consideration in bridging flocculation is the surface coverage or adsorbed amount. A set of particles with polymer sparsely adsorbed is a good candidate for bridging flocculation. This is because in order to form the bridge, there must be open space on the target surface. Since adsorption of polymers involves the connection of multiple segments to a surface, in order to reverse adsorption, many segments must simultaneously desorb, which is difficult. For this reason, two particles with high surface coverage are unlikely to form a bridge.[124]

Bridging flocculation is often used in separations. Aggregating the target particles can allow easier removal via such means as settling or straining. Glover et al.[125] studied the flocculation of colloidal alumina particles by addition of polymer as well as the coagulation of the same particles by addition of salt. The work used static light scattering and settling techniques in a side-by-side comparison. Reasonably comparable results were obtained by the two techniques for the salt-induced aggregation. For the polymer-flocculated system, the light scattering technique resulted in a larger dimension; however, the researchers suggested that the aggregates may have been too large to meet the requirements of the Rayleigh-Gans-Debye criteria.

2.3.3.2 Charge Neutralization Flocculation

Another approach to flocculation involves charged particles and polymer chains. In a given colloidal system with charged particles, electrostatic stabilization is likely to play a large role. Adsorption of oppositely charged polymer chains can neutralize the charge particles, resulting in aggregation. However, if the amount of adsorbed polymer is high enough, charge reversal happens and restabilization occurs based on electrostatic stabilization. One advantage of charge neutralization is that it is not highly dependent on molecular weight.

A variation on charge neutralization is the electrostatic-patch model.[124] If the adsorbing polymer has a much higher charge density than the surface of the particle, then the result is that although the overall charge of the particle with adsorbed polymer is neutral, there are sections that are highly charged. In the electrostatic-patch model, the charged patches

attract one another. This model in particular explains the unexpectedly low effect of polymer molecular weight on flocculation.

Charge density on the flocculent chain is essential for charge neutralization flocculation. As demonstrated by Ashmore et al., chitosan is a good candidate for charge neutralization flocculation, as it has a high enough charge density to induce charged patches on the particles.[126] A series of chitosan chains with various charge densities were used as flocculating agents for a stabilized system of polystyrene latex particles. A range of particle sizes (85 nm – 2.1 μm) was studied with the intention of identifying an optimum flocculent concentration. Two characteristics were measured: the increase in mean particle diameter and the increase in the rate of flocculation relative to a rapid rate associated with the addition of sodium chloride.

2.3.3.3 Depletion Flocculation

Another means of causing flocculation involves the addition of non-adsorbing polymer to the system. This phenomenon, originally described by Askura and Oosawa, is called depletion flocculation.[127] Depletion flocculation occurs when the distance separating two colloidal particles is too small to admit the presence of polymer coils in solution. They are forced out of the space in between, resulting in an osmotic pressure difference between the area in between the particles and the rest of the bulk solution. As a result, an attractive force is generated which pushes the particles together, causing coagulation. This happens above a critical volume fraction of polymer in solution.

Yan et al. used poly(acrylic acid) (PAA) to flocculate negatively charged latex particles in a study of floc structure.[128] The floc characteristics studied included size and compactness. The latex used consisted of spherical particles of polystyrene with an average radius of 165 nm at pH 10, at which pH adsorption of PAA did not occur. Small-angle static light scattering was used to determine the overall structure of the aggregates. Rheometry was used to characterize the floc strength by determination of the Bingham yield stress. Atomic force microscopy (AFM) was also used to directly measure force between particles. The growth rate of flocs depended on the initial concentration of both the latex particles and the PAA. The positive effect of latex particle concentration on rate

of flocculation is intuitive, as collisions must occur for aggregation. However, it was also found that the rate of aggregation was faster with lower concentrations of non-adsorbing PAA. The authors suggested that this was related to an increasing viscosity with PAA concentration, which is supported by their rheological data. The mechanical strength of the flocs was determined via measurement of the Bingham yield stresses. Increasing PAA concentration increased the Bingham yield stress; however, in all cases, a maximum was reached. Initial solids concentration was very strongly related to floc strength.

2.4 Colloidal Rheology

2.4.1 Hard Sphere Model

A system of hard spheres in a liquid will tend to exhibit a region of shear thinning with increasing velocity, bracketed on either end of the scale by plateau regions.[90] The shape of the curve is as generally shown in Figure 2-5 below. A low-shear limiting viscosity, η_o, and a high-shear limiting viscosity, η_∞ may be present as shown, depending on the volume fraction of spheres and nature of the liquid.

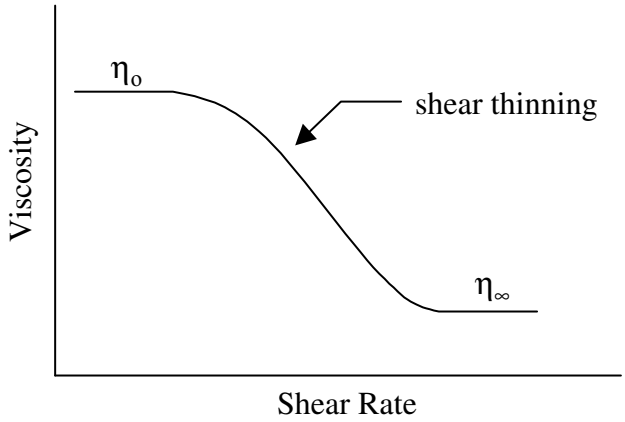

Figure 2-5. General schematic of shear thinning behavior.

As given by de Kruif et al.,[129] the relationship between volume fraction of particles, ϕ, and the limiting viscosities in the dilute limit is as given in Eq. 2-67, in which μ is the viscosity of the dispersing media. For the rest of the range of concentration, the relationship is as in Eq. 2-68. The order of the terms in the first set of equations correlates with the order of the interaction taking place. As may be seen from the coefficients, the difference between the two viscosity plateaus is related to the third order

interactions. This may be explained by assuming a lack of long-range ordering in the system. Long-range ordering allows third-order and higher interactions and imparts a structure.[90] This is also a measure of how significant non-hydrodynamic forces are in the system. The second set of equations indicates that at a higher shear rate, a higher volume fraction is required to cause divergence of the viscosity. This suggests that shearing causes orientation in the fluid.

$$\frac{\eta_o}{\mu} = 1 + 2.5\phi + (4 \pm 2)\phi^2 + (42 \pm 10)\phi^3 + \ldots$$
$$\frac{\eta_\infty}{\mu} = 1 + 2.5\phi + (4 \pm 2)\phi^2 + (25 \pm 7)\phi^3 + \ldots$$

Eq. 2-67

$$\frac{\eta_o}{\mu} = \left(1 - \frac{\phi}{0.63}\right)^{-2}$$
$$\frac{\eta_\infty}{\mu} = \left(1 - \frac{\phi}{0.71}\right)^{-2}$$

Eq. 2-68

A characteristic stress, σ_c, may be defined as the stress at which the viscosity is midway between the low and high shear limits. The shear-thinning regime may then be described by the model as follows:

$$\frac{\eta - \eta_\infty}{\eta_o - \eta_\infty} = \frac{1}{1 + \left(\frac{\sigma}{\sigma_c}\right)^{\mathrm{n}}} \qquad (1 \le \mathrm{n} \le 2)$$

Eq. 2-69

2.4.2 Charged Sphere Model

A surface charge on spherical particles in suspension leads to electrostatic interactions between spheres in addition to hydrodynamic interactions described by the semi-empirical equations above. If at moderate ionic strength a suspension is stable, its rheology is similar to the previously described case for hard spheres. However, a lower

ionic strength may result in drastically increased viscosity and a yield stress.[90] A transition occurs from a disordered fluid to a solid-like behavior at a volume fraction, ϕ_m, which is often readily apparent from experimental data. The low shear viscosity, η_o, may be described as:

$$\frac{\eta_o}{\mu} = \left(1 - \frac{\phi}{\phi_m}\right)^{-2}$$

Eq. 2-70

Above ϕ_m, the system exhibits viscoelasticity. Interaction potentials between pairs of particles must be overcome by energy input in order to strain the system. Long-range electrostatic repulsion between particles causes the material to behave like a solid. The shear modulus is proportional to the volume fraction of particles and is inversely proportional to both particle size and ionic strength.[90]

2.4.3 Stabilized Sphere Model

Polymers anchored to particles are often used as a means of stabilization for dispersions. Short-range repulsive interactions between polymer chains increase the viscosity. One aspect when considering the effect of stabilizing polymer chains on dispersions is that the effective volume fraction is increased when the polymer chains are added. This may be described by the following equation, in which a is the radius of the particle, d is the thickness of the polymer layer, and ϕ_o is the volume fraction of particles.

$$\phi = \phi_o\left[1 + \left(\frac{d}{a}\right)\right]^3$$

Eq. 2-71

Tadros et al.[130] examined the rheological behavior of polystyrene latex particles sterically stabilized with grafted poly(ethylene oxide) (PEO) chains. The dispersions studied had radii of 78, 303, and 502 nm. The authors examined the effect of the ratio of the adsorbed layer thickness, Δ, to the radius of the spheres, R. The same molecular weight of PEO chains (2 kg/mol) was used for all experiments. The two dispersions containing

larger particles were closer to the hard sphere behavior than the dispersion containing small particles. The authors noted that this is reasonable, as the value for Δ/R was about twice as large for the small particle case. This resulted in a soft layer of polymer.

2.5 Polymers in Nanomedicine

2.5.1 Polymers for Targeted Delivery

The use of polymers for drug delivery[131-139] and gene delivery[140, 141] has been examined by many investigators. Micelles are particularly promising, as they self-assemble into structures capable of encapsulating drugs with a range of solubilities. For instance, Hatton et al.[142, 143] examined copolymers consisting of Pluronic with crosslinked grafted poly(acrylic acid) as drug delivery vehicles. These were capable of encapsulating various hydrophobic drugs including Taxol, estradiol, progesterone, and camptothecin. Uhrich et al.[144-146] synthesized amphiphilic "scorpion-like" polymers with very low CMCs and examined encapsulation and release of the drug indomethacin. These macromolecules have a hydrophilic chain for stabilization and a backbone with hydrophobic side chains which form the core of self-assembled micelles. Sheihet et al.[147] prepared ABA triblock copolymers with PEO A blocks and oligomers of suberic acid and desaminotyrosyl-tyrosine esters. These self-assembled in solution and were capable of solubilizing paclitaxel, a hydrophobic drug.

For any of these bio-applications, there are several important design parameters for the particle-polymer complex. The first is compatibility with the body. PEO-containing polymers are especially interesting, as PEO does not trigger an immune response in-vivo and can also make other foreign materials less detectable by the immune system.[148] Another important characteristic is size. The complexes should be large enough (>10 nm) to avoid premature removal via extravasation from blood vessels into surrounding tissue and renal clearance, yet still small enough (10-70 nm) to pass into capillaries from larger blood vessels.[131] A final critical aspect is control of stability.

A primary drawback to using micelles for drug delivery is that upon dilution in the body they can disassemble. One approach to avoiding this problem is by crosslinking the micelles for use as a drug delivery vehicle.

Several groups have approached this by crosslinking the core of a micelle. For instance, Iijima et al. prepared a poly(ethylene glycol)-*b*-polylactide polymer with a methacryloyl group on one end which was then polymerized to crosslink the core.[149] This created a micelle that was stable in temperatures to 60°C, sodium dodecyl sulfate concentrations to 20 mg/mL, and in some organic solvents. These micelles were then used to solubilize paclitaxel.[150] Guo et al. made micelles of polystyrene-*b*-poly(2-cinnamoylethyl methacrylate) in organic solvents and used UV irradiation to crosslink the PCEMA core.[151] Bronich et al.[50] used Ca^{2+} to cause PEO-*b*-PMA polymers to form micelles which were subsequently cross-linked to form sterically stabilized hydrogel particles of approximately 100 nm in size. The anticancer drug cisplatin was incorporated into these particles for release.

The shell of a core-shell micelle may also be crosslinked. Zhang et al. demonstrated crosslinking of poly(ε-caprolactone)-b-poly(acrylic acid) micelles by a condensation reaction to form a crosslinked shell.[152] Weaver et al. created a so-called ionically crosslinked shell by addition of an anionic diblock copolymer to a micellar triblock copolymer.[153]

Carbodiimides are commonly used to mediate formation of an amide crosslink between carboxylate and amine groups via condensation.[154] One such carbodiimide is 1-ethyl-3-(3-dimethylaminopropyl)carbodiimide hydrochloride (EDC). It is water-soluble, as are the byproducts of the reaction, making isolation of the product relatively easy. Several papers by Bronich et al.[50, 155] describe the use of a divalent metal ion (Ca^{2+}) to cause PEO-b-PMA polymers to form into micelles, despite the charges on the polymethacrylate block. These micelles were subsequently cross-linked to form a drug delivery vessel for cisplatin.

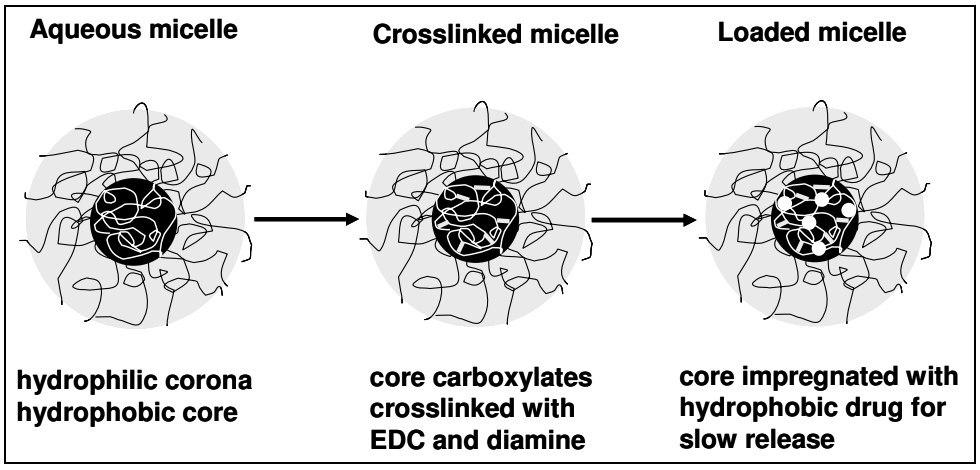

Figure 2-6. Approach to creating crosslinked micelles for drug delivery

EDC is frequently used in bio-conjugation reactions for formation of an amide link between a carboxylate and amine group. It has the advantage of being a water-phase reaction that may be performed at physiological pH. The major drawback in working with EDC is its limited effective life in water. In order to crosslink two carboxylate groups, a diamine such as ethylene diamine may be used. The crosslinking scheme is shown in Figure 2-7.

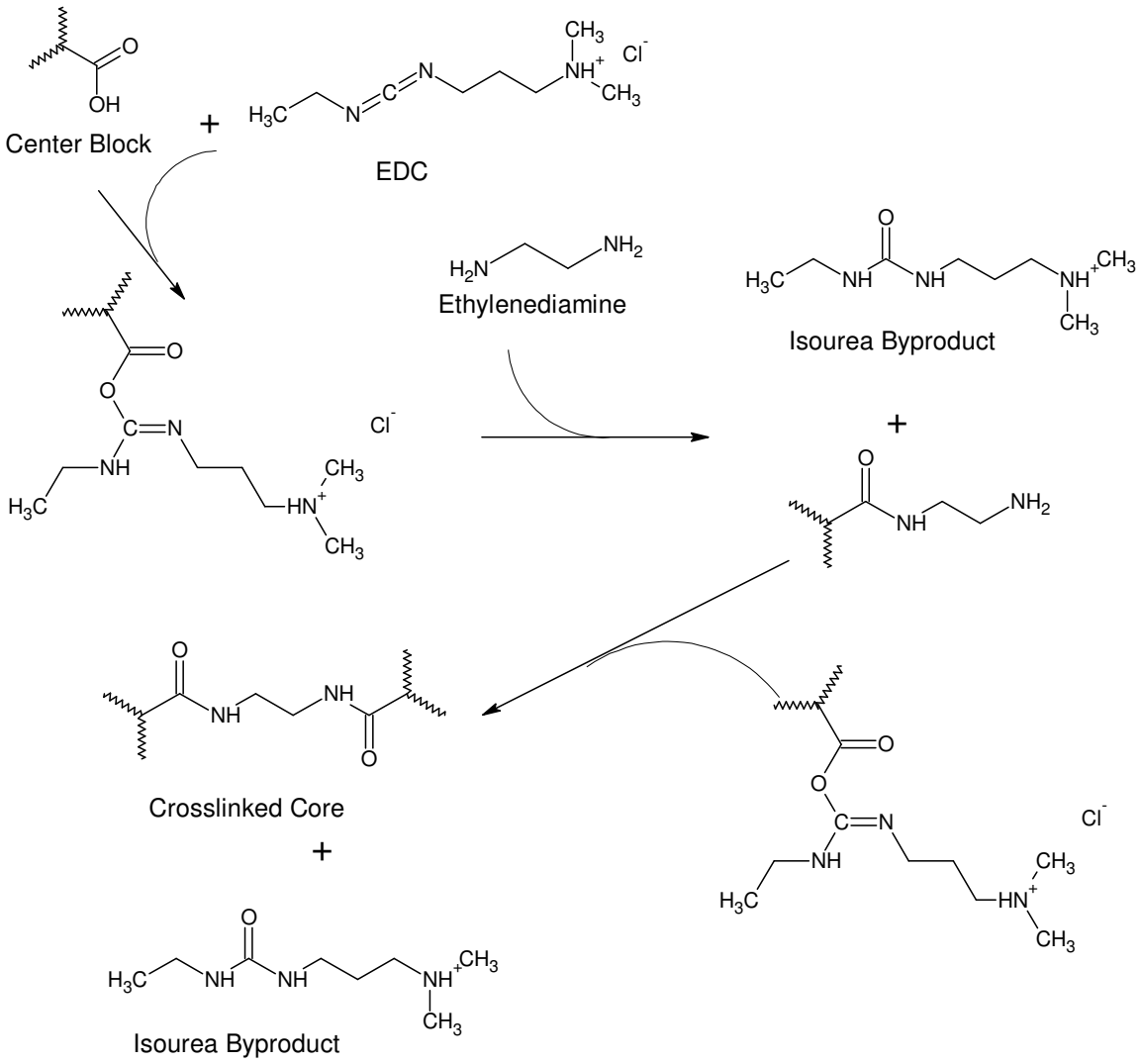

Figure 2-7. EDC crosslinking reaction of two carboxylate groups with ethylenediamine. An isourea by-product is formed.

One common approach to increase the efficiency of the reaction in Figure 2-7 is the addition of either N-hydroxysuccinimide (NHS) or N-hydroxysulfosuccinimide (sulfo-NHS) prior to crosslinking. Either may be reacted with a carboxylate in the presence of a carbodiimide such as EDC to form an ester which is more stable than the reactive intermediate in the previous scheme. This may be subsequently reacted with a diamine as before. The choice of NHS or sulfo-NHS alters the property of the resulting ester. NHS decreases water solubility, whereas sulfo-NHS maintains or increases water-solubility of the species. The scheme using NHS is summarized in Figure 2-8.

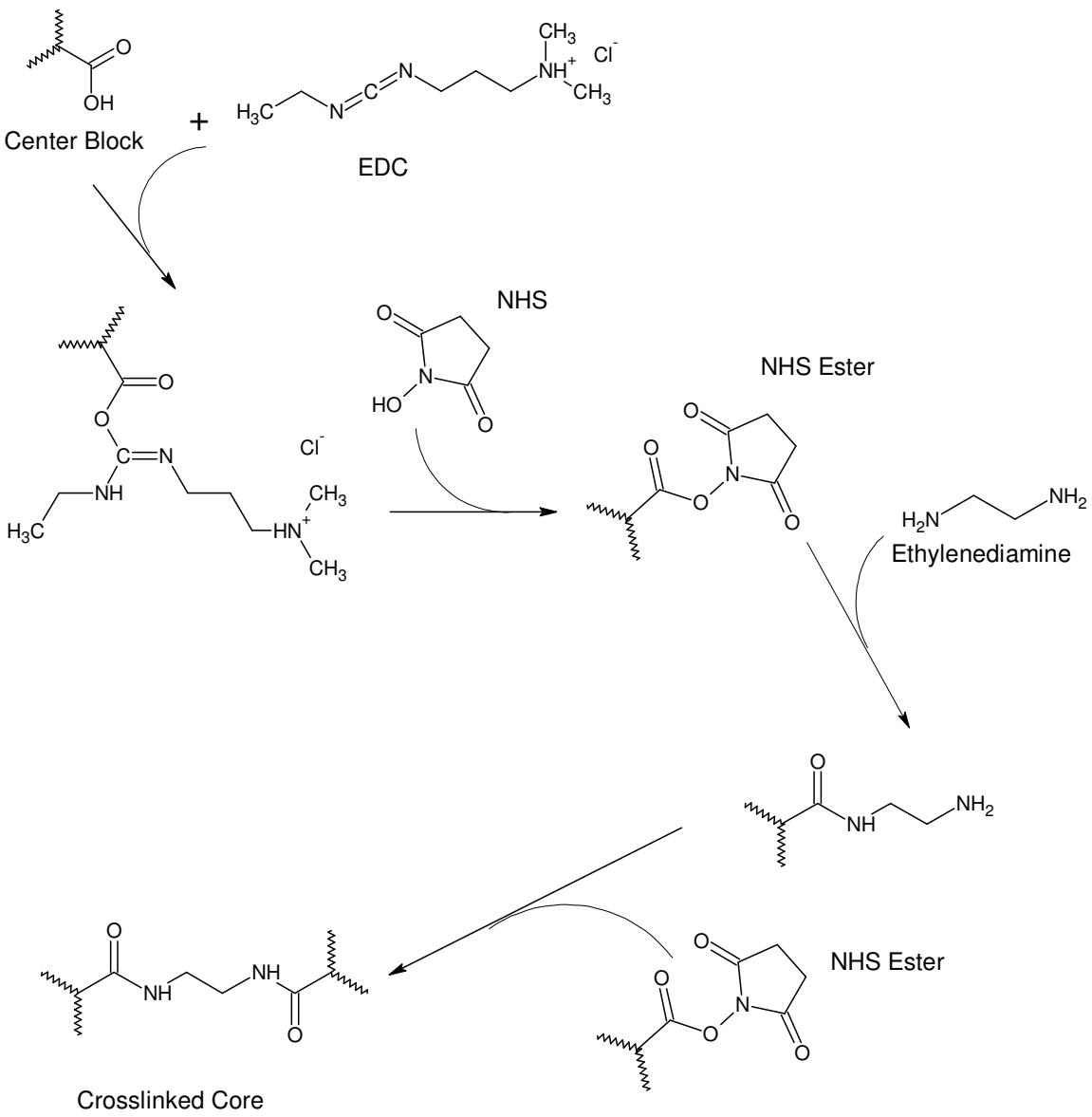

Figure 2-8. EDC crosslinking reaction of two carboxylate groups with ethylenediamine in the presence of NHS.

2.5.2 Magnetic Resonance Imaging (MRI)

Another potential application for polymers in medicine is stabilization of superparamagnetic iron oxide nanoparticles (SPIONS) with biodegradable polymers for bioapplications.[156-159] One major area is in targeted delivery designed to deliver a drug payload to specific locations.[160, 161] Another related application is in magnetic resonance imaging (MRI) for tumor detection.[162-165] SPIONS have a magnetic susceptibility that is much greater than gadolinium-based compounds for use in MRI imaging.[166] A recent review by Okuhata[167] indicated that state of the art gadolinium compounds have R_1

relaxivities of 4-34 mM^{-1} Gd s^{-1} as compared to recent advances in magnetite compounds, which have R_1 of 17-40 and R_2 of 35-190 mM^{-1} Fe s^{-1}.

MRI works on the same principle as nuclear magnetic resonance (NMR). Unpaired protons have a net spin, which is a magnetic moment vector. This is ½ for hydrogen. In a magnetic field, B, the magnetic moment of the proton aligns with the field in a low energy state. Upon application of energy, the particle can be excited to the high energy state, or spin state, whereupon it relaxes to the lower energy state. There are two such relaxations, T_1 and T_2.[168]

T_1, the spin-lattice relaxation constant, describes the return of magnetization along the longitudinal (z) axis, as shown in Figure 2-9.

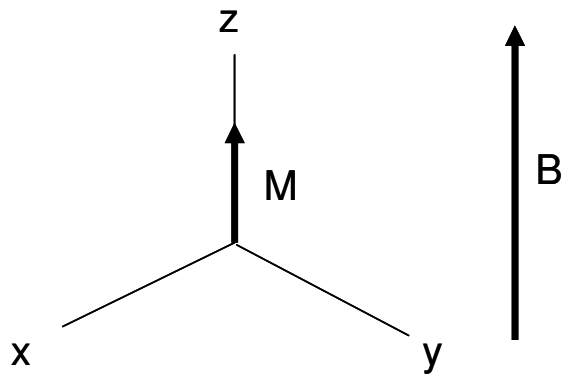

Figure 2-9. Longitudinal magnetization.

This process is described by:

$$M_z = M_o\left(1 - e^{-t/T_1}\right)$$

Eq. 2-72

in which M_o is the equilibrium magnetization, and t is the time.

Magnetization in the xy plane, M_{xy}, rotates about the z-axis at a frequency equal to the frequency of a photon that would cause a spin shift. Variations in frequency within the material cause dephasing of this vector.

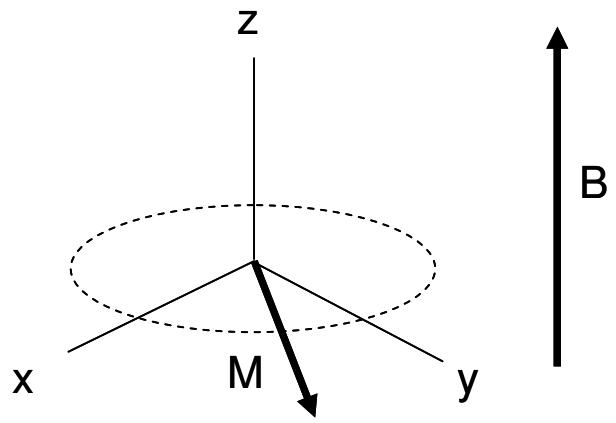

Figure 2-10. Transverse magnetization.

T_2 is the spin-spin relaxation time, which describes the time it takes for the xy magnetization to return to equilibrium according to:

$$M_{xy} = M_{xyo} e^{-t/T_2}$$

Eq. 2-73

in which M_{xyo} is the equilibrium magnetization in the xy plane.

Contrast enhancement may be accomplished by proximity of paramagnetic materials. Paramagnetic materials are those that have unpaired electrons of random orientation which align when attracted to a magnetic field. When the magnetic field is removed, they revert to random alignments. Below the Curie temperature, neighboring electrons are partially aligned, resulting in a ferromagnetic material. Superparamagnetic materials have preferred crystallographic directions for magnetization and have properties depending on particle size. Iron oxides commonly exhibit superparamagnetism at room temperature.[169]

Relaxivity parameters are described as:[170]

$$R_1 = \frac{1}{T_1[M]} \quad and \quad R_2 = \frac{1}{T_2[M]}$$

Eq. 2-74

in which [M] is the concentration of the Fe_3O_4.

An increase in relaxivity means that the time required to return to equilibrium has been decreased. Imaging weighted towards either T_1 or T_2 may be useful, depending on what sort of material in the body is under scrutiny. T_2 weighting is good for imaging fluids, and extra fluid is often present in the case of an injury or cancerous lesion.[171] SPIONS are of great potential usefulness as they are T_2 agents. T_2 agents do not require as close of an interaction with water as T_1 agents.[171] T_1 shortening is dependent on very close proximity of the protons to be relaxed and the magnetic contrast agent; therefore, adding a stabilizing or encapsulating material to the complex decreases relaxivity.[167] In general, decreasing the distance between the water molecules and the contrast agent increases R_1, as does increasing the speed with which relaxed water exchanges with bulk water.[170] T_2 imaging, on the other hand, is much less sensitive to distance. T_2 shortening works due to the effect of the paramagnetic material on the magnetic field. For instance, a T_2 agent coated in liposomes is more effective than the same agent without the liposomes because of T_2 agent clustering in the liposome.[167]

2.6 Biopolymers

2.6.1 Structure of Polypeptides

Polypeptides are comprised of a combination of amino acids. The amino acids may be grouped into four general categories: hydrophobic, uncharged polar, acidic, and basic (at physiological pH).[172] Proteins assume four levels of structure. The primary structure is the amino acid sequence. Secondary structure describes local structure such as α-helices and β-pleated sheets. Within a protein, tertiary structure occurs when larger scale folding occurs. Quaternary structure involves interaction between more than one protein.

2.6.2 Artificial Amino Acids

Work has been done by several groups to incorporate artificially created amino acids into proteins. Tirrell et al.[173] describes use of artificial amino acids, including

selenomethionine, p-fluorophenylalanine, 3-thienylalanine, 5',5',5'-trifluoroleucine, azetidine-2-carboxylic acid, and 3,4-dehydroproline. Each of these were provided to the host organism in place of their natural counterparts: methionine, alanine, leucine, and proline. The varying structures of the artificial amino acids extend possible choices for design of polypeptide functionality.

2.6.3 Transfer of Genetic Information

Genetic information is stored in deoxyribonucleic acid (DNA) and ribonucleic acid (RNA). The general structure of DNA is a double helix comprised of covalently linked sugar-phosphate backbones tied together by purine-pyrimidine base pairs. The amino acids are coded for by triplets of these base pairs in DNA. DNA is the primary storage location for genetic information.

Transfer of genetic information is primarily accomplished through various forms of RNA. RNA exists as ribosomal RNA (rRNA), messenger RNA (mRNA), and tranfer RNA (tRNA). The process of converting genetically coded material from base pairs to amino acids is called translation. Genetic information is transferred from DNA to RNA. mRNA codes each amino acid in the sequence. tRNA translates the code from base pairs to amino acids.

2.6.4 Deliberate Design

Proteins may be designed with a number of intentions in mind. For example, secondary and tertiary structures of proteins are determined by the sequence and interaction of the amino acids involved. The choice of amino acids is key, as is the sequence. In the case of block copolymers for adsorption onto surfaces, the design of the anchor and tail block are of a necessity very different. The anchor block is designed specifically to adsorb onto the target surface; the tail block must not adsorb, but must extend into solution to be effective.

2.6.5 Combinatorial Libraries

One approach to design of an artificial protein is the use of a combinatorial library of random peptides. A library consists of pieces of DNA sequences from a genome. They may be used to screen for certain desirable properties, such as adsorption to a particular

surface. Several different vectors may be used for libraries. The shortest sequences (<20kb) are found in bacteriophage lambda (λ) vectors. Bacteriophage P1 and cosmid vectors may have 40-100kb. Yeast artificial chromosome vectors can have up to 1Mb.[174] Filamentous phage display is one commonly used technique.[175] A large combinatorial library comprised of fragments of DNA may be incorporated into the bacteriophage. This phage is capable of attacking and infecting E. coli. The essential technique used is to select for phage containing the proper gene sequence by performing binding tests. Phages that do not adsorb may be readily washed away. The selected phages are removed from the surface, allowed to infect E. coli, and reproduce. Typically, several enrichment steps are performed.

Parmley and Smith[176] worked on improvements to previous expression vectors. They created fusion phage particles by inserting members of a DNA library into a protein gene of a filamentous phage. The resulting peptides were located on the surface. This allowed selection of those interacting with specific antibodies through a rapid screening technique.

A review by Samuelson et al.[177] describes a number of recent advances in techniques involving both gram negative and gram positive bacteria. Gram negative bacteria have a multi-layer membrane structure which requires transport of the protein through several membranes. This is commonly done by targeting proteins naturally designed to pass through these membranes. Gram negative techniques include outer membrane protein-based systems, lipoproteins, autotransporters, secreted proteins, subunits of surfaces appendages, and s-layer proteins. Gram positive bacteria do not have an outer membrane envelope; however, they do possess more rigid cell walls. Gram positive techniques include cell wall bound proteins, cell membrane anchored proteins, and cell surface associated proteins.

A bacterial display approach may also be simplified by use of display kits available from biotechnology companies. This eliminates the need to develop the library and streamlines design and synthesis. For example, the FliTrx™ Random Peptide Display,

marketed by Invitrogen, uses E. Coli to display a library of peptides. The dodecapeptides are displayed at the ends of flagellar filaments. This system makes use of a thioredoxin loop to constrain the peptide in order that it may adsorb to the surface.[178]

The FliTrx system was an innovation by Lu et al.[179] based on previous work to display surface fusion proteins. The technique makes use of a dispension region of the gene for flagellin (fliC) in E. coli. The researchers replaced this section with a sequence coding for thioredoxin (trxA). The intention was to create a strain of bacteria that would display the thioredoxin loop on the surface as part of the flagellae. This is very useful for observing surface interactions. The authors developed a panning method wherein the library was grown in a medium containing casamino acids, glucose, salts, and ampicillin. A sample of sufficient size to ensure that it contained 100 times the diversity of the library was grown in media containing tryptophan in order to induce the growth of fringe-like fimbriae. The authors used protein-antibody interactions as the basis for their study. They coated plates with antibody and added a blocking solution to prevent undesirable interactions before exposing the plate to the culture. They allowed the interaction to occur for one hour. They then washed the plates five times and then used mechanical agitation to shear off the remaining tightly-bound bacteria. This procedure was repeated several times. The resulting elutions from the final selection were plated onto ampicillin-containing plates, and individual colonies were selected. DNA was isolated from each. Three antibodies were studied (HIL8-NR7, HM7/7.7.10, and C11.5.14). The DNA from each colony was sequenced. For each antibody, a sequence could be identified that typically occurred (with some variations). The researchers performed separate confirmatory tests and concluded that the FliTrx system could be used to determine binding sequences for antibodies.

2.6.6 Environmental Applications

One application for protein adsorption is in design or discovery of peptides sequences that adsorb to specific metal and metal oxide surfaces. This field has particular application in the field of environmental remediation. Polymeric flocculants are in common use in wastewater treatment. One key issue is the removal of hazardous substances, such as heavy metals. Microbes are innately well-disposed towards this

work. Their surfaces tend to be polyanionic. In addition, a number of bacteria contain metallothionein proteins, which bind metal. One applications involves use of a polypeptide designed to adsorb with great specificity onto a particularly hazardous metal contaminant in wastewater could be used to remove and recover that metal Some work has been done towards development of specific peptide sequences both with and without combinatorial searching for zinc,[180-183] iron,[180, 184] copper,[180, 183] lead,[180] cerium,[180] nickel,[185] cadmium,[183, 185, 186] and mercury.[186, 187]

Investigation into bacteria binding to zinc has been undertaken by several groups. A combinatorial approach was used by Kjærgaard et al. to develop bacteria capable of chelating zinc oxide.[181] Type 1 fimbriae of E. Coli were used to contain a library of random sequences coding for eleven peptides. Sedimentation with a Percoll solution was used to identify cells adsorbing to the ZnO. Sequences found in multiple colonies were identified. By comparison with the SWISS-PROT database, the researchers discovered that a 63% level of identity existed between the relevant sequences and a helicase sequence thought to be part of a zinc binding sequence related to the unzipping of DNA. A comparative test was performed in which the researchers exposed the selected bacteria to cadmium oxide (CdO). They found that half of the clones demonstrated an affinity for the CdO. This work was followed up with a demonstration of bacteria capable of chelating Zn^{2+}.[182] In contrast to many other studies, no consistently repeated motif was observed. Instead, the authors found a greater percentage of histidines than typical (18.4% as opposed to 4.3%). However, one of the fifteen sequences contained no histidines. None of the fifteen sequences isolated contained portions matching those of known proteins involved in the binding of zinc. The authors suggested that they had identified many unique sequences. None of these sequences corresponded to those discovered by Barbas et al.[180] In 1993, Barbas et al. used a biopanning technique to develop bacteria adhering to zinc (Zn^{2+}) using a library coding for peptides 16 units in length. A suspension of $ZnCl_2$ particles was loaded with a chelating agent. The phage libraries were applied and shaken. After washing and elution, the adsorbing clones were identified. Several sequences were identified having affinity. This same technique was

used to study iron (Fe^{3+}), copper (Cu^{2}), lead (Pb^{2+}), and cerium (Ce^{3+}). Selection between similar metals was demonstrated.

As early as 1992, genetically engineered E. coli were developed that exhibited unique adherence to iron oxide (Fe_3O_4) particles.[184] This was done using a random library inserted into the phage λ receptor. A serial enrichment procedure was used. Particles of iron oxide were introduced to E. coli that had been induced to display the peptide library, which contained eleven codons. D-mannose was included to reduce nonspecific adhesion. This is not an unusual practice. The iron oxide particles were removed using a magnet, taking the adsorbed bacteria with them. After washing, the iron oxide containing culture was plated, specific colonies were selected, and the procedure was repeated four additional times. After PCR amplification and DNA sequencing, the resulting sequences were compared. In several experiments, the same sequence was identified.

In a deliberate design technique, Kotrba et al.[183] chemically synthesized sequences on the surface of E. coli intended to bind to cadmium (Cd^{2+}) in the presence of zinc (Zn^{2+}) and copper (Cu^{2+}). The sequences Gly-His-His-Pro-His-Gly (HP) and Gly-Cys-Gly-Cys-Pro-Cys-Gly-Cys-Gly (CP) were expressed in E. coli. For this experiment in selectivity, the HP sequence was chosen based on past work indicating an affinity for Cu^{2+} and Zn^{2+}. The CP sequence had previously shown selectivity for Cd^{2+}. The peptides were synthesized and immobilized on a resin. The ionic strength was kept constant. HP and CP sequences were used together, separately, and in multiples. Binding was improved significantly overall, but although experiments in selectivity demonstrated a preference for Cd^{2+}, substantial amounts of Cu^{2+} and Zn^{2+} were adsorbed as well.

Using deliberate design, Sousa et al. demonstrated specific adsorption to Cd^{2+} and Ni^{2+} for removal of heavy metals from wastewater in 1996.[185] E. coli were engineered to express clusters of histidine on the surface of the cells. Single and double clusters of six histidines expressed in the LamB protein were designed. Histidines form spheres about divalent cations. Both Cd^{2+} and Ni^{2+} were found to coordinate with the histidine-bearing bacteria.

Chen and Wilson studied deliberately designed E. coli for removal of mercury (Hg^{2+}) from contaminated water.[187] The approach taken was the over-expression of protein sequences containing cysteine, known to bind heavy metals. The strains developed showed both affinity and selectivity towards Hg^{2+}. Pazirandeh et al. also studied the removal of heavy metals from wastewater using a deliberate design technique.[186] E. coli were engineered to express a fusion protein with a metal binding motif containing a large portion of cysteine based on previous research. Induced cells carrying this gene were exposed to solutions of metal salts in the form of $CdCl_2$ (Cd^{2+}), $HgCl_2$ (Hg^{2+}), $Pb(NO_3)_2$ (Pb^{2+}), and Cu_2SO_4 (Cu^{2+}). After incubation, centrifugation was used to collect the bacteria. The amount of adsorbed metal was determined by measuring the content of metal in the supernatant. Cd^{2+} and Hg^{2+} were bound to a large degree as compared to control, whereas Pb^{2+} and Cu^{2+} were bound to a lesser degree. This result was good for the desired application in removal of heavy metals.

2.6.7 Processing Applications

Polypeptides have potential applications in processing applications, for example by improving suspension performance under heavy loading conditions or improving rheological behavior. Novel semiconductors are a potentially valuable application.[188] In addition, peptides may be used in material synthesis.[189]

Work has been done by Whaley et al.[188] to develop peptides sequences that selectively bind to semiconductors. Five semi-conductors were studied: GaAs(100), GaAs(111)A, GaAs(111)B, InP(100), and Si(100). Selectivity was found not only for difference compounds, but also for different crystallographic faces of GaAs. As is generally done, selection was performed several times, in this case five, to improve selection and reduce the possibility of contamination. The researchers hypothesized that the dodecamers in an extended state were larger than the crystal unit cells, and that as such, the essential sequences were smaller than the full length of the peptide. They subsequently reduced the length of the peptides in the screening library to further isolate the key combinations. The experimental procedure called for exposure of the surfaces to the library for one hour, after which the surfaces were washed ten times with Tri-buffered saline at pH 7.5.

Subsequently, elution was performed by decreasing the pH to 2.2 with glycine-HCl for 10 minutes, then neutralizing. The substrates were chemically etched immediately prior to phage exposure. XPS was used to characterize the surfaces of the substrates. These experiments were carried out using a phage display library containing approximately 10^9 peptide combinations. The creation of the phage library was as described by Parmley and Smith. [176] In their work, foreign DNA fragments were cloned into a phage vector. These fragments were then displayed on the surface of virions, allowing selectivity to antibodies to be observed. Whaley et al. applied this technique to semiconductor surfaces.

2.6.8 Recombinant DNA Technology for Synthesis of Biopolymers

Recombinant DNA technology, which is also sometimes called molecular cloning, makes use of a host cell to produce proteins. Advantages include control of chemical composition and chain length and that once the gene is created, an organism can produce it indefinitely.[190] The basic technique involves insertion of a base pair sequence into the DNA of a host organism, thereby causing the host to express the desired amino acid sequence. The original DNA sequence may be deliberately designed or discovered by use of a combinatorial library. Either way, it must be amplified before introduction into the host. The typical means of doing this is polymerase chain reaction (PCR), described in the next section. In simple terms, a DNA sequence is prepared by some means, then inserted into carrier DNA, which is used to inoculate the host cell. Typical vectors include plasmids and λ phages from bacteria. A good vector also includes a means of identification, such as antibiotic resistance. This allows for isolation of those host cells which have successfully incorporated the vector.

One issue commonly arising in the biological synthesis of protein polymers is that repetitive DNA sequences may be taken to be mistakes by the cellular machinery of the host and as such may be "corrected" to the detriment of the intended sequence. One technique to alleviate this issue is to take advantage of codon degeneracy by avoiding the repetitive use of the same triplet to code for an amino acid.[190] Instability may also occur in natural DNA sequences when a short palindromic DNA sequence is repeated frequently. A study by Lohe and Brutlag on the three relatively simple satellite DNA

sequences for Drosophila melanogaster showed that longer fragments were more susceptible to instability.[191]

2.6.9 Polymerase Chain Reaction

Polymerase Chain Reaction (PCR) is commonly used to amplify DNA in order to have sufficient material to work with. PCR involves a temperature cycle repeated many times. A high temperature (95°C) is used to denature the template DNA. The low temperature (37-55°C) portion of the cycle allows the primers to attach to the template strands. Taq DNA polymerase is used to catalyze the DNA synthesis at a moderate temperature (72°C). Repetition of the temperature cycle allows exponential production of DNA as each new strand becomes a template.[172]

2.6.10 Purification

Gel electrophoresis is commonly used as a means of separation of DNA based on molecular weight and charge. Protein polymers are frequently good candidates for this treatment if they contain a charge imbalance.[190] A commonly used gel is agarose, which has the necessary characteristic of porosity. When a voltage gradient is applied to the gel, molecules move at rates inversely proportional to the logarithm of the number of base pairs.[192] Maintaining constant gel geometry is important to consistent results. Dyes such as ethidium bromide may be used to stain the gels by binding to DNA and RNA.

2.7 Key Experimental Techniques

2.7.1 Light Scattering

Light scattering is a useful technique for characterizing soluble species and suspended particles in a liquid phase. Light scattering depends on the tendency of material to absorb and emit light. Essential to the concept is that the sample must display some sort of heterogeneity at some length scale. If the sample is homogeneous and isotropic, all scattered light will be cancelled out by destructive interference. A schematic is shown in Figure 2-11.

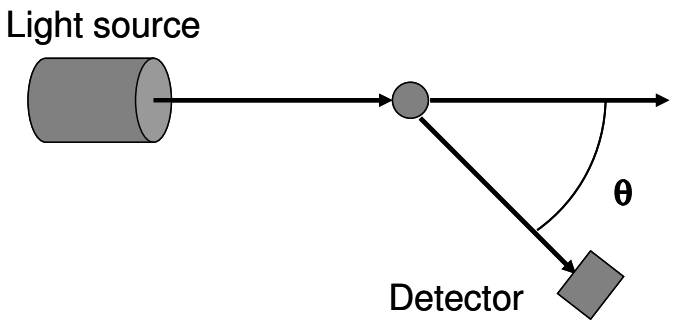

Figure 2-11. Light scattering experimental setup.

In this setup, monochromatic light from a laser source is directed into a sample. The incident beam is described by wavelength, λ_o, and a wave vector, $\vec{k}_i$. The magnitude of the wave vector is:

$$\left|\vec{k}_i\right| = \frac{2\pi\, m_1}{\lambda_o} = \frac{m_1 \omega_o}{c}$$

Eq. 2-75

in which ω_o is the frequency of the incident light, m_1 is the refractive index of the medium, and c is the speed of light in vacuum.[193] The scattered light is described by a wave vector, $\vec{k}_s$. The vector difference of $\vec{k}_i$ and $\vec{k}_s$ is $\vec{q}$. The magnitude of $\vec{q}$ is:

$$q = \frac{4\pi\, m_1}{\lambda_o} \sin\frac{\theta}{2}$$

Eq. 2-76

Concentration of the scattering species is important to scattering. At higher concentrations there is an increased incidence of multiple scattering. Light scattered from one particle at a given can strike a second particle at a different incident angle. As this can continue through additional particles, the resulting net value of θ can effectively be anything. At relatively low concentrations ($<10^{-4}$ g/cm^3), the singly scattered light dominates any multiple scattered light; however, at higher concentrations, the multiple scattered light becomes a problem.[193]

Light scattering is useful for particles in the size range comparable to the inverse of the magnitude of the scattering vector. Typical values for this range from 10-1000 nm.[193] There are two types of light scattering experiments for solutions and suspensions. They are static and dynamic light scattering.

2.7.1.1 Static Light Scattering

Static light scattering collects intensities over a long time as a function of the scattering angle. This yields time averaged properties, such as the molar mass and the radius of gyration. The measurement is described in the following equation in which T is the observation time and I is the scattered intensity.

$$\mathrm{I}(\theta) = \lim_{\mathrm{t}\to\infty} \frac{1}{\mathrm{T}} \int_0^{\mathrm{T}} \mathrm{I}(\theta, \mathrm{t})\mathrm{dt}$$

Eq. 2-77

In a solution, fluctuations in the intensity of light scattered are caused by variations in density and concentration. A central equation for static light scattering is:[194]

$$Kc/R_\theta = \frac{1}{P(\theta)}\left[1/M_w + 2A_2c\right]$$

Eq. 2-78

in which c is the concentration of the sample, M_w is the weight-average molecular weight, A_2 is the second virial coefficient, $P(\theta)$ is the form factor, and K is an optical constant. The Rayleigh ratio, R_θ, is defined as

$$R_\theta = \frac{I_A \tilde{n}_o^2}{I_T \tilde{n}_T^2} R_T$$

Eq. 2-79

where I_A is the difference in intensity between the scattering sample and the solvent, I_T is the scattering intensity of toluene, $\tilde{n}_o$ is the solvent refractive index, $\tilde{n}_T$ is the refractive index of toluene, and R_T is the Rayleigh ratio of toluene. The optical constant, K, for the instrument is defined by

$$K = \frac{4\pi^2 \left(n_{solvent} \frac{dn}{dc} \right)^2}{\lambda^4 N_A}$$

Eq. 2-80

in which dn/dc is the refractive index increment and N_A is Avogadro's number.

The shape and arrangement of the particles has a profound impact on scattering. For instance, a large particle may scatter from different scattering centers within itself. This necessitates the introduction of a particle scattering factor or form factor, P(θ), which is described by the equation below, in which N is the number of scattering centers and r_{ij} is the distance between the scattering centers. In the case of a polymeric chain, the scattering centers are the monomeric units.[194]

$$P(\theta) = \left(\frac{1}{N^2} \right) \sum_i^N \sum_j^N \left\langle \frac{\sin(qr_{ij})}{qr_{ij}} \right\rangle$$

Eq. 2-81

This equation may be expanded as a virial series.[194] This is shown in the following equation, in which $\langle s^2 \rangle_z$ is the mean square radius of gyration and A_2 is the second virial coefficient.

$$\frac{Kc}{R_\theta} = \left(\frac{1}{M_W} \right) \left(1 + \frac{1}{3\langle s^2 \rangle_z q^2} + ... \right) + 2A_2 c + ...$$

Eq. 2-82

This is especially useful in the context of a Zimm plot. In this graph, $\frac{Kc}{R_\theta}$ is plotted against $(q^2 + kc)$. In this case, k is an arbitrary constant. From the Zimm plot, shown as Figure 2-12, it is possible to obtain the mean square radius of gyration, the second virial coefficient, and the weight-average molecular weight.

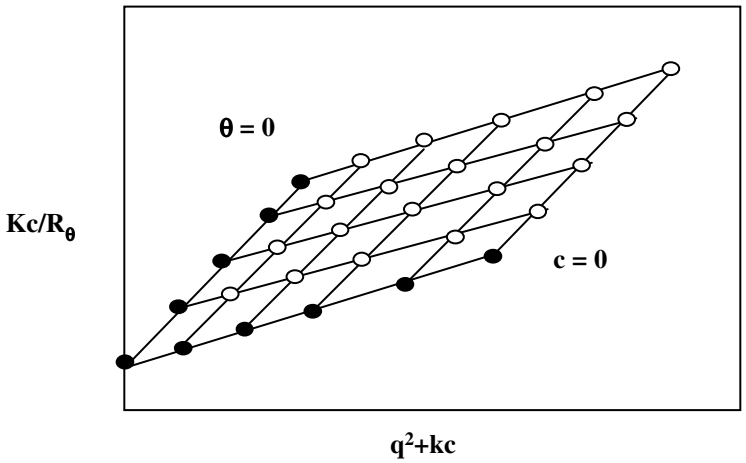

Figure 2-12. Example Zimm plot. The slope of the θ=0 line is the mean square radius of gyration; the slope of the c=0 line is the second virial coefficient. The y-intercept is the inverse of the weight-average molecular weight. Open circles are experimental data. Filled circles are extrapolated points.

If the scattering entities are small relative to the wavelength of the laser, SLS analysis may be done at a single angle using a Debye plot, which requires that q*Rg<<1 so that the form factor P(θ) approaches unity and therefore Eq. 2-78 reduces to:

$$Kc/R_\theta = 1/M_w + 2A_2C$$

Eq. 2-83

Static light scattering is useful in a variety of colloidal applications.[71, 195-198] For example, Lindner et al. used SLS to match a series of concentrations of oil-water emulsions with the Rayleigh-Debye-Gans single scattering theory.[195] They also examined the result of salt concentration on particle size. Quirantes et al. examined core-shell colloids.[196] In this study, hematite particles encased in a yttrium basic carbonate shell were used; particle size distribution was determined. A study was conducted by Pisárcik et al. on a series of alkanediyl-α,ω-bis(dimethylalkylammonium bromide) surfactants containing different alkyl tail lengths.[71] The aggregation number of each was determined. In another study, Wolff et al. examined a pair of biopolymers, both insulin fructans.[197] As the molar mass was known a priori, it was possible by determining the radius of gyration to draw conclusions regarding the conformation of the molecules in two solvents. In another biological study, Lehner et al. added chymosin to skim milk and observed the aggregation of casein molecules contained therein.[198] The size distributions determined were then compared with ultra low shear data.

2.7.1.2 Dynamic Light Scattering

Dynamic light scattering (DLS), also known as quasi-elastic light scattering, is used to study particle diffusion.[193] DLS is typically performed using an intensity autocorrelation, in which a Fourier transform is performed on the spectrum. This yields an autocorrelation function $G_2(\tau)$, in which the intensity I(t) is measured at an arbitrary time, t. After a time delay, τ, the intensity is measured again. The function $G_2(\tau)$ is given by an average of the product of the intensities at the two times as described as:

$$G_2(\tau) = \langle I(t) \cdot I(t+\tau) \rangle$$

Eq. 2-84

This may then be modeled by using the following equation, in which A and B are instrumental factors and Γ is the decay rate.

$$G_2(\tau) = \int_0^\infty G(\Gamma, t) \exp(-2\Gamma\tau) d\Gamma$$

Eq. 2-85

This may be used to determine the diffusion coefficient, D, according to:

$$\Gamma = Dq^2$$

Eq. 2-86

The scattering vector, q, is calculated according to the following equation, in which λ is the wavelength, n is the refractive index of the sample, and θ is the measurement angle.[199]

$$q = \frac{4\pi n}{\lambda} \sin\left(\frac{\theta}{2}\right)$$

Eq. 2-87

It is then possible to use a correlation between the diffusion coefficient and the particle size, such as the Stokes-Einstein relationship which is valid for non-interacting spherical particles:

$$R_H = \frac{kT}{6\pi\eta D_o}$$

Eq. 2-88

in which R_H is the hydrodynamic radius, D_o is the diffusion coefficient, and η is the viscosity. If a non-draining sphere in which the solvent moves as part of the spherical unit is assumed, the hydrodynamic radius may be related to the radius of gyration, R_g, by the following:[67]

$$R_H = 0.875 R_g$$

Eq. 2-89

For linear chain polymers, the radius of gyration may be approximated by a number of chain statistical models, including the freely jointed chain model:

$$\left\langle R^2 \right\rangle = nl^2 C_\infty$$

Eq. 2-90

in which n and l are the number and length of a Kuhn segment and C_∞ is the chain stiffness parameter. The radius of gyration of the chain, R_g, may then be calculated using:

$$\left\langle R_g^2 \right\rangle = \frac{\left\langle R^2 \right\rangle}{6}$$

Eq. 2-91

Dynamic light scattering is useful for a variety of applications. It is especially useful for use with polymers, as it may be used to determine the average particle size and size distribution for individual particles, as well as aggregates in dilute systems.

Dynamic light scattering has often been of use in studying behavior of gels. Many examples exist. In one instance, Nicolai and Cocard described a study in which colloidal disk-shaped particles of clay gelled in water.[200] They were able to observe the fluctuation of concentration in the system, along with the subsequent cessation of that fluctuation when the gel became too immobile to permit substantial movement. They were able to measure the behavior of aggregates in the system and note that they were semi-flexible in

nature. This has implications in processing. In another study, Narayanan et al. performed dynamic light scattering on aqueous solutions of pectin and calcium chloride in order to observe the gelation.[201] They used this data to support a coupling model.

Biological materials are frequently studied using DLS, as its non-destructive nature is very useful on potentially delicate molecules. For example, Tanaka et al. used DLS to investigate the oligomerization of a protein, bovine pancreatic trypsin inhibitor.[202] The studies were conducted in several salt solutions. In another study, Moradian-Oldak et al. examined engineered amelogenin proteins using DLS and AFM in order to observe self-assembly behavior.[203] By performing a time-dependent study, it was possible to observe the formation of particles and the subsequent aggregation. The objective was to study the interaction of specific domains in the protein.

2.7.2 Zeta Potential

Laser doppler spectroscopy may be used for measurement of zeta potential. Zeta potential is essentially the potential measured at the slip distance from the particle. Electrophoresis can be used to measure this by applying an electrical field, causing motion of the charged particle. Stokes's law allows calculation of the velocity of the particle in an electric field. This is given in the following equation, in which v is the velocity of the particle, η is the fluid viscosity, F is the force provided by the electrical field, and R is the radius of the particle.[31]

$$\vec{v} = \frac{\vec{F}}{6\pi\eta R}$$

Eq. 2-92

Zeta potential, ζ, is described by the following equation, in which q is the effective charge of the particle, R is the effective radius, and κ is the inverse of the Debye length.

$$\zeta = \frac{\left(q/R\right)}{4\pi\varepsilon_r\varepsilon_o}\left(1+\kappa R\right)^{-1}$$

Eq. 2-93

For the case of κR<<1 (a "thick" double layer), this simplifies to the following, in which u is the electrophoretic mobility, defined as the ratio of the velocity to the electric field.

$$\zeta = \frac{3}{2}\frac{\eta \mathrm{u}}{\varepsilon_r \varepsilon}$$

Eq. 2-94

For the case of κR>>1 (a "thin" double layer), the simplification is:

$$\zeta = \frac{\eta \mathrm{u}}{\varepsilon_r \varepsilon}$$

Eq. 2-95

2.7.3 Densiometry

Densiometry operates on the principle that a cell of constant volume oscillates at a frequency dependent on the density of the sample. This is described by the following equation in which T is the oscillation period, d is the sample density, V_c is the cell volume, M_c is the cell mass, and K is a temperature-dependent constant. K may be determined in advance using reference samples.

$$T = 2\pi\sqrt{\frac{dV_c + M_c}{K}}$$

Eq. 2-96

This method has been used to describe the specific gravity of the core and corona of micelles in solution for block copolymers.[204, 205] This may be accomplished by assuming that the volume contributions of the two blocks (B1 and B2) are additive as in:

$$V_{polymer} = m_{B1}v_{B1} + m_{B2}v_{B2}$$

Eq. 2-97

in which $V_{polymer}$ is the apparently specific volume of the copolymer, m_{B1} and m_{B2} are the mass fractions of B1 and B2, and v_{B1} and v_{B2} are the specific volumes of the two blocks. In order to use this approach, it is necessary to have one of the two blocks available as a homopolymer for separate measurement.

2.7.4 Small Angle Neutron Scattering (SANS)

Small angle neutron scattering (SANS) has been used by many researchers to examine the core-shell structure of micelles.[8, 26, 32, 34, 37, 44, 206] SANS is an especially useful technique for examining micelles because scattering can be done selectively from different portions of the structure provided there is sufficient difference in scattering length density (SLD). This may be achieved by either varying the solvent composition (for instance by using a deuterated solvent) or by deuterating portions of the polymer, as in a study on PEO-PPO-PEO by Goldmints et al.[44]

For SANS studies of polymeric micelles, a challenging aspect is fitting an appropriate model. There has been a large contribution to the body of this work with respect to polyoxamers (Pluronics), which have a poly(ethylene oxide)-b-poly(propylene oxide)-b-poly(ethylene oxide) structure. One approach treated the micelles as monodisperse homogeneous hard spheres. A hard sphere form factor is described by Ashcroft and Lekner.[207] The application to diblock copolymers forming spherical domains was later described by Kinning and Thomas.[208]. This has been used by several authors to describe micelles of Pluronics in aqueous solutions.[7, 209] More recent studies such as one by Svaneborg and Pedersen have involved numerical simulations to describe the form factor by treating the corona as a semi-dilute solution of polymer with a concentration profile varying from the surface.[210]

Contrast is a result of difference in the scattering length densities of the material and the medium. Scattering length density is given by the following equation, in which b_i is the bound coherent scattering length of the i^{th} atom in the volume, V, containing n atoms.

$$\rho = \frac{\sum_{i=1}^{n} b_i}{V}$$

Eq. 2-98

The Guinier approximation describes low q ($qR_g << 1$) scattering of dilute samples by Eq. 2-99 in which R_g is the radius of gyration and q is the modulus of the scattering vector, given by Eq. 2-100. The scattering angle is θ and λ is the wavelength.[211] The Guinier

law is not shape dependent, and is valid as long as $1<<1/R_g$, the system is sufficiently dilute to ensure independent scattering, and the system is isotropic. [212]

$$I(q) \approx I(0)\exp\left(-\frac{1}{3}q^2 R_g^2\right)$$

Eq. 2-99

$$q = \frac{4\pi}{\lambda}\sin\frac{\theta}{2}$$

Eq. 2-100

A slightly more complex representation describes the scattering according to a Debye function (Eq. 2-101), wherein Z is the degree of polymerization and υ_m is the monomer specific volume [212] This assumes that the polymer chains behave like Gaussian coils.

$$I(q) = \phi(\Delta\rho)^2 Z v_m \left(\frac{2\left(e^{-qR_g} + qR_g - 1\right)}{\left(qR_g\right)^2}\right)$$

Eq. 2-101

Core-shell models may be used to describe formation of micelles in solution. These models depend on being able to observe a difference in the scattering density between at least two of the three components: core, shell, and solvent. A core that is devoid of solvent simplifies the experiment, but is not essential. However, for simple models, one must make some assumptions about the degree of solvation of the core.

The form factor, P(q), for a monodisperse spherical core-shell system with a dry core is described by Eq. 2-102, in which R_c is the radius of the core and R_s is the total radius of the micelle.[213]

$$P(q) = \left[\frac{3V_c(\rho_c - \rho_s)j_1(qR_c)}{qR_c} + \frac{3V_s(\rho_s - \rho_{solv})j_1(qR_s)}{qR_s}\right]^2$$

Eq. 2-102

$$j_1(x) = \left(\frac{\sin x - x\cos x}{x^2}\right)$$

Eq. 2-103

$$V_c = \frac{4\pi}{3} R_c^3$$

Eq. 2-104

The scattered intensity is given by Eq. 2-105, in which S(q) is the structure factor and n_p is the number density of particles.

$$I(q) = n_p P(q) S(q)$$

Eq. 2-105

The structure factor, S(q), is used to describe ordering of the micelles in solution. For a dilute case, there is no micelle-micelle interaction, and S(q) = 1. For concentrated solutions, one option is to use a hard sphere structure factor, which for monodisperse spheres is calculated using the following interaction potentials:[214]

$$U(r) = \begin{Bmatrix} \infty, r < 2R \\ 0, r \geq 2R \end{Bmatrix}$$

Eq. 2-106

A SANS model for block copolymer micelles was developed by Pedersen et al.[34, 215, 216] This work was based on form factors for polymer stars using Gaussian statistics.[217, 218] The model describes a micelle with a homogeneous core (in this case PU) surrounded by a corona of non-interacting Gaussian chains (PEO), shown schematically in Figure 2-13.

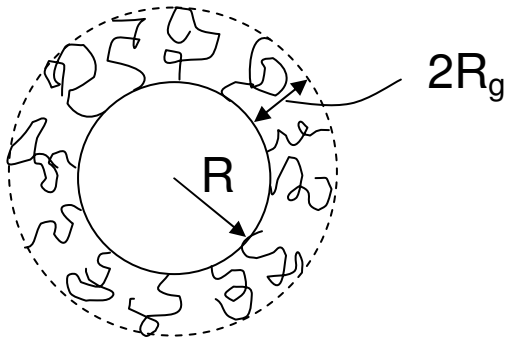

Figure 2-13. Illustration of a block copolymer micelle with nomenclature of the SANS model. R is the hard-sphere radius of the core. $2R_g$ is the thickness of the corona.

The overall expression for the intensity scattered by monodisperse micelles is given by Eq. 2-107. $F_{mic}(q)$ is the form factor for the micelle, S(q) is a hard sphere structure

factor, $A_{mic}(q)$ is the amplitude of the radial scattering length distribution of the micelle based on noninteracting chains, c is the concentration, and M_{mic} is the mass of a micelle.

$$\frac{I(q)}{c} = \frac{1}{M}\left(F\ (q) + A(q)^2\left[S(q) - 1\right]\right)$$

Eq. 2-107

The form factor, F(q) is given by the following.

$$F(q) = N^2\beta_{core}^2 A_{core}^2(q) + 2N\beta_{chain}^2 F_{chain}(q) + 4N^2\beta_{core}\beta_{chain}A_{core}A_{chain}(q) + 2N(2N-1)\beta_{chain}^2 A_{chain}^2(q)$$

Eq. 2-108

N is the aggregation number of the micelle and β_{core} and β_{chain} are the total excess scattering lengths of one PU block and one PEO block respectively. A_{core} is the form factor amplitude for a spherical homogeneous core with radius R and a smoothly decaying scattering length density over a width σ at the surface.

$$A_{core}(q) = \Phi(qR)\exp\frac{\left(-q^2\sigma^2\right)}{2}$$

Eq. 2-109

The form factor amplitude of a sphere with a sharp surface, Φ(qR), is given by the following.

$$\Phi(qR) = \frac{3\left(\sin(qR) - qR\cos(qR)\right)}{(qR)^3}$$

Eq. 2-110

F_{chain} is given by the Debye function in which R_g is the radius of gyration of a single polymer Gaussian chain.

$$F_{chain}(q) = \frac{2\left[\exp\left(-q^2R_g^2\right) - 1 + q^2R_g^2\right]}{\left(q^2R_g^2\right)^2}$$

Eq. 2-111

The form factor amplitude of the corona, $A_{chain}(q)$, is given by the following.

$$A_{chain}(q) = \frac{1-\exp\left(-q^2R_g^2\right)}{\left(q^2R_g^2\right)^2}\frac{\sin\left[q\left(dR_g+R\right)\right]}{q\left(dR_g+R\right)}$$

Eq. 2-112

The variable d is defined as the distance from the center of mass of the corona chains to the surface of the core divided by the radius of gyration of a corona chain. In other words, if d is equal to unity, the center of mass of the corona chains is located at a distance of R_g from the surface. This is the case in which the corona chains do not penetrate the core.

2.8 References

1. Riess, G., Micellization of block copolymers. *Progress in Polymer Science*, **2003**. 28(7): p. 1107-1170.

2. Gohy, J.F., Block copolymer micelles, in Block Copolymers II, V. Abetz, Editor. **2005**, Springer: London. p. 65-136.

3. Stuart, M.A.C., et al., Assembly of polyelectrolyte-containing block copolymers in aqueous media. *Current Opinion in Colloid & Interface Science*, **2005**. 10(1-2): p. 30-36.

4. Nolan, S.L., et al., Light scattering study on the effect of polymer composition on the structural properties of PEO-PPO-PEO micelles. *Journal of Colloid and Interface Science*, **1997**. 191(2): p. 291-302.

5. Alexandridis, P. and Hatton, T.A., Poly(ethylene oxide)-poly(propylene oxide)-poly(ethylene oxide) block copolymer surfactants in aqueous solutions and at interfaces: thermodynamics, structure, dynamics, and modeling. *Colloids and Surface A: Physicochemical and Engineering Aspects*, **1995**. 96: p. 1-46.

6. Almgren, M., Brown, W., and Hvidt, S., Self-Aggregation and Phase-Behavior of Poly(Ethylene Oxide) Poly(Propylene Oxide) Poly(Ethylene Oxide) Block-Copolymers in Aqueous-Solution. *Colloid and Polymer Science*, **1995**. 273(1): p. 2-15.

7. Mortensen, K. and Pedersen, J.S., Structural Study on the Micelle Formation of Poly(ethylene oxide)-Poly(propylene oxide)-Poly(ethylene oxide) Triblock Copolymer in Aqueous Solution. *Macromolecules*, **1993**. 26(805-812).

8. Jain, N.J., et al., Salt induced micellization and micelle structures of PEO/PPO/PEO block copolymers in aqueous solution. *Colloids and Surfaces A: Physicochemical and Engineering Aspects*, **2000**. 173(1-3): p. 85-94.

9. Guo, C., et al., Hydration and conformation of temperature-dependent micellization of PEO-PPO-PEO block copolymers in aqueous solutions by FT-Raman. *Langmuir*, **1999**. 15(8): p. 2703-2708.

10. Guo, C., et al., Conformational structure of triblock copolymers by FT-Raman and FTIR spectroscopy. *Journal of Colloid and Interface Science*, **1999**. 209(2): p. 368-373.

11. Alexandridis, P., Holzwarth, J.F., and Hatton, T.A., Micellization of Poly(Ethylene Oxide)-Poly(Propylene Oxide)-Poly(Ethylene Oxide) Triblock Copolymers in Aqueous-Solutions - Thermodynamics of Copolymer Association. *Macromolecules*, **1994**. 27(9): p. 2414-2425.

12. Chaibundit, C., et al., Association properties of triblock copolymers in aqueous solution: Copolymers of ethylene oxide and 1,2-butylene oxide with long E-blocks. *Langmuir*, **2000**. 16(24): p. 9645-9652.

13. Jada, A., et al., Structure of polystyrene-block-poly(ethylene oxide) diblock copolymer micelles in water. *Macromolecular Chemistry and Physics*, **1996**. 197(11): p. 3697-3710.

14. Xu, R.L., et al., Micellization of Polystyrene Poly(Ethylene Oxide) Block Copolymers in Water .5. a Test of the Star and Mean-Field Models. *Macromolecules*, **1992**. 25(2): p. 644-652.

15. Hurtrez, G., Dumas, P., and Riess, G., Polystyrene-poly(ethylene oxide) diblock copolymers micelles in water. *Polymer Bulletin*, **1998**. 40(2-3): p. 203-210.

16. Yu, K. and Eisenberg, A., Multiple morphologies in aqueous solutions of aggregates of polystyrene-block-poly(ethylene oxide) diblock copolymers. *Macromolecules*, **1996**. 29(19): p. 6359-6361.

17. Poe, G.D., et al., Enhanced Coil Expansion and Intrapolymer Complex Formation of Linear Poly(methacrylic acid) Containing Poly(ethylene glycol) Grafts. *Macromolecules*, **2004**. 37: p. 2603-2612.

18. Drescher, B., Scranton, A.B., and Klier, J., Synthesis and Characterization of Polymeric Emulsifiers Containing Reversible Hydrophobes: Poly(methacrylic acid-g-ethylene glycol). *Polymer*, **2001**. 42: p. 49-58.

19. Mathur, A.M., et al., Polymeric emulsifiers based on reversible formation of hydrophobic units. *Nature*, **1998**. 392(6674): p. 367-370.

20. Li, Y., Gong, Y.-K., and Nakashima, K., Nanoaggregate Formation of Poly(ethylene oxide)-b-polymethacrylate Copolymer Induced by Alkaline Earth Metal Binding. *Langmuir*, **2002**. 18: p. 6727-6729.

21. Moeser, G.D., et al., Water-based magnetic fluids as extractants for synthetic organic compounds. *Industrial & Engineering Chemistry Research*, **2002**. 41(19): p. 4739-4749.

22. Moeser, G.D., et al., Structure of polymer-stabilized magnetic fluids: Small-angle neutron scattering and mean-field lattice modeling. *Langmuir*, **2004**. 20(13): p. 5223-5234.

23. Matsuoka, H., et al., Polymer Micelle Formation without Gibbs Monolayer Formation: Synthesis and Characteristic Behavior of an Amphiphilic Diblock Copolymer Having Strong Acid Groups. *Macromolecules*, **2003**. 36: p. 5321-5330.

24. Matsuoka, H., et al., Micellization of Non-Surface-Active Diblock Copolymers in Water. Special Characteristics of Poly(Styrene)-block-Poly(Styrenesulfonate). *Langmuir*, **2004**. 20: p. 7412-7421.

25. Kaewsaiha, P., Matsumoto, K., and Matsuoka, H., Non-Surface Activity and Micellization of Ionic Amphiphilic Diblock Copolymers in Water. Hydrophobic Chain Length Dependence and Salt Effect on Surface Activity and the Critical Micelle Concentration. *Langmuir*, **2005**. 21: p. 9938-9945.

26. Moffitt, M., et al., Coronal Structure of Star-Like Block Ionomer Micelles: An Investigation by Small-Angle Neutron Scattering. *Macromolecules*, **1998**. 31: p. 2190-1297.

27. Moffitt, M. and Eisenberg, A., Scaling Relations and Size Control of Block Ionomer Microreactors Containing Different Metal Ions. *Macromolecules*, **1997**. 30: p. 4363-4373.

28. Khougaz, K., Gao, Z., and Eisenberg, A., Distribution of Water in Solutions of Reverse Micelles of Sodium Bis[2-ethylhexyl] Sulfosuccinate and Block Ionomers in Toluene. *Langmuir*, **1997**. 13: p. 623-631.

29. Israelachvili, J., Intermolecular and Surface Forces. 2nd ed. **1991**, London: Academic Press.

30. Shaw, D.J., Introduction fo Colloid and Surface Chemistry. **1966**, London: Butterworths.

31. Evans, D.F. and Wennerstrom, H., The Colloidal Domain. 2 ed. **1999**, New York: Wiley-VCH.

32. Yang, L., et al., Small-angle neutron scattering investigation of the temperature-dependent aggregation behavior of the block copolymer pluronic L64 in aqueous solution. *Langmuir*, **2000**. 16(23): p. 8555-8561.

33. Rassing, J. and Attwood, D., Ultrasonic velocity and light-scattering studies on the polyoxyethylene-polyoxypropylene copolymer Pluronic F127 in aqueous solution. *International Journal of Pharmaceutics*, **1983**. 13: p. 47-55.

34. Pedersen, J.S. and Gerstenberg, M.C., The structure of P85 Pluronic block copolymer micelles determined by small-angle neutron scattering. *Colloids and Surfaces a-Physicochemical and Engineering Aspects*, **2003**. 213(2-3): p. 175-187.

35. Pandit, N., et al., Effect of salts on the micellization, clouding, and solubilization behavior of pluronic F127 solutions. *Journal of Colloid and Interface Science*, **2000**. 222(2): p. 213-220.

36. Bohorquez, M., et al., A study of the temperature-dependent micellization of pluronic F127. *Journal of Colloid and Interface Science*, **1999**. 216(1): p. 34-40.

37. Wu, G.W., et al., SANS and SAXS studies of pluronic L64 in concentrated solution. *Physica A*, **1996**. 231(1-3): p. 73-81.

38. Mata, J.P., et al., Concentration, Temperature, and Salt-induced Micellization of a Triblock Copolymers Pluronic L64 in Aqueous Media. *Journal of Colloid and Interface Science*, **2005**. 292: p. 548-556.

39. Ghaouar, N., et al., Structure and thermodynamic modelling of Pluronic L64 solutions. *E-Polymers*, **2005**.

40. Sedev, R., Steitz, R., and Findenegg, G.H., The structure of PEO-PPO-PEO triblock copolymers at the water/air interface. *Physica B*, **2002**. 315(4): p. 267-272.

41. Prudhomme, R.K., Wu, G.W., and Schneider, D.K., Structure and rheology studies of poly(oxyethylene-oxypropylene-oxyethylene) aqueous solution. *Langmuir*, **1996**. 12(20): p. 4651-4659.

42. Almgren, M., et al., Static and Dynamic Properties of a (PEO---PPO---PEO) Block Copolymer in Aqueous Solution. *Journal of Colloid and Interface Science*, **1992**. 151: p. 157-165.

43. Arotcarena, M., et al., Switching the inside and the outside of aggregates of water-soluble block copolymers with double thermoresponsivity. *Journal of the American Chemical Society*, **2002**. 124(14): p. 3787-3793.

44. Goldmints, I., et al., Structure of (deuterated PEO) (PPO) (deuterated PEO) block copolymer micelles as determined by small angle neutron scattering. *Langmuir*, **1999**. 15(5): p. 1651-1656.

45. Zhou, Z. and Chu, B., Anomalous Micellization Behavior and Composition Heterogeneity of Triblock ABA Copolymer of (A) Ethylene Oxide and (B) Propylene Oxide in Aqueous Solution. *Macromolecules*, **1988**. 21: p. 2548-2554.

46. Malmsten, M. and Lindham, B., Self-Assembly in Aqueous Block Copolymer Solutions. *Macromolecules*, **1992**. 25: p. 5440-5445.

47. Brown, W., Schillen, K., and Almgren, M., Micelle and Gel Formation in a Poly(ethylene oxide)/Poly(propylene oxide)/Poly(ethylene oxide) Triblock Copolymer in Water Solution. Dynamic and Static Light Scattering and Oscillatory Shear Measurements. *Journal of Physical Chemistry*, **1991**. 95: p. 1850-1858.

48. Al-Saden, A.A., Whateley, T.L., and Florence, A.T., Poloxamer Association in Aqueous Solution. *Journal of Colloid and Interface Science*, **1982**. 90: p. 303-309.

49. Zeghal, M. and Auvray, L., Structure of Hydrophobically and Hydrogen-Bonded Complexes Between Amphiphilic Copolymer and Polyacid in Water. *The European Physical Journal E*, **2004**. 14: p. 259-268.

50. Bronich, T.K., et al., Polymer Micelle with Cross-Linked Ionic Core. *Journal of the American Chemical Society*, **2005**. 127: p. 8236-8237.

51. Solomatin, S.V., et al., Environmentally Responsive Nanoparticles from Block Ionomer Complexes: Effects of pH and Ionic Strength. *Langmuir*, **2003**. 19: p. 8069-8076.

52. Li, Y. and Nakashima, K., Fluorescence studies on the properties of the nanoaggregates of poly(ethylene oxide)-b-polymethacrylate copolymer formed by binding of cationic surfactants to polymethacrylate block. *Langmuir*, **2003**. 19(3): p. 548-553.

53. Khanal, A., et al., Fabrication of nanoaggregates of poly(ethylene oxide)-b-polymethacrylate by complex formation with chitosan or methylglycolchitosan. *Colloids and Surfaces A-Physicochemical and Engineering Aspects*, **2005**. 260(1-3): p. 129-135.

54. Oyama, H.T., Tang, W.T., and Frank, C.W., Complex-Formation between Poly(Acrylic Acid) and Pyrene-Labeled Poly(Ethylene Glycol) in Aqueous-Solution. *Macromolecules*, **1987**. 20(3): p. 474-480.

55. Ikawa, T., et al., Interpolymer Complex between Poly(Ethylene Oxide) and Poly(Carboxylic Acid). *Journal of Polymer Science Part a-Polymer Chemistry*, **1975**. 13(7): p. 1505-1514.

56. Tsuchida, E. and Abe, K., Interactions between Macromolecules in Solution and Intermacromolecular Complexes. *Advances in Polymer Science*, **1982**. 45: p. 1-119.

57. Gohy, J.F., Varshney, S.K., and Jerome, R., Water-soluble complexes formed by poly(2-vinylpyridinium)-block-poly(ethylene oxide) and poly(sodium methacrylate)-block-poly(ethylene oxide) copolymers. *Macromolecules*, **2001**. 34(10): p. 3361-3366.

58. Holappa, S., et al., Self-Complexation of Poly(ethylene oxide)-block-poly(methacrylic acid) Studied by Fluorescence Spectroscopy. *Macromolecules*, **2004**. 37: p. 7008-7018.

59. Holappa, S., et al., Soluble polyelectrolyte complexes composed of poly(ethylene oxide)-block-poly(sodium methacrylate) and poly(methacryloyloxyethyl trimethylammonium chloride). *Polymer*, **2003**. 44(26): p. 7907-7916.

60. Holappa, S., et al., Solution properties of linear and branched block copolymers consisting of acidic and PEO blocks. *Macromolecules*, **2002**. 35(12): p. 4733-4738.

61. Vagberg, L.J.M., Cogan, K.A., and Gast, A.P., Light-Scattering Study of Starlike Polymeric Micelles. *Macromolecules*, **1991**. 24(7): p. 1670-1677.

62. Daoud, M. and Cotton, J.P., Star shaped polymers: a model for the conformation and its concentration dependence. *Journal de Physique*, **1982**. 43: p. 531-538.

63. Farinha, J.P.S., et al., Structure in tethered chains: Polymeric micelles and chains anchored on polystyrene latex spheres. *Langmuir*, **1998**. 14(9): p. 2291-2296.

64. Harada, A. and Kataoka, K., Effect of charged segment length on physicochemical properties of core-shell type polyion complex micelles from block ionomers. *Macromolecules*, **2003**. 36(13): p. 4995-5001.

65. Johnsson, M., Hansson, P., and Edwards, K., Spherical micelles and other self-assembled structures in dilute aqueous mixtures of poly(ethylene glycol) lipids. *Journal of Physical Chemistry B*, **2001**. 105(35): p. 8420-8430.

66. FitzGerald, P.A., Davey, T.W., and Warr, G.G., Micellar structure in gemini nonionic surfactants from small-angle neutron scattering. *Langmuir*, **2005**. 21(16): p. 7121-7128.

67. Tanford, C., Physical Chemistry of Macromolecules. **1962**, New York: John Wiley and Sons.

68. Kawaguchi, S., et al., Aqueous solution properties of oligo- and poly(ethylene oxide) by static light scattering and intrinsic viscosity. *Polymer*, **1997**. 38(12): p. 2885-2891.

69. Devanand, K. and Selser, J.C., Asymptotic-Behavior and Long-Range Interactions in Aqueous-Solutions of Poly(Ethylene Oxide). *Macromolecules*, **1991**. 24(22): p. 5943-5947.

70. Striolo, A. and Prausnitz, J.M., Osmotic second virial coefficient for linear and star poly(ethylene oxide). *Polymer*, **2001**. 42(10): p. 4773-4775.

71. Pisarcik, M., Devinsky, F., and Lacko, I., Aggregation number of alkanediyl-alpha,omega-bis(dimethylalkylammonium bromide) surfactants determined by static light scattering. *Colloids and Surfaces a-Physicochemical and Engineering Aspects*, **2000**. 172(1-3): p. 139-144.

72. Vlassopoulos, D., et al., Multiarm star polymers dynamics. *Journal of Physics-Condensed Matter*, **2001**. 13(41): p. R855-R876.

73. Vlassopoulos, D., Colloidal star polymers: Models for studying dynamically arrested states in soft matter. *Journal of Polymer Science Part B-Polymer Physics*, **2004**. 42(16): p. 2931-2941.

74. Semenov, A.N., et al., Dynamic structure of interacting spherical polymer brushes. *Langmuir*, **1999**. 15(2): p. 358-368.

75. Seghrouchni, R., et al., Controlling the dynamics of soft spheres: From polymeric to colloidal behavior. *Europhysics Letters*, **1998**. 42(3): p. 271-276.

76. Vlassopoulos, D., et al., Ordering and dynamics of soft spheres in melt and solution. *Faraday Discussions*, **1999**: p. 225-235.

77. Roovers, J., et al., Regular Star Polymers with 64 and 128 Arms - Models for Polymeric Micelles. *Macromolecules*, **1993**. 26(16): p. 4324-4331.

78. Barnes, H.A., Hutton, J.F., and Walters, K., An Introduction to Rheology. Rheology Series, ed. K. Walter. **1989**, Amsterdam: Elsevier.

79. Fleer, G.J., et al., Polymers at Interfaces. **1993**, London: Chapman & Hall.

80. Kawaguchi, M. and Takahashi, A., Polymer Adorption at Solid-Liquid Interfaces. *Advances in Colloid and Interface Science*, **1992**. 73: p. 219-317.

81. Ploehn, H.J., Structure of Adsorbed Polymer Layers - Molecular Volume Effects. *Macromolecules*, **1994**. 27(6): p. 1617-1626.

82. Edwards, S.F., The statistical mechanics of polymers with excluded volume. *Proceedings of the Physical Society*, **1965**. 85: p. 613-624.

83. de Gennes, P.G., Some conformation problems for long macromolecules. *Rep. Prog. Phys.*, **1969**. 32: p. 187-205.

84. de Gennes, P.G. and Pincus, P., Scaling theory of polymer adsorption: proximal exponent. *J. Physique. Lett.*, **1983**. 44: p. 241-246.

85. Killmann, E. and Reiner, M., Adsorption of poly-L-lysine and poly-L-glutamic acid on silica surfaces. *Tenside Surf. Det.*, **1996**. 33: p. 220-227.

86. Marques, C.M. and Joanny, J.F., Block Copolymer Adsorption in a Nonselective Solvent. *Macromolecules*, **1989**. 22(3): p. 1454-1458.

87. Marques, C., Joanny, J.F., and Leibler, L., Adsorption of Block Copolymers in Selective Solvents. *Macromolecules*, **1988**. 21(4): p. 1051-1059.

88. Rudolph, J., Patzsch, J., and Meyer, W.H., Interaction of acrylic diblock copolymers with aluminium oxide surfaces. *Colloids and Surface A: Physicochemical and Engineering Aspects*, **1994**. 86: p. 299-309.

89. Prosser, A.J. and Franses, E.I., Adsorption and Surface Tension of Ionic Surfactants at the Air-water Interface: Review and Evaluation of Equilibrium Models. *Colloids and Surfaces A: Physicochem. Eng. Aspects*, **2001**. 178(1-40).

90. Russel, W.B., Saville, D.A., and Schowalter, W.R., Colloidal Dispersions. **1989**, Cambridge: Cambridge University Press.

91. Bockris, J.O.M. and Reddy, A.K.N., Chapter 3, in Modern Electrochemistry. **1970**, Plenum Press: New York.

92. Quesada-Perez, M., Callejas-Fernandez, J., and Hidalgo-Alvarez, R., Probing electrostatic forces in colloidal suspensions through turbidity data. *Journal of Colloid and Interface Science*, **1999**. 217(1): p. 177-185.

93. Tran, Y., Auroy, P., and Lee, L.T., Determination of the structure of polyelectrolyte brushes. *Macromolecules*, **1999**. 32(26): p. 8952-8964.

94. Napper, D.H., Polymeric Stabilization of Colloidal Dispersions. **1983**, London: Academic Press.

95. Vincent, B., Chapter 7, in Solid/Liquid Dispersions, T.F. Tadros, Editor. **1987**, Academic Press: London.

96. Buscall, R. and Ottewill, R.H., Chapter 5, in Polymer Colloids, R. Buscall, T. Corner, and J.F. Stageman, Editors. **1985**, Elsevier Applied Science Publishers: London.

97. de Laat, A.W.M. and Schoo, H.F.M., Novel poly(vinyl ether) block copolymers: Adsorption from aqueous solutions on alpha-Fe2O3 (Hematite) and the mechanism of colloidal stabilization. *Journal of Colloid and Interface Science*, **1997**. 191(2): p. 416-423.

98. Milner, S.T., Polymer Brushes. *Science*, **1991**. 251(4996): p. 905-914.

99. Alexander, S., *Journal of Physics (Paris)*, **1977**. 38: p. 977.

100. Alexander, S., *Journal of Physics (Paris)*, **1977**. 38: p. 983.

101. de Gennes, P.G., Conformations of Polymers Attached to an Interface. *Macromolecules*, **1980**. 13: p. 1069-1075.

102. Cantor, R., Nonionic Diblock Copolymers as Surfactants between Immiscible Solvents. *Macromolecules*, **1981**. 14: p. 1186-1193.

103. Milner, S.T., Witten, T.A., and Cates, M.E., Theory of the Grafted Polymer Brush. *Macromolecules*, **1988**. 21(8): p. 2610-2619.

104. Dolan, A.K. and Edwards, S.F., Theory of the stabilization of colloids by adsorbed polymer. *Proceedings of the Royal Society of London Series A-Mathematical and Physical Sciences*, **1974**. 337: p. 509-516.

105. Cosgrove, T., et al., Configuration of Terminally Attached Chains at the Solid Solvent Interface - Self-Consistent Field-Theory and a Monte-Carlo Model. *Macromolecules*, **1987**. 20(7): p. 1692-1696.

106. Ploehn, H.J. and Russel, W.B., Interactions Between Colloidal Particles and Soluble Polymers. *Advances in Chemical Engineering*, **1990**. 15: p. 137-228.

107. Dan, N. and Tirrell, M., Self-Assembly of Block-Copolymers with a Strongly Charged and a Hydrophobic Block in a Selective, Polar-Solvent - Micelles and Adsorbed Layers. *Macromolecules*, **1993**. 26(16): p. 4310-4315.

108. Biver, C., et al., Neutral and Charged Polymer Brushes: A Model Unifying Curvature Effects from Micelles to Flat Surfaces. *Macromolecules*, **1997**. 30: p. 1787-1792.

109. Halperin, A., Polymeric Micelles - a Star Model. *Macromolecules*, **1987**. 20(11): p. 2943-2946.

110. Doliveira, J.M.R., et al., Chains Anchored onto Convex Spherical Surfaces - Modification of the Daoud and Cotton Model. *Macromolecules*, **1995**. 28(13): p. 4750-4752.

111. Hedden, R.C. and Bauer, B.J., Structure and dimensions of PAMAM/PEG dendrimer-star polymers. *Macromolecules*, **2003**. 36(6): p. 1829-1835.

112. Lee, A.S., et al., Characterizing the structure of pH dependent polyelectrolyte block copolymer micelles. *Macromolecules*, **1999**. 32(13): p. 4302-4310.

113. Ducker, W.A., Senden, T.J., and Pashley, R.M., Measurement of Forces in Liquids Using a Force Microscope. *Langmuir*, **1992**. 8(7): p. 1831-1836.

114. Lin, E.K. and Gast, A.P., Self consistent field calculations of interactions between chains tethered to spherical interfaces. *Macromolecules*, **1996**. 29(1): p. 390-397.

115. Likos, C.N., et al., Star polymers viewed as ultrasoft colloidal particles. *Physical Review Letters*, **1998**. 80(20): p. 4450-4453.

116. Jusufi, A., Watzlawek, M., and Lowen, H., Effective interaction between star polymers. *Macromolecules*, **1999**. 32(13): p. 4470-4473.

117. Witten, T.A. and Pincus, P.A., Colloid Stabilization by Long Grafted Polymers. *Macromolecules*, **1986**. 19(10): p. 2509-2513.

118. Ashcroft, N.W. and Mermin, N.D., Solid State Physics. **1976**, Fort Worth: Harcourt Brace College Publishers.

119. Likos, C.N., Soft matter with soft particles. *Soft Matter*, **2006**. 2(6): p. 478-498.

120. Batchelor, F.R.S., Wunsch, C., and Rice, J., Ferrohydrodynamics. **1985**, Cambridge: Cambridge University Press.

121. Rosensweig, R.E., Ferrohydrodynamics. **1985**, New York: Cambridge University Press.

122. Plaza, R.C., et al., Stability of dispersions of colloidal nickel ferrite spheres. *Journal of Colloid and Interface Science*, **2001**. 242(2): p. 306-313.

123. Chin, C.J., Yiacoumi, S., and Tsouris, C., Probing DLVO forces using interparticle magnetic forces: Transition from secondary-minimum to primary-minimum aggregation. *Langmuir*, **2001**. 17(20): p. 6065-6071.

124. Gregory, J., Chapter 8, in Solid/Liquid Dispersions, T.F. Tadros, Editor. **1987**, Academic Press: London.

125. Glover, S.M., et al., Bridging flocculation studied by light scattering and settling. *Chemical Engineering Journal*, **2000**. 80: p. 3-12.

126. Ashmore, M., Hearn, J., and Karpowicz, F., Flocculation of latex particles of varying surface charge densities by chitosans. *Langmuir*, **2001**. 17(4): p. 1069-1073.

127. Tadros, T.F., Chapter 11, in Solid-Liquid Dispersions, T.F. Tadros, Editor. **1987**, Academic Press: London. p. xx.

128. Yan, Y.D., et al., The structure and strength of depletion force induced particle aggregates. *Chemical Engineering Journal*, **2000**. 80(1-3): p. 23-30.

129. de Kruif, C.G., et al., Hard sphere colloidal dispersions: Viscosity as a function of shear rate and volume fraction. *Journal of Chemical Physics*, **1985**. 83(9): p. 4717-4725.

130. Tadros, T.F., et al., Correlation of the Rheology of Concentrated Dispersions with Interparticle Interactions. *Colloids and Surfaces A-Physicochemical and Engineering Aspects*, **1993**. 79(1): p. 105-114.

131. Kabanov, A.V. and Alakhov, V., Pluronic (R) block copolymers in drug delivery: From micellar nanocontainers to biological response modifiers. *Critical Reviews in Therapeutic Drug Carrier Systems*, **2002**. 19(1): p. 1-72.

132. Kabanov, A.V., Batrakova, E.V., and Alakhov, V., Pluronic block copolymers as novel polymer therapeutics for drug and gene delivery. *Journal of Controlled Release*, **2002**. 82: p. 189-212.

133. Batrakova, E.V., et al., Effect of Pluronic P85 on ATPase Activity of Drug Efflux Transporters. *Pharmaceutical Research*, **2004**. 21(12): p. 2226-2233.

134. Nakayama, M. and Okano, T., Intelligent thermoresponsive polymeric micelles for targeted drug delivery. *Journal of Drug Delivery Science and Technology*, **2006**. 16(1): p. 35-44.

135. Rangel-Yagui, C.O., Pessoa, A., and Tavares, L.C., Micellar solubilization of drugs. *Journal of Pharmacy and Pharmaceutical Sciences*, **2005**. 8(2): p. 147-163.

136. Torchilin, V.P., Block copolymer micelles as a solution for drug delivery problems. *Expert Opinion on Therapeutic Patents*, **2005**. 15(1): p. 63-75.

137. Kabanov, A.V., Batrakova, E.V., and Miller, D.W., Pluronic((R)) block copolymers as modulators of drug efflux transporter activity in the blood-brain barrier. *Advanced Drug Delivery Reviews*, **2003**. 55(1): p. 151-164.

138. Lavasanifar, A., Samuel, J., and Kwon, G.S., Poly(ethylene oxide)-block-poly(L-amino acid) micelles for drug delivery. *Advanced Drug Delivery Reviews*, **2002**. 54(2): p. 169-190.

139. Rosler, A., Vandermeulen, G.W.M., and Klok, H.A., Advanced drug delivery devices via self-assembly of amphiphilic block copolymers. *Advanced Drug Delivery Reviews*, **2001**. 53(1): p. 95-108.

140. Park, T.G., Jeong, J.H., and Kim, S.W., Current status of polymeric gene delivery systems. *Advanced Drug Delivery Reviews*, **2006**. 58(4): p. 467-486.

141. Gebhart, C.L., et al., Design and Formulation of Polyplexes Based on Pluronic-Polyethyleneimine Conjugates for Gene Transfer. *Bioconjugate Chemistry*, **2002**. 13: p. 913-944.

142. Bromberg, L., Temchenko, M., and Hatton, T.A., Smart microgel studies. Polyelectrolyte and drug-absorbing properties of microgels from polyether-modified poly(acrylic. *Langmuir*, **2003**. 19(21): p. 8675-8684.

143. Barreiro-Iglesias, R., et al., Solubilization and stabilization of camptothecin in micellar solutions of pluronic-g-poly(acrylic acid) copolymers. *Journal of Controlled Release*, **2004**. 97(3): p. 537-549.

144. Djordjevic, J., Barch, M., and Uhrich, K.E., Polymeric micelles based on amphiphilic scorpion-like macromolecules: Novel carriers for water-insoluble drugs. *Pharmaceutical Research*, **2005**. 22(1): p. 24-32.

145. Tao, L. and Uhrich, K.E., Novel amphiphilic macromolecules and their in vitro characterization as stabilized micellar drug delivery systems. *Journal of Colloid and Interface Science*, **2006**. 298(1): p. 102-110.

146. Tian, L., et al., Amphiphilic scorpion-like macromolecules: Design, synthesis, and characterization. *Macromolecules*, **2004**. 37(2): p. 538-543.

147. Sheihet, L., et al., Hydrophobic drug delivery by self-assembling triblock copolymer-derived nanospheres. *Biomacromolecules*, **2005**. 6(5): p. 2726-2731.

148. Vert, M. and Domurado, D., Poly(ethylene glycol): Protein-repulsive or albumin-compatible? *Journal of Biomaterials Science - Polymer Edition*, **2000**. 11(12): p. 1307-1317.

149. Iijima, M., et al., Core-polymerized reactive micelles from heterotelechelic amphiphilic block copolymers. *Macromolecules*, **1999**. 32(4): p. 1140-1146.

150. Kim, J.H., et al., Core-stabilized polymeric micelle as potential drug carrier: Increased solubilization of taxol. *Polymers for Advanced Technologies*, **1999**. 10(11): p. 647-654.

151. Guo, A., Liu, G.J., and Tao, J., Star polymers and nanospheres from cross-linkable diblock copolymers. *Macromolecules*, **1996**. 29(7): p. 2487-2493.

152. Zhang, Q., Remsen, E.E., and Wooley, K.L., Shell cross-linked nanoparticles containing hydrolytically degradable, crystalline core domains. *Journal of the American Chemical Society*, **2000**. 122(15): p. 3642-3651.

153. Weaver, J.V.M., et al., Preparation of shell cross-linked micelles by polyelectrolyte complexation. *Angewandte Chemie-International Edition*, **2004**. 43(11): p. 1389-1392.

154. Hermanson, G.T., Bioconjugate Techniques. **1996**, San Diego: Academic Press.

155. Bontha, S., Kabanov, A.V., and Bronich, T.K., Polymer micelles with cross-linked ionic cores for delivery of anticancer drugs. *Journal of Controlled Release*, **2006**. 114(2): p. 163-174.

156. Gupta, A.K. and Gupta, M., Synthesis and surface engineering of iron oxide nanoparticles for biomedical applications. *Biomaterials*, **2005**. 26(18): p. 3995-4021.

157. Cheng, F.Y., et al., Characterization of aqueous dispersions of Fe3O4 nanoparticles and their biomedical applications. *Biomaterials*, **2005**. 26(7): p. 729-738.

158. hihIto, A., et al., Medical application of functionalized magnetic nanoparticles. *Journal of Bioscience and Bioengineering*, **2005**. 100(1): p. 1-11.

159. Neuberger, T., et al., Superparamagnetic nanoparticles for biomedical applications: Possibilities and limitations of a new drug delivery system. *Journal of Magnetism and Magnetic Materials*, **2005**. 293(1): p. 483-496.

160. Wassel, R.A., et al., Dispersion of super paramagnetic iron oxide nanoparticles in poly(D,L-lactide-co-glycolide) microparticles. *Colloids and Surfaces a-Physicochemical and Engineering Aspects*, **2007**. 292(2-3): p. 125-130.

161. Schulze, K., et al., Uptake and biocompatibility of functionalized poly(vinylalcohol) coated superparamagnetic maghemite nanoparticles by synoviocytes in vitro. *Journal of Nanoscience and Nanotechnology*, **2006**. 6(9-10): p. 2829-2840.

162. Lee, H., et al., Antibiofouling polymer-coated superparamagnetic iron oxide nanoparticles as potential magnetic resonance contrast agents for in vivo cancer imaging. *Journal of the American Chemical Society*, **2006**. 128(22): p. 7383-7389.

163. Leuschner, C., et al., LHRH-conjugated magnetic iron oxide nanoparticles for detection of breast cancer metastases. *Breast Cancer Research and Treatment*, **2006**. 99(2): p. 163-176.

164. Petri-Fink, A., et al., Development of functionalized superparamagnetic iron oxide nanoparticles for interaction with human cancer cells. *Biomaterials*, **2005**. 26(15): p. 2685-2694.

165. Kim, D.K., et al., Characterization and MRI study of surfactant-coated superparamagnetic nanoparticles administered into the rat brain. *Journal of Magnetism and Magnetic Materials*, **2001**. 225(1-2): p. 256-261.

166. Stark, D.D., et al., Superparamagnetic Iron-Oxide - Clinical-Application as a Contrast Agent for Mr Imaging of the Liver. *Radiology*, **1988**. 168(2): p. 297-301.

167. Okuhata, Y., Delivery of diagnostic agents for magnetic resonance imaging. *Advanced Drug Delivery Reviews*, **1999**. 37(1-3): p. 121-137.

168. Hornak, J.P. The Basics of MRI. **1996**; Available from: http://www.cis.rit.edu/htbooks/mri/.

169. Cornell, R.M. and Schwertmann, Y., The Iron Oxides. **1996**, Weinheim: VCH.

170. Caravan, P., Strategies for increasing the sensitivity of gadolinium based MRI contrast agents. *Chemical Society Reviews*, **2006**. 35(6): p. 512-523.

171. Mornet, S., et al., Magnetic nanoparticle design for medical diagnosis and therapy. *Journal of Materials Chemistry*, **2004**. 14(14): p. 2161-2175.

172. Boyer, R., Concepts in Biochemistry. **1999**, Pacific Grove, CA: Brooks/Cole Publishing Company.

173. Tirrell, J.G., et al., Chapter 3, in Protein-Based Materials, K. McGrath and D. Kaplan, Editors. **1997**, Birkhauser: Boston.

174. Kaiser, K. and Murray, N.E., Chapter 2, in DNA Cloning 1 Core Techniques, S.M. Glover and B.D. Hames, Editors. **1995**, Oxford University Press: Oxford.

175. Benhar, I., Biotechnological applications of phage and cell display. *Biotechnology Advances*, **2001**. 73: p. 305-318.

176. Parmley, S.F. and Smith, G.S., Antibody-selectable filamentous fd phage vectors: affinity purification of target genes. *Gene*, **1988**. 73: p. 305-318.

177. Samuelson, P., et al., Display of proteins on bacteria. *Journal of Biotechnology*, **2002**. 96: p. 129-154.

178. Invitrogen Life Technologies FliTrx(TM) Random Peptide Display Library Version G. **2002**.

179. Lu, Z., et al., Expression of thioredoxin random peptide libraries on the Escherichia coli cell surface as functional fusions to flagellin: a system designed for exploring protein-protein interactions. *Bio/Technology*, **1995**. 13: p. 366-372.

180. Barbas, C.F., Rosenblum, J.S., and Lerner, R.A., Direct selection of antibodies that coordinate metals from semisynthetic combinatorial libraries. *Proc. Natl. Acad. Sci. USA*, **1993**. 90: p. 6385-6389.

181. Kjaegaard, K., et al., Sequestration of zinc oxide by fimbrial designer chelators. *Applied and Environmental Microbiology*, **2000**. 66: p. 10-14.

182. Kjaegaard, K., Schembri, M.A., and Klemm, P., Novel Zn2+ -chelating peptides selected from a fimbria-displayed random peptide library. *Applied and Environmental Microbiology*, **2001**. 67: p. 5467-5473.

183. Kotrba, P., et al., Enhanced Bioaccumulation of heavy metal ions by bacterial cells due to surface display of short metal binding peptides. *Appl. Environ. Microbiol.*, **1999**. 65: p. 1092-1098.

184. Brown, S., Engineered iron oxide-adhesion mutants of the Escherichia coli phage lambda receptor. *Proc. Natl. Acad. Sci. USA*, **1992**. 89: p. 8651-8655.

185. Sousa, C., Cebolla, A., and de Lorenzo, V., Enhanced metalloadsorption of bacterial cells displaying poly-His peptides. *Nature Biotechnology*, **1996**. 14: p. 1017-1020.

186. Pazirandeh, M., Wells, B.M., and Ryan, R.L., Development of bacterium-based heavy metal biosorbents: enhanced uptake of cadmium and mercury by Escherichia coli expressing a metal binding motif. *Applied and Environmental Microbiology*, **1998**. 64: p. 4068-4072.

187. Chen, S. and Wilson, D.B., Construction and characterization of escherichia coli genetically engineered for bioremediation of Hg2+ -contaminated environments. *Appl. Environ. Microbiol.*, **1997**. 63: p. 2442-2445.

188. Whaley, S.R., et al., Selection of peptides with semiconductor binding specificity for directed nanocrystal assembly. *Nature*, **2000**. 405: p. 665-668.

189. Naik, R.R., et al., Silica-precipitating peptides isolated from a combinatorial phage display peptide library. *J. Nanosci. Nanotech.*, **2002**. 2: p. 95-100.

190. Ferrari, F.A. and Capello, J., Chapter 2, in Protein-Based Materials, K. McGrath and D. Kaplan, Editors. **1997**, Birkhauser: Boston.

191. Lohe, A.R. and Brutlag, D.L., Multiplicity of satellite DNA sequences in Drosophila Melanogaster. *Proc. Natl. Acad. Sci. USA*, **1986**. 83: p. 696-700.

192. Kroczek, R.A., Southern and Northern Analysis. *Journal of Chromatography*, **1993**. 618: p. 133-145.

193. Finsy, R., Particle Sizing by Quasi-Elastic Light-Scattering. *Advances in Colloid and Interface Science*, **1994**. 52: p. 79-143.

194. Burchard, W., Polymer Characterization: Quasi-Elastic and Elastic Light Scattering. *Makromolekulare Chemie - Macromolecular Symposia*, **1988**. 18: p. 1-35.

195. Lindner, H., Fritz, G., and Glatter, O., Measurements on concentrated oil in water emulsions using static light scattering. *Journal of Colloid and Interface Science*, **2001**. 242(1): p. 239-246.

196. Quirantes, A., Plaza, R., and Delgado, A., Static light scattering study of size parameters in core-shell colloidal systems. *Journal of Colloid and Interface Science*, **1997**. 189(2): p. 236-241.

197. Wolff, D., et al., Globular shape of high molar mass inulin revealed by static light scattering and viscometry. *Polymer*, **2000**. 41(22): p. 8009-8016.

198. Lehner, D., et al., Characterization of enzymatically induced aggregation of casein micelles in natural concentration by in situ static light scattering and ultra low shear viscosimetry. *Journal of Colloid and Interface Science*, **1999**. 213(2): p. 445-456.

199. Malvern_Instruments, CGS-3 User Manual, Chapter 8. **2005**.

200. Nicolai, T. and Cocard, S., Dynamic light-scattering study of aggregating and gelling colloidal disks. *Journal of Colloid and Interface Science*, **2001**. 244(1): p. 51-57.

201. Narayanan, J., et al., Gelation of aqueous pectin solutions: A dynamic light scattering study. *Journal of Colloid and Interface Science*, **2002**. 245(2): p. 267-273.

202. Tanaka, S., et al., pH-dependent oligomerization of BPTI in undersaturated and supersaturated solutions studied by dynamic light scattering. *Journal of Crystal Growth*, **2002**. 237: p. 289-294.

203. Moradian-Oldak, J., et al., Self-assembly properties of recombinant engineered amelogenin proteins analyzed by dynamic light scattering and atomic force microscopy. *Journal of Structural Biology*, **2000**. 131(1): p. 27-37.

204. Sommer, C., Pedersen, J.S., and Stein, P.C., Apparent Specific Volume Measurements of Poly(ethylene oxide), Poly(butylene oxide), Poly(propylene oxide), and Octadecyl Chains in the Micellar State as a Function of Temperature. *Journal of Physical Chemistry B*, **2004**. 108: p. 6242-6249.

205. Wen, X.G. and Verrall, R.E., Temperature Study of Sound Velocity and Volume-Related Specific Thermodynamic Properties of Aqueous Solutions of Poly(ethylene oxide)-Poly(propylene oxide)-Poly(ethylene oxide) Triblock Copolymers. *Journal of Colloid and Interface Science*, **1997**. 196: p. 215-223.

206. Soni, S.S., et al., Micellar structure of silicone surfactants in water from surface activity, SANS and viscosity studies. *Journal of Physical Chemistry B*, **2002**. 106(10): p. 2606-2617.

207. Ashcroft, N.W. and Lekner, J., *Physics Review*, **1966**. 145: p. 83-90.

208. Kinning, D.J. and Thomas, E.L., Hard-Sphere Interactions between Spherical Domains in Diblock Copolymers. *Macromolecules*, **1984**. 17: p. 1712-1718.

209. Pedersen, J.S. and Gerstenberg, M.C., Scattering Form Factor of Block Copolymer Micelles. *Macromolecules*, **1996**. 29: p. 1363-1365.

210. Svaneborg, C. and Pedersen, J.S., Form Factors of Block Copolymer Micelles with Excluded-Volume Interactions of Corona Chains Determined by Monte Carlo Simulations. *Macromolecules*, **2002**. 26: p. 1028-1037.

211. Higgins, J.S. and Benoit, H.C., Polymers and Neutron Scattering. Oxford Series on Neutron Scattering in Condensed Matter, ed. S.W. Lovesey and E.W.J. Mitchell. **1994**, Oxford: Clarendon Press.

212. Roe, R.-J., Methods of X-ray and Neutron Scattering in Polymer Science. Topics in Polymer Science, ed. J.M. Mark. **2000**, New York: Oxford University Press.

213. Guinier, A. and Fournet, G., Small-Angle Scattering of X-rays. **1955**, New York: John Wiley and Sons.

214. Percus, J.K. and Yevick, G.J., Analysis of Classical Statistical Mechanics by Means of Collective Coordinates. *The Physical Review*, **1958**. 110(1): p. 1-13.

215. Pedersen, J.S., Structure factors effects in small-angle scattering from block copolymer micelles and star polymers. *Journal of Chemical Physics*, **2001**. 114(6): p. 2839-2846.

216. Pedersen, J.S., et al., A Small-Angle Neutron and X-ray Contrast Variation Scattering Study of the Structure of Block Copolymer Micelles: Corona Shape and Excluded Volume Interactions. *Macromolecules*, **2003**. 36: p. 416-433.

217. Benoit, H.C., On the effect of branching and polydispersity on the angular distribution of the light scattered by gaussian coils *Journal of Polymer Science*, **1953**. 11: p. 507-510.

218. Marques, C.M., et al., Scattering from solutions of star polymers. *European Physical Journal B*, **1998**. 3(3): p. 353-358.

3 Solution properties and characterization of water-soluble triblock copolymers

3.1 Abstract

Symmetric A-B-A block copolymers consisting of poly(ethylene oxide) tailblocks and a polyurethane center block containing carboxylic acid groups have been shown to form micelles in aqueous solutions. The state of protonation of the acid groups can be adjusted by pH, thus affecting micellization. At low pH (2-6), neutralization of the carboxylic acid groups permitted hydrophobic interactions to drive the micellization, whereas at high pH (8), only unimers were present. Hydrodynamic radius, aggregation number, and second virial coefficient were measured using dynamic and static light scattering while varying pH, polymer composition, and temperature. A range of triblock compositions was studied - no micelles were formed for the triblock having the largest mass fraction of PEO (0.96) whereas micelles formed for all other PEO fractions studied (0.72-0.90). The effect of temperature in the range of 25-65°C on the micelle size and aggregation number depended on the composition. For most of the polymers (PEO mass fraction = 0.84-0.90), an increase in temperature caused a decrease in size, likely due to the disruption of hydrogen bonding in the corona and reduced solvation of the PEO corona chains. For one polymer (PEO mass fraction = 0.75), the size remained constant and the aggregation number increased with temperature. The measured micelle sizes were in semi-quantitative agreement with the density distribution model for star molecules.

3.2 Keywords

triblock copolymer; micelle; light scattering; SLS; DLS; refractive index increment; hydrophobicity; self-assembly; poly(ethylene oxide)

3.3 Introduction

Micelles which self-assemble from block copolymers are useful in a number of applications, such as emulsification, stabilization, drug delivery, and gene therapy.[1-5] There is a large body of literature describing studies of micellar systems where the

micellar cores consist of nonionic, insoluble polymer chains, such as poly(ethylene oxide)-poly(propylene oxide)-poly(ethylene oxide) triblocks[1, 6-14] poly(ethylene oxide)-poly(butylene oxide) diblocks,[7, 15] and poly(styrene)-poly(ethylene oxide) diblock[16-19] copolymers. However, the literature is much more limited on micelle-forming ionic block copolymers in water, particularly for those in which the ionic block forms the center of the micelle. There are some examples of aggregates composed of diblock copolymers where an ionic block forms a micellar core when neutralized. One such system concerned the pH-sensitive assembly of poly(methacrylic acid)-g-poly(ethylene glycol).[20] At low pH, shrinking of the aggregates was observed and was attributed to intramolecular complexes due to hydrogen bonding along the backbone. Another such poly(methacrylic acid)-g-poly(ethylene glycol) system was examined as an aqueous reversible emulsifier.[21, 22] Acid conditions caused hydrogen-bonding between the backbone and grafts to form hydrophobic segments. Li et al.[23] examined the formation of nanoaggregates of poly(ethylene oxide)-*b*-poly(methacrylate) (PEO-PMA) which formed when the PMA block was neutralized using alkaline earth metals. These systems formed a neutralized polyion core with a PEO corona. Such polymers may also be used for stabilizing solutions. For instance, Moeser and Hatton[24, 25] used PEO-PPO-PEO modified with poly(acrylic acid) (PAA) to stabilize magnetite particles in order to extract organics from water.

There are also several examples of micelle-forming amphiphilic block copolymers in aqueous solutions in which an ionic block is the hydrophilic corona block. Matsuoka et al.[26-28] describe micelle formation for several hydrophilic-hydrophobic diblock copolymers in which the corona chains were polysulfonic acids and the core block was poly(diethylsilacyclobutane). These novel copolymers micellized readily in water, yet did not show surface activity, i.e. did not form a Gibbs monolayer at the air-water interface. This was partly attributed to strong electrostatic repulsion between tailblock chains causing a destabilization in the monolayer. Examples may also be found of micelles with an ionic core;[29] however, these were in a hydrophobic solvent. Such polymers may be used for controlled synthesis of metal nanoparticles.[30] A similar study

involved trapping of water in the ionic core of a block copolymer micelle in a hydrocarbon solvent.[31]

The use of ion-containing polymers for biomedical applications such as drug delivery[32-40] and gene delivery[41, 42] has been examined by many investigators. PEO-containing polymers are especially interesting, as PEO does not trigger an immune response in-vivo and can also make other foreign materials less detectable by the immune system.[43] Micelles are also particularly promising, as they self-assemble into structures capable of encapsulating drugs with a range of solubilities. For instance, Hatton et al.[44, 45] examined copolymers consisting of Pluronic with crosslinked grafted poly(acrylic acid) as drug delivery vehicles. These were capable of encapsulating various hydrophobic drugs including Taxol, estradiol, progesterone, and camptothecin. Uhrich et al.[46-48] synthesized amphiphilic "scorpion-like" polymers with very low critical micelle concentrations and examined encapsulation and release of the drug indomethacin. These macromolecules have a hydrophilic chain for stabilization and a backbone with hydrophobic side chains which form the core of self-assembled micelles. Sheihet et al.[49] prepared ABA triblock copolymers with PEO A blocks and oligomers of suberic acid and desaminotyrosyl-tyrosine esters. These self-assembled in solution and were capable of solubilizing paclitaxel, a hydrophobic drug. Bronich et al.[50] used Ca^{2+} to cause PEO-*b*-PMA polymers to form micelles which were subsequently cross-linked to form sterically stabilized hydrogel particles of approximately 100 nm in size. The anticancer drug cisplatin was incorporated into these particles for release.

The matter of interactions between star polymers in semi-dilute and concentrated solutions has been addressed in a rich body of literature. In particular, Vlassopoulos et al. have examined multiarm star polymers in solution using dynamic scattering and viscometry techniques and have characterized interactions in semi-dilute solutions in terms of a structure factor.[51-56] Description of micelle interactions in dilute solutions using a second virial coefficient is addressed in another chapter.

This paper describes a solution study of unique materials that self-assemble with ionic, hydrophobic cores and was motivated by the desire to understand the behavior of such materials. Self-assembly with an ionic block in the center without the presence of multi-valent counterions is rare. These triblock copolymers consist of a symmetric PEO block at either end with a relatively hydrophobic polyurethane center block that contains a carboxylic acid.[57] This unique combination leads to an interesting balance between hydrogen bonding, hydrophobicity and charge effects in solution. Under conditions when the charge is suppressed such as at low pH and/or high ionic strength, the polymer chains self-assemble into micelles, whereas unimers alone are present under conditions where charge effects are important, such as high pH and low ionic strength. Light scattering is a valuable tool for examining behavior of polymers in solution,[58, 59] and has been used extensively to study micelle-forming systems of copolymers and low molecular weight surfactants. Static and dynamic light scattering data was used to determine the conditions under which these polymers form micelles in aqueous solution and to examine variations in size and aggregation number under these conditions. The results were also compared to a density distribution model by Vagberg,[60] which has been utilized for several other systems.[61-63]

3.4 Materials and Methods

3.4.1 Chemicals

PEO triblock copolymers (Figure 3-1) were synthesized as previously described.[57] In brief, synthesis of the copolymers consisted of several steps. First, a PEO oligomer was end-capped with excess isophorone diisocyanate. This was then chain-extended with bis(hydroxymethyl)propionic acid in dimethylformamide (DMF) with dibutyltin dilaurate as the catalyst. The reaction was monitored using Fourier transform infrared spectroscopy (FTIR) to observe the disappearance of the isocyanate peak at 2260 cm^{-1}. After removing the DMF, the polymer was dissolved in chloroform, washed three times with water, added to an excess of cold hexane, and isolated by filtration. The resulting triblock copolymers were characterized using ^{1}H and quantitative ^{13}C nuclear magnetic resonance (NMR), FTIR, and titration (to determine the concentration of COOH groups).

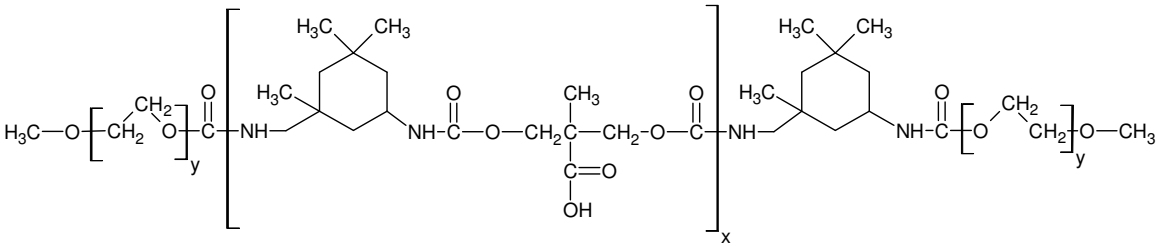

Figure 3-1. Structure of a representative triblock copolymer with PEO tail blocks and a polyurethane center block that contains carboxylic acid groups.

A series of these copolymers is described in overview in the table below. The nomenclature adopted herein for these triblock copolymers comprises the molecular weights of the PEO end blocks and the average number of carboxylic acid groups (derived by titration) in the central polyurethane section. For example, a 1930-3.1-1930 triblock consists of PEO end blocks with a number average molecular weight (M_n) of 1930 g/mol, and a polyurethane central block having an average of 3.1 carboxylic acid groups (DP).

Table 3-1. Properties of triblock copolymers.

Copolymer	M_n[a]	DP center[b]	DP tail	Mass fraction PEO
1930-3.1-1930	5160	3.1	44	0.75
4845-2.5-4845	10785	2.5	110	0.90
4845-4.7-4845	11540	4.7	110	0.84

[a]PEO tail block M_n from ^{1}H NMR. [b]Average number of COOH in the polyurethane center block from ^{13}C NMR.[57]

All solutions were prepared with deionized water from a NANOpure II ion exchanger (Barnstead) having a resistance above 17 MΩ·cm. ACS reagent grade sodium chloride (Fisher) was used as received to adjust background ionic strength. All pH adjustments were made using sodium hydroxide and hydrochloric acid (Fisher) as received or after dilution with deionized water.

3.4.2 Dynamic Light Scattering

Dynamic light scattering (DLS), also known as quasi-elastic light scattering, was used to study particle diffusion.[59] DLS was performed with a Malvern CGS-3 multi-angle goniometer and autocorrelator to investigate micellization and determine the hydrodynamic radii of both micelles and single triblock chains or unimers.

Hydrodynamic radii were determined using the Stokes-Einstein relationship, in which k is Boltzmann's constant, T is the temperature, η is the solvent viscosity, D_o is the diffusion coefficient, and R_H is the hydrodynamic radius:

$$R_H = \frac{kT}{6\pi\eta D_o}$$

Eq. 3-1

The Stokes-Einstein equation is valid in a range of particle sizes for which Brownian motion keeps the particles in suspension. The viscosity was corrected for temperature by the following equation, in which A and B are solvent-dependent parameters. This is essential since the viscosity is inversely proportional to the calculated hydrodynamic radius. For water, the expression used was:

$$\log_{10} \eta = A + \frac{B}{T} + CT + DT^2$$

Eq. 3-2

Measurements were made at a wavelength of 632.8 nm and at angles between 120° and 150°. Both static and dynamic light scattering measurements were made simultaneously. The DLS data were analyzed using an algorithm based on CONTIN, which is a program designed for inversion of noisy equations via a constrained regularization algorithm as described by Provencher.[64, 65] The basic features of CONTIN are prior knowledge about the data (that it is non-negative in this case) and parsimony (the solution with the fewest and smoothest peaks is probably best). The CGS-3 also employs a multiple-tau correlation technique where the delay time increment ($\Delta\tau$) between channels varies, which reduces error due to noise.[66]

DLS is typically performed using an intensity autocorrelation, in which a Fourier transform is performed on the spectrum. This yields an autocorrelation function $G_2(\tau)$, in which the intensity I(t) is measured at an arbitrary time, t. After a time delay, τ, the intensity is measured again. The function $G_2(\tau)$ is given by an average of the product of the intensities at the two times as described by:

$$G_2(\tau) = \langle I(t) \cdot I(t+\tau) \rangle$$

Eq. 3-3

This may then be modeled by using the following equation, in which A and B are instrumental factors and Γ is the decay rate.

$$G_2(\tau) = \int_0^\infty G(\Gamma, t) e^{-2\Gamma\tau} d\Gamma$$

Eq. 3-4

This may be used to determine the diffusion coefficient, D, according to:

$$\Gamma = Dq^2$$

Eq. 3-5

where the scattering vector, q, is calculated according to the following equation, in which λ is the wavelength, n is the refractive index of the sample, and θ is the measurement angle.[67]

$$q = \frac{4\pi n}{\lambda} \sin\left(\frac{\theta}{2}\right)$$

Eq. 3-6

It is then possible to use a correlation between the diffusion coefficient and the particle size, such as the Stokes-Einstein relationship (Eq. 3-1), which is valid for non-interacting spherical particles. If one assumes a non-draining sphere, the hydrodynamic radius may be related to the radius of gyration, R_g, by the following:[68]

$$R_H = 0.875 R_g$$

Eq. 3-7

For linear chain polymers, the radius of gyration may be approximated by a number of chain statistical models, including the freely jointed chain model:

$$\langle R^2 \rangle = nl^2 C_\infty$$

Eq. 3-8

$$\left\langle R_g^2 \right\rangle = \frac{\left\langle R^2 \right\rangle}{6}$$

Eq. 3-9

3.4.3 Static Light Scattering

Static light scattering (SLS) was also performed on the Malvern CGS-3 multi-angle goniometer. The static scattering data were analyzed by the following equation:

$$Kc/R_\theta = \frac{1}{P(\theta)}\left[1/M_w + 2A_2 c\right]$$

Eq. 3-10

in which c is the concentration of the sample, M_w is the weight-average molecular weight, A_2 is the second virial coefficient, $P(\theta)$ is the form factor, and K is an optical constant. The Rayleigh ratio, R_θ, is defined as

$$R_\theta = \frac{I_A \tilde{n}_o^2}{I_T \tilde{n}_T^2} R_T$$

Eq. 3-11

where I_A is the difference in intensity between the scattering sample and the solvent, I_T is the scattering intensity of toluene, $\tilde{n}_o$ is the solvent refractive index, $\tilde{n}_T$ is the refractive index of toluene, and R_T is the Rayleigh ratio of toluene. The optical constant, K, for the instrument is defined by

$$K = \frac{4\pi^2 \left(n_{solvent} \frac{dn}{dc} \right)^2}{\lambda^4 N_A}$$

Eq. 3-12

in which dn/dc is the refractive index increment and N_A is Avogadro's number.

Due to the small size of the micelles relative to the wavelength of the laser (633 nm), SLS analysis could be done at a single angle using a Debye plot, which requires that $q*R_g<<1$ so that the form factor $P(\theta)$ approaches unity and therefore Eq. 3-10 reduces to:

$$Kc/R_\theta = 1/M_w + 2A_2C$$

Eq. 3-13

As a check on the use of the Debye plot, measurements were made at several angles. This also enabled identification of any bad data due to flaws in the glass tubes.

3.4.4 Refractive Index Increment

The refractive index increment (dn/dc) was measured using an Optilab rEX by Wyatt Technology. The instrument operates at a wavelength of 685 nm and has a reference and sample cell. The reference cell was filled in each case with the solvent and isolated by a valve. Samples in the range of 1-10 mg/mL were then injected through the sample cell at a flow rate of 0.1 mL/min using a syringe pump. The samples used for dn/dc were prepared in the same manner as those used for light scattering. No filtration was used once the samples had been prepared, since light scattering on these samples had already shown them to be free of large particulates which might plug the flow cell. The relative refractive index was measured for each concentration and then dn/dc was calculated.

3.4.5 Sample Preparation for Light Scattering

Sample preparation is critical for light scattering.[58] The presence of dust or other contaminants severely affects the quality of the data. Dust is especially problematic, as it is typically on the order of 1000-10,000 nm in size, and contributes strongly to the intensity of scattered light. The two means of dust removal employed in this study were filtration and centrifugation. Both proved effective in removing most of the dust. Centrifugation was used most frequently as it had less effect on concentration.

Stock solutions were prepared by dissolving a known mass of sample (as measured by a Sartorius analytical scale) in a volumetric flask. The solvent was pre-filtered using two Whatman Anotop alumina filters (pore size 20 nm) directly in series on a syringe. The stock solutions were allowed to shake overnight, then diluted using a 1 mL volumetric

pipette and pre-filtered solvent. Adjustments in pH were performed using NaOH and HCl on the solvent and, as needed, the stock solution. The pH of individual samples was spot-checked after the light scattering measurements (when introduction of dust was no longer critical) to ensure that pH drift had not occurred.

In order to perform the centrifugation, 1.5 mL of each sample was placed into a plastic centrifuge tube. After centrifugation, a disposable pipette was used to remove the top 1 ml of sample while disturbing the sample as little as possible. In order to do this, the pipette tip was placed just slightly above the ending level in the tube. This was found to be a more effective means of eliminating dust in the sample as compared to decanting, presumably due to less disturbance of the sample. The samples were centrifuged on a Fisher Scientific accuSpin Micro for 60 minutes at 12,000 rpm. The relative centrifugal force (RCF) may be calculated by the following relationship, in which r is the radial distance from the center of rotation in cm and n is the speed of rotation in rpm.

$$RCF = 11.18 * \left(\frac{n}{1000} \right)^2 * r$$

Eq. 3-14

For the rotor used, r varies from 5.9 cm at the meniscus to 8.5 cm at the tip of the 1.5 mL plastic centrifuge tube. This corresponds to a range of 9498-13684 g.

Light scattering samples were prepared in disposable glass culture tubes with plastic caps. Dust was removed from these as much as possible by upending the tubes over a glass pipette passing through a rubber stopper in a round-bottomed flask containing boiling water. The steam was allowed to condense inside the culture tube and run out for about 10 seconds per tube, flushing dust particles away. The tubes were then placed upside down in a metal rack and heated to 50°C in an oven for approximately 45 minutes to dry them. The plastic caps were also held briefly over the stream of steam in order to flush out dust. These were placed on a watchglass facedown and dried in the same manner. The tubes and caps remained in the inverted position until just before the sample was pipetted from the centrifuge tube to the culture tube, whereupon they were immediately capped and marked.

These sample preparation procedures greatly reduced the appearance of dust in the DLS and SLS results. To deal with any remaining dust contamination, each sample was measured at several angles (120, 130, 140, and 150) and each run consisted of three 10-second measurements. Measuring each angle in triplicate allowed identification of individual runs in which dust was a problem. Measuring each sample at multiple angles made it obvious when there was a flaw in the glass tube causing an anomaly at a particular angle. The high angles were chosen to minimize the impact of large impurities or dust on the measured molecular weight.

3.5 Results and Discussion

3.5.1 Refractive index increment

The refractive index increment (RRI) or dn/dc was measured for each of the polymers in 0.1M NaCl at pH 2, 4, and 6 in duplicate. The Optilab rEX instrument has an operating temperature range of 25-50°C, so measurements were made at 25, 35, and 45°C. Light scattering with the CGS-3 was also performed at 55 and 65°C, so a linear extrapolation was made for those cases. RRI is determined by measuring the relative refractive index of a series of concentrations of polymer solutions as compared to the reference liquid (0.1M NaCl in water for this case). The refractive index, n, is plotted versus concentration; the slope of this linear plot is the refractive index increment.

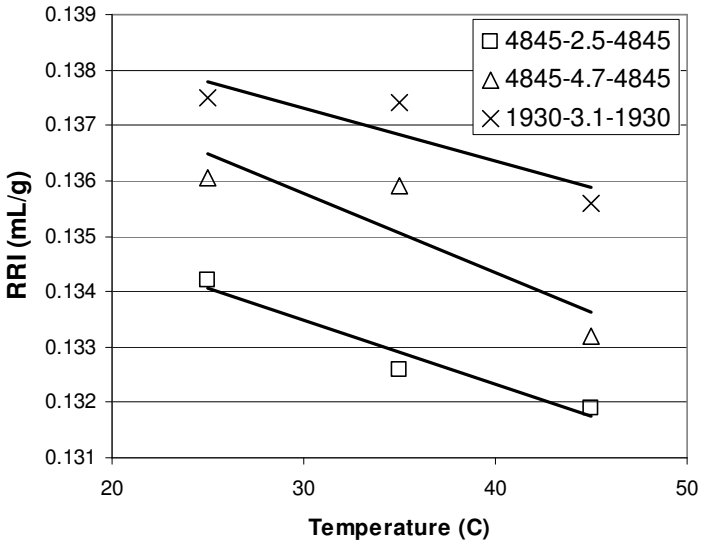

Figure 3-2. dn/dc for polymers in 0.1M NaCl at pH 2.

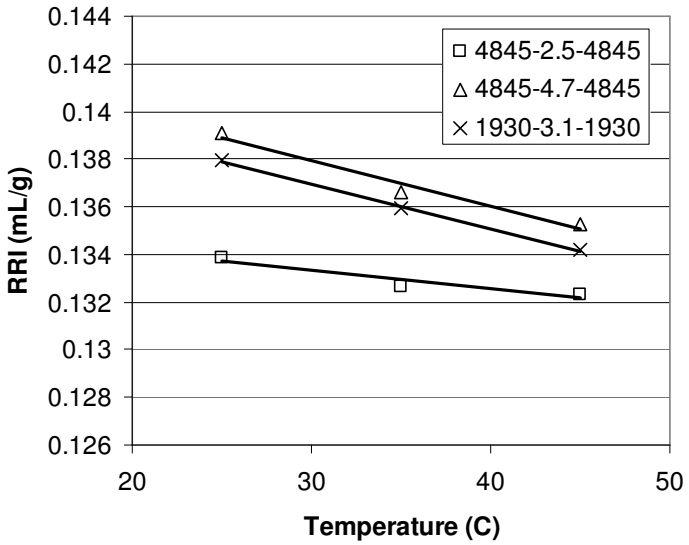

Figure 3-3. dn/dc for polymers in 0.1M NaCl at pH 4.

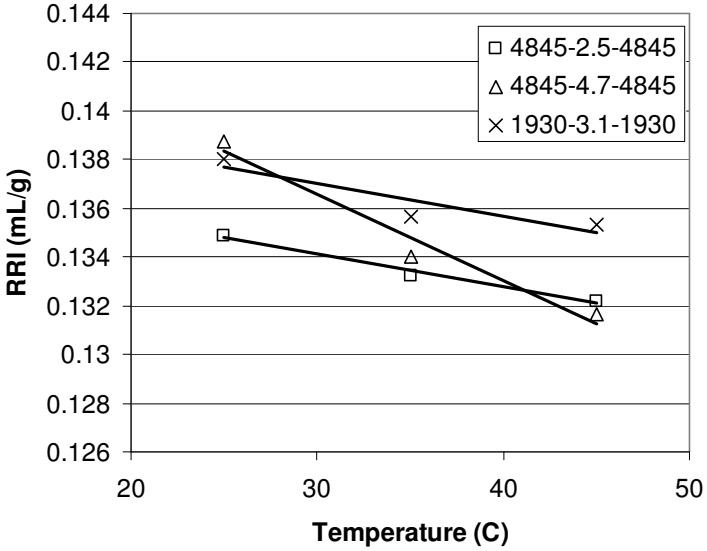

Figure 3-4. dn/dc for polymers in 0.1M NaCl at pH 6.

Measured values of dn/dc for the triblock copolymers were between 0.128 and 0.143 mL/g, depending on triblock composition and temperature. These values are shown in Figure 3-2 through Figure 3-4. By comparison, typical dn/dc values for aqueous solutions of PEO homopolymers with molecular weights between 1200 and 31,000 g/mol in water at a wavelength of 546 nm are typically between 0.128 and 0.141 mL/g.[58]

3.5.2 DLS for determination of hydrodynamic radius

The hydrodynamic radius is calculated from the diffusion coefficient based on the Stokes-Einstein equation (Eq. 3-1). The ALV-5000 multiple tau digital correlator was used to compute real-time photon correlations in 35 channels. These channels each corresponded to a time interval, t_s. The software counted the photons over each of these time intervals in parallel. A CONTIN algorithm is applied to describe the mean and distribution of the size peaks. In this work, an intensity-based distribution is always applied in order to determine the mean values of the scattering entities. Since the intensity distribution is calculated directly from the correlation function, it is desirable to report size values based on this. It is also possible to translate this to a volume distribution. However, there are two main drawbacks to this approach. First, any additional manipulation of the data will propagate errors in the initial measurements. Second, Mie theory is based on several assumptions: that the particles are spherical, that

the density is homogeneous throughout the particle, that the optical properties of the particles are known, and that there is no error in the intensity distribution. This becomes relevant due to a small fraction of larger aggregates in the scattering distribution. Practically, the volume distribution may be of assistance in describing proportions of scattering entities in a multi-modal distribution, but is less useful than the intensity distribution in describing absolute sizes. The intensity distribution, conversely, is not very useful for describing relative amounts, given the r^6 relationship between size and intensity. In this work, the size is reported as the mean of the peaks in the intensity-weighted distribution; the relative amounts are reported as the percent area of the peaks of the volume-weighted distribution.

These copolymers form two sorts of assemblies: a primary aggregate which is in a size range typical for micelles and a secondary aggregate. This secondary aggregate is believed to be the result of PEO-PEO interactions between micelles, as PEO is known to self-aggregate.[69] The aggregation number from SLS reported is based purely on the population of smaller aggregates.

3.5.3 SLS for determination of aggregation number and second virial coefficient: an example

In general, Rayleigh scattering may be assumed for scattering moieties up to 1/10 of the scattering wavelength. The largest of all micelles measured in this study were no more than 15 nm in radius (30 nm in diameter) and so meets this criterion for the laser wavelength of 632 nm. A more stringent check of appropriate use of the assumption of no angular dependence is that $qR_g \ll 1$. The variation of qR_H is shown below in Table 3-2. As R_H is larger than R_g, this is even more stringent.

Table 3-2. Angular dependence of qR_H for the largest copolymer micelle.

angle (°)	q (nm^{-1})	$q*R_H$
30	0.0051	0.07
45	0.0076	0.11
60	0.0099	0.14
75	0.0121	0.17
90	0.0141	0.20
105	0.0158	0.22
120	0.0172	0.24
150	0.0192	0.27

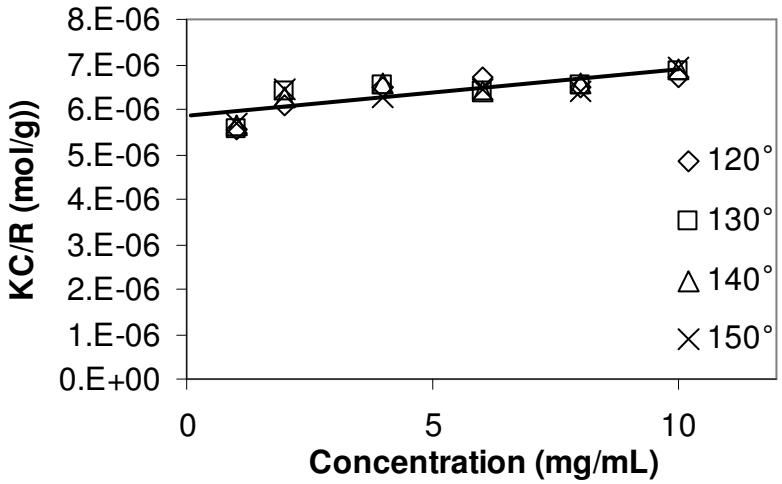

Figure 3-5. An example of a typical Debye plot. This is for micelles of 1930-3.1-1930 in 0.1M NaCl at pH 2 and 25℃ as measured on the CGS-3.

A Debye plot is constructed by calculating Kc/R for each concentration and plotting versus the concentration.[70] The intercept so determined is the reciprocal of the molecular weight, and the slope is proportional to the second virial coefficient. As may be seen in the example above, for the micelle of the 1930-3.1-1930 triblock with $R_H \cong$10nm, there was no angular dependence. The molecular weight determined here is that of the large scattering entity, the micelle. The aggregation number of the micelle is the molecular weight of the micelle divided by the molecular weight of a single polymer chain.

A brief note regarding measured intensity is appropriate here. The CGS-3 employs auto-attenuation of the measured light intensity, so the intensity reported is not absolute until scaled according to a monitor diode. In short, the entering laser light is split between a main beam that passes through the sample and a small side beam that is directed to a monitoring diode; this is recorded as I_{mon}. The software changes the laser intensity according to the scattering power of the sample. In order to recover the absolute scattered intensity at the measured angle, one must scale the measured intensity (I_{meas}) by a factor of (I_{mon} at maximum)/(I_{mon} during measurement).

There is some scattering intensity due to the unimers in solution. However, it is approximately two orders of magnitude smaller than that caused by the much larger micelles. Nonetheless, in order to account for this, the scattering intensity of the unimers must be subtracted. In order to do this, one would measure the scattering intensity of a solution just below the critical micelle concentration (CMC), then subtract this intensity. For this system, the CMC is quite low (~0.1 mg/mL). The resulting scattering intensity is on the order of twice that of water alone, thus is it very difficult to accurately measure scattering intensity. Therefore, this sample is taken to be the one where the autocorrelation function loses integrity, i.e. approximately at the CMC. The difference between subtracting the intensity of this sample versus subtracting the intensity of solvent alone typically causes a change in aggregation number of only about one.

3.5.4 Effect of Copolymer Composition on Micellization

The copolymer with the largest PEO tailblocks (15k-3-15k) did not micellize at the lowest pH tested (pH 2). This polymer is almost entirely PEO from either a repeat unit (341-3-341) or a mass fraction (0.96) perspective, and this composition likely accounts for the lack of micellization. The solubility of the PEO coils was sufficient to prevent micellization despite hydrophobic interaction or hydrogen bonding in the core. In light of this, no further tests were undertaken with the 15k-3-15k copolymer. The measured hydrodynamic radius and aggregation number (nearly unity) are shown below. Neither exhibited any temperature dependence.

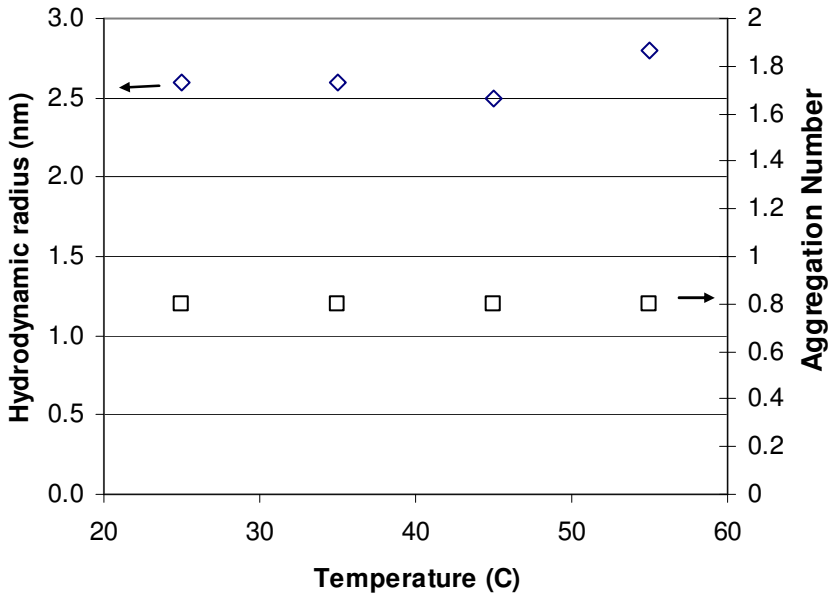

Figure 3-6. Hydrodynamic radius (DLS) and aggregation number (SLS) for 15k-3-15k copolymer at pH 2 and 0.1M NaCl. No micellization or temperature dependence was observed.

For the other polymers tested, it was possible to break up the micelle structure by raising the pH sufficiently and thus deprotonating the carboxylic acid groups in the center block.

The size of the unimers will be considered here; the size of the micelles will be discussed further in a later section. An empirical power law relationship between molecular weight (g/mol) and hydrodynamic radius (A) for PEO in water at 30°C was developed by Devanand and Selser.[69]

$$R_H = 0.0145 M_w^{0.571}$$

Eq. 3-15

The wormlike chain model may be applied to this system to estimate the radius of gyration[71] by:

$$R_g = L_k^2 \left\{ \frac{1}{6N_k} - \frac{1}{4N_k^2} + \frac{1}{4N_k^3} - \frac{1-e^{-2N_k}}{8N_k^4} \right\}$$

Eq. 3-16

in which L_k is the Kuhn length and N_k is the number of Kuhn segments, calculated by:

$$N_k = \frac{n}{C_\infty}$$

Eq. 3-17

in which n is the number of virtual bonds and C_∞ is the chain stiffness parameter. The value for C_∞ used was 4.1 for PEO.[72] L_k was calculated to be 0.61 nm by the following equation:

$$L_k = L_o C_\infty$$

Eq. 3-18

in which L_o is the length of a virtual bond for PEO (0.148 nm).[73]

The wormlike chain model is only strictly valid at the theta state ($\chi = 0.5$) where there are no excluded volume effects. Water is a good solvent for PEO ($\chi = 0.45$ for PEO chains of 10,000-20,000 g/mol),[74] so the coils would be more expanded than described by the wormlike chain model. Nonetheless, it provides a useful comparison. A non-draining coil was assumed,[68] allowing estimation of the hydrodynamic radius by:

$$R_H = 0.875 R_g$$

Eq. 3-19

The calculations for both of these models were made for a PEO coil of twice the DP of one of the tailblocks. The size of the unimers is summarized below, together with comparisons to the empirical relationship by Devanand and Selser and the predictions of the wormlike chain model. The results in Table 3-3 show semi-quantitative agreement between the measured and calculated values.

Table 3-3. Comparison of unimer size measured by DLS to: (a) an experimental correlation (Eq. 3-15)[69] and (b) wormlike chain prediction (Eq. 3-18).[71]

Copolymer	Measured R_H (nm)	Calculated R_H (nm), empirical[a]	Calculated R_H (nm), Worm-like chain[b]
1930-3.1-1930	2.3	1.7	1.7
4845-2.5-4845	3.4	2.8	2.7
4845-4.7-4845	4.3	2.8	2.7
15k-3-15k	2.6	5.2	4.8

DLS measurements were performed on samples in the concentration range of 0.1-10 mg/mL polymer at pH 8, 0.1M NaCl, and 25°C. The measured R_H is the peak mean for the primary intensity peak using a CONTIN algorithm.

For the other polymers, it was possible to break up the micelle structure by raising the pH sufficiently and thus deprotonating the carboxylic acid groups in the center block. The pH at which this happened for the 1930-3.1-1930, 4845-4.7-4845, and 4845-2.5-4845 copolymers was between 6 and 8 and correlated well with the measured pK_a of approximately 5 as determined by titration (Figure 3-7). The pK_a of COOH groups is strongly influenced by the surroundings. For instance, the pK_a of methacrylic acid monomer is 3.5, but the pK_a for poly(methacrylic acid) (PMAA) is 7.3. When complexed with PEO (M_w = 1300 g/mol), the pK_a increases to 7.5.[75]

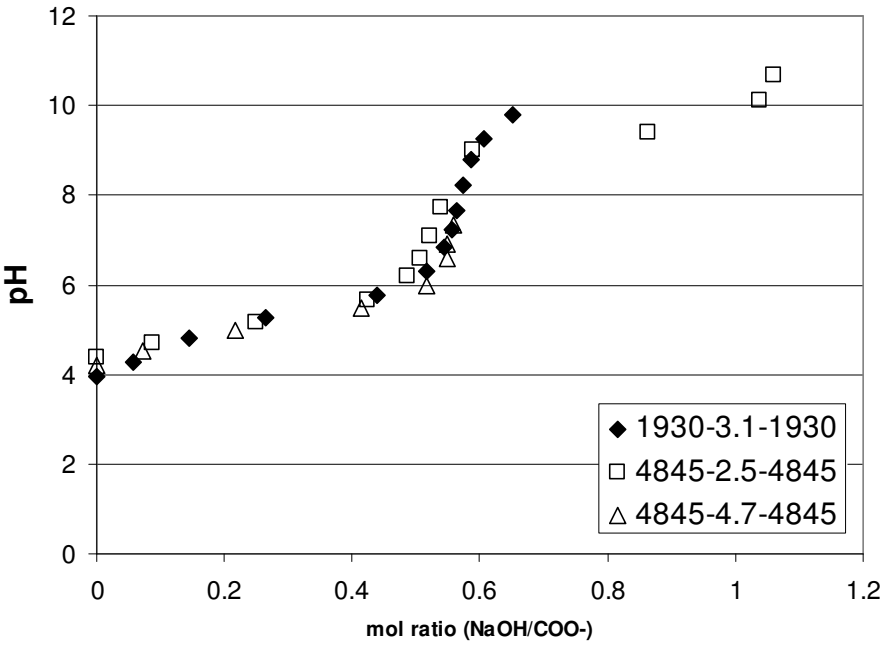

Figure 3-7. Titration data for the block copolymers with 0.1M NaCl in water. NaOH added was measured volumetrically using standardized 0.1M NaOH which was titrated to check concentration. Moles of COO- in the polymer expected are based on number of polyurethane repeat units previously measured by titration by Harris et al.[57]

3.5.5 Effect of Temperature on Micelle Size

Three of the polymers (1930-3.1-1930, 4845-2.5-4845, and 4845-4.7-4845) formed micelles in the pH range 2-6 with hydrodynamic radii typically in the range of 10-15 nm. The observed radii were insensitive to pH in the range 2-6 at a given temperature and composition. For comparison, results at pH 8 are shown as well in Figure 3-8 through Figure 3-10. No concentration dependence was observed for the size of the micelles in the range studied (0.1-10 mg/mL). In all cases, concentrations below 1 mg/mL were excluded from the size calculations, as they typically had a large amount of noise due to dust.

Two of the polymers, 4845-2.5-4845 and 4845-4.7-4845, behave in a very similar fashion. Each shows a steady, moderate decrease in hydrodynamic radius of about 10-15% with an increase in temperature from 25 to 65°C. Increasing the temperature would be expected to disrupt hydrogen bonding between PEO chains in the corona and the

solvent which would cause dehydration in the corona and a decrease in the size.[76] Micelles of the 4845-4.7-4845 copolymer were somewhat larger than micelles of the 4845-2.5-4845 copolymer, which is reasonable considering the larger center block and its greater contribution to the core diameter.

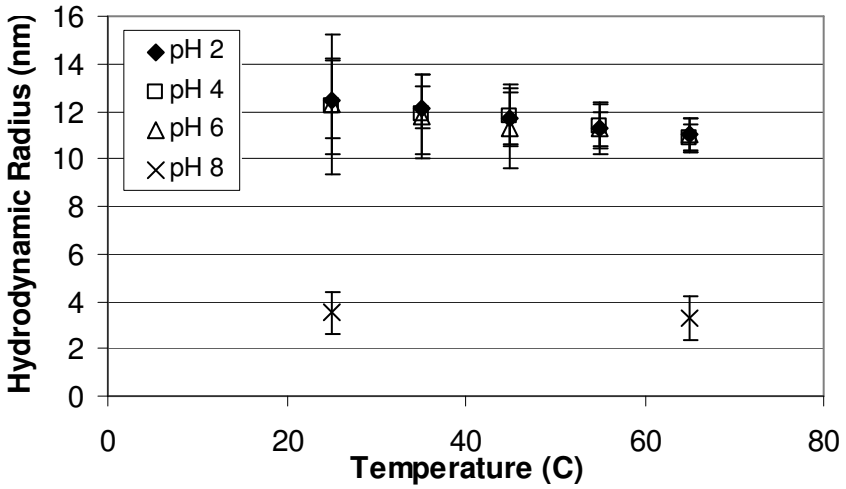

Figure 3-8. Hydrodynamic radius measured for 4845-2.5-4845 at 0.1M NaCl.

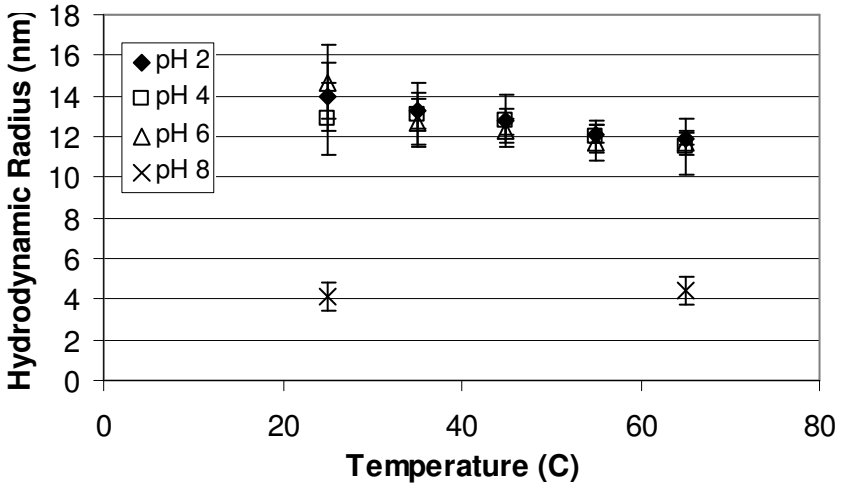

Figure 3-9. Hydrodynamic radius measured for 4845-4.7-4845 at 0.1M NaCl.

The 1930-3.1-1930 polymer exhibited behavior that differed from that of the other copolymers. At a given pH, the size was not very sensitive to increases in temperature. This is possibly due to decreased hydrogen bonding in the core, allowing more

hydrophobic interactions to take place, which would in turn counteract an increase in size. In addition, the reduced solubility of the PEO end blocks due to decreased hydrogen bonding, i.e. poorer solvent quality, would also drive micellization.

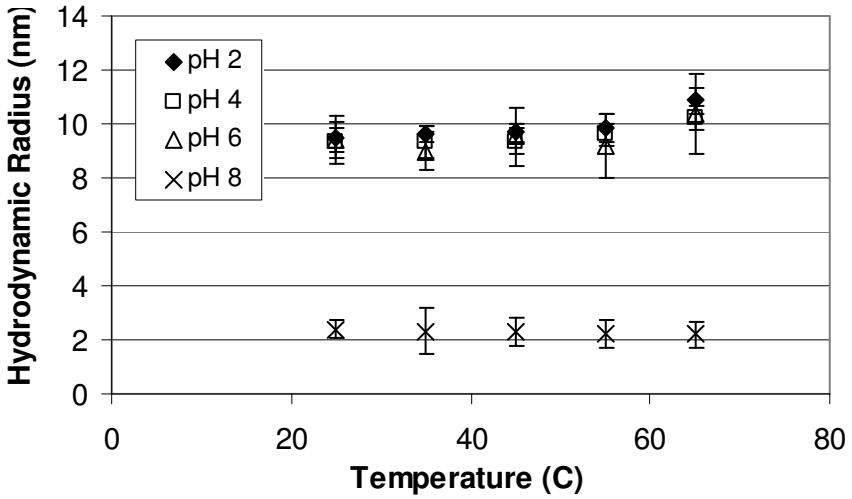

Figure 3-10. Hydrodynamic radius measured for 1930-3.1-1930 at 0.1M NaCl.

Previous studies of PEO-PPO-PEO triblocks have shown a similar trend. For example, Goldmints et al.[77] studied a deuterated PEO_{23}-PPO_{34}-PEO_{23} copolymer which formed micelles at temperatures above 40°C. The aggregation number increased with temperature above the critical micellization temperature (CMT), but the radius of the micelle remained the same. This was attributed to dehydration of the core. The increase in aggregation number without an increase in the overall size is typical for PEO-PPO-PEO copolymers as summarized by Alexandridis.[7] An increasing aggregation number with temperature was shown by several researchers for L64 (PEO_{14}-PPO_{31}-PEO_{14})[78, 79] and F127 (PEO_{95}-PPO_{62}-PEO_{95}).[80] This was also shown for P85 (PEO_{27}-PPO_{41}-PEO_{27}) by Brown et al.[81] However, a study on P85 by SANS showed an increase in both the radius and aggregation number between 20°C and 50°C[9] as did a study on F68 (PEO_{81}-PPO_{31}-PEO_{81}).[82] Some of the differences in observations can depend on the method employed, due to the dehydration of the PPO block with an increase in temperature.

One additional consideration in describing the aggregation behavior of these copolymers is the possibility of hydrogen bonding between the PEO tailblocks and the carboxylic

acid groups. Hydrogen bonding interactions between homopolymer polyacids and PEO have been observed in numerous instances.[83, 84] Poly(methyl methacrylate) PMAA and PEO complex under acidic conditions only if the molecular weight of the PEO is at least 2000 g/mol.[85] Investigators have found that hydrogen bonding also occurs between PEO and polyacids when they are present as a block copolymer, rather than as two separate homopolymers.[22, 86-89]

A carboxylic acid-containing polymer can also be incorporated into micelles with uncharged polymers containing a hydrophobic section by hydrogen bonding. This was demonstrated in a study by Zeghal and Auvray[90] in which they examined micelles composed of a mixture of Pluronic P105 (PEO_{34}-PPO_{52}-PEO_{34}) and PMA. Using a combination of SANS (with a deuterated polyacid) and NMR, they characterized the structure of the corona and investigated the effect of changing the degree of charge on the PMA and the temperature on the aggregation number and size of the resulting micelles. In this system, PMA was present in both the core and corona of the micelles, but in different ionization states. The PMA in the core was neutral whereas the PMA in the corona was ionized. They found that as the number of available hydroxyl groups increased, so did the number of PMA chains in the micelle. This being an electrostatic effect, it was strongly dependent on pH but only weakly dependent on temperature. The number of Pluronic chains in the micelle, however, was dependent on both pH and temperature, as micellization was driven by both hydrophobic interaction of the PPO chains and hydrogen bonding of the PMA with PPO.

3.5.6 Effect of Temperature on Aggregation Number

The aggregation number of the copolymers over a range of pH and temperature conditions was measured using SLS. As with the size measurements, the temperature effect on aggregation number was the same for 4845-2.5-4845 and 4845-4.7-4845 in that no dependence was observed as shown in Figure 3-11 and Figure 3-12.

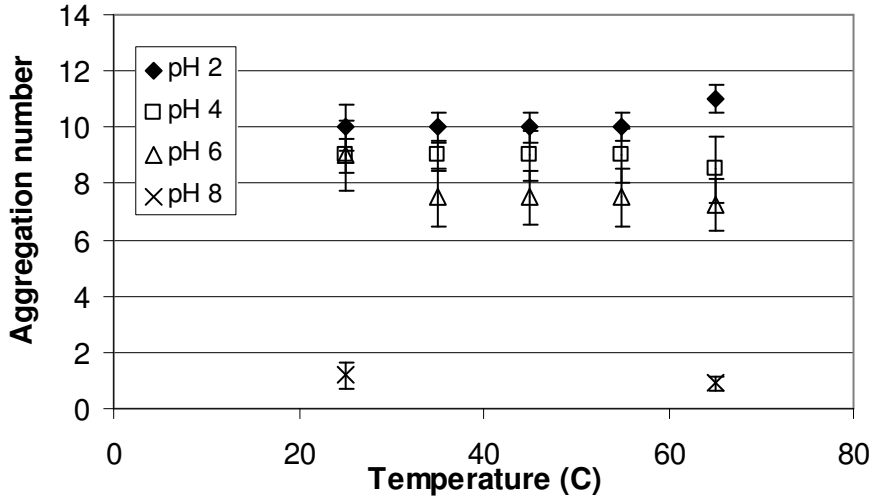

Figure 3-11. Aggregation number as a function of temperature and pH for 4845-2.5-4845 at 0.1M NaCl.

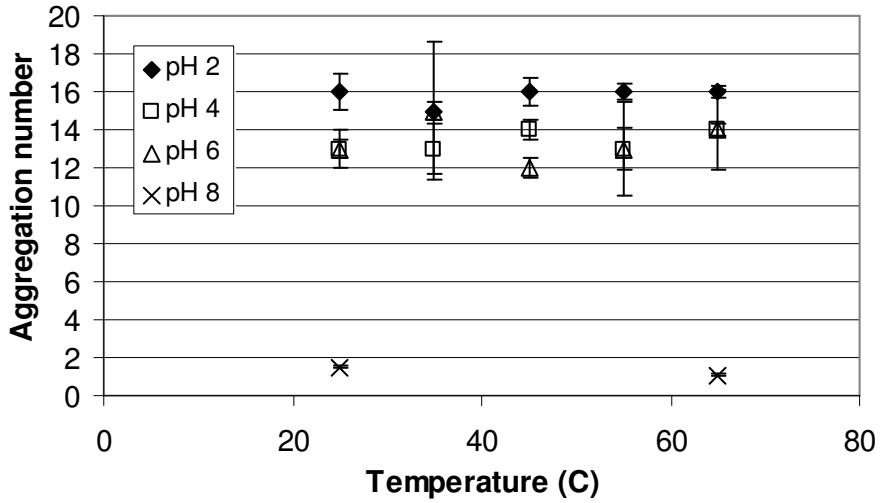

Figure 3-12. Aggregation number as a function of temperature and pH for 4845-4.7-4845 at 0.1M NaCl.

The 1930-3.1-1930 polymer showed an upswing in aggregation number with increasing temperature as shown in Figure 3-13. The increase in temperature may decrease hydrogen bonding in the core. This allows more hydrophobic interaction, encouraging addition of chains to the micelle.

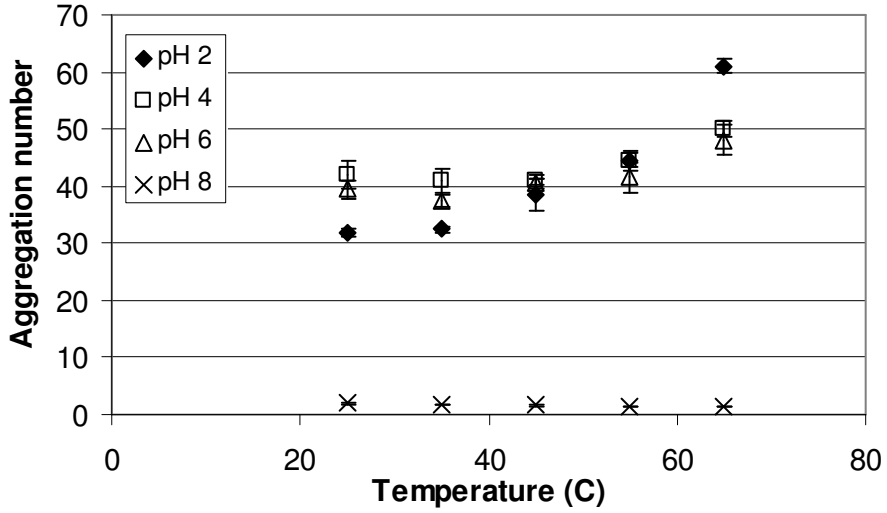

Figure 3-13. Aggregation number as a function of temperature and pH for 1930-3.1-1930 at 0.1M NaCl.

3.5.7 Comparison with the Density Distribution Prediction

Micelle dimensions were estimated with the density distribution (DD) model, developed by Vagberg et al.[60] This model, based on a model for star polymers by Daoud and Cotton[91] assumes concentric shells with a constant number of blobs. The blob number or number of corona chains is equal to twice the aggregation number in this case. Blob size $\xi(r)$, is a continuous function of distance from the surface. The segment density in the shell varies with distance from the core.

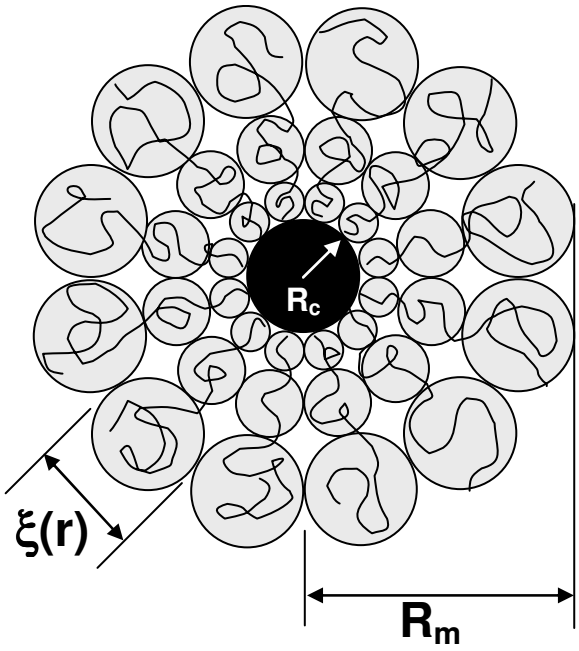

Figure 3-14. Schematic representation of the micelle showing the density distribution model[60] parameters.

The DD model predicts micelle radius, $R_{m,}$, as:

$$R_m = \left[N a_s^{1/\nu} \frac{8 f^{(1-\nu)/2\nu}}{3\nu 4^{1/\nu}} + R_c^{1/\nu} \right]^{\nu}$$

Eq. 3-20

where N is the number of Kuhn segments, ν is the Flory exponent, R_c is the radius of the core, a_s is the Kuhn length of the polymer, and f is the number of corona chains, which for these triblock copolymers is twice the aggregation number.

The blob diameter, ξ(r) is given by:

$$\xi(r) = \frac{4r}{f^{1/2}}$$

Eq. 3-21

in which r is the distance from the center.

The Flory exponent, ν, varies between 0.5 at a theta condition and 0.6 for a good solvent. For these calculations, ν=0.583[69] was used for PEO in water at room temperature. This

value was used in similar studies by other authors,[62, 63, 92] as described further below. The core radius, R_c, was estimated by setting the core diameter equal to the end-to-end distance of the center block, estimated using known bond lengths and angles. The resulting predictions for hydrodynamic radius were approximately 20% below the measured data as shown in Figure 3-15.

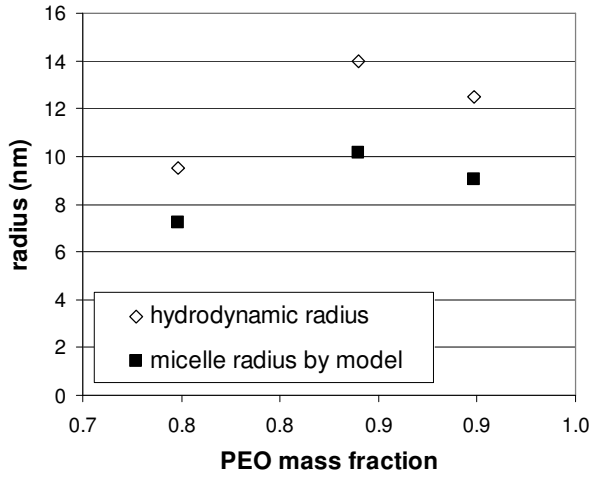

Figure 3-15. The hydrodynamic radius measured by DLS (25°C, pH 2, 0.1M NaCl) is compared to a prediction based on the density distribution model by Vagberg et al.[60]

Several groups have compared the density distribution prediction with experimental measurements of PEO-containing block copolymers or similar systems. Farhina et al.[92] examined the micellization of a series of PS-PEO copolymers in water and cyclopentane by DLS. They found that the model slightly overpredicted the brush thickness and partly attributed it to polydispersity and uncertainties in the input parameters to the model. Harada et al.[61] also found in their study of aqueous mixtures of poly(ethylene glycol)-b-poly(α,β-aspartic acid) and poly(ethylene glycol)-b-poly(L-lysine) that R_m values predicted were slightly larger than R_H values measured by DLS. These findings are both compatible with the original observations by Vagberg et al.[60] who attributed this difference to draining in the corona. Conversely, a study by Johnsson et al.[62] using PEG-derivatized lipids found that the predicted values tended to be slightly smaller than experimentally observed. For this study, the core of the radius was estimated using the measured aggregation number and the volume occupied by the components in the core. A study by Fitzgerald et al.[63] on dimeric PEO surfactants also indicated that the predicted

thickness of the shell was less than that experimentally fit from SANS data by 7-24% for the spherical micelles.

3.5.8 Volume Fraction Profile

The volume fraction profile in the micelle corona was examined using the Vagberg approach.[60] In this method, the volume fraction profile is divided into three sections. With the core, the density is constant. Beyond the micelle radius, calculated as R_m, the density is zero. Between R_c and R_m the profile as given below.

$$\rho(r) = \rho_c \qquad r < R_c$$
$$\rho(r) = A\left(\frac{r}{a_s}\right)^{\frac{1}{\nu}} r^{-3} \qquad R_c < r < R_m$$
$$\rho(r) = 0 \qquad R_m < r$$

Eq. 3-22

The constant of proportionality, A, is determined by the relationship between the blob size at the core-corona boundary and the number of corona chains.

$$A = \frac{3 * 4^{\frac{1}{\nu}} f^{\frac{3\nu-1}{2\nu}}}{32}$$

Eq. 3-23

The volume fraction profiles were calculated for 1930-3.1-1930, 4845-2.5-4845, and 4845-4.7-4845 in 0.1M NaCl at 25°C. The results are shown below in Figure 3-16. The relationship between core radius and aggregation number determines the maximum brush density. Longer PEO chains extend further into solution.

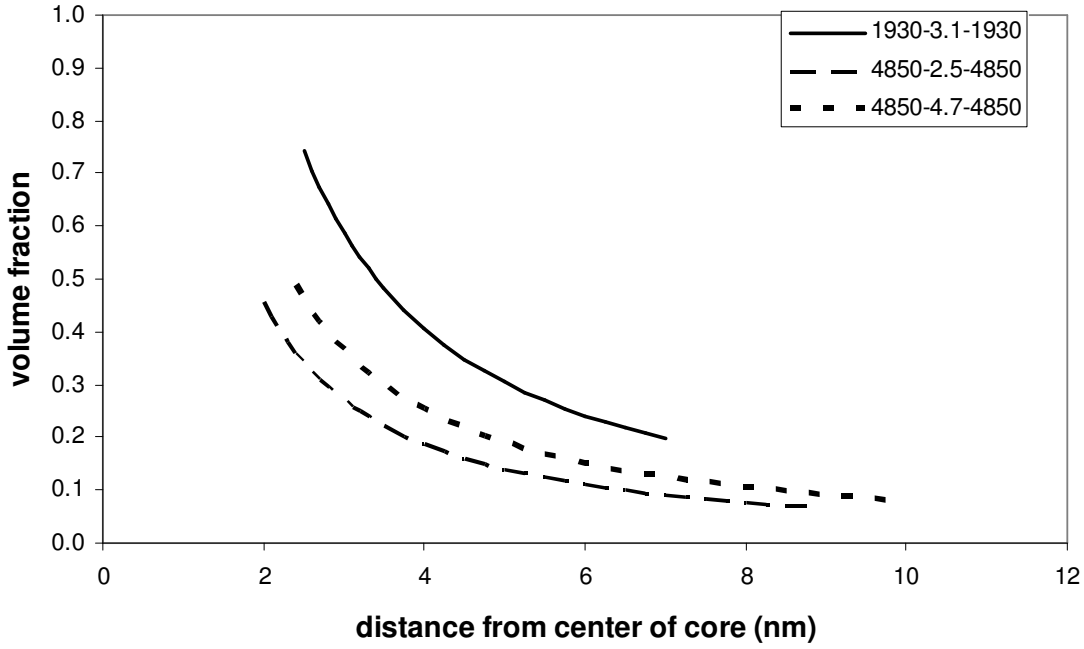

Figure 3-16. Volume fraction profiles for 1930-3.1-1930, 4845-2.5-4845, and 4845-4.7-4845 in 0.1M NaCl at 25C based on Vagberg's approach. Micelles with higher aggregation numbers form denser brushes, and those with longer PEO chains have the corona extending further into solution.

3.5.9 A Visual Comparison of Size

The figure below provides a graphical representation of the relative sizes of the micelles. The core is scaled to the end-to-end distance of the center block assuming that it is in a linear configuration. The overall size of the micelle is the hydrodynamic radius as measured by dynamic light scattering. The number appearing in the center of each micelle is the aggregation number as determined using SLS. The series down the left side shows what happens as one increases the length of the PEO tail blocks while keeping a short center block. 1930-3.1-1930 is most tightly packed and the PEO chains are more extended as compared to the unimer state. This means that there is more excluded volume, and in a sense, this micelle might behave more like a hard sphere than the others. 4845-2.5-4845 is more loosely packed, with less extended chains (relative to in solution as unimers). 15k-3-15k behaves like PEO homopolymer.

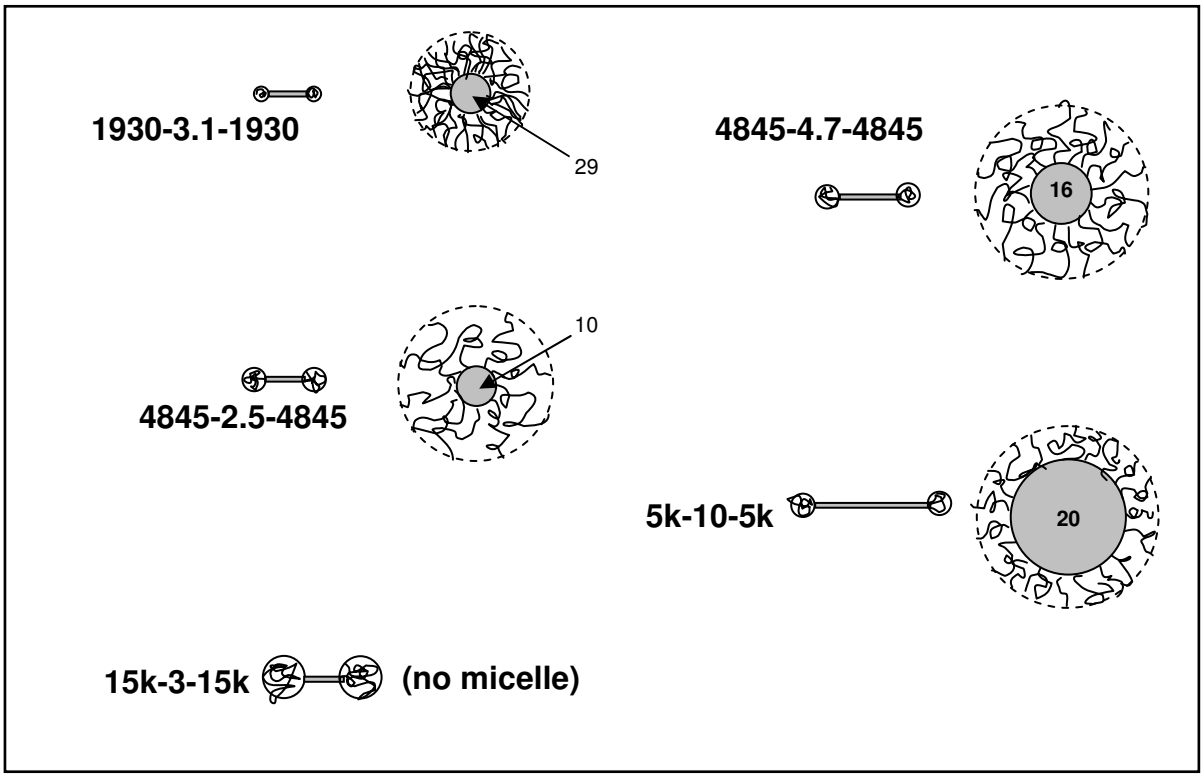

Figure 3-17. A visual representation of relative micelle sizes. The size of the center shown reflects the end-to-end distance if the center block were extended as far as possible without breaking or bending bonds. The number in the center of each is the aggregation number measured by SLS. The total size of the micelle is the hydrodynamic diameter as measured by DLS.

3.6 Conclusions

Hydrophilic triblock copolymers have been shown to micellize under conditions of low electrostatic repulsion. Dynamic light scattering was used to determine the hydrodynamic radii of the micelles. Static light scattering was used to determine the micelle molecular weights and aggregation numbers.

The pH of the solution had the most marked effect on the micellization properties. At low pH, all of the copolymers with the exception of 15k-3-15k micellized, presumably due to protonation of the carboxylic acid groups. The 15k-3-15k polymer did not micellize under any conditions studied. It consists of largely PEO (0.96 mass fraction), which is highly water soluble. For the other polymers, a transition to unimers occurred between pH 6 and 8, with no micelles found at pH 8. The temperature was varied in the range from 25-65°C. Two of the polymers (4845-2.5-4845 and 4845-4.7-4845) display a

steady decrease in hydrodynamic radius with increasing temperature which was attributed to temperature-induced disruption of hydrogen bonding in the PEO corona. The aggregation number did not vary in this range. The 1930-3.1-1930 polymer showed no change in the hydrodynamic radius with an increase in temperature. However, the aggregation number increased with temperature, indicating that the typical decrease in size not seen in this polymer with an increase in temperature may have been simply offset by the increasing molecular weight of the micelle. This increase in aggregation number may have been allowed by increased hydrophobic interactions in the core promoted by the decrease in hydrogen bonding, as well as the reduction of solubility in the corona. The relative sizes of the polymers studied were compared to the density distribution model. Although the predicted sizes were typically 20% less than the measured hydrodynamic radii, the model predicted observed trends as the triblock composition was changed.

3.7 References

1. Riess, G., Micellization of block copolymers. *Progress in Polymer Science*, **2003**. 28(7): p. 1107-1170.

2. Gohy, J.F., Block copolymer micelles, in Block Copolymers II, V. Abetz, Editor. **2005**, Springer: London. p. 65-136.

3. Stuart, M.A.C., et al., Assembly of polyelectrolyte-containing block copolymers in aqueous media. *Current Opinion in Colloid & Interface Science*, **2005**. 10(1-2): p. 30-36.

4. Alexandridis, P. and Spontak, R.J., Solvent-regulated ordering in block copolymers. *Current Opinion in Colloid & Interface Science*, **1999**. 4(2): p. 130-139.

5. Spontak, R.J. and Alexandridis, P., Advances in self-ordering macromolecules and nanostructure design. *Current Opinion in Colloid & Interface Science*, **1999**. 4(2): p. 140-146.

6. Nolan, S.L., et al., Light scattering study on the effect of polymer composition on the structural properties of PEO-PPO-PEO micelles. *Journal of Colloid and Interface Science*, **1997**. 191(2): p. 291-302.

7. Alexandridis, P. and Hatton, T.A., Poly(ethylene oxide)-poly(propylene oxide)-poly(ethylene oxide) block copolymer surfactants in aqueous solutions and at interfaces: thermodynamics, structure, dynamics, and modeling. *Colloids and Surface A: Physicochemical and Engineering Aspects*, **1995**. 96: p. 1-46.

8. Almgren, M., Brown, W., and Hvidt, S., Self-Aggregation and Phase-Behavior of Poly(Ethylene Oxide) Poly(Propylene Oxide) Poly(Ethylene Oxide) Block-Copolymers in Aqueous-Solution. *Colloid and Polymer Science*, **1995**. 273(1): p. 2-15.

9. Mortensen, K. and Pedersen, J.S., Structural Study on the Micelle Formation of Poly(ethylene oxide)-Poly(propylene oxide)-Poly(ethylene oxide) Triblock Copolymer in Aqueous Solution. *Macromolecules*, **1993**. 26(805-812).

10. Jain, N.J., et al., Salt induced micellization and micelle structures of PEO/PPO/PEO block copolymers in aqueous solution. *Colloids and Surfaces A: Physicochemical and Engineering Aspects*, **2000**. 173(1-3): p. 85-94.

11. Guo, C., et al., Hydration and conformation of temperature-dependent micellization of PEO-PPO-PEO block copolymers in aqueous solutions by FT-Raman. *Langmuir*, **1999**. 15(8): p. 2703-2708.

12. Guo, C., et al., Conformational structure of triblock copolymers by FT-Raman and FTIR spectroscopy. *Journal of Colloid and Interface Science*, **1999**. 209(2): p. 368-373.

13. Alexandridis, P., Holzwarth, J.F., and Hatton, T.A., Micellization of Poly(Ethylene Oxide)-Poly(Propylene Oxide)-Poly(Ethylene Oxide) Triblock Copolymers in Aqueous-Solutions - Thermodynamics of Copolymer Association. *Macromolecules*, **1994**. 27(9): p. 2414-2425.

14. Yang, L., et al., Small-angle neutron scattering investigation of the temperature-dependent aggregation behavior of the block copolymer pluronic L64 in aqueous solution. *Langmuir*, **2000**. 16(23): p. 8555-8561.

15. Chaibundit, C., et al., Association properties of triblock copolymers in aqueous solution: Copolymers of ethylene oxide and 1,2-butylene oxide with long E-blocks. *Langmuir*, **2000**. 16(24): p. 9645-9652.

16. Jada, A., et al., Structure of polystyrene-block-poly(ethylene oxide) diblock copolymer micelles in water. *Macromolecular Chemistry and Physics*, **1996**. 197(11): p. 3697-3710.

17. Xu, R.L., et al., Micellization of Polystyrene Poly(Ethylene Oxide) Block Copolymers in Water .5. a Test of the Star and Mean-Field Models. *Macromolecules*, **1992**. 25(2): p. 644-652.

18. Hurtrez, G., Dumas, P., and Riess, G., Polystyrene-poly(ethylene oxide) diblock copolymers micelles in water. *Polymer Bulletin*, **1998**. 40(2-3): p. 203-210.

19. Yu, K. and Eisenberg, A., Multiple morphologies in aqueous solutions of aggregates of polystyrene-block-poly(ethylene oxide) diblock copolymers. *Macromolecules*, **1996**. 29(19): p. 6359-6361.

20. Poe, G.D., et al., Enhanced Coil Expansion and Intrapolymer Complex Formation of Linear Poly(methacrylic acid) Containing Poly(ethylene glycol) Grafts. *Macromolecules*, **2004**. 37: p. 2603-2612.

21. Drescher, B., Scranton, A.B., and Klier, J., Synthesis and Characterization of Polymeric Emulsifiers Containing Reversible Hydrophobes: Poly(methacrylic acid-g-ethylene glycol). *Polymer*, **2001**. 42: p. 49-58.

22. Mathur, A.M., et al., Polymeric emulsifiers based on reversible formation of hydrophobic units. *Nature*, **1998**. 392(6674): p. 367-370.

23. Li, Y., Gong, Y.-K., and Nakashima, K., Nanoaggregate Formation of Poly(ethylene oxide)-b-polymethacrylate Copolymer Induced by Alkaline Earth Metal Binding. *Langmuir*, **2002**. 18: p. 6727-6729.

24. Moeser, G.D., et al., Water-based magnetic fluids as extractants for synthetic organic compounds. *Industrial & Engineering Chemistry Research*, **2002**. 41(19): p. 4739-4749.

25. Moeser, G.D., et al., Structure of polymer-stabilized magnetic fluids: Small-angle neutron scattering and mean-field lattice modeling. *Langmuir*, **2004**. 20(13): p. 5223-5234.

26. Matsuoka, H., et al., Polymer Micelle Formation without Gibbs Monolayer Formation: Synthesis and Characteristic Behavior of an Amphiphilic Diblock Copolymer Having Strong Acid Groups. *Macromolecules*, **2003**. 36: p. 5321-5330.

27. Matsuoka, H., et al., Micellization of Non-Surface-Active Diblock Copolymers in Water. Special Characteristics of Poly(Styrene)-block-Poly(Styrenesulfonate). *Langmuir*, **2004**. 20: p. 7412-7421.

28. Kaewsaiha, P., Matsumoto, K., and Matsuoka, H., Non-Surface Activity and Micellization of Ionic Amphiphilic Diblock Copolymers in Water. Hydrophobic Chain Length Dependence and Salt Effect on Surface Activity and the Critical Micelle Concentration. *Langmuir*, **2005**. 21: p. 9938-9945.

29. Moffitt, M., et al., Coronal Structure of Star-Like Block Ionomer Micelles: An Investigation by Small-Angle Neutron Scattering. *Macromolecules*, **1998**. 31: p. 2190-1297.

30. Moffitt, M. and Eisenberg, A., Scaling Relations and Size Control of Block Ionomer Microreactors Containing Different Metal Ions. *Macromolecules*, **1997**. 30: p. 4363-4373.

31. Khougaz, K., Gao, Z., and Eisenberg, A., Distribution of Water in Solutions of Reverse Micelles of Sodium Bis[2-ethylhexyl] Sulfosuccinate and Block Ionomers in Toluene. *Langmuir*, **1997**. 13: p. 623-631.

32. Kabanov, A.V. and Alakhov, V., Pluronic (R) block copolymers in drug delivery: From micellar nanocontainers to biological response modifiers. *Critical Reviews in Therapeutic Drug Carrier Systems*, **2002**. 19(1): p. 1-72.

33. Kabanov, A.V., Batrakova, E.V., and Alakhov, V., Pluronic block copolymers as novel polymer therapeutics for drug and gene delivery. *Journal of Controlled Release*, **2002**. 82: p. 189-212.

34. Batrakova, E.V., et al., Effect of Pluronic P85 on ATPase Activity of Drug Efflux Transporters. *Pharmaceutical Research*, **2004**. 21(12): p. 2226-2233.

35. Nakayama, M. and Okano, T., Intelligent thermoresponsive polymeric micelles for targeted drug delivery. *Journal of Drug Delivery Science and Technology*, **2006**. 16(1): p. 35-44.

36. Rangel-Yagui, C.O., Pessoa, A., and Tavares, L.C., Micellar solubilization of drugs. *Journal of Pharmacy and Pharmaceutical Sciences*, **2005**. 8(2): p. 147-163.

37. Torchilin, V.P., Block copolymer micelles as a solution for drug delivery problems. *Expert Opinion on Therapeutic Patents*, **2005**. 15(1): p. 63-75.

38. Kabanov, A.V., Batrakova, E.V., and Miller, D.W., Pluronic((R)) block copolymers as modulators of drug efflux transporter activity in the blood-brain barrier. *Advanced Drug Delivery Reviews*, **2003**. 55(1): p. 151-164.

39. Lavasanifar, A., Samuel, J., and Kwon, G.S., Poly(ethylene oxide)-block-poly(L-amino acid) micelles for drug delivery. *Advanced Drug Delivery Reviews*, **2002**. 54(2): p. 169-190.

40. Rosler, A., Vandermeulen, G.W.M., and Klok, H.A., Advanced drug delivery devices via self-assembly of amphiphilic block copolymers. *Advanced Drug Delivery Reviews*, **2001**. 53(1): p. 95-108.

41. Park, T.G., Jeong, J.H., and Kim, S.W., Current status of polymeric gene delivery systems. *Advanced Drug Delivery Reviews*, **2006**. 58(4): p. 467-486.

42. Gebhart, C.L., et al., Design and Formulation of Polyplexes Based on Pluronic-Polyethyleneimine Conjugates for Gene Transfer. *Bioconjugate Chemistry*, **2002**. 13: p. 913-944.

43. Vert, M. and Domurado, D., Poly(ethylene glycol): Protein-repulsive or albumin-compatible? *Journal of Biomaterials Science - Polymer Edition*, **2000**. 11(12): p. 1307-1317.

44. Bromberg, L., Temchenko, M., and Hatton, T.A., Smart microgel studies. Polyelectrolyte and drug-absorbing properties of microgels from polyether-modified poly(acrylic. *Langmuir*, **2003**. 19(21): p. 8675-8684.

45. Barreiro-Iglesias, R., et al., Solubilization and stabilization of camptothecin in micellar solutions of pluronic-g-poly(acrylic acid) copolymers. *Journal of Controlled Release*, **2004**. 97(3): p. 537-549.

46. Djordjevic, J., Barch, M., and Uhrich, K.E., Polymeric micelles based on amphiphilic scorpion-like macromolecules: Novel carriers for water-insoluble drugs. *Pharmaceutical Research*, **2005**. 22(1): p. 24-32.

47. Tao, L. and Uhrich, K.E., Novel amphiphilic macromolecules and their in vitro characterization as stabilized micellar drug delivery systems. *Journal of Colloid and Interface Science*, **2006**. 298(1): p. 102-110.

48. Tian, L., et al., Amphiphilic scorpion-like macromolecules: Design, synthesis, and characterization. *Macromolecules*, **2004**. 37(2): p. 538-543.

49. Sheihet, L., et al., Hydrophobic drug delivery by self-assembling triblock copolymer-derived nanospheres. *Biomacromolecules*, **2005**. 6(5): p. 2726-2731.

50. Bronich, T.K., et al., Polymer Micelle with Cross-Linked Ionic Core. *Journal of the American Chemical Society*, **2005**. 127: p. 8236-8237.

51. Vlassopoulos, D., et al., Multiarm star polymers dynamics. *Journal of Physics-Condensed Matter*, **2001**. 13(41): p. R855-R876.

52. Vlassopoulos, D., Colloidal star polymers: Models for studying dynamically arrested states in soft matter. *Journal of Polymer Science Part B-Polymer Physics*, **2004**. 42(16): p. 2931-2941.

53. Semenov, A.N., et al., Dynamic structure of interacting spherical polymer brushes. *Langmuir*, **1999**. 15(2): p. 358-368.

54. Seghrouchni, R., et al., Controlling the dynamics of soft spheres: From polymeric to colloidal behavior. *Europhysics Letters*, **1998**. 42(3): p. 271-276.

55. Vlassopoulos, D., et al., Ordering and dynamics of soft spheres in melt and solution. *Faraday Discussions*, **1999**: p. 225-235.

56. Roovers, J., et al., Regular Star Polymers with 64 and 128 Arms - Models for Polymeric Micelles. *Macromolecules*, **1993**. 26(16): p. 4324-4331.

57. Harris, L.A., et al., Magnetite nanoparticle dispersions stabilized with triblock copolymers. *Chemistry of Materials*, **2003**. 15(6): p. 1367-1377.

58. Huglin, M.B., ed. Light Scattering from Polymer Solutions. Physical Chemistry A Series of Monographs, ed. E.M. Loebl. **1972**, Academic Press: London.

59. Finsy, R., Particle Sizing by Quasi-Elastic Light-Scattering. *Advances in Colloid and Interface Science*, **1994**. 52: p. 79-143.

60. Vagberg, L.J.M., Cogan, K.A., and Gast, A.P., Light-Scattering Study of Starlike Polymeric Micelles. *Macromolecules*, **1991**. 24(7): p. 1670-1677.

61. Harada, A. and Kataoka, K., Effect of charged segment length on physicochemical properties of core-shell type polyion complex micelles from block ionomers. *Macromolecules*, **2003**. 36(13): p. 4995-5001.

62. Johnsson, M., Hansson, P., and Edwards, K., Spherical micelles and other self-assembled structures in dilute aqueous mixtures of poly(ethylene glycol) lipids. *Journal of Physical Chemistry B*, **2001**. 105(35): p. 8420-8430.

63. FitzGerald, P.A., Davey, T.W., and Warr, G.G., Micellar structure in gemini nonionic surfactants from small-angle neutron scattering. *Langmuir*, **2005**. 21(16): p. 7121-7128.

64. Provencher, S.W., A Contrstrained Regularization Method for Inverting Data Represented by Linear Algebraic or Integral Equations. *Computer Physics Communications*, **1982**. 27: p. 213-227.

65. Provencher, S.W., CONTIN: A General PurposeConstrained Regularization Program for Inverting Noisy Linear Algebraic and Integral Equations. *Computer Physics Communications*, **1982**. 27: p. 229-242.

66. Peters, R., Noise on photon correlation functions and its effect on data reduction algorithms., in Dynamic Light Scattering: The Method and Some Applications, W. Brown, Editor. **1993**, Clarendon Press: Oxford.

67. Malvern_Instruments, CGS-3 User Manual, Chapter 8. **2005**.

68. Tanford, C., Physical Chemistry of Macromolecules. **1962**, New York: John Wiley and Sons.

69. Devanand, K. and Selser, J.C., Asymptotic-Behavior and Long-Range Interactions in Aqueous-Solutions of Poly(Ethylene Oxide). *Macromolecules*, **1991**. 24(22): p. 5943-5947.

70. Heimenz, P.C., Polymer Chemistry. **1984**, New York: Marcel Dekker, Inc.

71. Davis, R.M., Analysis of Dilute Solutions of (Carboxymethyl)cellulose with the Electrostatic Wormlike Chain Theory. *Macromolecules*, **1991**. 24: p. 1149-1155.

72. Brandrup, J. and Immergut, E.H., eds. Polymer Handbook. **1999**, John Wiley: New York.

73. Russel, W.B., Saville, D.A., and Schowalter, W.R., Colloidal Dispersions. **1989**, Cambridge: Cambridge University Press.

74. Venohr, H., et al., Static and Dynamic Light Scattering from Aqueous Poly(Ethylene Oxide) Solutions. *European Polymer Journal*, **1998**. 34: p. 723-732.

75. Tsuchida, E. and Abe, K., Interactions Between Macromolecules in Solution and Intermacromolecular Complexes. *Advances in Polymer Sciencd*, **1982**. 45: p. 1-119.

76. Ghaouar, N., et al., Structure and thermodynamic modelling of Pluronic L64 solutions. *E-Polymers*, **2005**.

77. Goldmints, I., et al., Structure of (deuterated PEO) (PPO) (deuterated PEO) block copolymer micelles as determined by small angle neutron scattering. *Langmuir*, **1999**. 15(5): p. 1651-1656.

78. Zhou, Z. and Chu, B., Anomalous Micellization Behavior and Composition Heterogeneity of Triblock ABA Copolymer of (A) Ethylene Oxide and (B) Propylene Oxide in Aqueous Solution. *Macromolecules*, **1988**. 21: p. 2548-2554.

79. Almgren, M., et al., Static and Dynamic Properties of a (PEO---PPO---PEO) Block Copolymer in Aqueous Solution. *Journal of Colloid and Interface Science*, **1992**. 151: p. 157-165.

80. Malmsten, M. and Lindham, B., Self-Assembly in Aqueous Block Copolymer Solutions. *Macromolecules*, **1992**. 25: p. 5440-5445.

81. Brown, W., Schillen, K., and Almgren, M., Micelle and Gel Formation in a Poly(ethylene oxide)/Poly(propylene oxide)/Poly(ethylene oxide) Triblock Copolymer in Water Solution. Dynamic and Static Light Scattering and Oscillatory Shear Measurements. *Journal of Physical Chemistry*, **1991**. 95: p. 1850-1858.

82. Al-Saden, A.A., Whateley, T.L., and Florence, A.T., Poloxamer Association in Aqueous Solution. *Journal of Colloid and Interface Science*, **1982**. 90: p. 303-309.

83. Oyama, H.T., Tang, W.T., and Frank, C.W., Complex-Formation between Poly(Acrylic Acid) and Pyrene-Labeled Poly(Ethylene Glycol) in Aqueous-Solution. *Macromolecules*, **1987**. 20(3): p. 474-480.

84. Ikawa, T., et al., Interpolymer Complex between Poly(Ethylene Oxide) and Poly(Carboxylic Acid). *Journal of Polymer Science Part a-Polymer Chemistry*, **1975**. 13(7): p. 1505-1514.

85. Tsuchida, E. and Abe, K., Interactions between Macromolecules in Solution and Intermacromolecular Complexes. *Advances in Polymer Science*, **1982**. 45: p. 1-119.

86. Gohy, J.F., Varshney, S.K., and Jerome, R., Water-soluble complexes formed by poly(2-vinylpyridinium)-block-poly(ethylene oxide) and poly(sodium methacrylate)-block-poly(ethylene oxide) copolymers. *Macromolecules*, **2001**. 34(10): p. 3361-3366.

87. Holappa, S., et al., Self-Complexation of Poly(ethylene oxide)-block-poly(methacrylic acid) Studied by Fluorescence Spectroscopy. *Macromolecules*, **2004**. 37: p. 7008-7018.

88. Holappa, S., et al., Soluble polyelectrolyte complexes composed of poly(ethylene oxide)-block-poly(sodium methacrylate) and poly(methacryloyloxyethyl trimethylammonium chloride). *Polymer*, **2003**. 44(26): p. 7907-7916.

89. Holappa, S., et al., Solution properties of linear and branched block copolymers consisting of acidic and PEO blocks. *Macromolecules*, **2002**. 35(12): p. 4733-4738.

90. Zeghal, M. and Auvray, L., Structure of Hydrophobically and Hydrogen-Bonded Complexes Between Amphiphilic Copolymer and Polyacid in Water. *The European Physical Journal E*, **2004**. 14: p. 259-268.

91. Daoud, M. and Cotton, J.P., Star shaped polymers: a model for the conformation and its concentration dependence. *Journal de Physique*, **1982**. 43: p. 531-538.

92. Farinha, J.P.S., et al., Structure in tethered chains: Polymeric micelles and chains anchored on polystyrene latex spheres. *Langmuir*, **1998**. 14(9): p. 2291-2296.

4 A SANS study of controlled aggregation of polyurethane-containing PEO block copolymers in water

4.1 Abstract

A new class of novel hydrophilic triblock copolymers which form micelles in aqueous solution was studied by static and dynamic light scattering (SLS and DLS), small angle neutron scattering (SANS), and densiometry. The polymers were symmetric A-B-A block copolymers having two poly(ethylene oxide) tailblocks and a carboxylic acid containing polyurethane center block. Previous studies using SLS and DLS on three of these polymers with varying center and tail block lengths revealed pH-induced micellization. The internal structure of the micelle was examined to determine the relative sizes of core and corona, the degree of hydration of the core, and the interpenetration of PEO chains into the core. The SANS data were fit to a triblock model consisting of a homogeneous core with a corona of non-interacting Gaussian chains. All three polymers were fit to a model having only three free parameters: the radius of the core, the radius of gyration of the corona, and concentration. Good agreement with size as measured by DLS was obtained. All three micelles had effectively dry cores, but the amount of PEO present in the core was greater for micelles with lower aggregation numbers.

4.2 Keywords

triblock copolymer, swelling, SANS, hydrophobicity, hydrogen bonding, charged micelle, PEO, core, corona, DLS, SLS,

4.3 Introduction

Novel PEO triblock copolymers consisting of poly(ethylene oxide) end blocks and a center block consisting of urethane and carboxylic acid groups[1] have been shown to exhibit micellization in aqueous solutions using static and dynamic light scattering. Solution pH has been used to control the formation of the micelles. At low pHs,

protonation of the carboxylic groups in the core led to micellization which is believed to be driven in part by hydrophobic and hydrogen bonding interactions in the center block. Additionally, an effect of temperature on micellization was observed. Two of the polymers exhibited a steady decrease in hydrodynamic radius with increasing temperature which was attributed to temperature-induced disruption of hydrogen bonding in the PEO corona. One polymer, which had a smaller fraction of PEO, exhibited the opposite trend, growing larger and exhibiting an increase in aggregation number. The light scattering studies allowed measurement of hydrodynamic radii, aggregation numbers, and second virial coefficients for the micelles. However, in order to gain insight into the internal structure of the micelles, a SANS study was required.

Small angle neutron scattering (SANS) has been used by many researchers to examine the core-shell structure of micelles.[2-8] SANS is an especially useful technique for examining micelles because scattering can be done selectively from different portions of the structure provided there is sufficient difference in scattering length density (SLD). This may be achieved by either varying the solvent composition (for instance by using a deuterated solvent) or by deuterating portions of the polymer, as in a study on PEO-PPO-PEO by Goldmints et al.[4]

For SANS studies of polymeric micelles, a challenging aspect is fitting an appropriate model. There has been a large contribution to the body of this work with respect to polyoxamers (Pluronics), which have a poly(ethylene oxide)-b-poly(propylene oxide)-b-poly(ethylene oxide) structure. One approach treated the micelles as monodisperse homogeneous hard spheres. A hard sphere form factor is described by Ashcroft and Lekner.[9] The application to diblock copolymers forming spherical domains was later described by Kinning and Thomas.[10]. This has been used by several authors to describe micelles of Pluronics in aqueous solutions.[11, 12] More recent studies such as one by Svaneborg and Pedersen have involved numerical simulations to describe the form factor by treating the corona as a semi-dilute solution of polymer with a concentration profile varying from the surface.[13]

No other system like the one in the present study is available in the scientific literature. The unique structure of the triblock copolymers allows for formation of micelles with a charged block in the center at conditions where the center block is not entirely neutralized.

There are examples in the literature of diblock copolymers containing an ionic block which forms a micellar core, but the ionic block must be neutralized. For instance, work by Li et al.[14] described nanoaggregates of poly(ethylene oxide)-b-poly(methacrylic acid) where the ionic block was neutralized using alkaline earth metals. This resulted in a neutralized polyion core with a PEO corona. Also, Bronich et al.[15] describe the use of a divalent metal ion (Ca^{2+}) to cause poly(ethylene oxide)-b-poly(methacrylate) polymers to form into micelles, despite the charges on the poly(methacrylate) block. Block ionic complexes can also be formed by combining poly(ethylene oxide)-b-poly(sodium methacrylate) with surfactants such as hexadecyltrimethylammonium bromide.[16] This complexation has also been demonstrated with poly(ethylene oxide)-b-poly(methacrylate) and cetyltrimetylammonium chloride[17] or chitosan.[18]

There are also examples in the literature of self-assembly of hydrogen-bonding graft copolymers in water. One such system concerned the pH-sensitive assembly of poly(methacrylic acid)-g-poly(ethylene glycol).[19] At low pH, collapse of the aggregates was observed and was thought to be the result of intramolecular complexes due to hydrogen bonding along the backbone. Another such poly(methacrylic acid)-g-poly(ethylene glycol) system was examined as an aqueous reversible emulsifier.[20, 21] Acid conditions caused hydrogen-bonding between the backbone and grafts to form hydrophobic segments.

This present study concerns SANS measurements on a series of novel polyurethane-containing triblock copolymers. Previous studies using static and dynamic light scattering revealed pH-induced micellization. In this study SANS was used to probe the internal structure of the micelle. In addition to understanding of the micelle formation processes of the polymers, this work will provide additional information regarding the

use of these and similar triblock copolymers as stabilizing agents for magnetite nanoparticles in aqueous solutions.[1, 22] By gaining an understanding of the micelle structure in absence of magnetite nanoparticles, better models may be developed for the stabilized particles.

4.4 Materials and Methods

4.4.1 Chemicals

PEO triblock copolymers were synthesized as previously described.[1] In brief, synthesis of the copolymers consisted of several steps. First, a PEO oligomer was end-capped with isophorone diisocyanate. This was then chain-extended with bis(hydroxymethyl)propionic acid in dimethylformamide (DMF) with dibutyltin dilaurate as the catalyst. The reaction was monitored using FTIR to observe the disappearance of the isocyanate peak at 2260 cm^{-1}. After removing the DMF, the polymer was dissolved in chloroform, washed three times with, added to an excess of cold hexane, and isolated by filtration. The resulting triblock copolymers were characterized using ^{1}H and quantitative ^{13}C NMR, FTIR, and titration (to determine the concentration of COOH groups).

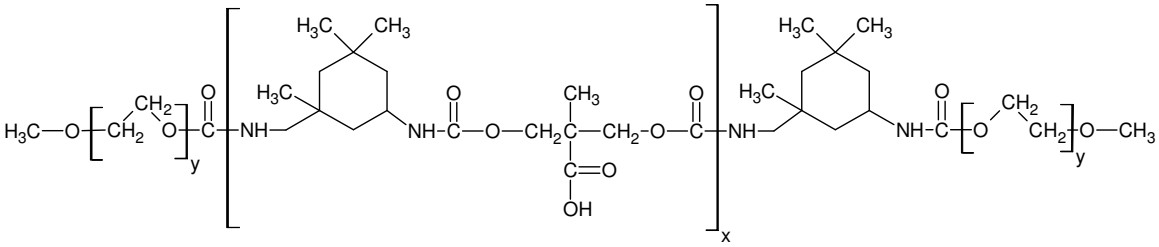

Figure 4-1. Structure of a representative triblock copolymer with PEO tail blocks and a polyurethane center block that contains carboxylic acid groups.

A series of these copolymers is described in overview in the table below. The nomenclature adopted herein for these triblock copolymers comprises the molecular weights of the PEO end blocks and the average number of carboxylic acid groups (derived by titration) in the central polyurethane section. For example, a 1930-3.1-1930 triblock consists of PEO end blocks with a number average molecular weight of 1930 g/mol, and a polyurethane central block having an average of 3.1 carboxylic acid groups.

Table 4-1. Properties of triblock copolymers.

Copolymer	M_n[a]	DP center[b]	DP tail	Mass fraction PEO
1930-3.1-1930	5160	3.1	44	0.75
4850-2.5-4850	10785	2.5	110	0.90
4850-4.7-4850	11540	4.7	110	0.84

[a]PEO tail block M_n from ^{1}H NMR. [b]Average number of COOH in the polyurethane center block from ^{13}C NMR.[1]

Solutions for SANS were prepared using D_2O (Cambridge Isotope Laboratories, Inc, Andover, MA) as received or deionized water from a NANOpure II ion exchanger (Barnstead) having a resistance above 17 MΩ·cm. Ionic strength for the deuterated solutions was adjusted using NaCl in D_2O and pD was adjusted using NaOH or HCl in D_2O. The pD measurements were made using an ordinary glass electrode (Orion Model 720 pH meter) according to the correction of Glasoe:[23]

$$pD = pH\ meter\ reading + 0.40$$

Eq. 4-1

NaOH, NaCl, and the polymers were dried at slightly elevated temperature (30°C) in a vacuum oven until no further change in weight was observed (overnight). Stock solutions of NaCl, NaOH, and HCl were prepared in each solvent to be studied (H_2O, D_2O, and a 50:50 mixture) by weight. Stock solutions of each polymer were prepared in the salt solutions by weight to slightly above the target concentration and were placed on a shaker overnight, then the pH was adjusted using the previously prepared solutions. After the pH adjustment and any dilution to the stock solutions, the actual concentrations were calculated and noted. Further dilutions were also prepared by weight using the pH-adjusted stock solutions of polymer and salt while mixing on a magnetic stir plate. No purification steps (such as filtration or centrifugation) were deemed necessary, as dust contamination was expected to be of a size too large to be detected by SANS.

4.4.2 Small Angle Neutron Scattering

SANS measurements were made on the NG3-SANS beamline at a wavelength of 5 Å at the National Institute of Science and Technology (NIST) National Center for Neutron Research (NCNR) in Gaithersburg, MD.[24] Two sample-to-detector distances were used

(2.5 m and 13 m) in order to cover a q-range from 0.0029-0.26 $Å^{-1}$. The beam intensity at the shorter distance was 1.4E6 counts/s, and a typical experiment was 20 minutes in duration. At the longer distance, the beam intensity was 3.1E5 counts/s, and a typical experiment was 2 hours in duration. Transmission measurements were made on all samples. The sample aperture diameter was 1.26 cm.

SANS samples were loaded into demountable titanium sample cells with quartz windows. The titanium portions of the cells were previously scrubbed with Sparkleen detergent, rinsed thoroughly with deionized water, and allowed to dry. The quartz windows were gently rubbed under a flow of deionized water, rinsed, and allowed to air-dry before being gently brushed free of dust using a Kimwipe. The sample cells had screw-in caps at the top to prevent evaporation of the sample, which was particularly important in the runs at elevated temperatures. In order to avoid under-tightening (leading to evaporation) or over-tightening (resulting in broken cell windows), a torque wrench set to 25 in-lb was used.

Initially, samples were run using pure H_2O, pure D_2O, and a 50:50 mix (by weight) as the solvent. Experiments in H_2O used a 1 mm thick sample, whereas D_2O required 4 mm and the 50:50 mixture required 2 mm. The sample thickness was chosen to maximize scattering and transmission, which typically occurs when the transmission ratio (I/I_o) is approximately 0.5.[25] This may be determined using the Beer-Lambert law:

$$\frac{I}{I_o} = e^{-n\sigma_T t}$$

Eq. 4-2

I is the transmitted neutron flux, I_o is the incident neutron flux, σ_T is the total cross section, n is the number of units per unit volume, and t is the sample thickness. The total cross section is defined as the sum of the coherent and incoherent cross sections. A transmission ratio of approximately 0.5 corresponds to a thickness of about 1 mm in water.

The partial specific volumes of the core and corona components were necessary in order to model the data. These were measured using a DA-300 Density/Specific Gravity Meter (Mettler). The partial specific volumes of the 2K and 5K PEO at 25°C were determined using solutions in D_2O the range of 0.1-5 wt %. The partial specific volume of the micelles for each copolymer was measured in the weight range of 0.2-2%. The partial specific volumes of the poly(urethane) block in the cores were calculated from these measurements as described later in this paper.

4.4.3 Light Scattering

Static and dynamic light scattering measurements were made on these polymer micelles in solution in D_2O. Dynamic light scattering is performed by measuring the variation of intensity with time. This is also known as quasi-elastic light scattering. This can be used to study electrophoretic motion, electrokinetic potential, and particle diffusion.[26] Hydrodynamic radii were determined using the Stokes-Einstein relationship, in which k is Boltzmann's constant, T is the temperature, η is the solvent viscosity, D_o is the diffusion coefficient, and R_H is the hydrodynamic radius:

$$R_H = \frac{kT}{6\pi\eta D_o}$$

Eq. 4-3

The viscosity was corrected for temperature by the following equation, in which A and B are solvent-dependent parameters. This is essential since the viscosity is inversely proportional to the calculated hydrodynamic radius. For D_2O, Eq. 4-4 was used to calculate viscosity in cP relative to temperature in K (A = 3.4931, B = 9.3628E2, C = 1.7670E-3, D = -1.1438E-6).[27] For water, a simpler expression containing only the first stwo terms was used.

$$\log_{10}\eta = A + \frac{B}{T} + CT + DT^2$$

Eq. 4-4

Dynamic light scattering (DLS) was performed using a Malvern NanoZS operating at a fixed angle of 173° and a wavelength of 633 nm. The viscosity and refractive index were

adjusted as appropriate for H_2O, D_2O, or the mixture. The DLS data from this device was analyzed using Distribution Technology Software (DTS). This uses an algorithm based on CONTIN, which is a program designed for inversion of noisy equations via a constrained regularization algorithm as described by Provencher.[28, 29] The basic features of CONTIN are prior knowledge (in this case, that the sizes must be non-negative) and parsimony (the solution with the fewest and smoothest peaks is probably best). The CGS-3 also employs a multiple-tau correlation technique, meaning that the Δt value between channels varies; this reduces error due to noise.[30]

DLS is typically performed using an intensity autocorrelation, in which a Fourier transform is performed on the spectrum. This yields an autocorrelation function $G_2(\tau)$, in which the intensity is measured at an arbitrary time, t. After a time delay, τ, the intensity is measured again. The function $G_2(\tau)$ is given by an average of the product of the intensities at the two times as described as:

$$G_2(\tau) = \langle I(t) \cdot I(t+\tau) \rangle$$

Eq. 4-5

This may then be modeled by using the following equation, in which Γ is the decay rate.

$$G_2(\tau) = \int_0^\infty G(\Gamma, t) \exp(-2\Gamma\tau) d\Gamma$$

Eq. 4-6

This may be used to determine the diffusion coefficient, D, according to:

$$\Gamma = Dq^2$$

Eq. 4-7

Particle size may be determined using a correlation with the diffusion coefficient such as the Stokes-Einstein relationship, which is valid for non-interacting spherical particles. This is given by:

$$D_o = \frac{kT}{3\pi\eta d}$$

Eq. 4-8

in which k is Boltzmann's constant, T is the temperature, η is the viscosity, and d is the particle diameter.

If one assumes a non-draining sphere, the hydrodynamic radius may be related to the radius of gyration, R_g, by the following:[31]

$$R_H = 0.875 R_g$$

Eq. 4-9

Static light scattering (SLS) was also performed on the Malvern NanoZS. Previous measurements using the multi-angle capability of the Malvern CGS-3 had indicated that these scattering moieties had no angular dependence, so the single-angle NanoZS was acceptable. Scattering is described by:

$$Kc/R_\theta = 1/M_w + 2A_2C$$

Eq. 4-10

in which c is the concentration of the sample, M_w is the weight-average molecular weight, A_2 is the second virial coefficient, P(θ) is the form factor, q is the scattering vector, and K is an optical constant. The Rayleigh ratio, R_θ, is defined as

$$R_\theta = \frac{I_A \tilde{n}_o^2}{I_T \tilde{n}_T^2} R_T$$

Eq. 4-11

where I_A is the difference in intensity between the scattering sample and the solvent, I_T is the scattering intensity of toluene, $\tilde{n}_o$ is the solvent refractive index, $\tilde{n}_T$ is the refractive index of toluene, and R_T is the Rayleigh ratio of toluene. The scattering vector, q, is calculated according to:

$$q = \frac{4\pi n}{\lambda}\sin\left(\frac{\theta}{2}\right)$$

Eq. 4-12

in which λ is the wavelength, n is the refractive index of the sample, and θ is the measurement angle.[32] The optical constant, K, for the instrument is defined by the following, in which dn/dc is the refractive index increment and N_A is Avogadro's number.

$$K = \frac{4\pi^2\left(n_{solvent}\frac{dn}{dc}\right)^2}{\lambda^4 N_A}$$

Eq. 4-13

Due to the small size of the scattering entities (micelles) relative to the wavelength of the laser (633 nm), the SLS analysis could be done at a single angle using a Debye approach, which requires that qRg<<1.

$$Kc/R_\theta = 1/M_w + 2A_2C$$

Eq. 4-14

The refractive index increment, dn/dc, was measured using a Wyatt Optilab REx differential refractometer. Measured values of dn/dc for the triblock copolymers were between 0.128 and 0.143 mL/g, depending on triblock composition and temperature. All measurements were made in H_2O. The method outlined by Charron[33] was used to check the expected difference for dn/dc between H_2O and D_2O. The refractive index for a mixture of polymer and solvent was calculated by the Lorentz-Lorez equation:[34]

$$\frac{n^2-1}{n^2+2} = \frac{A_w}{M_w}\rho_w + \frac{A_p}{M_p}\rho_p$$

Eq. 4-15

in which n is the refractive index, M_w is the molecular weight of water, M_p is the molecular weight of a polymer repeat unit, ρ_w is the mass concentration of the solvent, ρ_p

is the mass concentration of the polymer, A_w is the molar refractivity of solvent, and A_p is the molar refractivity of a polymer repeat unit. The molar refractivity of the repeat unit was calculated using the molar refractivities of the bonds according to Vogel.[35] The relationship between polymer mass concentration and refractive index of the solution is:

$$\rho_p = \frac{3}{\frac{A_p}{M_p} - V_p \frac{n_w^2 - 1}{n_w^2 + 2}} \frac{n^2 - n_w^2}{(n^2 + 2)(n_w^2 + 2)}$$

Eq. 4-16

in which V_p is the partial specific volume of the polymer. This was measured as described later in this paper. The variation in dn/dc from the different solvents was expected to be less than 2%; therefore, using values measured in water alone was justifiable.

4.4.4 Densiometry

Partial specific volumes were measured using a DA-300 Density/Specific Gravity Meter (Mettler). The partial specific volumes of the 2k and 5k PEO at 25°C were determined using aqueous solutions in the range of 0.1-5 wt %. The partial specific volume of the micelles for each copolymer was measured in the weight range of 0.2-2%.

Densiometry operates on the principle that a cell of constant volume oscillates at a frequency dependent on the density of the sample. This is described by the following equation in which T is the oscillation period, d is the sample density, V_c is the cell volume, M_c is the cell mass, and K is a temperature-dependent constant. K may be determined in advance using reference samples. This procedure was performed daily using air and degassed water.

$$T = 2\pi\sqrt{\frac{dV_c + M_c}{K}}$$

Eq. 4-17

4.5 Results and Discussion

4.5.1 Light scattering

Static and dynamic light scattering measurements were performed on the polymers in D_2O and H_2O to provide input to the SANS model. These copolymers form two sorts of assemblies: a primary aggregate which is in size range typical for micelles and a secondary aggregate. This secondary aggregate is believed to be the result of PEO-PEO interactions between micelles, as PEO is known to self-aggregate.[36] The aggregation number from SLS used in the SANS modeling is based purely on the population of smaller aggregates. A summary is provided in Table 4-2.

Table 4-2. Summary of static and dynamic light scattering data on polymers in D_2O and H_2O, both with 0.1M NaCl and pH or pD 2.

		H_2O		D_2O	
	T (°C)	R_H (nm)	N_{agg}	R_H (nm)	N_{agg}
1930-3.1-1930	25	10.7	29.2	9.3	31.9
	35	10.0	31.6		
	45	10.4	34.9	9.5	39.0
	55	10.0	32.9		
	65	10.4	39.3	10.0	44.7
4850-2.5-4850	25	12.5	10.0	13.5	9.5
	35	12.2	10.0		
	45	11.7	10.0	12.3	9.3
	55	11.3	10.0		
	65	11.0	11.0	11.3	10.2
4850-4.7-4850	25	14.0	16.0	16.0	15.3
	35	13.3	15.0		
	45	12.8	16.0	13.3	17.5
	55	12.1	16.0		
	65	11.9	16.0	11.5	17.8

4.5.2 Partial Specific Volumes

The model is quite sensitive to the partial specific volume of core and corona. These were measured using a DA-300 Density/Specific Gravity Meter (Mettler). The partial specific volume of PEO was determined for both 2k and 5k blocks. These were provided by Dr. Riffle's group, and were the same materials subsequently used to prepare the triblock copolymers. The specific gravity was measured at each of five concentrations, then plotted as the inverse of solution density versus concentration. The partial specific

volume of the solution is obtained by drawing a tangent through a point on this curve and extrapolating to the bulk. In the case of PEO, it has been found previously that the plot is linear for concentrations up to approximately 50 wt.%.[37]

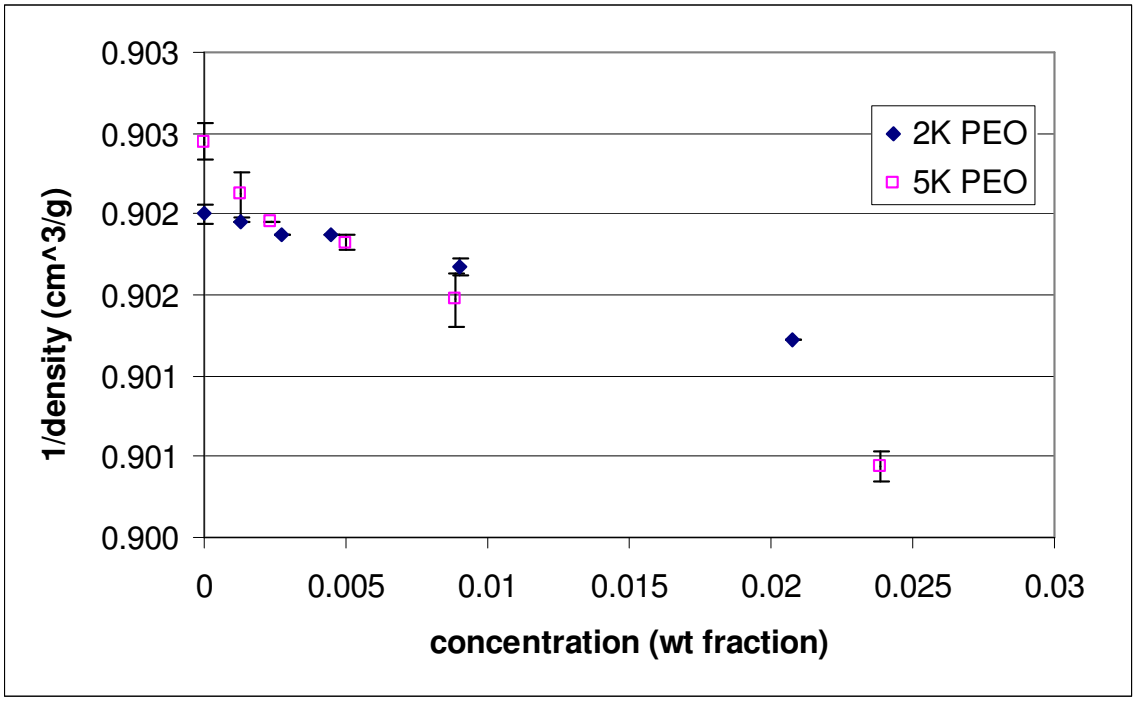

Figure 4-2. Density measurements for PEO homopolymer in D_2O at pH 2 with 0.1M NaCl.

In order to use these measurements in the SANS model, it was necessary to determine that the PEO fraction in the corona was in the linear range (<50 wt. %). 1930-3.1-1930 was used as the example for this, as it was expected to have the most crowded corona due to a much higher aggregation number than 4850-2.5-4850 or 4850-4.7-4850. Initial SANS fitting treating the entire micelle as if it had the density of PEO yielded a core radius of about 2.5 nm (assuming no solvation of the core) and a total radius of about 6.7 nm. The aggregation number of 32 was previously measured using SLS. The volume of the core was calculated as 1215 nm^3. The volume fraction of PEO, ϕ_{PEO}, in the corona was determined by:

$$\phi_{PEO} = \frac{V_{PEO}}{V_{corona}}$$

Eq. 4-18

in which the volume of PEO in the corona, V_{PEO}, is calculated using simple geometry by:

$$V_{PEO} = \frac{2N_{agg}M_{unimer}v_{PEo}}{N_{AV}}$$

Eq. 4-19

in which v_{PEO} is the partial specific volume of PEO measured by densiometry. The volume of the corona, V_{corona}, is calculated as the difference between the volume of a spherical micelle based on dynamic light scattering and the volume of the core based on SANS modeling described later. This approach yielded a PEO volume fraction of approximately 0.15 in the corona. As this is substantially below 50%, the partial specific volume measured at low wt% was deemed adequate. Density measurements on the micelles were carried out at conditions similar to those in the SANS experiment. Concentrations from 0.2 to 2 wt % were chosen to bracket the concentration range of interest. This is shown in the figure below.

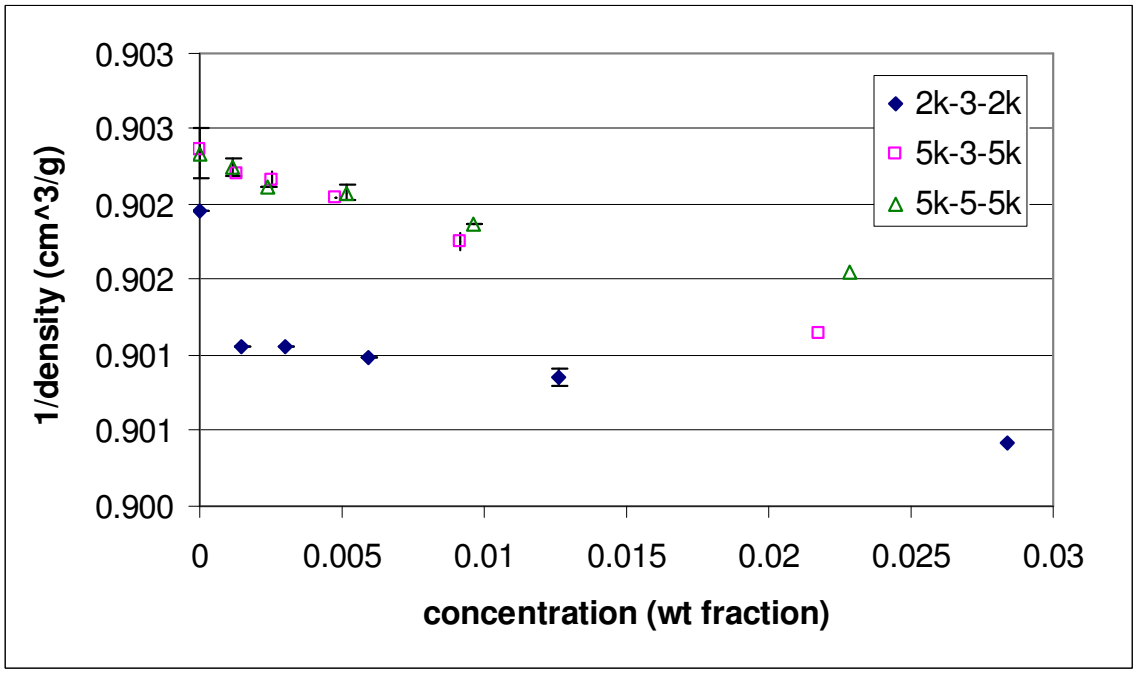

Figure 4-3. Density measurements for triblock copolymers in D_2O at pH 2 with 0.1M NaCl.

The specific volume of the copolymer was assumed to have additive contributions from the block portion, as described by several authors.[38, 39] This is according to the following relationship:

$$V_{micelle} = m_{PEO} v_{PEO} + m_{PU} v_{PU}$$

Eq. 4-20

in which m_{PEO} is the mass fraction of the PEO corona, m_{PU} is the mass fraction of the polyurethane core, and v_{PEO} and v_{PU} are the partial specific volumes of the corona and core, respectively. This enabled calculation of the specific volume of the polyurethane-containing core of the micelle. The results are summarized below:

Table 4-3. Summary of densiometry on the triblock copolymers with 0.1M NaCl, pD or pH 2.

	mass fraction PEO	mass fraction PU	specific volume of PEO (cm^3/g)	specific volume of micelle (cm^3/g)	Specific volume of core (calc) (cm^3/g)
1930-3.1-1930 (D_2O)	0.75	0.26	0.8648	0.8766	0.9116
1930-3.1-1930 (50:50)			0.8806	0.8902	0.9187
1930-3.1-1930 (H_2O)			0.8198	0.8081	0.7734
4850-2.5-4850 (D_2O)	0.90	0.10	0.8246	0.8480	1.0551
4850-4.7-4850 (D_2O)	0.84	0.16	0.8246	0.8697	1.1059

4.5.3 Small Angle Neutron Scattering (SANS)

Contrast is a result of difference in the scattering length densities of the material and the medium. Scattering length density is given by the following equation, in which b_i is the bound coherent scattering length of the i^{th} atom in the volume, V, containing n atoms.

$$\rho = \frac{\sum_{i=1}^{n} b_i}{V}$$

Eq. 4-21

The Guinier approximation describes low q ($qR_g << 1$) scattering of dilute samples by Eq. 4-22 in which R_g is the radius of gyration and q is the modulus of the scattering vector, given by Eq. 4-23. The scattering angle is θ and λ is the wavelength.[25] The Guinier law is not shape dependent, and is valid as long as $1 << q/R_g$, the system is sufficiently dilute to ensure independent scattering, and the system is isotropic. [40]

$$I(q) \approx I(0)\exp\left(-\frac{1}{3}q^2 R_g^2\right)$$

Eq. 4-22

$$q = \frac{4\pi}{\lambda}\sin\frac{\theta}{2}$$

Eq. 4-23

A slightly more complex representation describes the scattering according to a Debye function (Eq. 4-24), wherein Z is the degree of polymerization and υ_m is the monomer specific volume [40] This assumes that the polymer chains behave like Gaussian coils.

$$I(q) = \phi(\Delta\rho)^2 Z v_m \left(\frac{2\left(e^{-qR_g} + qR_g - 1\right)}{\left(qR_g\right)^2}\right)$$

Eq. 4-24

Core-shell models may be used to describe formation of micelles in solution. These models depend on being able to observe a difference in the scattering density between at least two of the three components: core, shell, and solvent. A core that is devoid of solvent simplifies the experiment, but is not essential. However, for simple models, one must make some assumptions about the degree of solvation of the core.

The form factor, P(q), for a monodisperse spherical core-shell system with a dry core is described by Eq. 4-25, in which R_c is the radius of the core and R_s is the total radius of the micelle.[41]

$$P(q) = \left[\frac{3V_c(\rho_c - \rho_s)j_1(qR_c)}{qR_c} + \frac{3V_s(\rho_s - \rho_{solv})j_1(qR_s)}{qR_s}\right]^2$$

Eq. 4-25

$$j_1(x) = \left(\frac{\sin x - x\cos x}{x^2}\right)$$

Eq. 4-26

$$V_c = \frac{4\pi}{3}R_c^3$$

Eq. 4-27

The scattered intensity is given by Eq. 4-28, in which S(q) is the structure factor and n_p is the number density of particles.

$$I(q) = n_p P(q) S(q)$$

Eq. 4-28

The structure factor, S(q), is used to describe ordering of the micelles in solution. For a dilute case, there is no micelle-micelle interaction, and S(q) = 1. For concentrated solutions, one option is to use a hard sphere structure factor, which for monodisperse spheres is calculated using the following interaction potentials:[42]

$$U(r) = \begin{Bmatrix} \infty, r < 2R \\ 0, r \geq 2R \end{Bmatrix}$$

Eq. 4-29

4.5.4 Data Reduction

Data reduction was carried out using IGOR Pro 5 and macros provided by NIST.[43] The reduction scheme consisted of several steps. A background consisting of a blocked beam and an empty cell was subtracted. The sensitivity of the detector was accounted for by comparing the scattering across all pixels to Plexiglas, a known isotropic scatterer. A file containing these data was provided by the NG3 SANS staff. Transmission for each sample was used to normalize the data. The data were masked to eliminate the edges and any bad pixels using a mask provided by the NG3 SANS staff. The resulting data were circularly averaged to yield 1-D data. After reduction, overlapping q-ranges were combined to yield single curves.

4.5.5 Solvent Selection

Scattering contrast is defined as the difference between the scattering length density (SLD or ρ) of the scattering moiety and the solvent. Scattering lengths for the elements are available in tabulated form, but for ease the scattering length densities for the polyurethane center block and the PEO end block were calculated using an algorithm provided by NIST and available at http://www.ncnr.nist.gov. Estimated contrasts are listed in the table below.

Table 4-4. Scattering length densities for polymers and solvents.

		Contrast (A-2)		
	SLD (A^{-2})	D_2O	H_2O	D_2O:H_2O mix
D_2O	6.36e-6			
H_2O	-5.60e-7			
50:50 D_2O:H_2O	2.9e-6			
polyurethane core	1.13e-6	-5.23e-6	1.69e-6	-1.77e-6
PEO tail	6.17e-7	5.74e-6	1.18e-6	-2.28e-6

The expectation was that D_2O would provide the most pronounced contrast. D_2O has the additional advantage of resulting in less incoherent scattering than H_2O. Typical background scattering for D_2O is 0.06 cm^{-2} as compared to 1 cm^{-2} for H_2O. An initial experiment was conducted to ascertain the solvent compositions giving the best scattering. As expected, D_2O provided data with the most distinctive shape. However, subsequent experiments were performed in several solvents and modeled using a global fit.

4.5.6 Data Analysis

The SANS model used for the data analysis was developed from the model for block copolymer micelles of Pedersen et al.[8, 44, 45] This work was based on form factors for polymer stars using Gaussian statistics.[46, 47] The model describes a micelle with a homogeneous core (in this case PU) surrounded by a corona of non-interacting Gaussian chains (PEO), shown schematically in Figure 4-4. The model was modified from Pedersen's work to account for the presence of two PEO chains for each PU center block.

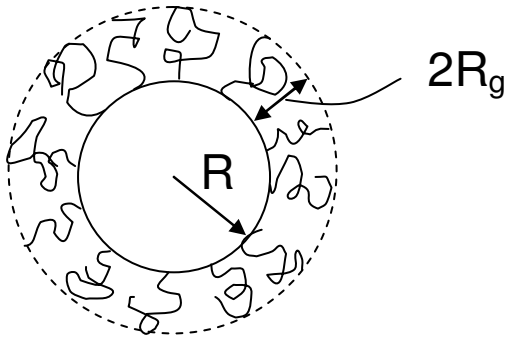

Figure 4-4. Illustration of a block copolymer micelle with nomenclature of the SANS model. R is the hard-sphere radius of the core. $2R_g$ is the thickness of the corona.

The overall expression for the intensity scattered by monodisperse micelles is given by Eq. 4-30. $F_{mic}(q)$ is the form factor for the micelle, S(q) is a hard sphere structure factor, $A_{mic}(q)$ is the amplitude of the radial scattering length distribution of the micelle based on noninteracting chains, c is the concentration, and M_{mic} is the mass of a micelle.

$$\frac{I(q)}{c} = \frac{1}{M}\left(F\ (q) + A(q)^2\left[S(q) - 1\right]\right)$$

Eq. 4-30

No evidence was seen to indicate particle-particle interactions so this simplifies to:

$$\frac{I(q)}{c} = \frac{1}{M}F\ (q)$$

Eq. 4-31

The form factor, F(q) is given by the following.

$$F(q) = N^2\beta_{core}^2 A_{core}^2(q) + 2N\beta_{chain}^2 F_{chain}(q) + 4N^2\beta_{core}\beta_{chain}A_{core}A_{chain}(q) + 2N(2N-1)\beta_{chain}^2 A_{chain}^2(q)$$

Eq. 4-32

N is the aggregation number of the micelle and β_{core} and β_{chain} are the total excess scattering lengths of one PU block and one PEO block respectively. A_{core} is the form factor amplitude for a spherical homogeneous core with radius R and a smoothly decaying scattering length density over a width σ at the surface.

$$A_{core}(q) = \Phi(qR)\exp\frac{\left(-q^2\sigma^2\right)}{2}$$

Eq. 4-33

The form factor amplitude of a sphere with a sharp surface, Φ(qR), is given by the following.

$$\Phi(qR) = \frac{3\left(\sin(qR) - qR\cos(qR)\right)}{(qR)^3}$$

Eq. 4-34

F_{chain} is given by the Debye function in which R_g is the radius of gyration of a single polymer Gaussian chain.

$$F_{chain}(q) = \frac{2\left[\exp\left(-q^2R_g^2\right) - 1 + q^2R_g^2\right]}{\left(q^2R_g^2\right)^2}$$

Eq. 4-35

The form factor amplitude of the corona, $A_{chain}(q)$, is given by the following.

$$A_{chain}(q) = \frac{1-\exp\left(-q^2R_g^2\right)}{\left(q^2R_g^2\right)^2}\frac{\sin\left[q\left(dR_g + R\right)\right]}{q\left(dR_g + R\right)}$$

Eq. 4-36

The variable d is defined as the distance from the center of mass of the corona chains to the surface of the core divided by the radius of gyration of a corona chain. In other words, if d is equal to unity, the center of mass of the corona chains is located at a distance of R_g from the surface. This is the case in which the corona chains do not penetrate the core.

4.5.7 Model Fits

The results for the triblock model fitting for the three polymers are shown in Figure 4-5, Figure 4-6, and Figure 4-7. It was found that the background was relatively independent of other parameters in the model and was allowed to vary in all the fittings. There was an upturn in the data at $q<0.01$ suggesting the presence of aggregates in the samples. This is consistent with the DLS results which showed a quantity of larger aggregates in the solutions, even immediately following solution filtration. As a result, the data was fitted using $q = 0.01$ Å^{-1} as the lower boundary.

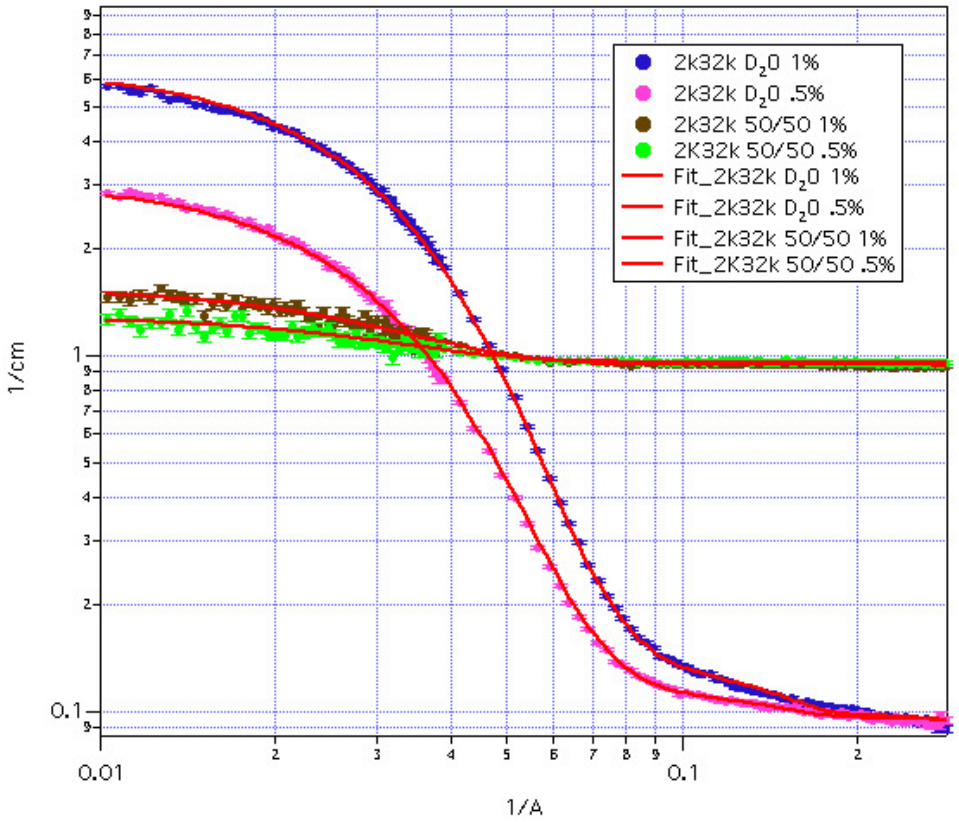

Figure 4-5. SANS data and global fits to a triblock copolymer micellar model for 1930-3.1-1930. The H_2O solvent data has been omitted from the graph for clarity.

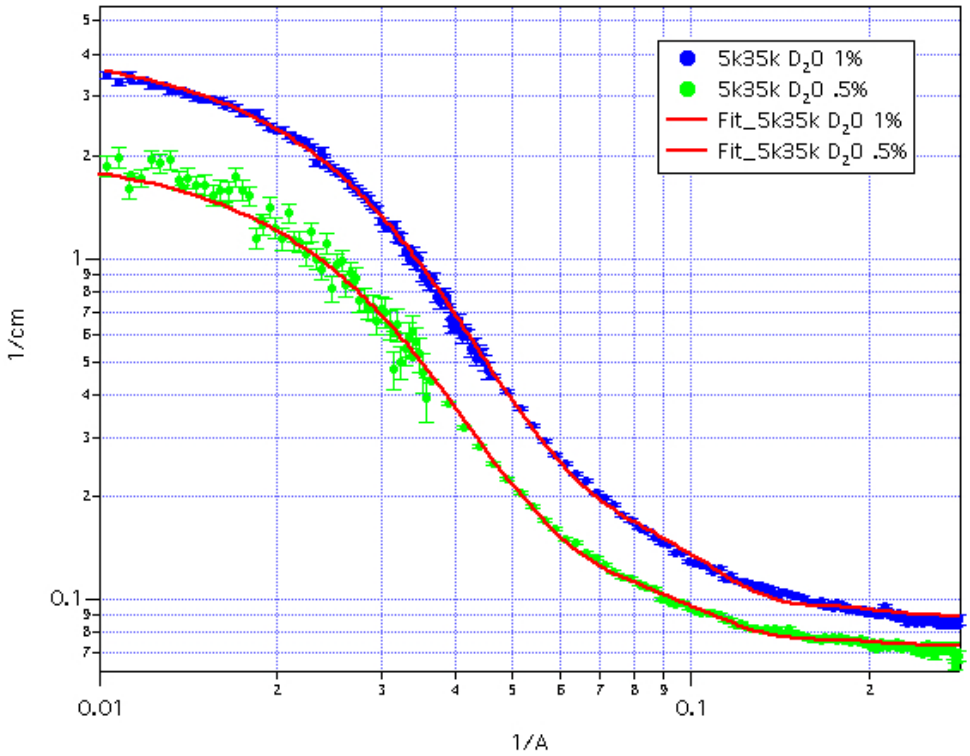

Figure 4-6. SANS data and global fits to a triblock copolymer micellar model for4850-2.5-4850.

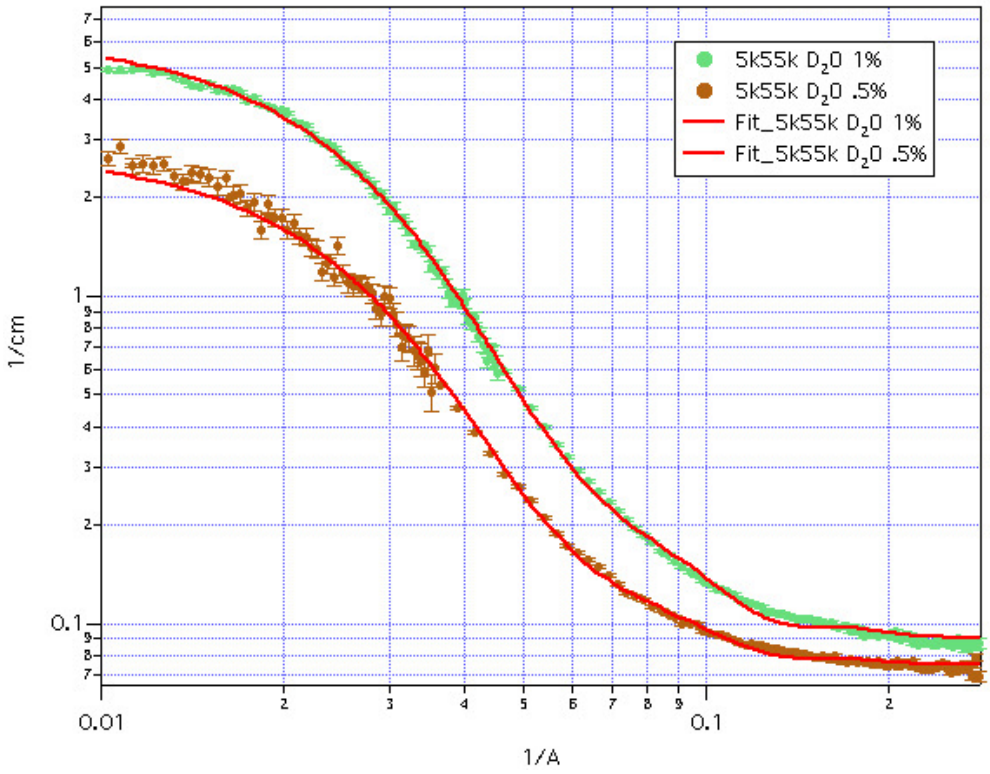

Figure 4-7. SANS data and global fits to a triblock copolymer micellar model for 4850-4.7-4850.

In some of the fitted curves there are features such as small bumps that are not present in the data. These features are a result of the monodisperse nature of the fitted model. They will tend to smear out if even a small amount of polydispersity is added to the model.

From knowledge of the aggregation number, physical density, chemical composition, and concentration, it was possible to model the 1930-3.1-1930 data using the triblock model with just 2 free parameters: the radius of the core, R, and the radius of gyration of the chain, R_g. The triblock model was used to globally fit two concentrations and three separate solvent contrasts. In other words, six independent data sets were globally refined giving a core radius of 27 Å and an R_g for the PEO chains of 22 Å.

However, the fit significantly improves if the concentration is allowed to refine, showing a reduction of approximately 25% from the original value. It is assumed that this apparent reduction in micelle concentration is as a result of the formation of larger aggregates as mentioned previously. Allowing the concentration to refine also allows for improvements in the fits for the 4850-2.5-4850 and 4850-4.7-4850 data by simultaneously fitting two concentrations in D_2O solvent only. The concentrations drop by 35% and 40% respectively.

Initial attempts at fitting the triblock model to the 4850-2.5-4850 data with just 2 free parameters, R and R_g, resulted in the radius of the core dropping to zero and a finite Gaussian chain dimension. This is reminiscent of a star polymer system in which polymer chains effectively converge at a point. A model of this form was found to fit the data equally well. The fitting of the triblock model could, however, be significantly improved if penetration of the core by the PEO chains was allowed. This could be achieved by either allowing the parameter d to refine (values of less than 1 correspond to an overlap between the core and the chains) or by allowing the scattering length of the core, β_{core} to refine. When β_{core} is allowed to refine it shows a significant increase in magnitude consistent with the presence of PEO in the core. While the 4850-4.7-4850 data can be fitted well by just allowing R, R_g, and concentration to refine, like the 4850-2.5-4850, a significant improvement is shown if PEO is allowed to penetrate the core.

This is plausible as PEO and carboxylates are known to form complexes by hydrogen bonding.[19, 21]

Table 4-5. Summary of fitting of SANS data for in 0.1M NaCl, equivalent pH 2.

No of data sets refined	1930-3.1-1930 6 (3 contrasts, 2 concentrations)	4850-2.5-4850 2 (1 contrasts, 2 concentrations)	4850-4.7-4850 2 (1 contrasts, 2 concentrations)
Aggregation number (N)	31.9	9.5	15.3
Radius of core (R) Å Igor	24.5 ± 0.1	30.1 ± 0.1	32.5 ± 0.1
Radius of core (R) Å densiometry	24.7	17.3	23.1
Rg of chain Å Igor	21.1 ± 0.01	28.8 ± 0.1	28.4 ± 0.1
Total radius (R + 2Rg - σ) Å	61.7	82.6	84.6
Rg (Guinier approximation) Å	51.5	61.7	64.3
R_H from DLS Å	93	135	160
R_H/total radius	1.51	1.63	1.88
R_H /R_g	1.80	2.19	2.48
Reduction in concentration	25%?	35%	40%
Initial βcore (predicted) Å	-0.0103	-0.0103	-0.0285
Final β core (fit) Å	- 0.0084	-0.0305	-0.0338
Reduced χ^2	2.1	4.2	5.8
Volume of PU (from density) $Å^3$	62766	18223	51972
Volume (from SANS fitting) $Å^3$	61600	113097	145125
Core composition:	0% PEO 101.8±10.0%PU*	76.3±1.5% PEO 17.7±5.6% PU	61.1±6.9% PEO 37.9±9.1% PU

A summary of the results of the triblock model fitting is presented in Table 4-5. By taking the overall micelle radius as $R+2R_g$, the 1930-3.1-1930, 4850-2.5-4850, and 4850-4.7-4850 micelles have radii of 68.2 Å, 87.6Å, and 89.6 Å, respectively. By light scattering, the hydrodynamic radii are 107, 125, and 150 Å, respectively.

From knowledge of the density and mass of PU and the aggregation number from DLS in each of the samples the volume of PU within the core for the three samples can be determined. By comparing this with the core volumes based on the SANS fits and assuming no water penetration it is possible to determine the core composition. These results are also shown in Table 4-5. This indicates that the core in 1930-3.1-1930 is predominantly PU, while the cores of the 4850-2.5-4850 and 4850-4.7-4850 micelles contain some PEO with the concentration of PEO increasing as the aggregation number decreases.

4.5.8 Comparison with the Density Distribution Prediction

Micelle dimensions were also estimated with the density distribution (DD) model, developed by Vagberg et al.[48] This model, based on a model for star polymers by Daoud and Cotton[49] assumes concentric shells with a constant number of blobs equal to twice the aggregation number in this case. Blob size $\xi(r)$, is a continuous function of distance from the surface. The segment density in the shell varies with distance from the core.

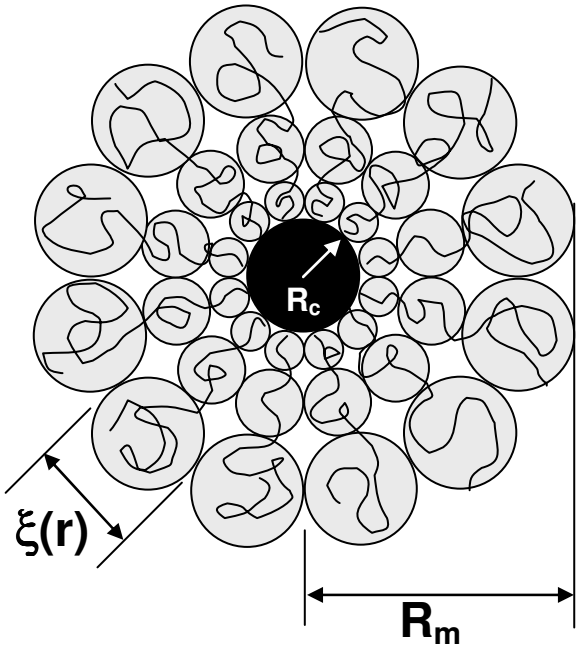

Figure 4-8. Schematic representation of the micelle showing the density distribution model[48] parameters.

The DD model predicts micelle radius, R_m, as:

$$R_m = \left[N a_s^{1/\nu} \frac{8 f^{(1-\nu)/2\nu}}{3\nu 4^{1/\nu}} + R_c^{1/\nu} \right]^{\nu}$$

Eq. 4-37

where N is the number of Kuhn segments, ν is the Flory exponent, R_c is the radius of the core, and f is the number of corona chains, which for these triblock copolymers is twice the aggregation number.

The blob diameter, $\xi(r)$ is given by:

$$\xi(r) = \frac{4r}{f^{1/2}}$$

Eq. 4-38

in which r is the distance from the center.

The Flory exponent, ν, varies between 0.5 at a theta condition and 0.6 for a good solvent. The calculations used ν = 0.583[36] for PEO in water at room temperature for these calculations, a value used in similar studies by other authors.[50-52]

The radius predicted by the density distribution model is compared with a measured hydrodynamic radius and a modeled radius by SANS in Figure 4-9. The agreement between SANS and the model is within 6-15% for the three polymers.

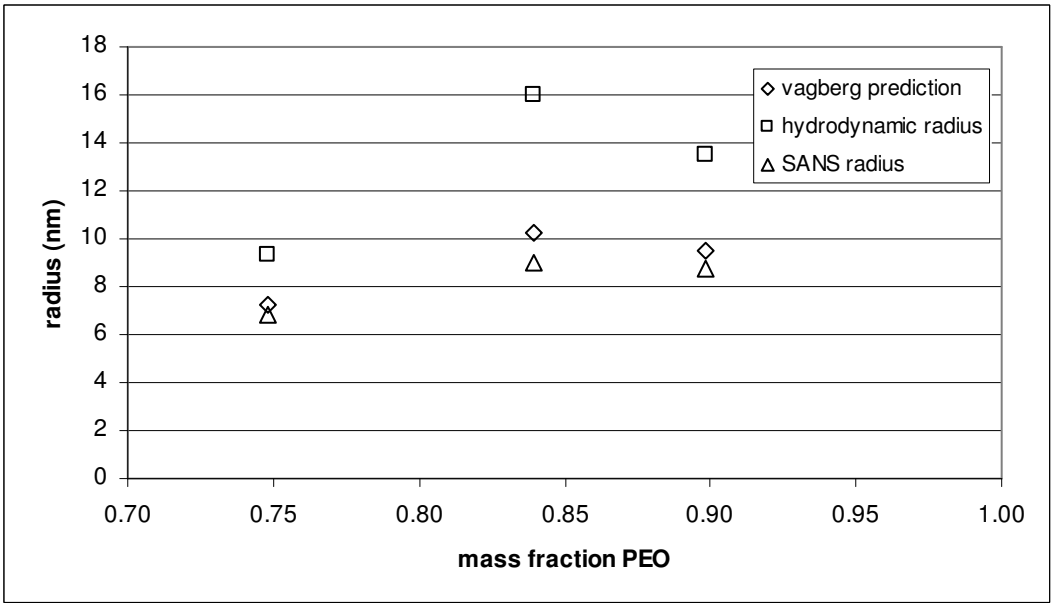

Figure 4-9. Comparison of the density distribution[48] prediction for micelle radius with measured hydrodynamic radius (DLS) and total radius by SANS. All measurements were in D_2O at pD 2.

4.6 Conclusions

By using a modified SANS model consisting of a homogeneous polyurethane core and a non-interacting Gaussian corona, good fits (reduced χ^2 = 2-6) were obtained for scattering data on three species of triblock copolymer micelles. The triblock model is a

better fit for the data from samples with a higher aggregation number. The model is consistent with micelles in which the cores of all three micelles are predominantly composed of PU with the addition of PEO for the micelles with lower aggregation numbers.

There is little experimental evidence for the presence of any water in the core, although the calculations of PEO content in the core may be incorrect if in addition to PEO there was also some water present in the core. However, this water content is likely to be only a small fraction of the total volume.

4.7 References

1. Harris, L.A., et al., Magnetite nanoparticle dispersions stabilized with triblock copolymers. *Chemistry of Materials*, **2003**. 15(6): p. 1367-1377.

2. Wu, G.W., et al., SANS and SAXS studies of pluronic L64 in concentrated solution. *Physica A*, **1996**. 231(1-3): p. 73-81.

3. Moffitt, M., et al., Coronal Structure of Star-Like Block Ionomer Micelles: An Investigation by Small-Angle Neutron Scattering. *Macromolecules*, **1998**. 31: p. 2190-1297.

4. Goldmints, I., et al., Structure of (deuterated PEO) (PPO) (deuterated PEO) block copolymer micelles as determined by small angle neutron scattering. *Langmuir*, **1999**. 15(5): p. 1651-1656.

5. Jain, N.J., et al., Salt induced micellization and micelle structures of PEO/PPO/PEO block copolymers in aqueous solution. *Colloids and Surfaces A: Physicochemical and Engineering Aspects*, **2000**. 173(1-3): p. 85-94.

6. Soni, S.S., et al., Micellar structure of silicone surfactants in water from surface activity, SANS and viscosity studies. *Journal of Physical Chemistry B*, **2002**. 106(10): p. 2606-2617.

7. Yang, L., et al., Small-angle neutron scattering investigation of the temperature-dependent aggregation behavior of the block copolymer pluronic L64 in aqueous solution. *Langmuir*, **2000**. 16(23): p. 8555-8561.

8. Pedersen, J.S. and Gerstenberg, M.C., The structure of P85 Pluronic block copolymer micelles determined by small-angle neutron scattering. *Colloids and Surfaces a-Physicochemical and Engineering Aspects*, **2003**. 213(2-3): p. 175-187.

9. Ashcroft, N.W. and Lekner, J., *Physics Review*, **1966**. 145: p. 83-90.

10. Kinning, D.J. and Thomas, E.L., Hard-Sphere Interactions between Spherical Domains in Diblock Copolymers. *Macromolecules*, **1984**. 17: p. 1712-1718.

11. Mortensen, K. and Pedersen, J.S., Structural Study on the Micelle Formation of Poly(ethylene oxide)-Poly(propylene oxide)-Poly(ethylene oxide) Triblock Copolymer in Aqueous Solution. *Macromolecules*, **1993**. 26(805-812).

12. Pedersen, J.S. and Gerstenberg, M.C., Scattering Form Factor of Block Copolymer Micelles. *Macromolecules*, **1996**. 29: p. 1363-1365.

13. Svaneborg, C. and Pedersen, J.S., Form Factors of Block Copolymer Micelles with Excluded-Volume Interactions of Corona Chains Determined by Monte Carlo Simulations. *Macromolecules*, **2002**. 26: p. 1028-1037.

14. Li, Y., Gong, Y.-K., and Nakashima, K., Nanoaggregate Formation of Poly(ethylene oxide)-b-polymethacrylate Copolymer Induced by Alkaline Earth Metal Binding. *Langmuir*, **2002**. 18: p. 6727-6729.

15. Bronich, T.K., et al., Polymer Micelle with Cross-Linked Ionic Core. *Journal of the American Chemical Society*, **2005**. 127: p. 8236-8237.

16. Solomatin, S.V., et al., Environmentally Responsive Nanoparticles from Block Ionomer Complexes: Effects of pH and Ionic Strength. *Langmuir*, **2003**. 19: p. 8069-8076.

17. Li, Y. and Nakashima, K., Fluorescence studies on the properties of the nanoaggregates of poly(ethylene oxide)-b-polymethacrylate copolymer formed by binding of cationic surfactants to polymethacrylate block. *Langmuir*, **2003**. 19(3): p. 548-553.

18. Khanal, A., et al., Fabrication of nanoaggregates of poly(ethylene oxide)-b-polymethacrylate by complex formation with chitosan or methylglycolchitosan. *Colloids and Surfaces A-Physicochemical and Engineering Aspects*, **2005**. 260(1-3): p. 129-135.

19. Poe, G.D., et al., Enhanced Coil Expansion and Intrapolymer Complex Formation of Linear Poly(methacrylic acid) Containing Poly(ethylene glycol) Grafts. *Macromolecules*, **2004**. 37: p. 2603-2612.

20. Drescher, B., Scranton, A.B., and Klier, J., Synthesis and Characterization of Polymeric Emulsifiers Containing Reversible Hydrophobes: Poly(methacrylic acid-g-ethylene glycol). *Polymer*, **2001**. 42: p. 49-58.

21. Mathur, A.M., et al., Polymeric emulsifiers based on reversible formation of hydrophobic units. *Nature*, **1998**. 392(6674): p. 367-370.

22. Woodward, R.C., et al., *Journal of Applied Crystallography, accepted*, **2007**.

23. Glasoe, P.K. and Long, F.A., Use of Glass Electrodes to Measure Acidities in Deuterium Oxide. *Journal of Physical Chemistry*, **1960**. 64: p. 188-190.

24. Glinka, C.J., et al., The 30 m Small-Angle Neutron cattering Instruments at the National Institute of Standards and Technology. *Journal of Applied Crystallography*, **1998**. 31(3): p. 430-445.

25. Higgins, J.S. and Benoit, H.C., Polymers and Neutron Scattering. Oxford Series on Neutron Scattering in Condensed Matter, ed. S.W. Lovesey and E.W.J. Mitchell. **1994**, Oxford: Clarendon Press.

26. Finsy, R., Particle Sizing by Quasi-Elastic Light-Scattering. *Advances in Colloid and Interface Science*, **1994**. 52: p. 79-143.

27. Yaws, C.L., ed. Chemical Properties Handbook. **1999**, McGraw-Hill: New York.

28. Provencher, S.W., A Contrstrained Regularization Method for Inverting Data Represented by Linear Algebraic or Integral Equations. *Computer Physics Communications*, **1982**. 27: p. 213-227.

29. Provencher, S.W., CONTIN: A General PurposeConstrained Regularization Program for Inverting Noisy Linear Algebraic and Integral Equations. *Computer Physics Communications*, **1982**. 27: p. 229-242.

30. Peters, R., Noise on photon correlation functions and its effect on data reduction algorithms., in Dynamic Light Scattering: The Method and Some Applications, W. Brown, Editor. **1993**, Clarendon Press: Oxford.

31. Tanford, C., Physical Chemistry of Macromolecules. **1962**, New York: John Wiley and Sons.

32. Malvern_Instruments, CGS-3 User Manual, Chapter 8. **2005**.

33. Charron, J.R., Block Copolymer Adsorption to Phospholipid Monolayers at the Air-Water Interface, in Chemical Engineering. **1996**, Carnegie Mellon.

34. Cuypers, P.A., et al., The Adsorption of Prothrombin to Phosphatidylserine Multilayers Quantitated by Ellipsometry. *The Journal of Biological Chemistry*, **1983**. 25(2426-2431).

35. Vogel, A.I., et al., Physical Properties and Chemical Constitution. Part XXIV. Aliphatic Aldoximes, Ketoximes, and Ketoxime O-Alkyl Ethers, NN-Dialkylhydrazines, Aliphatic Ketazines, Mono- and Di-alkyl-aminopropionitriles, Alkoxypropionitriles, Dialkyl Azodiformates, and Dialkyl Carbonates. Bond Parachors, Bond Refractions, and Bond-refraction Coefficients. *Journal of the Chemical Society*, **1952**: p. 514-549.

36. Devanand, K. and Selser, J.C., Asymptotic-Behavior and Long-Range Interactions in Aqueous-Solutions of Poly(Ethylene Oxide). *Macromolecules*, **1991**. 24(22): p. 5943-5947.

37. Muller, E.A. and Rasmussen, P., Densities and Excess Volumes in Aqueous Poly(ethylene glycol) Solutions. *Journal of Chemical and Engineering Data*, **1991**. 36: p. 214-217.

38. Sommer, C., Pedersen, J.S., and Stein, P.C., Apparent Specific Volume Measurements of Poly(ethylene oxide), Poly(butylene oxide), Poly(propylene oxide), and Octadecyl Chains in the Micellar State as a Function of Temperature. *Journal of Physical Chemistry B*, **2004**. 108: p. 6242-6249.

39. Wen, X.G. and Verrall, R.E., Temperature Study of Sound Velocity and Volume-Related Specific Thermodynamic Properties of Aqueous Solutions of Poly(ethylene oxide)-Poly(propylene oxide)-Poly(ethylene oxide) Triblock Copolymers. *Journal of Colloid and Interface Science*, **1997**. 196: p. 215-223.

40. Roe, R.-J., Methods of X-ray and Neutron Scattering in Polymer Science. Topics in Polymer Science, ed. J.M. Mark. **2000**, New York: Oxford University Press.

41. Guinier, A. and Fournet, G., Small-Angle Scattering of X-rays. **1955**, New York: John Wiley and Sons.

42. Percus, J.K. and Yevick, G.J., Analysis of Classical Statistical Mechanics by Means of Collective Coordinates. *The Physical Review*, **1958**. 110(1): p. 1-13.

43. Greenwald, B. and Krzywon, J. SANS Reduction Macros Version 4.2. Available from: http://www.ncnr.nist.gov/programs/sans/data/data_red.html

44. Pedersen, J.S., Structure factors effects in small-angle scattering from block copolymer micelles and star polymers. *Journal of Chemical Physics*, **2001**. 114(6): p. 2839-2846.

45. Pedersen, J.S., et al., A Small-Angle Neutron and X-ray Contrast Variation Scattering Study of the Structure of Block Copolymer Micelles: Corona Shape and Excluded Volume Interactions. *Macromolecules*, **2003**. 36: p. 416-433.

46. Benoit, H.C., On the effect of branching and polydispersity on the angular distribution of the light scattered by gaussian coils *Journal of Polymer Science*, **1953**. 11: p. 507-510.

47. Marques, C.M., et al., Scattering from solutions of star polymers. *European Physical Journal B*, **1998**. 3(3): p. 353-358.

48. Vagberg, L.J.M., Cogan, K.A., and Gast, A.P., Light-Scattering Study of Starlike Polymeric Micelles. *Macromolecules*, **1991**. 24(7): p. 1670-1677.

49. Daoud, M. and Cotton, J.P., Star shaped polymers: a model for the conformation and its concentration dependence. *Journal de Physique*, **1982**. 43: p. 531-538.

50. Farinha, J.P.S., et al., Structure in tethered chains: Polymeric micelles and chains anchored on polystyrene latex spheres. *Langmuir*, **1998**. 14(9): p. 2291-2296.

51. FitzGerald, P.A., Davey, T.W., and Warr, G.G., Micellar structure in gemini nonionic surfactants from small-angle neutron scattering. *Langmuir*, **2005**. 21(16): p. 7121-7128.

52. Johnsson, M., Hansson, P., and Edwards, K., Spherical micelles and other self-assembled structures in dilute aqueous mixtures of poly(ethylene glycol) lipids. *Journal of Physical Chemistry B*, **2001**. 105(35): p. 8420-8430.

5 Pair Interactions Between Micelles: Prediction of the Second Virial Coefficient for Micelles Using a Star Model

5.1 Abstract

A method is presented for predicting the second virial coefficient, A_2, for micelles in solution based on the pair potential model for a star polymer developed by Likos et al.[1, 2] Static and dynamic light scattering data for a series of novel polyurethane-containing hydrophilic triblock copolymers in water as well as data from previous studies were used to test the model. Comparison of the experimentally determined A_2 values to the star model and hard sphere approximations revealed that the star model more accurately predicted interactions for micelles, particularly in the case of micelles having lower aggregation numbers indicative of softer potentials.

5.2 Keywords

soft colloid; second virial coefficient; interaction potential; blob model; triblock copolymer; micelle

5.3 Introduction

Brush formation due to terminally attached chains on flat surfaces has thus been studied extensively. Scaling models employing stepwise density functions were developed by Alexander,[3, 4] de Gennes,[5] and Cantor,[6] while self consistent mean field (SCF) models[7-9] used continuous functions to describe polymer segment density.

Polymer chains on curved surfaces are less extended at a given adsorption density than their flat counterparts due to the curvature of the surfaces that provides additional space for the polymer chains at a given graft density as compared to a flat plate. The resulting segment density profile for terminally attached chains on highly curved surfaces was described by Daoud and Cotton in a model to describe the structure of star polymers.[10]

Their model, based on scaling theory, proposed that polymers tethered to a spherical surface assumed the conformation of a string of blobs increasing in size with distance from the surface. This model has been applied to a number of systems to describe aggregation and adsorption behavior of neutral and charged block copolymers.[11-13] Halperin performed a scaling analysis by applying the star model allowing for a small insoluble core to polymer micelles in selective solvents.[14]

The Daoud and Cotton model contains an adjustable integration constant that relates to scaling the number of chains to the surface area of the core and so the model has been extended in at least two ways to provide quantitative modeling capability. The Density Distribution (DD) model by Vagberg et al.[15] described the increasing diameters of the blobs as a continuous function, also allowing direct computation of the brush length. Vagberg et al. also extended the star polymer model to include a finite core, R_c. This allowed prediction of micelle size based on aggregation number. This model has been used to describe a number of systems, including dendrimer-star polymers,[16, 17] poly(ethylene oxide) lipid micelles,[18] and polyelectrolyte block copolymer micelles.[19] D'Oliveira et al.[20] developed the Discrete Blob (DB) model, which was based on distinct layers and assumed dense packing of blobs on the surface. Based on the premise that the number of blobs in each sublayer was equal to the number of tethered chains, an expression for the diameter of the discretely packed blobs was developed, which allowed prediction of the total layer thickness. Farinha et al.[21] examined the DB and DD models using PS-PEO block copolymers both in micellar solution and adsorbed onto PS latex spheres and found them to be comparable both with experimental results and one another.

The interaction potential between two particles is critical to the stability of the suspension. For nanoparticles of metal oxides and metals, particularly polar solvents, attractive Van der Waals forces are typically so strong that, for steric stabilization, layer thicknesses may need to be on the order of the particle radius. Thus the problem of modeling and describing steric interaction energies on highly curved surfaces is expected to be of widespread interest for nanoparticle processing. The interaction potential may in some instances be measured directly using atomic force microscopy (AFM) with a sphere

glued to the cantilever, as pioneered by Ducker.[22] However, AFM is generally limited to particles on the order of a micron or larger in size. Other geometries such as crossed cylinders are possible using the surface force apparatus (SFA).[23-26] However, the radius of curvature of the cylinders is limited to macroscopic dimensions and the area of interest effectively has flat plate geometry, allowing use of the Derjaguin approximation.[23] For particles with radii less than 20 nm, such as the particles of interest in this study, it is not presently possible to directly measure the interaction energies. The ability to predict interaction potential of small colloids becomes increasingly useful, particularly as the radius of the particle and the thickness of the polymer brush become similar in dimension (i.e. the brush becomes increasingly curved.) The matter of interactions between star polymers in semi-dilute and concentrate solutions has been addressed in a rich body of literature. In particular, Vlassopoulos et al. have examined multiarm star polymers in solution using static and dynamic scattering techniques and have characterized interactions in semi-dilute solutions in terms of a structure factor.[17, 27-31]

Several groups have examined the steric interaction for polymer-coated curved surfaces. Lin and Gast employed a self consistent mean field theory with a Derjaguin approximation to describe the interaction potential for chains tethered on colloidal surfaces.[32] Likos and coworkers developed an expression for effective pair potential between star polymers.[2, 33] This expression describes the interaction potential in two regimes as exponentially decaying for large separations and a logarithmic repulsion at close distances. The form of the expression at small separations is derived from work by Witten and Pincus using scaling theory to describe stabilization of colloidal particles by long grafted polymer chains.[34] The chain conformations for a single star are compatible with the blob model of star polymers.[15] One key point regarding this approach is that as it is based on star polymers, it is designed for use with highly curved brushes and so translates well to smaller particles or micelles. As the interaction potential is difficult to measure directly, two means of testing the model are by measurement of a structure factor (such as by small angle neutron scattering) or by measurement of the second virial coefficient, A_2 (such as by light scattering and also SANS).

In this work, I use the model for effective interaction between star polymers developed by Likos et al.[1, 2, 33] to obtain an expression for A_2 for micelles in solution. I compare the values of A_2 obtained using this method with experimentally determined values for PEO-PPO-PEO micelles[35] and novel polyurethane-containing hydrophilic triblock copolymer micelles.[36] In doing so, I not only introduce a new means of calculating A_2 a priori, but also demonstrate the applicability of the expression introduced by Likos et al. for star polymers to micellar systems. Through the analogy of micelles to sterically stabilized nanoparticles, this study demonstrates that this model can be used to model steric interactions for the latter class of materials.

5.4 Materials and Methods

5.4.1 Chemicals

PEO triblock copolymers (Figure 5-1) were synthesized as previously described.[36] In brief, synthesis of the copolymers consisted of several steps. First, a PEO oligomer was end-capped with isophorone diisocyanate. This was then chain-extended with bis(hydroxymethyl)propionic acid in dimethylformamide (DMF) with dibutyltin dilaurate as the catalyst. The reaction was monitored using FTIR to observe the disappearance of the isocyanate peak at 2260 cm^{-1}. After removing the DMF, the polymer was dissolved in chloroform, washed three times with, added to an excess of cold hexane, and isolated by filtration. The resulting triblock copolymers were characterized using ^{1}H and quantitative ^{13}C NMR, FTIR, and titration (to determine the concentration of COOH groups).

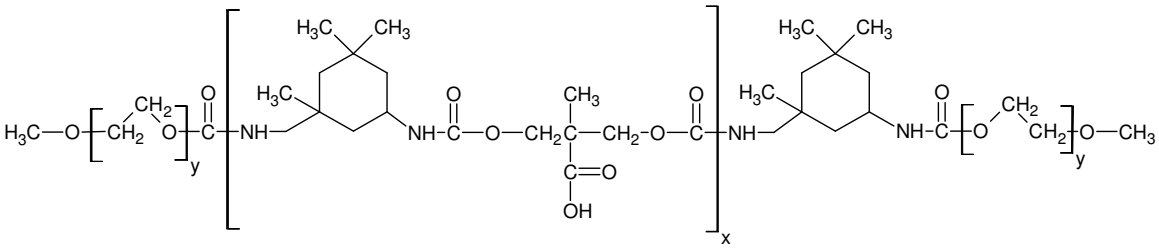

Figure 5-1. Structure of a representative triblock copolymer with PEO tail blocks and a polyurethane center block that contains carboxylic acid groups.

A series of these copolymers is described in overview in the table below. The nomenclature adopted herein for these triblock copolymers comprises the molecular

weights of the PEO end blocks and the average number of carboxylic acid groups (derived by titration) in the central polyurethane section. For example, a 1930-3.1-1930 triblock consists of PEO end blocks with a number average molecular weight of 1930 g/mol, and a polyurethane central block having an average of 3.1 carboxylic acid groups.

Table 5-1. Properties of triblock copolymers.

Copolymer	M_n[a]	DP center[b]	DP tail	Mass fraction PEO
1930-3.1-1930	5160	3.1	44	0.75
4850-2.5-4850	10800	2.5	110	0.90
4850-4.7-4850	11500	4.7	110	0.84

[a]PEO tail block M_n from ^{1}H NMR. [b]Average number of COOH in the polyurethane center block from ^{13}C NMR.[36]

Solution properties of these copolymers were studied extensively using light scattering to measure aggregation number, second virial coefficient, and hydrodynamic radius (Chapter 3) and small angle neutron scattering to measure core and shell sizes (Chapter 4). The reader is referred to those previous chapters for detailed descriptions; certain key results are summarized in this chapter as well for the reader's convenience.

Solutions were prepared with deionized water from a NANOpure II ion exchanger (Barnstead) having a resistance above 17 MΩ·cm. ACS reagent grade sodium chloride (Fisher) was used as received to adjust background ionic strength. All pH adjustments were made using sodium hydroxide and hydrochloric acid (Fisher) as received or after dilution with deionized water.

Solutions for SANS were prepared using D_2O (Cambridge Isotope Laboratories, Inc, Andover, MA) as received or deionized water from a NANOpure II ion exchanger (Barnstead) having a resistance above 17 MΩ·cm. Ionic strength for the deuterated solutions was adjusted using NaCl in D_2O and pD was adjusted using NaOH or HCl in D_2O. The pD measurements were made using an ordinary glass electrode (Orion Model 720 pH meter) according to the correction of Glasoe:[37]

$$pD = pH\ meter\ reading + 0.40$$

Eq. 5-1

5.4.2 Light Scattering

Static and dynamic light scattering measurements were made on these polymer micelles in solution in D_2O. Dynamic light scattering is performed by measuring the variation of intensity with time. This is also known as quasi-elastic light scattering. This can be used to study electrophoretic motion, electrokinetic potential, and particle diffusion.[38] Hydrodynamic radii were determined using the Stokes-Einstein relationship, in which k is Boltzmann's constant, T is the temperature, η is the solvent viscosity, D_o is the diffusion coefficient, and R_H is the hydrodynamic radius:

$$R_H = \frac{kT}{6\pi\eta D_o}$$

Eq. 5-2

The viscosity was corrected for temperature by the following equation, in which A and B are solvent-dependent parameters. This is essential since the viscosity is inversely proportional to the calculated hydrodynamic radius. For D_2O, Eq. 5-3 was used to calculate viscosity in cP relative to temperature in K (A = 3.4931, B = 9.3628E2, C = 1.7670E-3, D = -1.1438E-6).[39] For water, a simpler expression containing only the first two terms built into the Malvern software was used.

$$\log_{10} \eta = A + \frac{B}{T} + CT + DT^2$$

Eq. 5-3

Dynamic light scattering (DLS) was performed using a Malvern NanoZS operating at a fixed angle of 173° and a wavelength of 633 nm. The viscosity and refractive index were adjusted as appropriate for H_2O, D_2O, or the mixture. The DLS data from this device was analyzed using Distribution Technology Software (DTS). This uses an algorithm based on CONTIN, which is a program designed for inversion of noisy equations via a constrained regularization algorithm as described by Provencher.[40, 41] The basic features of CONTIN are prior knowledge (in this case, that the sizes must be non-negative) and parsimony (the solution with the fewest and smoothest peaks is probably best).

DLS is typically performed using an intensity autocorrelation, in which a Fourier transform is performed on the spectrum. This yields an autocorrelation function $G_2(\tau)$, in

which the intensity is measured at an arbitrary time, t. After a time delay, τ, the intensity is measured again. The function $G_2(\tau)$ is given by an average of the product of the intensities at the two times as described as:

$$G_2(\tau) = \langle I(t) \cdot I(t+\tau) \rangle$$

Eq. 5-4

This may then be modeled by using the following equation, in which A and B are instrumental factors and Γ is the decay rate.

$$G_2(\tau) = \int_0^\infty G(\Gamma, t) \exp(-2\Gamma\tau) d\Gamma$$

Eq. 5-5

This may be used to determine the diffusion coefficient, D, according to:

$$\Gamma = Dq^2$$

Eq. 5-6

Particle size may be determined using a correlation with the diffusion coefficient such as the Stokes-Einstein relationship, which is valid for non-interacting spherical particles. This is given by:

$$D_o = \frac{kT}{3\pi\eta d_H}$$

Eq. 5-7

in which k is Boltzmann's constant, T is the temperature, η is the viscosity, and d_H is the particle hydrodynamic diameter.

If one assumes a non-draining sphere, the hydrodynamic radius may be related to the radius of gyration, R_g, by the following:[42]

$$R_H = 0.875 R_g$$

Eq. 5-8

Static light scattering (SLS) was also performed on the Malvern NanoZS. Previous measurements using the multi-angle capability of the Malvern CGS-3 had indicated that these scattering moieties had no angular dependence, so the single-angle NanoZS was acceptable. Scattering is described by:

$$Kc/R_\theta = \frac{1}{P(\theta)}\left[1/M_w + 2A_2C\right]$$

Eq. 5-9

in which c is the concentration of the sample, M_w is the weight-average molecular weight, A_2 is the second virial coefficient, P(θ) is the form factor, q is the scattering vector, and K is an optical constant. The Rayleigh ratio, R_θ, is defined as

$$R_\theta = \frac{I_A \tilde{n}_o^2}{I_T \tilde{n}_T^2} R_T$$

Eq. 5-10

where I_A is the difference in intensity between the scattering sample and the solvent, I_T is the scattering intensity of toluene, $\tilde{n}_o$ is the solvent refractive index, $\tilde{n}_T$ is the refractive index of toluene, and R_T is the Rayleigh ratio of toluene. The scattering vector, q, is calculated according to:

$$q = \frac{4\pi n}{\lambda}\sin\left(\frac{\theta}{2}\right)$$

Eq. 5-11

in which λ is the wavelength, n is the refractive index of the sample, and θ is the measurement angle.[43] The optical constant, K, for the instrument is defined by the following, in which dn/dc is the refractive index increment and N_A is Avogadro's number.

$$K = \frac{4\pi^2\left(n_{solvent}\frac{dn}{dc}\right)^2}{\lambda^4 N_A}$$

Eq. 5-12

Due to the small size of the scattering entities (micelles) relative to the wavelength of the laser (633 nm), the SLS analysis could be done at a single angle using a Debye approach:

$$Kc/R_\theta = 1/M_w + 2A_2c + \ldots$$

Eq. 5-13

as illustrated in Figure 5-2, which requires that qRg<<1.

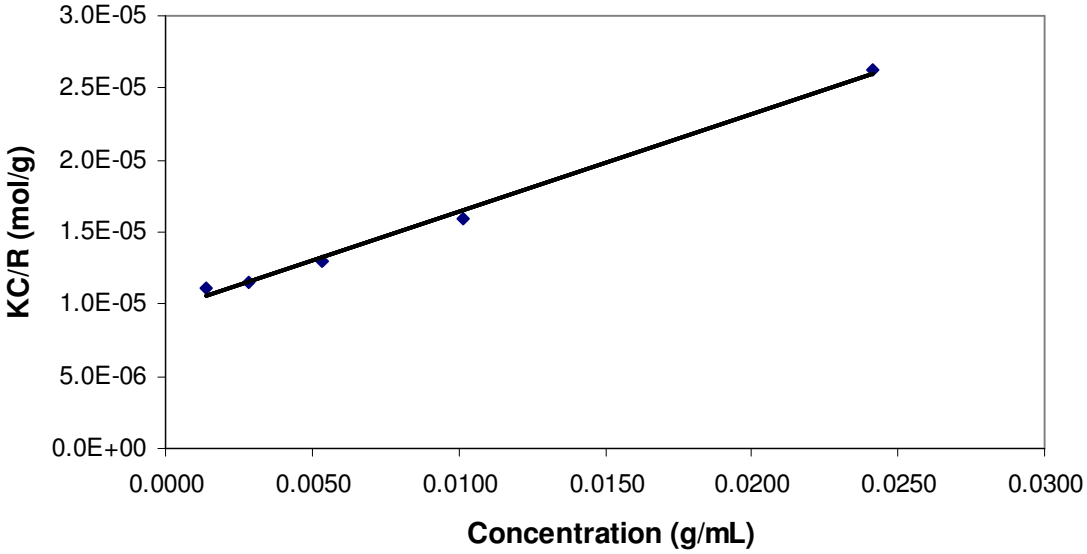

Figure 5-2. Example of a Debye plot for 4850-2.5-4850 polymer in D_2O with 0.1M NaCl and a pD of 2.

The refractive index increment, dn/dc, was measured using a Wyatt Optilab REx differential refractometer. Measured values of dn/dc in H_2O for the triblock copolymers were between 0.128 and 0.143 mL/g, depending on triblock composition. The method outlined by Charron[44] was used to check the expected difference for dn/dc between H_2O and D_2O. The refractive index for a mixture of polymer and solvent was calculated by the Lorentz-Lorez equation:[45]

$$\frac{n^2-1}{n^2+2} = \frac{A_w}{M_w}\rho_w + \frac{A_p}{M_p}\rho_p$$

Eq. 5-14

in which n is the refractive index, M_w is the molecular weight of water, M_p is the molecular weight of a polymer repeat unit, ρ_w is the mass concentration of the solvent, ρ_p

is the mass concentration of the polymer, A_w is the molar refractivity of solvent, and A_p is the molar refractivity of a polymer repeat unit. The molar refractivity of the repeat unit was calculated using the molar refractivities of the bonds according to Vogel.[46] The relationship between polymer mass concentration and refractive index of the solution is:

$$\rho_p = \frac{3}{\frac{A_p}{M_p} - V_p \frac{n_w^2 - 1}{n_w^2 + 2}} \frac{n^2 - n_w^2}{(n^2 + 2)(n_w^2 + 2)}$$

Eq. 5-15

in which V_p is the partial specific volume of the polymer. This was measured using densiometry. The group contribution method predicted variation in dn/dc from the different solvents of less than 2%; thus justifying the use of values measured in water alone.

5.4.3 Densiometry

Partial specific volumes were measured using a DA-300 Density/Specific Gravity Meter (Mettler) in order to determine the size of the micelles cores as well as to provide input to SANS modeling reported elsewhere. The partial specific volumes of the 2000 and 5000 molecular weight PEO at 25°C were determined using aqueous solutions in the range of 0.1-5 wt %. The partial specific volume of the micelles for each copolymer was measured in the weight range of 0.2-2%.

Densiometry operates on the principle that a cell of constant volume oscillates at a frequency dependent on the density of the sample. This is described by the following equation in which T is the oscillation period, d is the sample density, V_c is the cell volume, M_c is the cell mass, and K is a temperature-dependent constant. K may be determined in advance using reference samples. This procedure was performed daily using air and degassed water.

$$T = 2\pi\sqrt{\frac{dV_c + M_c}{K}}$$

Eq. 5-16

5.5 Results and Discussion

5.5.1 Estimation of Micelle Size with the Density Distribution Prediction

Static and dynamic light scattering measurements were performed on the polymers in D_2O and H_2O. These copolymers form two sorts of assemblies: a primary aggregate which is in size range typical for micelles and a secondary aggregate. This secondary aggregate is believed to be the result of PEO-PEO interactions between micelles, as PEO is known to self-aggregate.[47]

Micelle radius, R_m was estimated for the polymers with the density distribution (DD) model, developed by Vagberg et al.[15] This model, based on a model for star polymers by Daoud and Cotton[10] assumes concentric shells with a constant number of blobs equal to twice the aggregation number in this case. Blob size $\xi(r)$, is a continuous function of distance from the surface. The segment density in the shell varies with distance from the core.

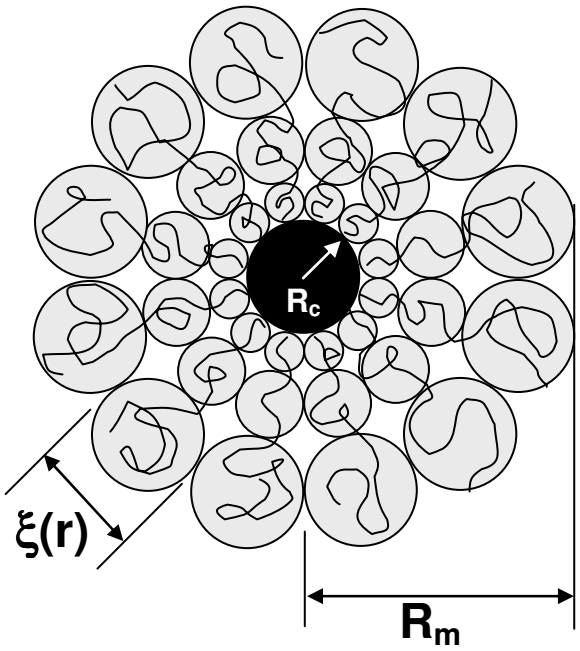

Figure 5-3. Schematic representation of the micelle showing the density distribution model[15] parameters.

The DD model predicts micelle radius, R_m, as:

$$R_m = \left[N a_s^{1/\nu} \frac{8 f^{(1-\nu)/2\nu}}{3\nu 4^{1/\nu}} + R_c^{1/\nu} \right]^{\nu}$$

Eq. 5-17

where N is the number of Kuhn segments, ν is the Flory exponent, R_c is the radius of the core, and f is the number of corona chains. For these triblock copolymers, f is twice the aggregation number, N_{agg}, as measured by SLS.

The blob diameter, ξ(r) is given by:

$$\xi(r) = \frac{4r}{f^{1/2}}$$

Eq. 5-18

in which r is the distance from the center.

The Flory exponent, ν, varies between 0.5 at a theta condition and 0.6 for a good solvent. The value ν = 0.583[47] for PEO in water at room temperature was used for these calculations, as used in similar studies by other authors.[18, 21, 48]

R_c was estimated by:

$$R_c = \left(\frac{N_{agg} M_{PU} \rho_{PU}}{N_{AV}} \right)^{1/3}$$

Eq. 5-19

in which M_{PU} is the molecular weight of the polyurethane block that comprises the core and ρ_{PU} is the measured specific gravity of the core. This assumes a dry core and a sharp interface between the core and corona.

The specific volume of the copolymer was assumed to have additive contributions from the block portion, as described in several previous studies.[49, 50] This is according to the following relationship:

$$V_{micelle} = m_{PEO} v_{PEO} + m_{PU} v_{PU}$$

Eq. 5-20

in which m_{PEO} is the mass fraction of the PEO corona, m_{PU} is the mass fraction of the polyurethane core, and v_{PEO} and v_{PU} are the partial specific volumes of the corona and core, respectively. This enabled calculation of the specific volume of the polyurethane-containing core of the micelle. The results are summarized in Table 5-2.

Table 5-2 Summary of densiometry on the triblock copolymers with 0.1M NaCl, pD 2.

	mass fraction PEO	mass fraction PU	specific volume of PEO (cm^3/g)	specific volume of micelle (cm^3/g)	Specific volume of core[a] (cm^3/g)
1930-3.1-1930 (H_2O)	0.75	0.26	0.8198	0.8081	0.7734
1930-3.1-1930 (D_2O)	0.75	0.26	0.8648	0.8766	0.9116
4850-2.5-4850 (D_2O)	0.90	0.10	0.8246	0.8480	1.0551
4850-4.7-4850 (D_2O)	0.84	0.16	0.8246	0.8697	1.1059

[a]The specific volume of the core was calculated using Eq. 5-20.

5.5.2 Extension of the Star Polymer Interaction Model to Determine A_2

The Likos expression for the effective pair potential between star polymers is given as:

$$A_{\text{int}} = \frac{5}{18} f^{3/2} \begin{cases} -\ln\left(\frac{r}{\sigma} + \frac{1}{1+\frac{\sqrt{f}}{2}}\right); & r \le \sigma \\ \frac{1}{1+\frac{\sqrt{f}}{2}}\left(\frac{\sigma}{r}\right)\exp\left(-\frac{\sqrt{f}}{2\sigma}(r-\sigma)\right); & r > \sigma \end{cases}$$

Eq. 5-21

in which r is the center-to-center separation, f is the number of arms, and $\sigma/2$ is the distance from the center of the core to the center of the outermost blob layer. For this expression, σ is defined as $1.3*R_g$, the radius of gyration of the ensemble.[33] The first portion of the equation (relating to close approach) is a logarithmic relationship based on a model developed by Witten and Pincus[34] which describes the entropic repulsion when chains from adjacent stars overlap. The exponential longer distance relationship ($r>\sigma$) has

the form of a Yukawa-type exponential screening term similar in form to that used to describe a screened Coulomb potential[51] with the decay length set to the diameter of the largest blobs.[1] The prefactor 5/18 is based on machine simulations and causes the two portions to merge smoothly at r=σ.

One significant advantage of the Likos model is that it illustrates increasing "hardness" with an increase in the number of star arms, f. This may be seen in Figure 5-4.

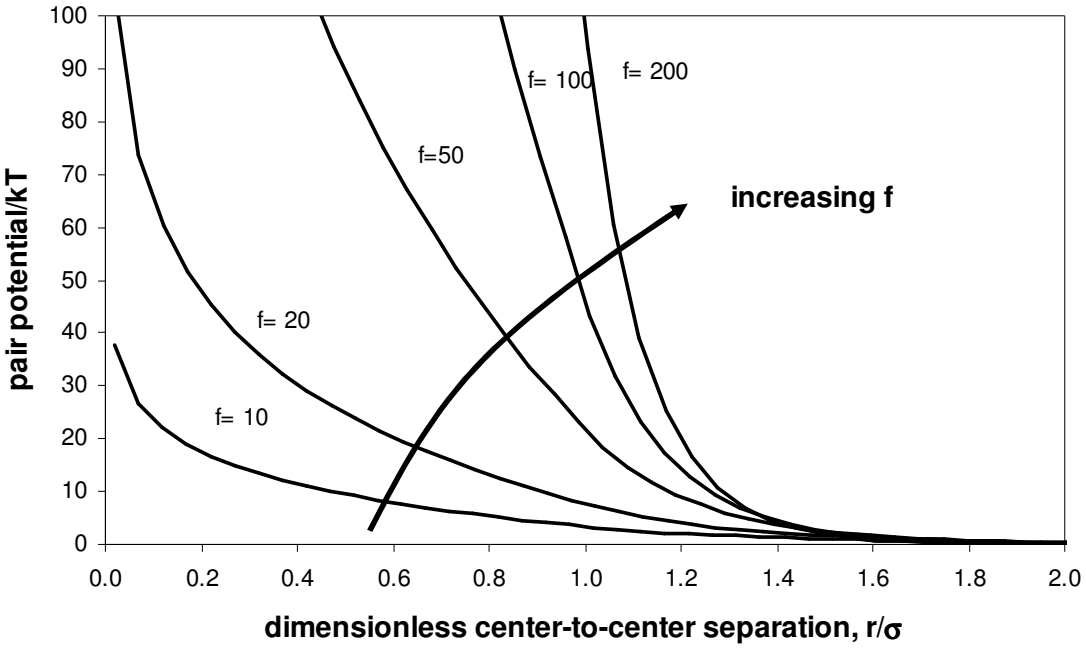

Figure 5-4. Pair potential for an example system with 2000 g/mol PEO grafted to a sphere with R_c = 5 nm and f = 10, 20, 50, 100, and 200. The transition from a soft to hard interaction potential with increasing f may be observed.

The volume fraction of polymer in the corona as a function of distance from the surface of the core may be calculated using the Vagberg approach.[15] In this method, the volume fraction profile is divided into three sections. With the core, the density is constant. Beyond the complex radius, calculated as R_m, the density is zero. Between R_c and R_m the profile is:

$$\Phi(r) = \rho_{polymer} A \left(\frac{r}{a_s} \right)^{\frac{1}{\nu}} r^{-3}$$

Eq. 5-22

in which ρ_{PEO} is the density of the polymer. This is illustrated in Figure 5-5.

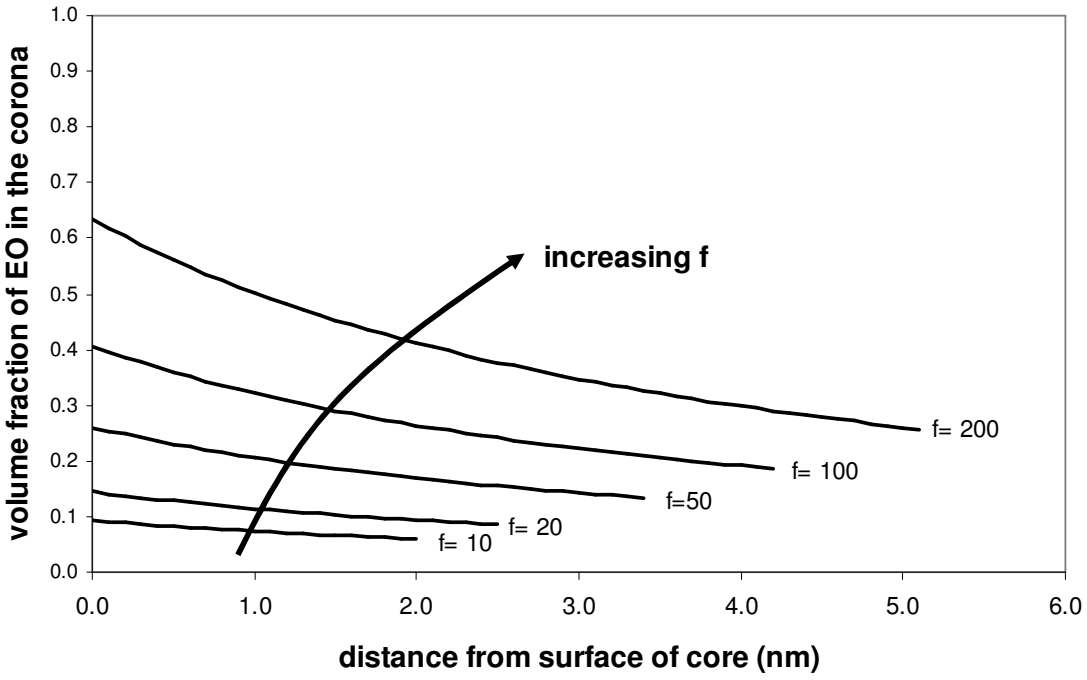

Figure 5-5. Volume fraction profile for an example system with 2000 g/mol PEO grafted to a sphere with R_c = 5 nm and f = 10, 20, 50, 100, and 200.

The second virial coefficient may be calculated by:

$$A_2 = \frac{N_a}{M^2} 2\pi \int_{2a}^{\infty} (1 - \exp(-A_{\text{int}})) r^2 dr$$

Eq. 5-23

in which A_{int} is the pair potential, r is the center-to-center separation of two particles of radius a, M is the molecular weight of the ensemble, and N_a is Avogadro's number.[52]

The resulting expression for A_2 is:

$$A_2 = 2\pi \frac{N_A}{M^2}\left(\int_{2R_c}^{\sigma} 1-\exp\left(\frac{5}{18} f^{3/2} \ln\left(\frac{r}{\sigma} + \frac{1}{1+\frac{\sqrt{f}}{2}} \right) \right) r^2 dr + \int_{\sigma}^{\infty} 1-\exp\left(-\frac{5}{18} f^{3/2} \frac{1}{1+\frac{\sqrt{f}}{2}} \left(\frac{\sigma}{r} \right) \exp\left(-\frac{\sqrt{f}}{2\sigma}(r-\sigma) \right) \right) r^2 dr \right)$$

Eq. 5-24

Mathematica 5.2 was used to symbolically integrate the first half of the expression and to numerically integrate the second half.

In addition to the prediction from the soft colloid model, a comparison was made to a hard sphere model:

$$A_2 = \frac{16\pi N_{AV} R^3}{3M_2^2}$$

Eq. 5-25

in which N_{AV} is Avagadro's number, R is the radius of the micelle, and M_2 is the molecular weight of the micelle.[42] For R, the hydrodynamic radius as determined by DLS was used, and for M_2 the micellar molecular weight found using SLS was used. For this study, the 4850-2.5-4850 and 4850-4.7-4850 experiments were in D_2O only to correspond with the SANS study; calculations in both H_2O and D_2O are provided for 1930-3.1-1930.

Two values of R_g are included in Table 5-3. R_g experimentally determined from a Guinier analysis on SANS data was used to model A_2. However, R_g may also be estimated by directly integrating the segment distribution function. This is covered in detail in Chapter 6. Briefly, the radius of gyration, R_g, is given as:

$$R_g = \sqrt{\frac{I_{total}}{m_{total}}}$$

Eq. 5-26

in which m_{total} is the mass of one micelle and I_{total} is the total inertia of the micelle and is the sum of I_{core} and I_{corona}. These are given by:

$$I_{core} = \int_0^{R_c} r^2 \rho_{magnetite} 4\pi r^2 dr = \frac{4\pi R_c^5 \rho_{magnetite}}{5}$$

Eq. 5-27

and

$$I_{corona} = \int_{R_c}^{R_m} r^2 m_s A \left(\frac{r}{a_s}\right)^{\frac{1}{\nu}} r^{-3} 4\pi r^2 dr = \frac{4\pi A m_s}{a_s^{1/\nu}\left(2+\frac{1}{\nu}\right)}\left(R_m^{\left(2+1/\nu\right)} - \left(R_c\right)^{\left(2+1/\nu\right)}\right)$$

Eq. 5-28

respectively, in which all parameters are as defined previously for the Vagberg star model.

Table 5-3. Comparison of experimental A_2 to star and hard sphere values for novel polyurethane-containing hydrophilic triblock copolymers at 25°C, pD 2, 0.1M NaCl in D_2O. R_H was determined by DLS, R_g is from a Guinier analysis on SANS data, and f is from SLS.

Sample	M (kg/ mol)	f	R_m (nm)	R_H (nm)	R_c (nm)	R_g (nm) inertia	R_g (nm) SANS	A_2 (mL *mol/g^2) SLS	Star (R_g from inertia)	Star (R_g from SANS)	Hard sphere
1930-3.1-1930 (H_2O)	150	58 (±1.7)	7.0	10.7	2.3	4.0	5.2	2.1e-4 (±5.8e-6)	4.7e-5	1.1e-4	1.5e-4
1930-3.1-1930 (D_2O)	165	64 (±2.5)	7.2	9.3	2.5	4.2	5.2	2.2e-4 (±7.8e-6)	4.4e-5	8.7e-5	1.4e-4
4850-2.5-4850 (D_2O)	102	19 (±0.6)	9.0	13.5	1.6	5.3	6.2	3.4e-4 (±1.3e-5)	3.2e-4	5.1e-4	7.0e-4
4850-4.7-4850 (D_2O)	176	31 (±1.8)	10.1	16.0	2.3	5.8	6.4	2.8e-4 (±1.3e-5)	1.3e-4	1.8e-4	3.3e-4

Note: Propagation of errors for A_2 and f are described in detail in the Appendix. R_g as determined by SANS is reported as the same for both D_2O and H_2O because the Guinier fit was on a combination of data.

The hard sphere A_2 is similar to the experimentally measured values for 1930-3.1-1930, the polymer with the highest aggregation number and smallest radius. This is reasonable, as that polymer is the most densely packed of those studied and as such would be

expected to resemble a hard sphere more than the others. However, in the case of the polymer with lower aggregation numbers (4850-2.5-4850 and 4850-4.7-4850), the hard sphere approximation overpredicts A_2 by approximately an order of magnitude. The star model is a closer match, which reflects the less dense packing of PEO chains around the core.

This can be understood by considering how the mass fraction of PEO in the corona varies as a function of distance from the surface of the core. The mass density profile in the micelle corona was divided into three sections using the approach by Vagberg et al.[15] With the core, the density is constant. Beyond the micelle radius, calculated as R_m, the density is zero. Between R_c and R_m the profile as given below.

$$\rho(r) = \rho_c \qquad r < R_c$$
$$\rho(r) = m_s A\left(\frac{r}{a_s}\right)^{\frac{1}{\nu}} r^{-3} \qquad R_c < r < R_m$$
$$\rho(r) = 0 \qquad R_m < r$$

Eq. 5-29

The constant of proportionality, A, is determined by the relationship between the blob size at the core-corona boundary and the number of corona chains.

$$A = \frac{3 * 4^{\frac{1}{\nu}} f^{\frac{3\nu-1}{2\nu}}}{32}$$

Eq. 5-30

The mass fraction profiles for 1930-3.1-1930, 4850-2.5-4850, and 4850-4.7-4850 in 0.1M NaCl at 25°C were calculated, and the results are shown below in Figure 5-6. The relationship between core radius and aggregation number determines the maximum brush density. Longer PEO chains extend further into solution.

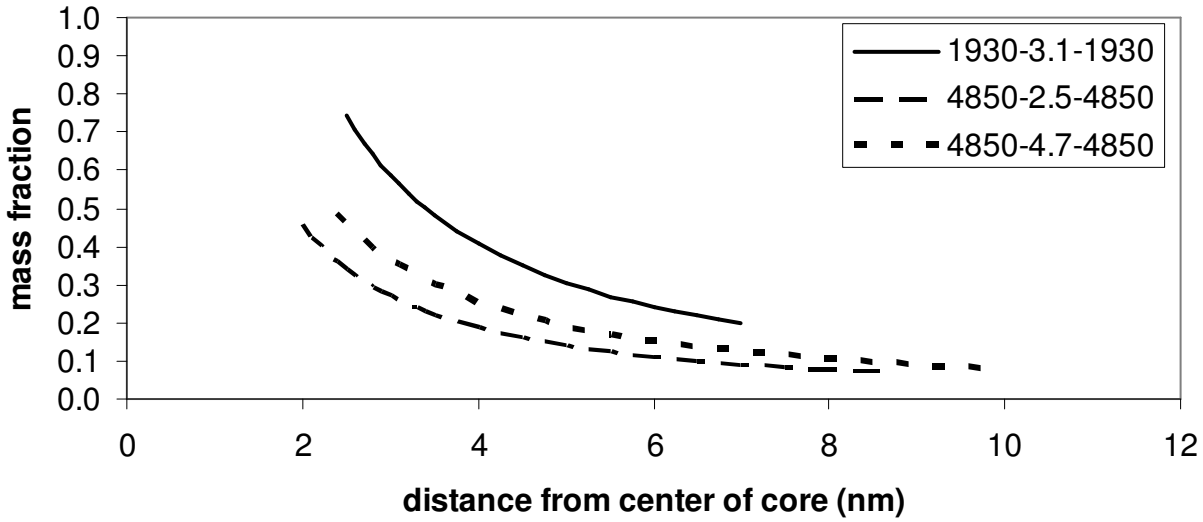

Figure 5-6. Mass fraction profiles for 1930-3.1-1930, 4850-2.5-4850, and 4850-4.7-4850 in 0.1M NaCl at 25C based on Vagberg's approach. Micelles with higher aggregation numbers form denser brushes, and those with longer PEO chains have the corona extending further into solution.

In addition to the data on novel polyurethane-containing hydrophilic triblock copolymers, A_2 values predicted with the Likos interaction potential were also compared to experimental values from the literature. Nolan et al.[35] measured R_H, N_{agg}, and A_2 using dynamic and static light scattering on a series of poly(ethylene oxide)-poly(propylene oxide)-poly(ethylene oxide) (PEO-PPO-PEO) copolymer micelles in water. Vagberg et al.[15] also used light scattering to determine the micellization behavior of poly(ethylene oxide)-polystyrene (PS-PEO) in cyclopentane. Both examined their findings using the starlike polymer model, but they did not calculate A_2 as described in this chapter. Parameters from these papers that were used are described below in Table 5-4, as are the resulting values of A_2 from the star model.

Table 5-4. Comparison of experimental A_2 to star and hard sphere values for studies on PEO-PPO-PEO in water and PEO-PS in cyclopentane.

Sample	M (g/mol)	f	R_H (nm)	R_c (nm)	Rg inertia (nm)	R_g SLS (nm)	A_2 (mL*mol/g^2)			
							SLS	Star (R_g from inertia)	Star (Rg from SLS)	Hard sphere
[a]$EO_{32}PO_{61}EO_{32}$	428,000	172	8.4	4.9	6.6	---	2.7e-5	1.5e-5	---	3.7e-5
[a]$EO_{54}PO_{61}EO_{54}$	173,000	60	8.6	3.5	5.9	---	4.9e-5	1.1e-4	---	2.0e-4
[a]$EO_{68}PO_{61}EO_{68}$	201,000	62	8.6	3.5	6.6	---	5.6e-5	1.2e-4	---	2.1e-4
[a]$EO_{38}PO69EO_{38}$	689,000	240	8.9	5.5	7.6	---	1.9e-5	7.8e-6	---	2.3e-4
[b]PEO/PS 30-40 ppm water	3,190,000	17	34.9	3.5	21.2	27.9	-2e-5	2.2e-5	4.9e-5	3.9e-5
[b]PEO/PS sat. with water	14,400,000	77	43.9	6.4	31.1	31.7	3.1e-6	2.5e-6	2.7e-6	5.9e-6

[a]PEO-PPO-PEO micelles were in water at 25°C.[35] M and f were determined by SLS. R_c was determined by authors as $R_c = (3anv_{PO}/4\pi)^{1/3}$ where n is the number of PO units per surfactant, a is the aggregation number, and v_{PO} is the volume per PO molecule. [b]PEO-PS copolymers were in cyclopentane at 25°C.[15] M, f, and R_g were determined by SLS. R_c was determined by the authors in an equivalent manner.

The predictions by the star model for A_2 are closer to the experimental values than the hard sphere A_2, which is reasonable for these softer colloids. Those micelles with more densely packed corona chains behave more like hard spheres. For the examples with lower aggregation numbers, notably $EO_{54}PO_{61}EO_{54}$ and $EO_{68}PO_{61}EO_{68}$, the A_2 expression based on the star model provides a much closer match. This is illustrated in Figure 5-7, which shows the mass fraction profile in the PEO corona. $EO_{54}PO_{61}EO_{54}$ and $EO_{68}PO_{61}EO_{68}$ have very similar profiles and are less densely packed than $EO_{32}PO_{61}EO_{32}$.

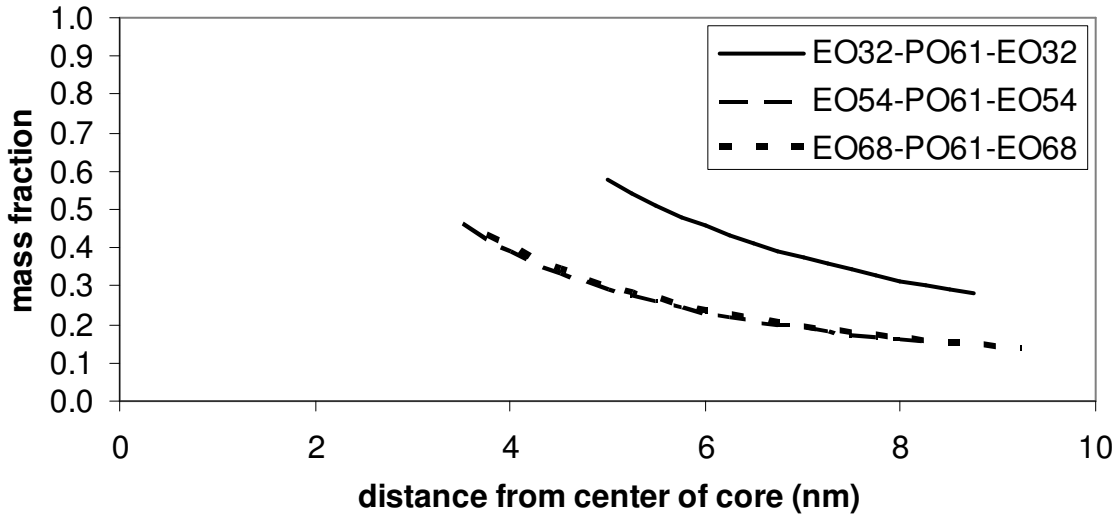

Figure 5-7. Mass fraction profiles for PEO-PPO-PEO micelles in water at 25 ℃.

The examples of PS-PEO in cyclopentane are rather different from the novel triblock copolymer micelles and the PEO-PPO-PEO micelles previously discussed. In this system, the hydrophilic PEO chains form the core of the micelle and solubilize a small amount of water while the PS chains extend into solution. The polymer chains themselves are much bigger with an overall molecular weight of 187,500 g/mol, of which only 4% by weight was PEO. The micelles are therefore much larger and have a relatively small core. Addition of water increased both the size of the micelle and the aggregation number (17 to 77). The large increase in aggregation number caused an increase in the mass fraction of PEO in the corona, as may be seen in Figure 5-8. As the authors noted, the negative value of A_2 measured for the sample with lower content could be due to the presence of a number of aggregating chains, as that polymer was measured closer to the CMC.[15] However, for the sample saturated with water, the agreement between the star model and experimental data is quite good.

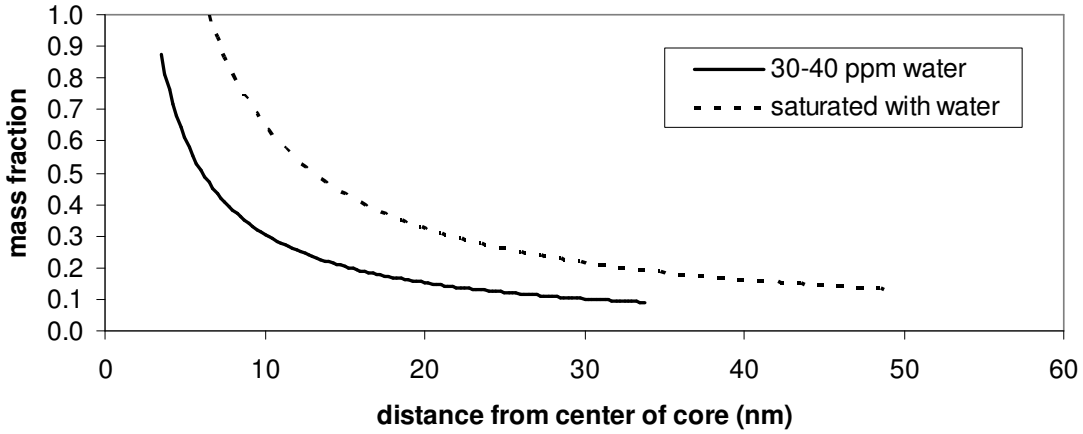

Figure 5-8. Mass fraction profiles for PEO-PS copolymers in cyclopentane at 25 °C.

Additional comparisons were made to two studies of star polymers in good solvents. Bauer et al. synthesized a series of chlorosilane-linked polyisoprene stars and measured their properties in cyclohexane.[53] Roovers et al. prepared star polybutadiene polymers in cyclohexane.[17] The methodology described in the preceding micellar examples was applied to these star polymers with excellent results, which results are summarized below.

Table 5-5. Prediction of R_g and A_2 for star polymers.

Sample	M (g/mol)	f	R_H (nm)	Rg inertia (nm)	R_g SLS (nm)	A_2 (mL*mol/g^2) SLS	Star (R_g from inertia)	Star (R_g from SLS)	Hard sphere
8-II[a]	610000	6.9	25.4	25.5	25.5	4.9E-04	9.6E-04	9.6E-04	2.0e-3
8-IV[a]	1760000	7.8	44.4	48.5	45.5	3.1E-04	8.1E-04	6.7E-04	1.5e-3
12-II[a]	810000	11.8	25.9	24.9	25.0	3.4E-04	5.4E-04	5.5E-04	1.1e-3
12-VIII[a]	3900000	12.0	62.7	60.1	58.7	1.9E-04	3.3E-04	3.1E-04	6.7e-4
12-V[a]	5280000	12.2	75.0	74.6	72.0	1.9E-04	3.4E-04	3.1E-04	6.5e-4
18-II[a]	218000	18.0	9.5	10.7	9.6	3.9E-04	5.9E-04	4.3E-04	1.1e-3
18-III[a]	800000	17.4	21.8	22.8	21.4	2.7E-04	4.2E-04	3.5E-04	7.7e-4
18-IV[a]	1480000	18.0	32.5	30.2	29.9	2.3E-04	2.9E-04	2.8E-04	5.7e-4
18-V[a]	3570000	17.9	50.8	50.1	50.0	2.0E-04	2.3E-04	2.2E-04	4.5e-4
6430[b]	1340000	56	17.5	19.2	18.5	9.6E-05	7.5E-05	6.7E-05	1.8e-4
6460[b]	2890000	61	26.5	29.4	28.0	7.2E-05	5.6E-05	4.9E-05	1.3e-4
6480[b]	4200000	59	32.0	36.2	34.1	6.6E-05	5.0E-05	4.2E-05	1.2e-4
12828[c]	2980000	114	22.4	23.5	21.6	4.2E-05	1.7E-05	1.8E-05	6.6e-5
12856[c]	5950000	127	32.2	33.7	34.5	3.1E-05	1.6E-05	1.7E-05	4.9e-5
12880[c]	8800000	122	38.7	42.6	42.4	3.0E-05	1.5E-05	1.5E-05	4.9e-5

[a]Chlorosilane-linked polyisoprene stars in cyclohexane at 23°C with a core radius of 0.7 nm.[53] R_g calculations were performed with $\nu = 0.58$, C_∞=5.99[54] and a_s = 0.92 nm[55] for the polyisoprene stars. [b]Polybutadiene stars in cyclohexane with core radius 1.8 nm.[17] [c]Polybutadiene stars in cyclohexane with core radius 2.6 nm.[17] R_g was calculated with $\nu = 0.58$, C_∞=5.1 and a_s=0.75 nm.[17]

These two well known and much cited papers from the star polymer literature illustrate the utility of the star polymer interaction model to for calculating A_2. The agreement is good between the calculated and experimentally observed values. These star polymers are close to the hard sphere limit. For a given core size with approximately the same values of f, an increase in the length of the polymer chains yields a lower value of A_2. This softer interaction is consistent with the expected lower mass fraction at the outermost edge of the micelle brush layer. As the interaction becomes softer, the newly

developed star polymer model for A_2 does a better job of matching experimental data than the hard sphere approximation.

5.5.3 Micelle-micelle separation

The micelle-micelle separation based on a hard sphere model may be calculated by the relationship

$$\frac{\bar{h}}{d} = \left[\left(\frac{1}{3\pi\phi} + \frac{5}{6} \right)^{1/2} - 1 \right]$$

Eq. 5-31

in which d is the diameter of a micelle, ϕ is the volume fraction of micelles in solution, and $\bar{h}$ is the average separation between micelles.[56]

The average separation between micelles at a concentration of 10 mg/ml was determined for the experimental polymers in D_2O. The results are summarized in Table 5-6.

Table 5-6. Volume fraction and micelle-micelle separation for the triblock copolymers.

Sample	M_{unimer} (g/mol)	$M_{micelle}$ (g/mol)	N_{agg}	R_m (nm)	ϕ	$\bar{h}/d$	$\bar{h}$ (nm)
1930-3.1-1930	5160	165,000	32	7.2	0.06	0.64	9.2
4850-2.5-4850	10800	102,000	9	9.0	0.18	0.19	3.5
4850-4.7-4850	11500	176,000	15	10.1	0.15	0.25	5.0

Note: Calculations are for the polymers in D_2O with 0.1M NaCl, pD 2, 10 mg/mL.

Due to the higher aggregation number for 1930-3.1-1930, the denser and more compact micelle yields a lower volume fraction at a given concentration in solution and thus a larger separation. However, in all cases the micelle-micelle separation calculated indicates that the micelles are separated by several nanometers on average, meaning that they are not being forced into impingement by their concentration in solution.

5.6 Conclusions

A star polymer model for the pair potential between two particles was used to develop for the first time an expression for the second virial coefficient, A_2, for micelles with no adjustable parameters that accounts for variations in the hardness of the pair potential in terms of the number of corona chains and the radius of the core, both of which can be measured. In addition, a means of calculating R_g from the mass distribution in the

micelle or star polymer was derived. The expression for A_2 was tested with data on a series of novel polyurethane-containing hydrophilic triblock copolymers that form micelles in water. R_g and A_2 were calculated for two literature examples of micellar systems (PEO-PPO-PEO in water and PEO-PS in cyclopentane). In addition, two star polymer systems (polyisoprene and polybutadiene in cyclohexane) were tested. In all cases, the star model for A_2 demonstrated semi-quantitative agreement with the experimentally measured values and illustrated the utility of the star polymer interaction model for calculating A_2.

5.7 References

1. Likos, C.N., Soft matter with soft particles. *Soft Matter*, **2006**. 2(6): p. 478-498.

2. Likos, C.N., et al., Star polymers viewed as ultrasoft colloidal particles. *Physical Review Letters*, **1998**. 80(20): p. 4450-4453.

3. Alexander, S., *Journal of Physics (Paris)*, **1977**. 38: p. 977.

4. Alexander, S., *Journal of Physics (Paris)*, **1977**. 38: p. 983.

5. de Gennes, P.G., Conformations of Polymers Attached to an Interface. *Macromolecules*, **1980**. 13: p. 1069-1075.

6. Cantor, R., Nonionic Diblock Copolymers as Surfactants between Immiscible Solvents. *Macromolecules*, **1981**. 14: p. 1186-1193.

7. Milner, S.T., Witten, T.A., and Cates, M.E., Theory of the Grafted Polymer Brush. *Macromolecules*, **1988**. 21(8): p. 2610-2619.

8. Dolan, A.K. and Edwards, S.F., Theory of the stabilization of colloids by adsorbed polymer. *Proceedings of the Royal Society of London Series A-Mathematical and Physical Sciences*, **1974**. 337: p. 509-516.

9. Cosgrove, T., et al., Configuration of Terminally Attached Chains at the Solid Solvent Interface - Self-Consistent Field-Theory and a Monte-Carlo Model. *Macromolecules*, **1987**. 20(7): p. 1692-1696.

10. Daoud, M. and Cotton, J.P., Star shaped polymers: a model for the conformation and its concentration dependence. *Journal de Physique*, **1982**. 43: p. 531-538.

11. Marques, C., Joanny, J.F., and Leibler, L., Adsorption of Block Copolymers in Selective Solvents. *Macromolecules*, **1988**. 21(4): p. 1051-1059.

12. Dan, N. and Tirrell, M., Self-Assembly of Block-Copolymers with a Strongly Charged and a Hydrophobic Block in a Selective, Polar-Solvent - Micelles and Adsorbed Layers. *Macromolecules*, **1993**. 26(16): p. 4310-4315.

13. Biver, C., et al., Neutral and Charged Polymer Brushes: A Model Unifying Curvature Effects from Micelles to Flat Surfaces. *Macromolecules*, **1997**. 30: p. 1787-1792.

14. Halperin, A., Polymeric Micelles - a Star Model. *Macromolecules*, **1987**. 20(11): p. 2943-2946.

15. Vagberg, L.J.M., Cogan, K.A., and Gast, A.P., Light-Scattering Study of Starlike Polymeric Micelles. *Macromolecules*, **1991**. 24(7): p. 1670-1677.

16. Hedden, R.C. and Bauer, B.J., Structure and dimensions of PAMAM/PEG dendrimer-star polymers. *Macromolecules*, **2003**. 36(6): p. 1829-1835.

17. Roovers, J., et al., Regular Star Polymers with 64 and 128 Arms - Models for Polymeric Micelles. *Macromolecules*, **1993**. 26(16): p. 4324-4331.

18. Johnsson, M., Hansson, P., and Edwards, K., Spherical micelles and other self-assembled structures in dilute aqueous mixtures of poly(ethylene glycol) lipids. *Journal of Physical Chemistry B*, **2001**. 105(35): p. 8420-8430.

19. Lee, A.S., et al., Characterizing the structure of pH dependent polyelectrolyte block copolymer micelles. *Macromolecules*, **1999**. 32(13): p. 4302-4310.

20. Doliveira, J.M.R., et al., Chains Anchored onto Convex Spherical Surfaces - Modification of the Daoud and Cotton Model. *Macromolecules*, **1995**. 28(13): p. 4750-4752.

21. Farinha, J.P.S., et al., Structure in tethered chains: Polymeric micelles and chains anchored on polystyrene latex spheres. *Langmuir*, **1998**. 14(9): p. 2291-2296.

22. Ducker, W.A., Senden, T.J., and Pashley, R.M., Measurement of Forces in Liquids Using a Force Microscope. *Langmuir*, **1992**. 8(7): p. 1831-1836.

23. Israelachvili, J., Intermolecular and Surface Forces. 2nd ed. **1991**, London: Academic Press.

24. Guenoun, P., Argillier, J.F., and Tirrell, M., End-tethered charged chains at surfaces. *Comptes Rendus De L Academie Des Sciences Serie Iv Physique Astrophysique*, **2000**. 1(9): p. 1163-1169.

25. Balastre, M., et al., A study of polyelectrolyte brushes formed from adsorption of amphiphilic diblock copolymers using the surface forces apparatus. *Macromolecules*, **2002**. 35(25): p. 9480-9486.

26. Sennerfors, T., Froberg, J.C., and Tiberg, F., Adsorption of polyelectrolyte-nanoparticle systems on silica: Influence on interaction forces. *Journal of Colloid and Interface Science*, **2000**. 228(1): p. 127-134.

27. Vlassopoulos, D., et al., Multiarm star polymers dynamics. *Journal of Physics-Condensed Matter*, **2001**. 13(41): p. R855-R876.

28. Vlassopoulos, D., Colloidal star polymers: Models for studying dynamically arrested states in soft matter. *Journal of Polymer Science Part B-Polymer Physics*, **2004**. 42(16): p. 2931-2941.

29. Semenov, A.N., et al., Dynamic structure of interacting spherical polymer brushes. *Langmuir*, **1999**. 15(2): p. 358-368.

30. Seghrouchni, R., et al., Controlling the dynamics of soft spheres: From polymeric to colloidal behavior. *Europhysics Letters*, **1998**. 42(3): p. 271-276.

31. Vlassopoulos, D., et al., Ordering and dynamics of soft spheres in melt and solution. *Faraday Discussions*, **1999**: p. 225-235.

32. Lin, E.K. and Gast, A.P., Self consistent field calculations of interactions between chains tethered to spherical interfaces. *Macromolecules*, **1996**. 29(1): p. 390-397.

33. Jusufi, A., Watzlawek, M., and Lowen, H., Effective interaction between star polymers. *Macromolecules*, **1999**. 32(13): p. 4470-4473.

34. Witten, T.A. and Pincus, P.A., Colloid Stabilization by Long Grafted Polymers. *Macromolecules*, **1986**. 19(10): p. 2509-2513.

35. Nolan, S.L., et al., Light scattering study on the effect of polymer composition on the structural properties of PEO-PPO-PEO micelles. *Journal of Colloid and Interface Science*, **1997**. 191(2): p. 291-302.

36. Harris, L.A., et al., Magnetite nanoparticle dispersions stabilized with triblock copolymers. *Chemistry of Materials*, **2003**. 15(6): p. 1367-1377.

37. Glasoe, P.K. and Long, F.A., Use of Glass Electrodes to Measure Acidities in Deuterium Oxide. *Journal of Physical Chemistry*, **1960**. 64: p. 188-190.

38. Finsy, R., Particle Sizing by Quasi-Elastic Light-Scattering. *Advances in Colloid and Interface Science*, **1994**. 52: p. 79-143.

39. Yaws, C.L., ed. Chemical Properties Handbook. **1999**, McGraw-Hill: New York.

40. Provencher, S.W., A Contrstrained Regularization Method for Inverting Data Represented by Linear Algebraic or Integral Equations. *Computer Physics Communications*, **1982**. 27: p. 213-227.

41. Provencher, S.W., CONTIN: A General PurposeConstrained Regularization Program for Inverting Noisy Linear Algebraic and Integral Equations. *Computer Physics Communications*, **1982**. 27: p. 229-242.

42. Tanford, C., Physical Chemistry of Macromolecules. **1962**, New York: John Wiley and Sons.

43. Malvern_Instruments, CGS-3 User Manual, Chapter 8. **2005**.

44. Charron, J.R., Block Copolymer Adsorption to Phospholipid Monolayers at the Air-Water Interface, in Chemical Engineering. **1996**, Carnegie Mellon.

45. Cuypers, P.A., et al., The Adsorption of Prothrombin to Phosphatidylserine Multilayers Quantitated by Ellipsometry. *The Journal of Biological Chemistry*, **1983**. 25(2426-2431).

46. Vogel, A.I., et al., Physical Properties and Chemical Constitution. Part XXIV. Aliphatic Aldoximes, Ketoximes, and Ketoxime O-Alkyl Ethers, NN-Dialkylhydrazines, Aliphatic Ketazines, Mono- and Di-alkyl-aminopropionitriles, Alkoxypropionitriles, Dialkyl Azodiformates, and Dialkyl Carbonates. Bond Parachors, Bond Refractions, and Bond-refraction Coefficients. *Journal of the Chemical Society*, **1952**: p. 514-549.

47. Devanand, K. and Selser, J.C., Asymptotic-Behavior and Long-Range Interactions in Aqueous-Solutions of Poly(Ethylene Oxide). *Macromolecules*, **1991**. 24(22): p. 5943-5947.

48. FitzGerald, P.A., Davey, T.W., and Warr, G.G., Micellar structure in gemini nonionic surfactants from small-angle neutron scattering. *Langmuir*, **2005**. 21(16): p. 7121-7128.

49. Sommer, C., Pedersen, J.S., and Stein, P.C., Apparent Specific Volume Measurements of Poly(ethylene oxide), Poly(butylene oxide), Poly(propylene oxide), and Octadecyl Chains in the Micellar State as a Function of Temperature. *Journal of Physical Chemistry B*, **2004**. 108: p. 6242-6249.

50. Wen, X.G. and Verrall, R.E., Temperature Study of Sound Velocity and Volume-Related Specific Thermodynamic Properties of Aqueous Solutions of Poly(ethylene oxide)-Poly(propylene oxide)-Poly(ethylene oxide) Triblock Copolymers. *Journal of Colloid and Interface Science*, **1997**. 196: p. 215-223.

51. Ashcroft, N.W. and Mermin, N.D., Solid State Physics. **1976**, Fort Worth: Harcourt Brace College Publishers.

52. Jansen, J.W., Dekruif, C.G., and Vrij, A., Attractions in Sterically Stabilized Silica Dispersions .3. 2nd Virial-Coefficient as a Function of Temperature, as Measured by Means of Turbidity. *Journal of Colloid and Interface Science*, **1986**. 114(2): p. 492-500.

53. Bauer, B.J., et al., Chain Dimensions in Dilute Polymer-Solutions - a Light-Scattering and Viscometric Study of Multiarmed Polyisoprene Stars in Good and Theta-Solvents. *Macromolecules*, **1989**. 22(5): p. 2337-2347.

54. Brandrup, J. and Immergut, E.H., eds. Polymer Handbook. **1999**, John Wiley: New York.

55. Thudium, R.N. and Han, C.C., Microstructure effect on the phase behavior of blends of deuterated polybutadiene and protonated polyisoprene. *Macromolecules*, **1996**. 29(6): p. 2143-2149.

56. Barnes, H.A., Hutton, J.F., and Walters, K., An Introduction to Rheology. Rheology Series, ed. K. Walter. **1989**, Amsterdam: Elsevier.

6 Adsorption of Brush-Forming Copolymers on Magnetite Nanoparticles

6.1 Abstract

Adsorption of several water-soluble block copolymers on magnetite nanoparticles was examined for the purpose of tailoring a steric stabilizing brush layer. The copolymers included a poly(ethylene oxide) (PEO) chain with three carboxylic acid groups on one end, several block copolymers of PEO and poly(ethyleneimine) (PEI), and a symmetric pentablock copolymer having PEO, poly(propylene oxide) (PPO), and a carboxylic acid-containing urethane block. The sizes of the magnetite-polymer complexes were predicted using a star polymer model and compared to sizes measured by dynamic light scattering. Colloidal stability in water and phosphate buffered saline was predicted using an extended DLVO theory. The volume fraction in the PEO corona was calculated with the blob model and related to the mobility of water in the corona.

6.2 Keywords

adsorption; brush extension; triblock copolymer; surface; colloidal stabilization; blob model; magnetite

6.3 Introduction

Colloidal science is essential to many industrial applications, including ceramics, microelectronics, coatings, paints, filled adhesives, foods, detergents, and cosmetics.[1] Dispersion stabilization is important in colloidal systems to prevent undesirable agglomeration, which can increase viscosity and lead to significant difficulty in processing. In many cases, high particle loading (30-40% by weight) is required, making control of viscosity imperative.[2] Polymers are frequently used to stabilize dispersions of colloids.[3, 4]

The use of polymers and polymer-stabilized nanoparticles for drug delivery[5-13] and gene delivery[14, 15] has been examined by many investigators. Currently, a potential application

is stabilization of superparamagnetic iron oxide nanoparticles (SPIONS) with biodegradable polymers for bioapplications.[16-19] One major area is in targeted delivery designed to deliver a drug payload to specific locations.[20, 21] Another related application is in magnetic resonance imaging (MRI) for tumor detection.[22-25] In 1998, Stark et al. reported that superparamagnetic iron oxide has a magnetic susceptibility that was 50 times greater than traditional gadolinium-based compounds for use in MRI imaging[26] A recent review by Okuhata[27] indicated that state of the art gadolinium compounds have R_1 relaxivities of 4-34 mM^{-1} Gd s^{-1} as compared to recent advances in magnetite compounds, which have R_1 of 17-40 and R_2 of 35-190 mM^{-1} Fe s^{-1}.

For any of these bioapplications, there are several important design parameters for the particle-polymer complex. The first is compatibility with the body. PEO-containing polymers are especially interesting, as PEO does not trigger an immune response in-vivo and can also make other foreign materials less detectable by the immune system.[28] Another important characteristic is size. The complexes should be large enough (>10 nm) to avoid premature removal via extravasation from blood vessels into surrounding tissue and renal clearance, yet still small enough (10-70 nm) to pass into capillaries.[5] A final critical aspect is control of colloidal stability. This will be a primary focus of the present chapter.

Steric stabilization using adsorbed polymer can be particularly efficient when nonadsorbing chains are terminally attached, forming an extended, brush-like layer.[29] Many contributions have been made to describe the extension behavior of adsorbed polymers, initially on flat surfaces.[30, 31] Scaling models employing stepwise density functions were developed by Alexander,[32, 33] de Gennes,[34] and Cantor,[35] while self consistent mean field (SCF) models[36-38] used continuous functions to describe polymer density.

Polymer chains on curved surfaces are less extended at a given adsorption density than their flat counterparts. The curvature of the surfaces provides additional space for the polymer chains at a given graft density as compared to a flat plate. The resulting density

profile was described originally for a star polymer by Daoud and Cotton.[39] Their model, based on scaling theory, proposed that polymers tethered to a spherical surface assumed the conformation of a string of blobs increasing in size with distance from the surface. This model has been applied to a number of systems to describe aggregation and adsorption behavior of neutral and charged block copolymers.[40-42] Halperin performed a scaling analysis by applying the star model to polymer micelles in selective solvents.[43]

Since the Daoud and Cotton model contains an adjustable parameter constant that relates to scaling the number of chains to the surface area of the core, the model was extended in two ways. D'Oliveira et al. [44] developed the Discrete Blob (DB) model, which was based on distinct layers and assumed dense packing of blobs on the surface. Based on the premise that the number of blobs in each sublayer was equal to the number of tethered chains, an expression for the diameter of the discretely packed blobs was developed, which allowed prediction of the total layer thickness. The Density Distribution (DD) model by Vagberg et al.[45] described the increasing diameters of the blobs as a continuous function, also allowing direct computation of the brush length. Farinha et al.[46] examined the DB and DD models using PS-PEO block copolymers both in micellar solution and adsorbed onto PS latex spheres and found them to be comparable both with experimental results and one another. Vagberg et al. also extended the star polymer model to include a finite core, R_c. This allowed prediction of micelle size based on aggregation number. This model has been used to describe a number of systems, including dendrimer-star polymers,[47, 48] poly(ethylene oxide) lipid micelles,[49] and polyelectrolyte block copolymer micelles.[50]

The interaction potential between two particles is critical to the stability of the suspension. For nanoparticles of metal oxides and metals, particularly polar solvents, attractive Van der Waals forces are typically so strong that, for steric stabilization, layer thicknesses may need to be on the order of the particle radius. Thus the problem of modeling and describing steric interaction energies on highly curved surfaces is expected to be of widespread interest for nanoparticles processing. The interaction potential may in some instances be measured directly using atomic force microscopy (AFM) with a

sphere glued to the cantilever, as pioneered by Ducker.[51] However, AFM is limited to particles on the order of a micron or larger in size. Other geometries such as crossed cylinders are possible using a surface force apparatus (SFA). However, the radius of curvature of the cylinders is limited to macroscopic dimensions and the area of interest effectively has flat plate geometry, allowing use of the Derjaguin approximation.[52] For particles with diameter less than 20 nm, such as the particles of interest in this study, it is not presently possible to directly measure the interaction energies. The ability to predict interaction potential of small colloids becomes increasingly useful, particularly as the radius of the particle and the thickness of the polymer brush become similar in dimension (i.e. the brush becomes increasingly curved.) The matter of interactions between star polymers in semi-dilute and concentrate solutions has been addressed in a rich body of literature. In particular, Vlassopoulos et al. have examined multiarm star polymers in solution using static and dynamic scattering techniques and have characterized interactions in semi-dilute solutions in terms of a structure factor.[48, 53-57] Description of particle interactions in dilute solutions using a second virial coefficient is addressed in another chapter.

Several groups have examined the steric interaction for polymer-coated curved surfaces. Lin and Gast employed a self consistent mean field theory with a Derjaguin approximation to describe the interaction potential for chains tethered on colloidal surfaces.[58] As an extension of the blob model for steric interaction potential pioneered by Witten and Pincus,[59] Likos and coworkers developed an analytical expression for effective pair potential between star polymers.[60, 61] This expression describes the interaction potential in two regimes as exponentially decaying for large separations and a logarithmic repulsion at close distances. The form of the expression at small separations is derived from work by Witten and Pincus using scaling theory to describe stabilization of colloidal particles by long grafted polymer chains.[59] The chain conformations for a single star are compatible with the blob model of star polymers.[45] A key point regarding this approach is that as it is based on star polymers it is designed for use with highly curved brushes. As such, it should describe interactions between particles with star-like structures, i.e. micelle and nanoparticles where there is an inner core with length scale 4-

6 nm and a soluble corona around the core. As the interaction potential is difficult to measure directly, two means of testing the model are by measurement of a structure factor (such as by small angle neutron scattering) or by measurement of the second virial coefficient, A_2 (such as by light scattering). The latter approach was described in Chapter 5 of this thesis.

This work concerns a study of polymer-magnetite complexes consisting of block copolymers strongly bound to magnetite particles and forming a sterically stabilizing layer of PEO brush. The adsorption of several copolymers on magnetite nanoparticles in water and phosphate buffered saline is described. The copolymers included poly(ethyleneoxide)-*g*-poly(ethyleneimine), poly(ethylene oxide) with three carboxylate groups grafted to one end of the chain, and a symmetric pentablock consisting of poly(ethylene oxide), poly(propylene oxide), and a novel carboxylic acid-containing urethane center block. The size and zeta potential on the particles was measured before and after adsorption and stability was examined in the two solvents. In addition, a model for effective interaction between star polymers developed by Likos et al.[60-62] was used to predict the steric interaction potential between two polymer-coated particles based on an extension of Vagberg's density distribution model to include a surface layer of adsorbed anchor block.[45] This was used in conjunction with extended DLVO theory to predict colloidal stability of the complexes. These magnetite complexes are being developed for use as MRI contrast agents.

6.4 Materials and Methods

6.4.1 Chemicals

The magnetite nanoparticles were synthesized by Nikorn Pothayee using a method he developed from the work of Pinna et al.[63] Briefly, 2.12 g (6 mmol) of iron(III) acetylacetonate was added to 40 mL of deoxygenated benzyl alcohol in a 250-mL 3-neck round bottom flask equipped with a condenser and mechanical stirring. The reaction mixture was heated to 200°C at a rate of 4-5°C/min and kept at this temperature for 4 hours under nitrogen. The resulting black particles were collected by centrifugation and washed with acetone. The dried particles were then redispersed in chloroform containing

0.15 ml oleic acid to ensure a stable dispersion. Chloroform was then evaporated, and the dried particles were washed with acetone to remove the excess oleic acid. Finally, the magnetite particles were redispersed and stored in chloroform. The radii of the bare magnetite particles were characterized by dynamic light scattering (DLS) as 5.1 nm and transmission electron microscopy (TEM) as 3.8 nm. Additional details on the measurements are given in a later section. The TEM value was used in all modeling in this paper.

Adsorption of polymeric stabilizers onto the magnetite particles was accomplished in chloroform. The complex was then precipitated using hexane and dried. After that, it was redispersed in water or phosphate buffered saline as appropriate.

The polymers were synthesized by Professor Riffle's group. There were three types of polymers. The first was a pentablock copolymer with a hydrophobic carboxylic acid containing urethane center block. The structure of this polymer was PEO-PPO-urethane-PPO-PEO, and it is illustrated below in Figure 6-1.

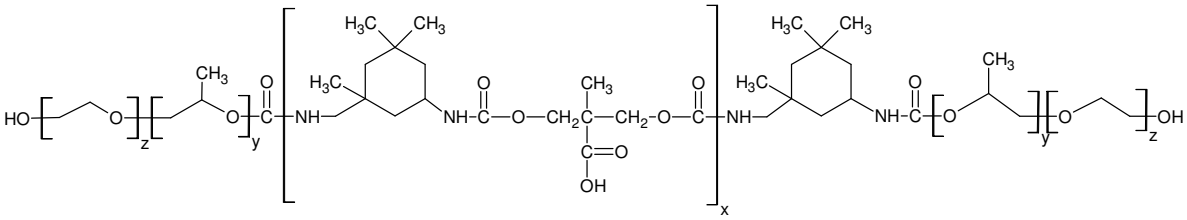

Figure 6-1. Structure of the pentablock stabilizer with PEO-PPO tail blocks and polyurethane center block containing carboxylic acid groups.

The second basic structure employed was a PEO-*g*-PEI copolymer. This is illustrated in Figure 6-2. For this structure, either one or two PEO chains were attached at random points on the PEI chain. Both branched (3kPEO-0.6KPEI(b)) and linear (5kPEO-1.4kPEI(l) PEI structures were used.

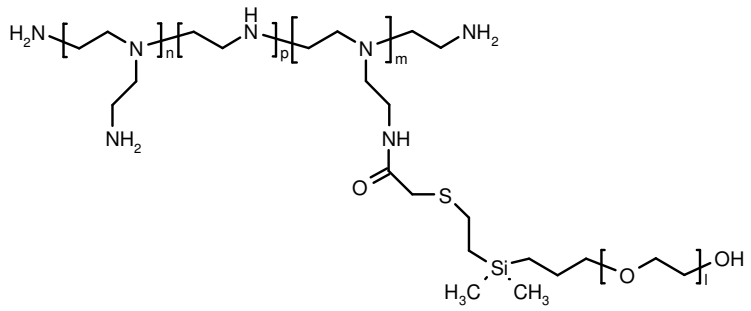

Figure 6-2. Structure of the PEO-g-PEI stabilizer. For these polymers, m can be either 1 or 2.

The third stabilizer design was a PEO chain with three carboxylic acid groups on one end to act as an attachment point on the magnetite.

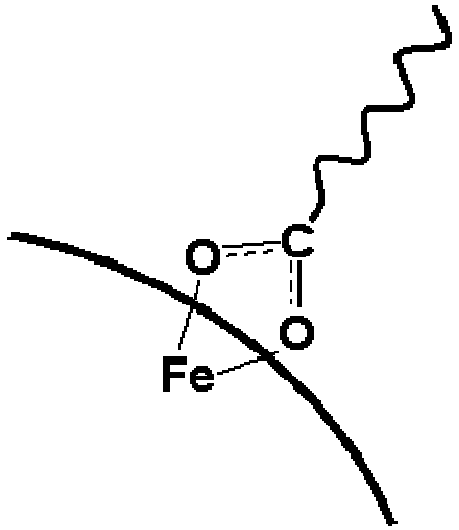

Figure 6-3. Adsorption of carboxylic acid onto magnetite.

The characteristics of the stabilizers are shown below in Table 6-1.

Table 6-1. Properties of the polymeric stabilizers.

	PEO tail block M_n (g/mol)[a]	Number of PEO tail blocks	Ave. number of ionizable groups per molecule[b]	Wt% magnetite[c]
Urethane pentablock	3,000	2	3	35
3kPEO-0.6kPEI(b) (m=1)[d]	3,000	1	14	39
3kPEO-0.6kPEI(b) (m=2)[d]	3,000	2	14	41
5kPEO-1.4KPEI(l)[e]	5,000	1	32	39
7kPEO-3COOH	7,000	1	3	40

[a]PEO tail block M_n from ^1H NMR. [b]Average number of COOH/mol of polymer from ^{13}C NMR. [c]Weight % magnetite by TGA for the complex in water. [d]3kPEO-0.6kPEI(b) contains branched PEI. [e]5kPEO-1.4KPEI(l) contains linear PEI.

6.4.2 Light Scattering

Dynamic light scattering is performed by measuring the variation of intensity with time. This is also known as quasi-elastic light scattering. This can be used to study electrophoretic motion, electrokinetic potential, and particle diffusion.[64] Hydrodynamic radii were determined using the Stokes-Einstein relationship, in which k is Boltzmann's constant, T is the temperature, η is the solvent viscosity, D_o is the diffusion coefficient, and d_H is the hydrodynamic diameter:

$$d_H = \frac{kT}{3\pi\eta D_o}$$

Eq. 6-1

Dynamic light scattering (DLS) was performed using a Malvern NanoZS operating at a fixed angle of 173° and a wavelength of 633 nm. The viscosity and refractive index were adjusted as appropriate for water or PBS at 25°C. The DLS data from this device were analyzed using Distribution Technology Software (DTS). This uses an algorithm based on CONTIN, which is a program designed for inversion of noisy equations via a constrained regularization algorithm as described by Provencher.[65, 66] The basic features of CONTIN are prior knowledge (in this case, that the sizes must be non-negative) and parsimony (the solution with the fewest and smoothest peaks is probably best).

Eq. 6-2

Particle size may be determined using a correlation with the diffusion coefficient such as the Stokes-Einstein relationship, which is valid for non-interacting spherical particles. This is given by:

$$\mathrm{D_o} = \frac{\mathrm{kT}}{3\pi\eta\mathrm{d_H}}$$

Eq. 6-3

in which k is Boltzmann's constant, T is the temperature, η is the viscosity, and d_H is the particle hydrodynamic diameter. If one assumes a non-draining sphere, the hydrodynamic radius, R_H, may be related to the radius of gyration, R_g, by the following:[67]

$$R_H = 0.875 R_g$$

Eq. 6-4

6.4.3 Zeta Potential

The zeta potential was measured using a Malvern NanoZS operating at a fixed angle of 173° and a wavelength of 633 nm. The choice of a model for zeta potential depends on the thickness of the Debye layer, κ^{-1}, relative to the radius of the particle, a.

The Debye length, κ^{-1}, can be calculated from the ionic strength, I, in an aqueous system as:

$$\kappa^{-1} = \left(\frac{0.304}{\sqrt{I}} \right)$$

Eq. 6-5

The ionic strength for a solution may be calculated as:

$$I = \frac{\sum c_i z_i^2}{2}$$

Eq. 6-6

in which c_i and z_i are the concentration and charge on a given ion in solution. The PBS solution used was purchased from Mediatech Inc., andcontained 0.2 g/L KCl, 0.2 g/L KH_2PO_4, 1.15 g/L Na_2PO_4 (anhydrous), and 8 g/L NaCl. The effective ionic strength as calculated using Eq. 6-6 was 0.197 M and the debye length (Eq. 6-5) was 0.7 nm. For deionized water, an ionic strength of ~10^{-5}M was assumed, with a resulting debye length of 96 nm.

For the case of a thin double layer with κa large, the zeta potential, ζ, is related to the electrophoretic mobility, μ, by the viscosity, η, and the electric permittivity of the medium, ε, according to the Smoluchowski approximation:

$$u = \frac{\zeta \varepsilon}{\eta}$$

Eq. 6-7

This limit assumes that the double layer is quite thin relative to the size of the particles; therefore, the electrical field is uniform and is at all times parallel to the surface of the particle.

The magnetite particles used were very small (approximately 4 nm radius); therefore, the Smoluchowski limit commonly employed for aqueous measurements was not appropriate. The measured zeta potential was corrected using:

$$\zeta_{corrected} = \frac{\zeta_{measured}}{\frac{2}{3} f(a\kappa)}$$

Eq. 6-8

The function $f(a\kappa)$ is given by[68]

$$f(\kappa a) = \frac{3}{2} - \frac{9}{2\kappa a} + \frac{75}{2\kappa^2 a^2} - \frac{330}{\kappa^3 a^3}$$

Eq. 6-9

which interpolates smoothly between the Smoluchowski and Huckel limits.

In water, the conditions more closely resembled the Huckel approximation, in which the particle does not deform the electrical field. In PBS, despite the significant ionic strength, the situation was intermediate between the two extremes. Zeta potentials measured under the Smoluchowski limit with f(κa)=1.5 were subsequently corrected using f(κa) appropriate for water (1.0) and PBS (1.2).[68]

6.4.4 Densiometry

The partial specific volumes of 2k and 5k PEO at 25°C were determined using aqueous solutions in the range of 0.1-5 wt % to be used in determination of the radius of gyration of the complex as described later in this chapter. Partial specific volumes were measured using a DA-300 Density/Specific Gravity Meter (Mettler). The partial specific volume of a micelle of a symmetric triblock copolymer consisting of two poly(ethylene oxide) chains flanking a three repeat unit urethane center block was also measured in the weight range of 0.2-2%. This was done in order to determine the specific volume of the urethane center block, which is the same as the anchor block in the urethane pentablock used in this study. The experimental procedure is described in detail in Chapter 5.

6.4.5 Transmission Electron Microscopy

Transmission electron microscopy (TEM) was conducted by Matthew Carroll with a JEOL 3000F field-emission transmission electron microscope (operated at 300kV)

equipped with a Gatan image filter (GIF) and digital imaging system at the University of Western Australia in Perth, Australia. Dry samples of the magnetite complexes were dispersed in de-ionized water and cast onto an amorphous carbon-coated copper grids for analysis. An image is included as Figure 6-4.

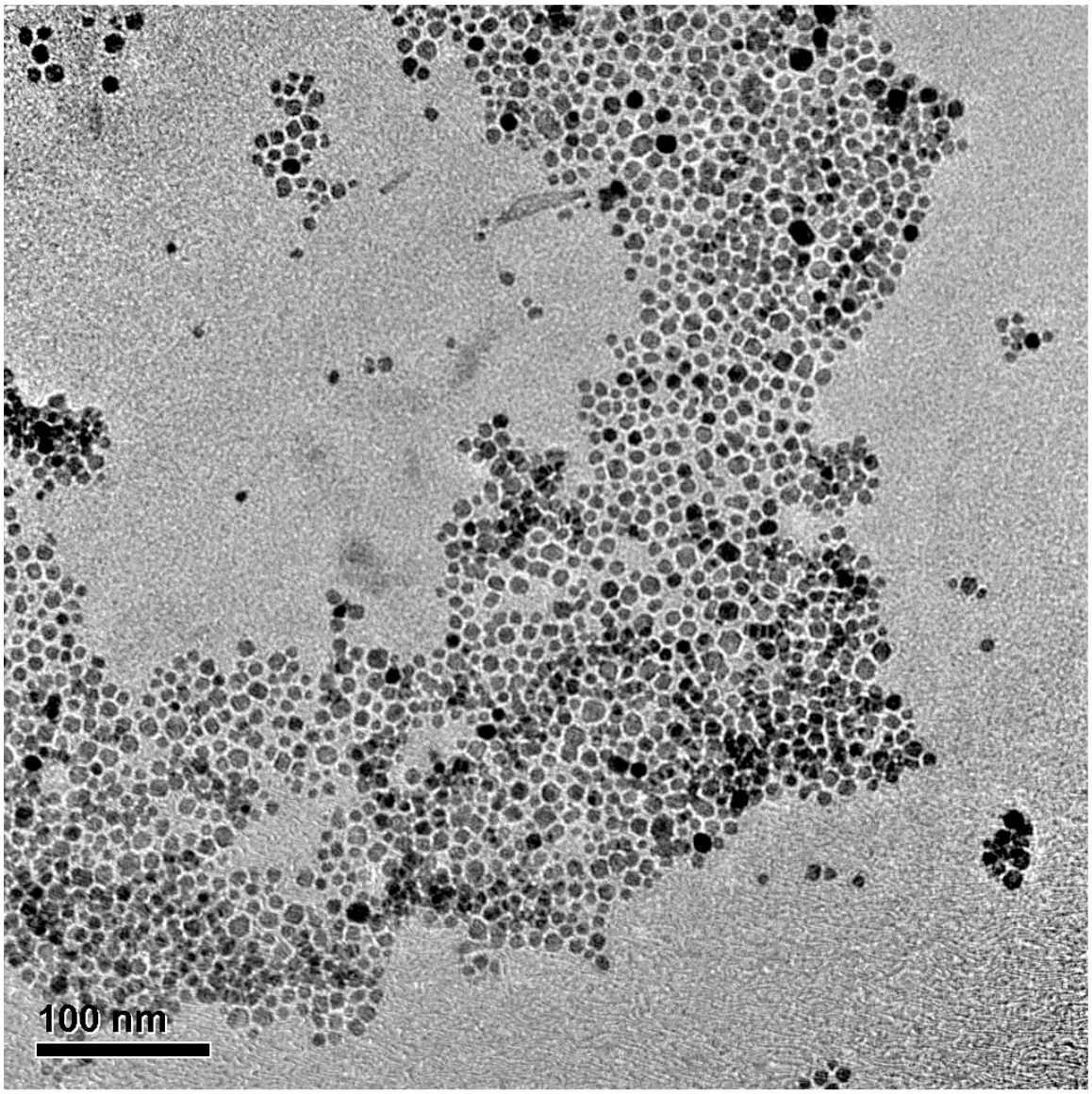

Figure 6-4. Transmission electron microscopy (TEM) image of the magnetite used in this study. TEM was performed by Thompson Mefford.

Particle size analysis was performed by Thompson Mefford using Reindeer Graphics's Fovea Pro 4 plug-in for Adobe Photoshop CS2. Mean and standard deviation of the particle size diameters were calculated and particle size distributions were fitted with a Weibull distribution function as shown in Figure 6-5. A total of 4759 particles were analyzed with a mean diameter of 7.6 nm and a standard deviation of 2.9 nm.

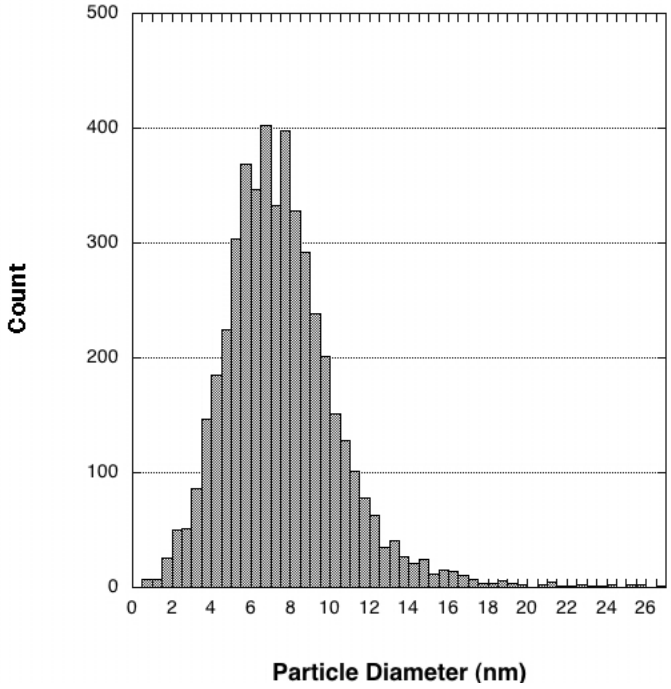

Figure 6-5. Particle size distribution for the magnetite used in this study. TEM and analysis was performed by Thompson Mefford.

6.4.6 Thermal Gravimetric Analysis

The amount of polymer adsorbed on the magnetite was characterized by Nikorn Pothayee by thermogravimetric analysis (TGA) using a TA Instruments TGA Q500 in nitrogen at a rate of 10°C/min. In addition to the adsorbed polymer, a small amount of organic contaminant (benzyl alcohol or oleic acid) remained on the surface. Typical amounts were 5-10% by weight. This is illustrated in Figure 6-6, and the percent of magnetite in each complex is listed in Table 6-1.

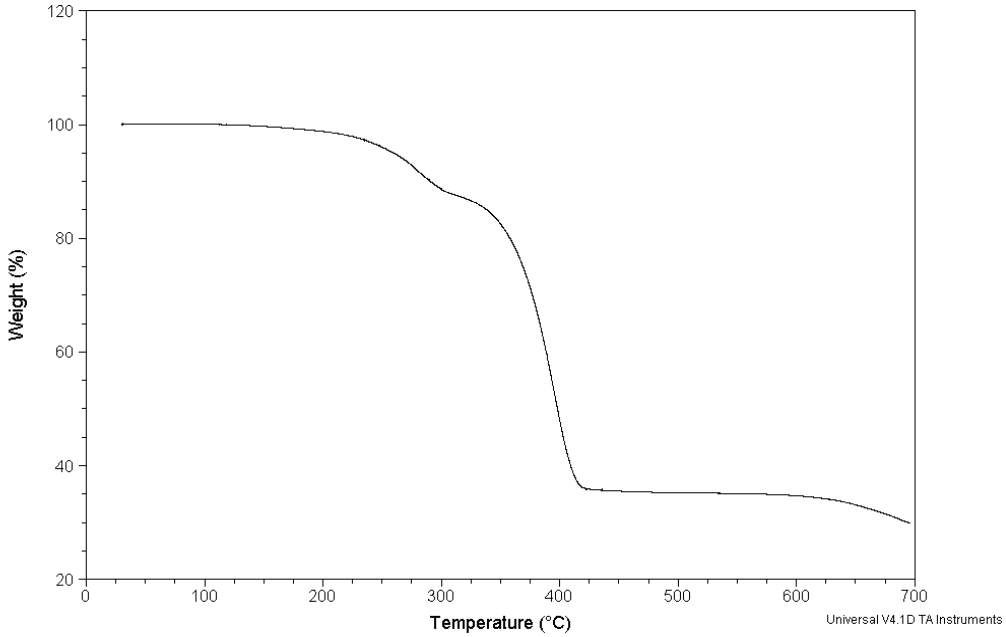

Figure 6-6. TGA scan for the urethane pentablock on magnetite.

6.5 Results and Discussion

6.5.1 Estimation of R_m with the Density Distribution Prediction

The magnetite complex size, R_m, was estimated for the complex with the density distribution (DD) model, developed by Vagberg et al.[45] This model, based on a model for star polymers by Daoud and Cotton[39] assumes concentric shells with a constant number of blobs equal to the number of adsorbed chains per particle. Blob size $\xi(r)$, is a continuous function of distance from the surface. The segment density in the shell varies with distance from the core.

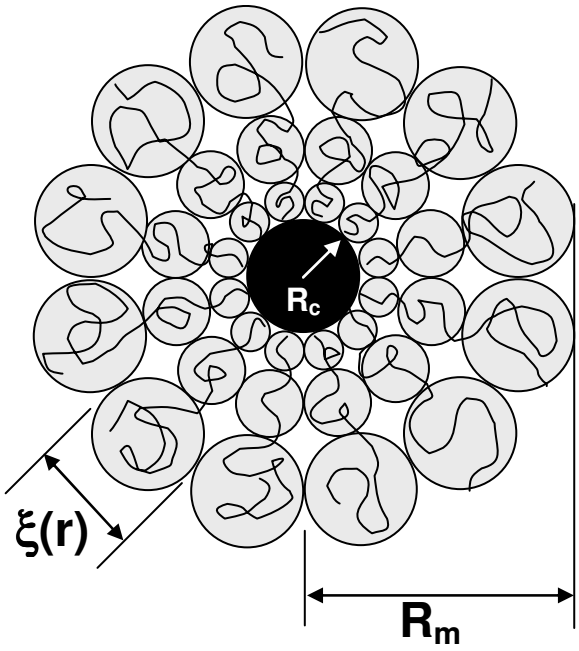

Figure 6-7. Schematic representation of the complex showing the density distribution model[45] parameters.

The DD model predicts complex radius, R_m, as:

$$R_m = \left[N a_s^{1/\nu} \frac{8 f^{(1-\nu)/2\nu}}{3\nu 4^{1/\nu}} + R_c^{1/\nu} \right]^{\nu}$$

Eq. 6-10

where N is the number of Kuhn segments, ν is the Flory exponent, R_c is the radius of the core, f is the number of corona chains, and a_s is the Kuhn segment length for PEO (0.6 nm). For the copolymers, f is determined from the weight ratio of magnetite and polymer measured by TGA and knowledge of the polymer properties. R_c was measured using TEM and by DLS on the bare particles.

The blob diameter, ξ(r) is given by:

$$\xi(r) = \frac{4r}{f^{1/2}}$$

Eq. 6-11

in which r is the distance from the center of the complex. This expression was used for the 7k-3COOH polymer, in which the size of the graft points is quite small compared to the size of the polymer chains.

The Flory exponent, ν, varies between 0.5 at a theta condition and 0.6 for a good solvent. The calculations used ν = 0.583[69] for PEO in water at room temperature for these calculations, as used in similar studies by other authors.[46, 49, 70]

6.5.2 Extension of the DD Model to Include an Anchor Layer

The Vagberg model is based on a star polymer and is applicable in the case of polymer chains grafted onto a hard core. However, a slight modification was necessary to apply this method to a complex to account for the presence of the anchor block. For block copolymers, the anchor block was assumed to form a flat, dry layer surrounding the core with thickness t_a as shown in Figure 6-8. The thickness of the anchor block was calculated from the volume of a solid shell of the appropriate density based on the known weight ratio of polymer to magnetite and the composition of the polymer. For the pentablock copolymer, the density was a weighted average between the density of PPO and the density of the urethane center block. The density of the urethane center block was measured as 0.77 cm^3/g as described in detail in Chapter 4.

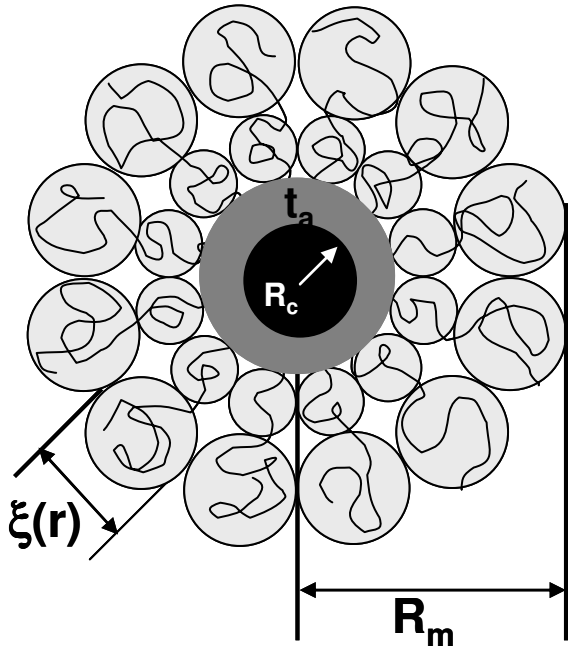

Figure 6-8. Parameters of the density distribution model[45] extended to include an anchor layer.

The Vagberg model was adapted by addition of a new effective core size which is equal to R_c+t_a. In effect, the number of attached chains, f, remains the same, but is spread out over a larger surface area. The resulting expression is:

$$R_m = \left[Nl^{1/\nu} \frac{8f^{(1-\nu)/2\nu}}{3\nu 4^{1/\nu}} + (R_c + t_a)^{1/\nu} \right]^{\nu}$$

Eq. 6-12

This expression was used for the urethane pentablock and the three PEO-PEI copolymers, as each had a significant anchor block. The measured and predicted sizes of the polymer-magnetite complexes (based on R_c = 3.8) are shown below in Table 6-2. The volume fractions for all complexes at r = (R_c+t_a) were less than 1.0.

Table 6-2. Complex size measured by DLS and predicted using the Density Distribution model.[a]

Sample	d_H (nm) volume[b]	d_H (nm) number[b]	$2R_m$ (nm)	t_a (nm)	f	polymer (mg/m^2)
Urethane pentablock	36.8	27.6	27.2	2.2	288	12.2
3kPEO-0.6kPEI(b) (m = 1)	23.5	19.1	26.2	1.1	288	9.5
3kPEO-0.6kPEI(b) (m = 2)	27.5	22.5	26.6	0.7	341	10.3
5kPEO-1.4KPEI(l)	28.3	20.1	31.0	1.5	176	10.3
7kPEO-3COOH	29.6	23.9	34.8	0	155	9.9

[a]The model was fit using R_c = 3.8 nm as measured by TEM. [b]Volume and number average distributions are discussed further in the text below.

Two values are reported for the measured hydrodynamic diameter of the complexes, a volume average and a number average. To understand the significance of the two numbers, a brief digression on how light scattering is used to measure size is necessary. The technique of DLS involves measuring the intensity of light scattered from a sample at a given angle. By use of a Fourier transform, the autocorrelation function is translated into a distribution of sizes. This distribution is based on intensity. Since the intensity of scattered light goes as r^6, the intensity-weighted average is heavily weighted towards larger particles in the distribution. This may be converted to a volume distribution (~r^3) or a number distribution. In a manner analogous to molecular weight distributions, all are fair ways to represent an average of the size distribution. It makes sense to compare whichever distribution is most comparable to any other experimental technique being employed. The disadvantage to using the volume or particularly the number average is that any error present in the initial distribution may be magnified. However, for these

complexes, repeatable results were obtained. Also, these are spherical complexes and are small relative to the wavelength of the light source ($r < \lambda/20$), so the Rayleigh approximation holds.

The weight fraction of polymer is based on TGA measurements and represents a maximum value. It is possible that the true weight fraction is less for two reasons. The first is that the polymer weight fraction counts any organic impurities in the complex. The second is that if the TGA sample contained any unbound polymer, then that would be counted as well. The polymer was adsorbed from chloroform, then the complex was precipitated using hexane and dried before redispersing in aqueous solvent. If any unbound polymer precipitated in hexane, it would have been present in the TGA sample. With that in mind, the predicted complex sizes are likewise maximum values.

The single most sensitive input to the model is the magnetite radius, R_c. An accurate measurement of that value is critical for the predictions. In general, the agreement between the model fits for $2*R_m$ and the measured hydrodynamic diameters were good. The closest fits were for the 3kPEO-0.6kPEI (both m = 1 and m = 2) and the urethane pentablock copolymers. The volume fraction PEO in the corona is higher for these three complexes than the remaining two as will be discussed in a later section. Physically, that means that these complexes are more similar to a hard sphere than the others and a size measured by DLS, which is an equivalent hard sphere measurement, should be closer to the actual size. The remaining polymers (7kPEO-3COOH and 5kPEO-1.4kPEI) have lower volume fractions in the corona, indicating that they are softer particles. As a result, the equivalent hard sphere radius measured by DLS is smaller than the prediction from the density distribution model.

6.5.3 Colloidal Stability

According to the classical Derjaguin-Landau-Verwey-Overbook (DLVO) theory, stabilization depends on the combination of electrostatic and van der Waals (vdW) interactions between surfaces. The curve describing the total interaction potential, Φ, can be used to predict stability. At very close ranges the vdW forces will dominate, resulting in coagulation. However a repulsive barrier of $\Phi/kT >> 1$ caused by electrostatic or

steric forces can lead to kinetic stability, which is often sufficient for stabilization. In addition, it is possible to have a secondary minimum, which would provide a relatively low energy state and encourage kinetic stabilization.[30] As the particles approach, they become trapped in the secondary minimum and are loosely flocculated. However, if the energy well is shallow, the flocculated system may be readily redispersed with the application of agitation. By contrast, particles that reach the primary minimum typically cannot be readily redispersed.

Attachment of soluble chains to form a brush on a surface generally increases colloidal stability due to steric stabilization. This arises from a combination of enthalpic and entropic effects resulting from the confinement of soluble tail chains in the gap between two particles. Steric stabilization occur when the steric forces keep the particles separated by a distance that prevents coagulation due to dispersion forces. With sufficiently thick brushes, the interaction curve can be entirely repulsive, resulting in a very stable dispersion. Calculation of the interaction potential due to steric effects is discussed in more detail below.

For the case of the magnetic substrate, an additional contribution to the interaction potential comes from the magnetic forces. However, the magnetite particles in this study are small enough to fall into the superparamagnetic regime so their magnetic dipoles have no overall orientation in the absence of an applied magnetic field.[71] For the discussions in this chapter, the magnetic potential has been neglected except in the presence of an applied magnetic field.

The general expression for interaction potential,Φ, is the sum of the interaction potentials $\Phi = \Phi_{ES} + \Phi_{vdW} + \Phi_{M} + \Phi_{S}$ in which the subscript ES is electrostatic, vdW is van der Waals, M is magnetite, and S is steric (adsorbed polymer). All potential curves will be reported in this manuscript as a ratio of potential (Φ) to thermal energy (kT) for ease of interpretation.

The electrostatic interaction is described with a constant potential expression useful for curved surfaces having a thick electrical double layer ($\kappa a<5$) and surface potentials of approximately 25 mV or less.[52] This expression was used for the samples in water, for which an ionic strength of ~10^{-5}M was assumed, corresponding to κ^{-1}=96 nm.

$$\Phi_{ES} = 2\pi a \varepsilon \varepsilon_o \psi_o^2 e^{-\kappa(r-2a)}$$

Eq. 6-13

In this equation, ε is the dielectric constant of the medium (water), ε_o is the permittivity of free space, ψ_o is the surface potential, and κ is the inverse Debye length. For a thin electrical double layer ($\kappa a >10$) the equivalent expression is

$$\Phi_{ES} = 2\pi a \varepsilon \varepsilon_o \psi_o^2 \ln\left(1 + e^{-k(r-2a)}\right)$$

Eq. 6-14

This expression was used for the samples in PBS where I_{eff}=0.197 M and κ^{-1}=0.7 nm, although in PBS the zeta potential was so low that the difference is trivial.

Determination of a true surface potential is difficult given the complexities that can arise with defining the structure of a Stern layer and given that the presence of the PEO brush shifts the shear plane away from the magnetite particle surface. Therefore, the surface potential was approximated in these calculations with the zeta potential.

Table 6-3. Zeta potential and stability observations for the complexes.

	Water (pH ~ 7)[a]		PBS (pH = 7.4)	
Sample	zp (mV)	stability	zp (mV)	Stability[b]
Urethane pentablock	-11.1	yes	-7.6	Aggregated overnight
3kPEO-0.6kPEI(b)	27.1	yes	0.3	yes
3kPEO-0.6kPEI(b)-3kPEO	15.2	yes	-2.1	yes
5kPEO-1.4KPEI(l)	25.3	yes		yes
7kPEO-3COOH	6.1	yes	-11.9	Aggregated immediately

[a]Samples in water contained no buffer, so some downward pH drift was expected. [b]Stability was quantitatively determined by visual observation. Aggregation was noted when a fine layer of magnetite formed at the bottom of the vial. Those samples referenced as stable remained entirely free of sediment for a minimum of several days.

The magnetite pair potential, Φ_M, for two spheres of equal size aligned in a uniform magnetite field with θ=0 is given by the following:

$$V_M = -\frac{8\pi\mu_0 a^3 M^2}{9\left(\frac{h}{a}+2\right)^3}$$

Eq. 6-15

in which M is the magnetization (345,000 A/m), μ_o is the magnetite permeability of vacuum (1.26e^{-6}Tm/A), h is the surface-to-surface separation of two particles, and a is the radius of the magnetite particle.[72] This represents the maximum pair potential and thus leads to an upper bound on the effect of a magnetite field on doublet formation.

The vdW contribution to the interaction potential is described as:

$$\Phi_{vdW} = -\frac{1}{6}A_{eff}\left(\frac{2a^2}{r^2-4a^2}+\frac{2a^2}{r^2}+\ln\left(\frac{r^2-4a^2}{r^2}\right)\right)$$

Eq. 6-16

in which a is the particle radius and r is the center-to-center separation of two particles. A_{eff} is the effective retarded Hamaker constant, calculated from the following equation:

$$A_{eff} = A_{\nu=0} + A_{\nu>0} = \frac{3}{4}kT\left(\frac{\bar{\varepsilon}(0)-\varepsilon(0)}{\bar{\varepsilon}(0)+\varepsilon(0)}\right)^2 + \frac{3\hbar\omega}{16\sqrt{2}}\frac{\left(\bar{n}_o^2-n_o^2\right)^2}{\left(\bar{n}_o^2+n_o^2\right)^{3/2}}F(H)$$

Eq. 6-17

In this equation, k is the Boltzmann constant, T is the temperature, $\varepsilon(0)$ and $\bar{\varepsilon}(0)$ are the dielectric constants for the medium and the substrate, n_o and $\bar{n}_o$ are the refractive indices (in the visible range) of the medium and substrate, $2\pi\hbar$ is Planck's constant, and ω is the frequency of the dominant relaxation in the uv. F(H) accounts for retardation effects, and is unity at the nonretarded limit:

$$F(H) \approx \left(1+\left(\frac{\pi H}{4\sqrt{2}}\right)^{3/2}\right)^{-2/3}$$

Eq. 6-18

H is given by the following equation in which h is the surface to surface separation and c is the speed of light.

$$H = n_o \left(\bar{n}_o^2 + n_o^2 \right)^{1/2} \frac{h\omega}{c}$$

Eq. 6-19

For magnetite a dielectric constant of 20,000[73] and refractive index of 1.97[74] were used. The calculated Hamaker constant in the nonretarded limit for Fe_3O_4 was $9.0*10^{-20}$ J. The Hamaker constant for magnetite has been reported elsewhere as $16.4*10^{-20}$ J.[75] One additional correction to the Hamaker constant was made in order to account for screening by the electrolyte. This is as described in the following equation and has an effect only for the zero frequency portion of the Hamaker constant evaluated in the limit of zero frequency.[52]

$$A = A_{\nu=0}(2\kappa h) e^{-2\kappa h} + A_{\nu>0}$$

Eq. 6-20

The maximum effect of this correction at a separation distance of 25 nm (beyond which distance is beyond the range of interest for this study), is a decrease in the Hamaker constant of 4% for water and 10% for PBS.

The resulting complete expression is:

$$A_{eff} = \frac{3}{4} kT \left(\frac{\bar{\varepsilon}(0) - \varepsilon(0)}{\bar{\varepsilon}(0) + \varepsilon(0)} \right)^2 e^{-2\kappa h} + \frac{3\hbar\omega}{16\sqrt{2}} \frac{\left(\bar{n}_o^2 - n_o^2 \right)^2}{\left(\bar{n}_o^2 + n_o^2 \right)^{3/2}} F(H)$$

Eq. 6-21

The treatment in this chapter does not include a contribution to the vdW forces from the adsorbed polymer; the vdW force is based on the magnetite alone. This is not an uncommon assumption; for instance, Bevan et al. used this assumption when examining a system of PEO-PPO-PEO triblocks adsorbed on latex spheres.[76] In the present work, the magnetite makes a significantly larger contribution to the vdW force both because it comprises much more of the complex by mass and also because polymers typically have significantly lower Hamaker constants than metals or metal oxides. Inclusion of the

contribution from the polymer layer would have caused the effect of the vdW force to have taken effect at a larger separation distance, r. However, this expansion of the vdW effect would not unduly influence the stability predictions of this model, as most of the mass of polymer is still concentrated close to the surface of the magnetite particle. This distribution of mass will be further addressed in a calculation for R_g later in this chapter. Methods do exist to characterize the effective Hamaker constant for a particle-polymer compex. For instance, latexes present in paint can be described by a many-layered Hamaker constant.[77] Tadmor and Klein described the force between surfactant-coated particles; they also make the point that for thin layers of polymer, the contribution to energy is small.[78] Prieve and Russel predicted Hamaker constant for coatings using Lifshitz theory.[79]

For the case of a densely adsorbed brush layer, the steric contribution to the interaction potential may be described by the Likos expression:

$$\frac{\Phi_S}{kT} = \frac{5}{18} f^{3/2} \begin{cases} -\ln\left(\frac{r}{\sigma} + \frac{1}{1+\frac{\sqrt{f}}{2}}\right); & r \le \sigma \\ \frac{1}{1+\frac{\sqrt{f}}{2}}\left(\frac{\sigma}{r}\right)\exp\left(-\frac{\sqrt{f}}{2\sigma}(r-\sigma)\right); & r > \sigma \end{cases}$$

Eq. 6-22

in which r is the center-to-center separation, f is the number of arms, and $\sigma/2$ is the distance from the center of the core to the center of the outermost blob layer. For this expression, σ is defined as $1.3*R_g$, the radius of gyration of the ensemble.[61] The first portion of the equation (relating to close approaches) is a logarithmic relationship derived originally by Witten and Pincus[59] which describes the entropic repulsion when chains from adjacent stars overlap. The exponential longer distance relationship ($r>\sigma$) is based on a Yukawa-type decay (such as that used to describe a screened Coulomb potential[80]) with the decay length set to the diameter of the largest blobs and has been extensively tested using machine simulation.[62] The two portions of the expression have been formulated to meet smoothly at $r=\sigma$. The geometry of this model is shown in Figure 6-9.

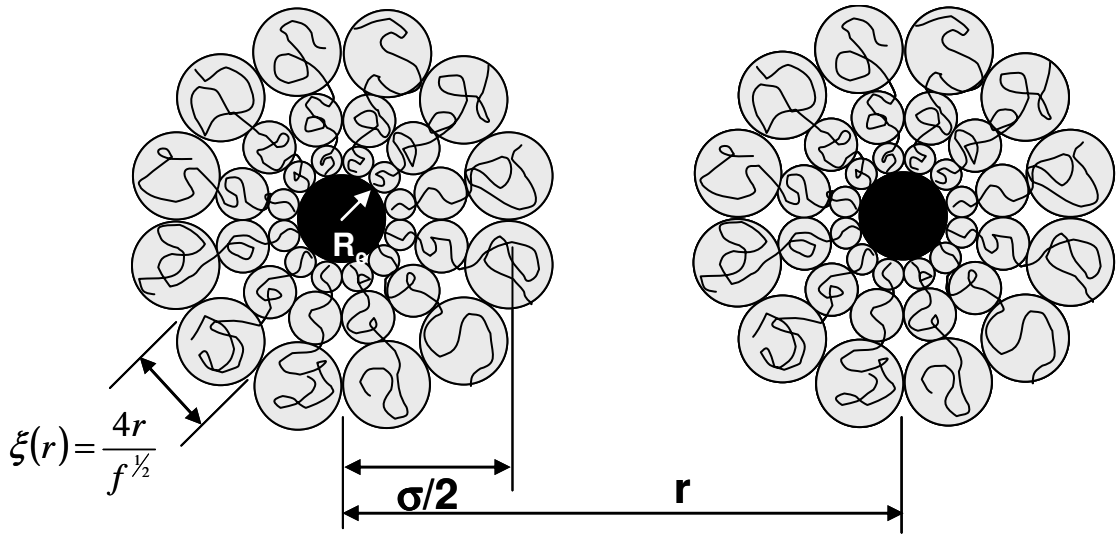

Figure 6-9. Geometry for the Likos-Lowen[62] star polymer model.

One critical parameter for this mode is R_g, the radius of gyration of the particle-polymer ensemble. One approach is to experimentally measure this using a scattering technique such as SLS or SANS. Alternately, one can approximate R_g using the moment of inertia of the complex.

The moment of inertia of a mass, m, rotated about an axis at a distance r is given by:[81]

$$I = \int r^2 dm$$

Eq. 6-23

Extending this to the moment of inertia of a sphere with density ρ at a distance r from the origin yields:

$$I = \int r^2 \rho(r) 4\pi r^2 dr$$

Eq. 6-24

The radius of gyration is related to the moment of inertia and the mass by:

$$R_g = \sqrt{\frac{I}{m}}$$

Eq. 6-25

The moment of inertia of a composite body is the sum of the moments of inertias of the various components. For the case of a magnetite core with a shell of adsorbed anchor block and a corona of extended PEO chains, the moment of inertia could be described as:

$$I_{total} = I_{magnetite} + I_{anchor} + I_{corona}$$

Eq. 6-26

Correspondingly, the mass of the ensemble is:

$$m_{total} = m_{magnetite} + m_{anchor} + m_{corona}$$

Eq. 6-27

and the radius of gyration of the entire complex is:

$$R_g = \sqrt{\frac{I_{total}}{m_{total}}}$$

Eq. 6-28

All that remains is to define the density as a function of distance from the center, r. For $r<R_c$, the density is the bulk density of magnetite, $\rho_{magnetite}$. For the distance from R_c to R_c+t_a, the density is assumed to be the bulk density of the dry anchor block. For the pentablock copolymer, this was taken to be a weighted average between the densities of the urethane anchor block (measured by densiometry as described Chapter 4) and that of PPO.

$$\rho(r) = \rho_{magnetite} \qquad for \quad r < R_c$$
$$\rho(r) = \rho_{anchor} \qquad for \quad R_c < r < (R_c + t_a)$$

Eq. 6-29

For the PEO corona, the density is defined in the density distribution model by Vagberg[45] as:

$$\rho(r) = m_s A \left(\frac{r}{a_s}\right)^{\frac{1}{\nu}} r^{-3} \quad for \quad (R_c + t_a) < r < R_m$$

Eq. 6-30

in which m_s is the mass of a segment of PEO, and the constant of proportionality, A, is determined by the relationship between the blob size at the core-corona boundary and the number of corona chains.

$$A = \frac{3 * 4^{\frac{1}{\nu}} f^{\frac{3\nu-1}{2\nu}}}{32}$$

Eq. 6-31

Inserting the expressions in Eq. 6-24 and Eq. 6-29 into the formula for inertia given as Eq. 6-24 yields these expressions for the inertia of the core, anchor, and corona respectively.

$$I_{core} = \int_0^{R_c} r^2 \rho_{magnetite} 4\pi r^2 dr = \frac{4\pi R_c^5 \rho_{magnetite}}{5}$$

Eq. 6-32

$$I_{anchor} = \int_{R_c}^{R_c+t_a} r^2 \rho_{anchor} 4\pi r^2 dr = \frac{4\pi\rho_{anchor}}{5}\left((R_c + t_a)^5 - R_c^5\right)$$

Eq. 6-33

$$I_{corona} = \int_{R_c+t_a}^{R_m} r^2 m_s A\left(\frac{r}{a_s}\right)^{\frac{1}{\nu}} r^{-3} 4\pi r^2 dr = \frac{4\pi A m_s}{a_s^{1/\nu}\left(2+\frac{1}{\nu}\right)}\left(R_m^{\left(2+1/\nu\right)} - \left(R_c + t_a\right)^{\left(2+1/\nu\right)}\right)$$

Eq. 6-34

To test this method, the calculated R_g were compared to measured values of R_g in the literature for PEO-PPO-PEO[82] and PS-PEO[45] micelles with good agreement (within 2-24% of experimental values).

Table 6-4. Estimation of R_g and σ.

Sample	R_m (nm)	t_a (nm)	f	R_g (nm)	σ (nm)
Urethane pentablock	13.3	2.3	288	7.4	9.6
3kPEO-0.6kPEI(b) (m=1)	12.7	1.1	288	7.2	9.4
3kPEO-0.6kPEI(b) (m=2)	12.9	0.7	341	7.5	9.8
5kPEO-1.4KPEI(l)	15.1	1.4	176	8.3	10.7
7kPEO-3COOH	16.8	0	155	9.7	12.6

Note: These predictions are based on R_c = 3.8 nm from TEM measurements.

An interesting feature of the Likos and Lowen model is the transition from a steep logarithmic decay at small separations ($r<\sigma$) to a very gradual exponential decay at further distances. Pragmatically, that means that steric stabilization does not become significant until r/σ gets close to unity. As the number of chains attached, f, decreases, the brushes must move closer together to achieve steric repulsion. This can be seen in the example plot in Figure 6-10.

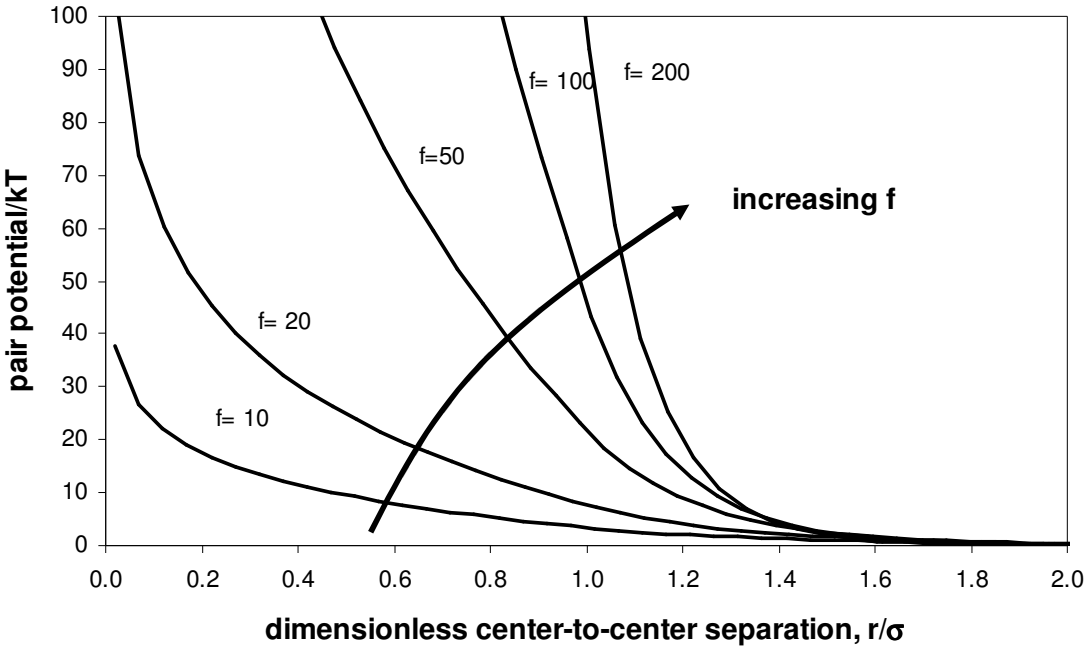

*Figure 6-10. Example plot showing the effect of increasing the number of corona chains per particle, f on steric repulsion. The dimensionless center-to-center distance is r/σ. These example calculations assume f = 10, 20, 50, 100, and 200. R_c was 5 nm, ν was 0.583, and the attached chains were 2000 g/mol PEO. The value of σ was calculated as 1.3*R_g, and R_g for the complex was calculated using the moment of inertia approach described earlier in the chapter, and as such varies with f.*

As may be seen in Table 6-4, R_g is significantly smaller than R_m, and as such σ is significantly smaller than R_m. This means that counter to intuition, the large steric stabilization effect doesn't occur immediately upon the outermost edge of the complexes touching ($r = 2R_m$). Physically, this corresponds to the decrease in brush density towards the outside of the corona due to the large effect from curvature. This is different from other brush models based originally on flat plate brush models adapted for spherical particles using the Derjaguin approximation, such as those by Russel[30] and Ploehn.[31] Lin and Gast examined the effect of using the volume fraction profile from a flat plate model on interaction potential between curved surfaces and found that the interaction was overpredicted, especially in cases where the thickness of the polymer brush was greater than the size of the hard core.[58]

The steric potential for the experimental polymer-magnetite complexes is shown in Figure 6-11.

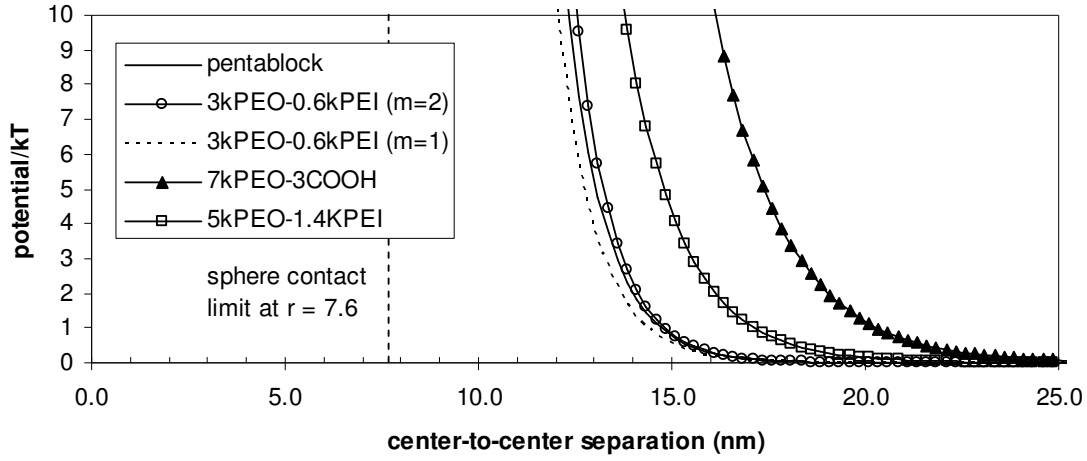

Figure 6-11. Steric potential by the Likos and Lowen expression for a core radius of 3.8 nm.

This highlights another point, which is that the volume fraction in the corona, which is a radial profile as shown in Eq. 6-30, has a strong effect on steric repulsion. The volume fraction of PEO in the corona as a function of distance from the surface of the core may be calculated using the Vagberg approach.[45] In this method, the volume fraction profile is divided into three sections. With the core, the density is constant. Beyond the complex radius, calculated as R_m, the density is zero. Between R_c and R_m the profile is the following, in which ρ_{PEO} is the density of PEO.

$$\Phi(r) = \rho_{PEO} A \left(\frac{r}{a_s} \right)^{\frac{1}{\nu}} r^{-3}$$

Eq. 6-35

As f increases, so does the volume fraction throughout the corona. This is illustrated in Figure 6-12.

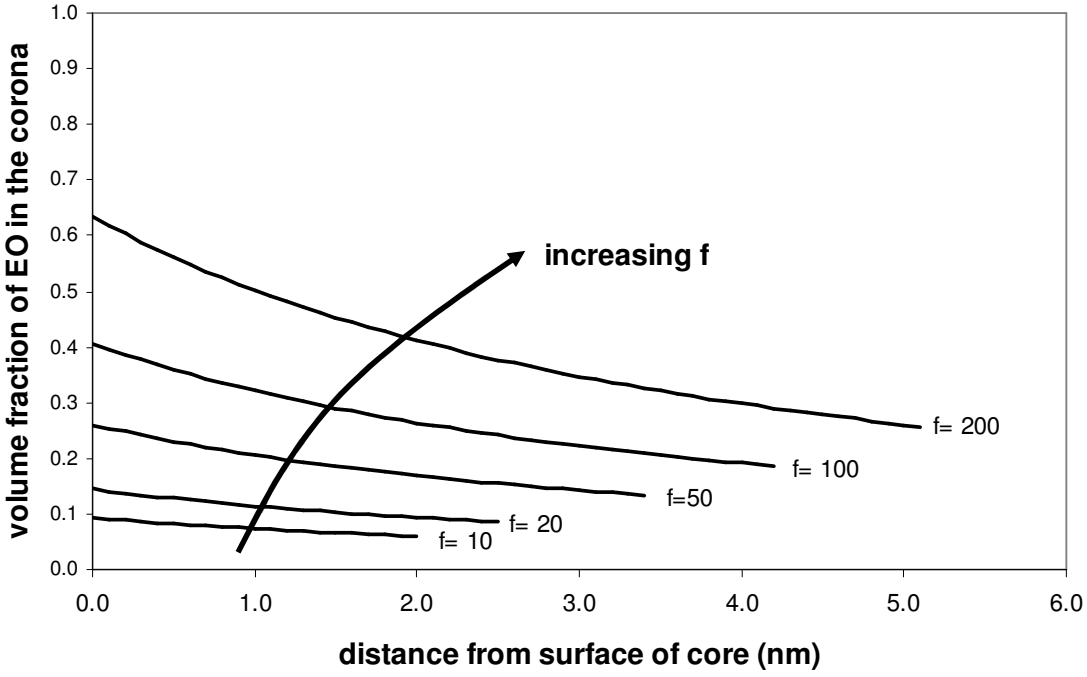

*Figure 6-12. Example plot showing the effect of increasing the number of corona chains per particle,,f on volume fraction in the corona. The center-to-center distance is r. These example calculations assume f = 10, 20, 50, 100, and 200. R_c was 5 nm, ν was 0.583, and the attached chains were 2000 g/mol PEO. The value of σ was calculated as 1.3*R_g, and R_g for the complex was calculated using the moment of inertia approach described earlier in the chapter, and as such varies with f.*

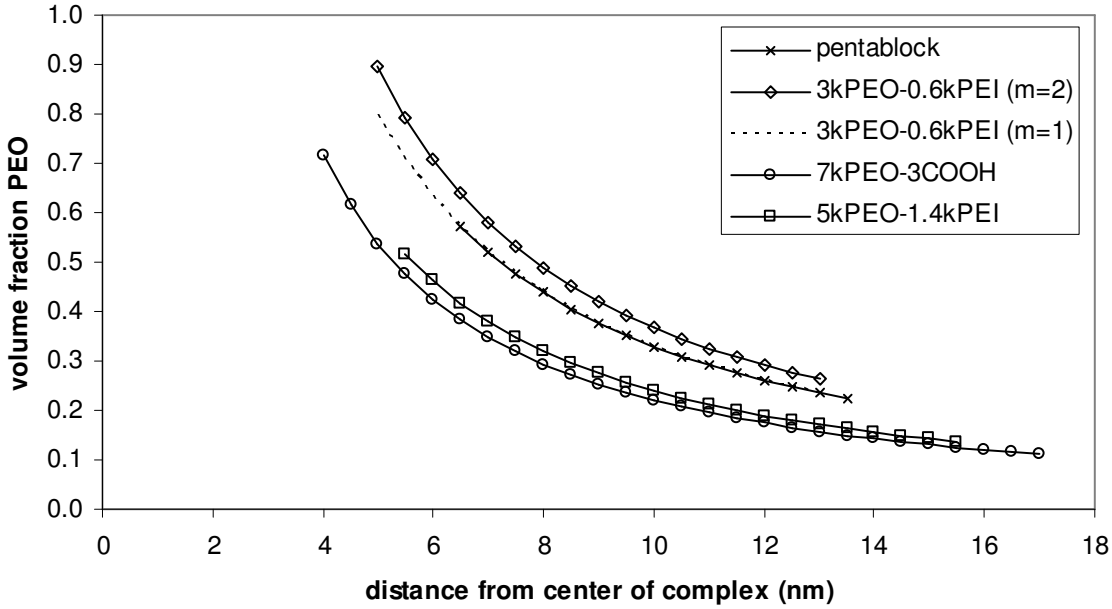

Figure 6-13. Volume fraction in the PEO corona for the polymer-magnetite complexes for R_c = 3.8 nm. The starting point for each sample depends on the thickness R_c+t_a.

The volume fraction profile for each PEO corona is shown in Figure 6-13. The polymer with the longest PEO chains (7kPEO-3COOH) has a corona which extends further into solution; it also has the lowest volume fraction at the periphery of the corona. The highest volume fraction is the triblock 3kPEO-0.6kPEI (m=2), which has a denser brush than its diblock counterpart, 3kPEO-0.6kPEI (m=1).

A typical DLVO plot for a polymer-magnetite complex in water is shown in Figure 6-14 for 3kPEO-0.6kPEI (m=2). There is a significant electrostatic contribution to stabilization due to its relatively zeta potential of 27 mV in water (Table 6-3); nonetheless the steric repulsion generated by the dense PEO brush is the main component of stability.

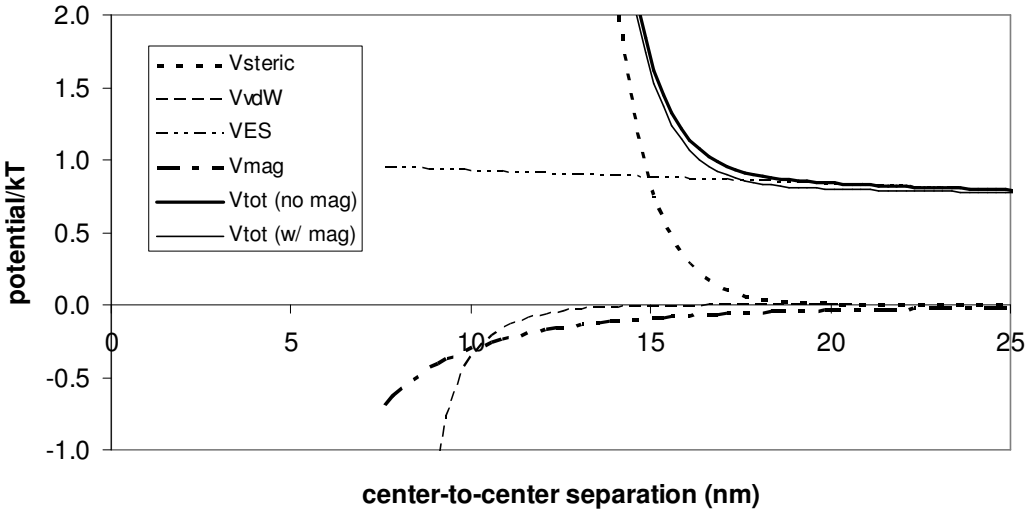

Figure 6-14. DLVO interaction potential for 3kPEO-0.6kPEI (m=2) in deionized water with R_c = 3.8 nm. The magnetization used was measured by Nikorn Pothayee using a 7 Tesla Quantum Design MPMS SQUID magnetometer (345,000 A/m).

Figure 6-15 shows the hypothetical DLVO diagram for the same 3kPEO-0.6kPEI (m=2) and magnetite complex, but in PBS and assuming that no polymer desorbs in PBS. The high ionic strength of the PBS screens out most of the electrostatic interaction, leaving just the steric repulsion for stabilization. If the amount of polymer present on the magnetite surface is the same in water or PBS, then one would expect that the complex would still be stable in PBS, and so it is. This is the case for both 3kPEO-0.6kPEI (m=2) and 3kPEO-0.6kPEI (m=1). Even if the Flory interaction exponent is changed from

0.583 (good solvent) to 0.5 (theta solvent), representing the case where the enthalpic contribution to stability disappears, the entropic contribution is sufficient for stability.

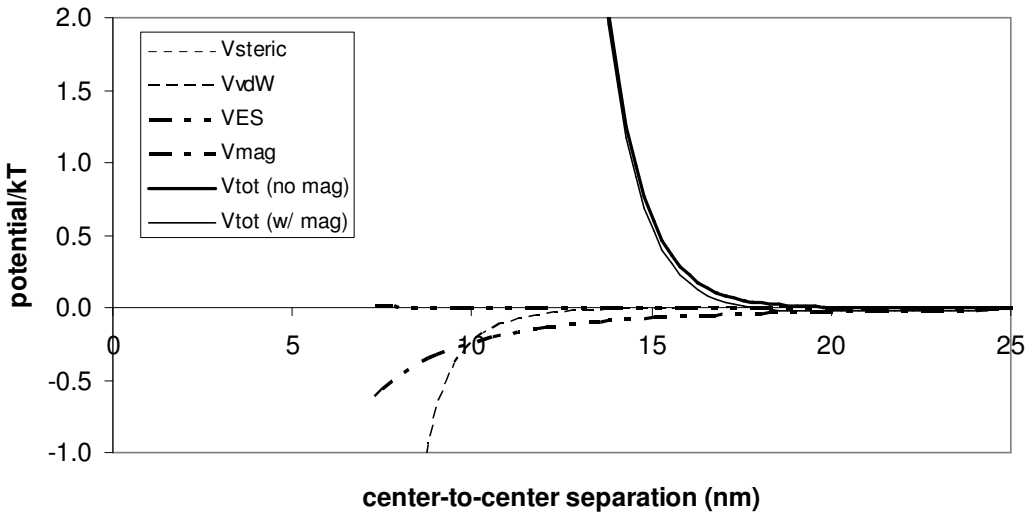

Figure 6-15. A hypothetical DLVO prediction for magnetite (R_c = 3.8 nm) with adsorbed 3kPEO-0.6kPEI (m=2) in PBS based on the assumption that no desorption occurs in PBS. The magnetization used was (345,000 A/m).

On the other hand, both of the carboxylate-containing polymers were stable in water, but unstable in PBS. The urethane pentablock complex had some limited stability, but aggregated overnight; the 7kPEO-3COOH visibly precipitated with a few hours. The DLVO calculations for both of these cases indicated that if the adsorbed amount in PBS remained the same as in water, they should be stable regardless of the screening effect of the raised ionic strength. It appears likely, then, that the polymer is desorbing from the magnetite on exposure to PBS.

One possible explanation for this is that some component of the PBS preferentially adsorbs to the magnetite, displacing the polymer. Although ordinarily polymers are quite difficult to desorb since the entire chain must be detached at once to free it, in this case the number of attachment points is quite low for those polymers with stability issues (only 3 COO^- groups per molecule for either the 7kPEO-3COOH or the urethane pentablock as compared to 14-32 amine groups for the PEI-containing polymers). The

longer time required for sufficient desorption to trigger instability in the pentablock copolymer may be explained by the shell of hydrophobic PPO surrounding the urethane anchor block. This would provide a diffusive barrier to the ionic medium.

Several authors have measured IEP for monovalent electrolytes under various conditions. In $NaClO_4$ at several concentrations, the IEP was at approximately pH 6.[83] In several concentration of $NaNO_3$, it was measured as 6.3.[84] In several concentrations of NaCl, it was 7.9.[85] These are all indifferent electrolytes.

The working pH of the buffer (7.4) is very close to the measured IEP of magnetite in water (~6.2) as shown in Figure 6-16. The next charge on magnetite is close to zero, and adsorption of ions from PBS could make a large difference in the surface charge. This would be consistent with a study by Heimstra and Riemsdijk on a similar iron oxide, goerthite.[86] In this work, the isoelectric point of goerthite shifted downward about 4 pH units as the phosphate ion concentration increased from 1.5 to 5.7 mmol/L in a background concentration of 0.01M $NaNO_3$.

The carboxylic acid units may also influence the IEP. A 2006 study by Illes et al. found that the IEP of magnetite decreased with addition of humic acid (in a background solution of 0.002 mol/L NaCl).[87] With no humic acid, the IEP was around 8. At 0.09 mmol humic acid per gram of magnetite, the IEP dropped to about 4.3. At 0.14 mm/g humic acid, the IEP was about 3.3. At higher concentration of humic acid, the charge was always negative.

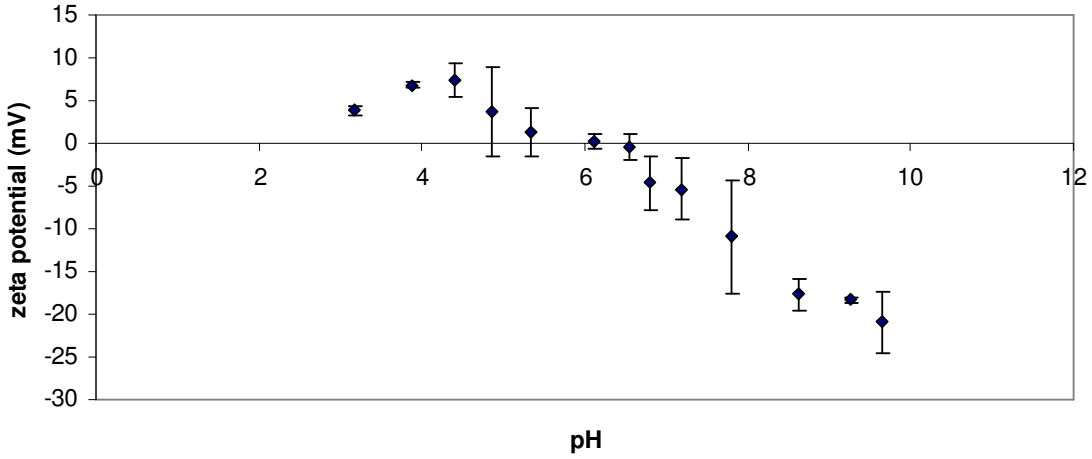

Figure 6-16. Titration of magnetite in water with 0.1M H_2SO_4 under a nitrogen purge.

6.5.4 Self-diffusion of water in a PEO brush

One further application of the corona volume fraction profile is in predicting how readily water molecules may penetrate through the corona. This is important since one of the potential applications of these complexes is as NMR contrast agents. In order for the complexes to be useful, the polymer shells must be permeable to water. T_2 weighting is good for imaging fluids, and extra fluid is often present in the case of an injury or cancerous lesion.[88] SPIONS are of great potential usefulness as they are T_2 agents. T_2 agents do not require as close of an interaction with water as T_1 agents.[88] T_1 shortening is dependent on direct contact between the protons to be relaxed and the magnetic contrast agent; therefore, adding a stabilizing or encapsulating material to the complex decreases relaxivity.[27] In general, decreasing the distance between the water molecules and the contrast agent increases relaxivity, as does increasing the speed with which relaxed water exchanges with bulk water.[89] T_2 imaging, on the other hand, is much less sensitive to distance. T_2 shortening works due to the effect of the paramagnetic material on the magnetic field. For instance, a T_2 agent coated in liposomes is more effective than the same agent without the liposomes because of T_2 clustering in the liposome.[27]

One relevant measure of water permeability is the self-diffusion coefficient of water in a PEO brush. The self-diffusion of water varies with concentration of PEO in a PEO-water

solution. The volume fraction of PEO in the corona was previously described in Eq. 5-22.

Borodin et al. used molecular dynamics simulations to model the self-diffusion coefficient of water in solutions of a 12-repeat unit oligomeric PEO at various concentrations between 17.0 and 99.9 wt%.[90] By fitting a simple polynomial curve to their data as shown in Figure 6-17, a relationship between the self-diffusion coefficient of water, D_w, with units of m^2/s and the weight fraction of PEO, w_p was obtained. This is:

$$D_w = 3.4e^{-8}w_p^5 - 9.6e^{-8}w_p^4 + 1.0e^{-7}w_p^3 - 4.1e^{-8}w_p^2 - 1.3e^{-9}w_p + 5.0e^{-9}$$

Eq. 6-36

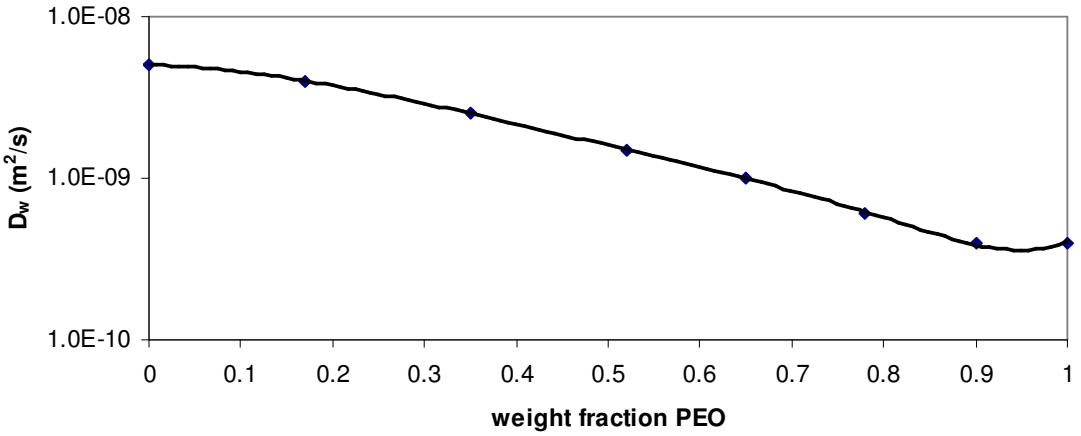

Figure 6-17. Simple polynomial fit relating the self-diffusion coefficient of water and the weight fraction of PEO. Data is from Borodin et al.[90]

The volume fraction of PEO may be converted to the weight fraction of PEO as such:

$$w_{PEO} = \frac{\rho_{PEO} A \left(\frac{r}{a_s}\right)^{1/\nu} r^{-3}}{\left(\rho_{PEO} - \rho_{H_2O}\right) A \left(\frac{r}{a_s}\right)^{1/\nu} r^{-3} + \rho_{H_2O}}$$

Eq. 6-37

Substituting Eq. 6-37 into Eq. 6-36 results in an expression for $D_w(r)$. One consideration for comparison of magnetite-polymer complexes is the maximum value of

$D_w(r)$, which occurs at the attachment point and is either $D_w(R_c)$ or $D_w(R_c+t_a)$ depending on whether an anchor layer is present.

Table 6-5. Estimated diffusion parameters in the complexes.

Sample	t_a (nm)	PEO brush thickness (nm)	Diffusion parameters at $r = R_c+t_a$ (base of brush)		
			w_{PEO}	D_w[a] (m^2/s)	X_{bound}[b]
Urethane pentablock	2.3	7.2	0.57	1.3e-9	>0.95
3kPEO-0.6kPEI(b) (m=1)	1.1	7.8	0.80	5.5e-10	>0.98
3kPEO-0.6kPEI(b) (m=2)	0.7	8.4	0.89	3.8e-10	>0.99
5kPEO-1.4KPEI(l)	1.4	9.9	0.52	1.5e09	>0.90
7kPEO-3COOH	0	13.0	0.72	7.7e-10	>0.96

[a]The self-diffusion coefficient for water, D_w, was determined using Eq. 6-36. [b]The bound fraction of water, X_{bound} was estimated from Figure 1 in a study by Borodin et al.[90]

Another way to consider this is in terms of an average diffusion coefficient, D_{AV} over the entire corona shell. This has the form:

$$D_{AV} = \int_{R^*}^{R_m} D_w(r) 2\pi r dr$$

Eq. 6-38

In which R^* represents either R_c or R_c+t_a as appropriate.

6.6 Conclusions

In this chapter, the adsorption of several block copolymers on magnetite nanoparticles and subsequent stabilization in water and phosphate buffered saline was examined. The Vagberg model for a star polymer was extended for application to nanoparticles with an adsorbed polymer chain consisting of a flat anchor block and an extended corona block. The star polymer model is applicable in this case because the size of the core particle is of a size similar to the extended brush length. In this regime, the effect of curvature on brush extension is very pronounced. The predicted sizes were compared hydrodynamic sizes of the complexes measured by dynamic light scattering. Good agreement was found between the predicted and measured sizes.

In addition, an extended DLVO theory including steric potential based on a model compatible with star polymers was used to predict colloidal stability of these complexes in water and PBS. According to the prediction, all of the complexes were expected to be

stable in both water and PBS, despite electrostatic screening from the higher ionic strength. This is because the amount of polymer adsorbed on the particles should have been sufficient for steric interactions to cause stabilization. However, the experimental observation was that although all of the complexes were stable in water, two aggregated in PBS. The urethane pentablock aggregated overnight, and the 7kPEO-3COOH polymer aggregated almost immediately. A likely cause of this is that the polymers desorbed in the presence of PBS, which has a pH close to that of magnetite. The two polymers have the same number of COO^- groups per chain, however, the pentablock has a hydrophobic PO layer which likely slowed the desorption.

The volume fraction of PEO segments in the core for these complexes was also described using Vagberg's approach. This is significant both for understanding of colloidal stability and also for predicting which complexes will be useful for their proposed application as NMR contrast agents. In order to function well, water must be able to reach the magnetite. As the volume fraction increases, the self-diffusion coefficient decreases.

6.7 References

1. Ogden, A.L. and Lewis, J.A., Effect of nonadsorbed polymer on the stability of weakly flocculated suspensions. *Langmuir*, **1996**. 12(14): p. 3413-3424.

2. SenGupta, A.K. and Papadopoulos, K.D., Stability of concentrated colloids: The controlling parameters. *Journal of Colloid and Interface Science*, **1998**. 203(2): p. 345-353.

3. Napper, D.H., Polymeric Stabilization of Colloidal Dispersions. **1983**, London: Academic Press.

4. Fleer, G.J., et al., Polymers at Interfaces. **1993**, London: Chapman & Hall.

5. Kabanov, A.V. and Alakhov, V., Pluronic (R) block copolymers in drug delivery: From micellar nanocontainers to biological response modifiers. *Critical Reviews in Therapeutic Drug Carrier Systems*, **2002**. 19(1): p. 1-72.

6. Kabanov, A.V., Batrakova, E.V., and Alakhov, V., Pluronic block copolymers as novel polymer therapeutics for drug and gene delivery. *Journal of Controlled Release*, **2002**. 82: p. 189-212.

7. Batrakova, E.V., et al., Effect of Pluronic P85 on ATPase Activity of Drug Efflux Transporters. *Pharmaceutical Research*, **2004**. 21(12): p. 2226-2233.

8. Nakayama, M. and Okano, T., Intelligent thermoresponsive polymeric micelles for targeted drug delivery. *Journal of Drug Delivery Science and Technology*, **2006**. 16(1): p. 35-44.

9. Rangel-Yagui, C.O., Pessoa, A., and Tavares, L.C., Micellar solubilization of drugs. *Journal of Pharmacy and Pharmaceutical Sciences*, **2005**. 8(2): p. 147-163.

10. Torchilin, V.P., Block copolymer micelles as a solution for drug delivery problems. *Expert Opinion on Therapeutic Patents*, **2005**. 15(1): p. 63-75.

11. Kabanov, A.V., Batrakova, E.V., and Miller, D.W., Pluronic((R)) block copolymers as modulators of drug efflux transporter activity in the blood-brain barrier. *Advanced Drug Delivery Reviews*, **2003**. 55(1): p. 151-164.

12. Lavasanifar, A., Samuel, J., and Kwon, G.S., Poly(ethylene oxide)-block-poly(L-amino acid) micelles for drug delivery. *Advanced Drug Delivery Reviews*, **2002**. 54(2): p. 169-190.

13. Rosler, A., Vandermeulen, G.W.M., and Klok, H.A., Advanced drug delivery devices via self-assembly of amphiphilic block copolymers. *Advanced Drug Delivery Reviews*, **2001**. 53(1): p. 95-108.

14. Park, T.G., Jeong, J.H., and Kim, S.W., Current status of polymeric gene delivery systems. *Advanced Drug Delivery Reviews*, **2006**. 58(4): p. 467-486.

15. Gebhart, C.L., et al., Design and Formulation of Polyplexes Based on Pluronic-Polyethyleneimine Conjugates for Gene Transfer. *Bioconjugate Chemistry*, **2002**. 13: p. 913-944.

16. Gupta, A.K. and Gupta, M., Synthesis and surface engineering of iron oxide nanoparticles for biomedical applications. *Biomaterials*, **2005**. 26(18): p. 3995-4021.

17. Cheng, F.Y., et al., Characterization of aqueous dispersions of Fe3O4 nanoparticles and their biomedical applications. *Biomaterials*, **2005**. 26(7): p. 729-738.

18. hihIto, A., et al., Medical application of functionalized magnetic nanoparticles. *Journal of Bioscience and Bioengineering*, **2005**. 100(1): p. 1-11.

19. Neuberger, T., et al., Superparamagnetic nanoparticles for biomedical applications: Possibilities and limitations of a new drug delivery system. *Journal of Magnetism and Magnetic Materials*, **2005**. 293(1): p. 483-496.

20. Wassel, R.A., et al., Dispersion of super paramagnetic iron oxide nanoparticles in poly(D,L-lactide-co-glycolide) microparticles. *Colloids and Surfaces a-Physicochemical and Engineering Aspects*, **2007**. 292(2-3): p. 125-130.

21. Schulze, K., et al., Uptake and biocompatibility of functionalized poly(vinylalcohol) coated superparamagnetic maghemite nanoparticles by synoviocytes in vitro. *Journal of Nanoscience and Nanotechnology*, **2006**. 6(9-10): p. 2829-2840.

22. Lee, H., et al., Antibiofouling polymer-coated superparamagnetic iron oxide nanoparticles as potential magnetic resonance contrast agents for in vivo cancer imaging. *Journal of the American Chemical Society*, **2006**. 128(22): p. 7383-7389.

23. Leuschner, C., et al., LHRH-conjugated magnetic iron oxide nanoparticles for detection of breast cancer metastases. *Breast Cancer Research and Treatment*, **2006**. 99(2): p. 163-176.

24. Petri-Fink, A., et al., Development of functionalized superparamagnetic iron oxide nanoparticles for interaction with human cancer cells. *Biomaterials*, **2005**. 26(15): p. 2685-2694.

25. Kim, D.K., et al., Characterization and MRI study of surfactant-coated superparamagnetic nanoparticles administered into the rat brain. *Journal of Magnetism and Magnetic Materials*, **2001**. 225(1-2): p. 256-261.

26. Stark, D.D., et al., Superparamagnetic Iron-Oxide - Clinical-Application as a Contrast Agent for Mr Imaging of the Liver. *Radiology*, **1988**. 168(2): p. 297-301.

27. Okuhata, Y., Delivery of diagnostic agents for magnetic resonance imaging. *Advanced Drug Delivery Reviews*, **1999**. 37(1-3): p. 121-137.

28. Vert, M. and Domurado, D., Poly(ethylene glycol): Protein-repulsive or albumin-compatible? *Journal of Biomaterials Science - Polymer Edition*, **2000**. 11(12): p. 1307-1317.

29. Milner, S.T., Polymer Brushes. *Science*, **1991**. 251(4996): p. 905-914.

30. Russel, W.B., Saville, D.A., and Schowalter, W.R., Colloidal Dispersions. **1989**, Cambridge: Cambridge University Press.

31. Ploehn, H.J. and Russel, W.B., Interactions Between Colloidal Particles and Soluble Polymers. *Advances in Chemical Engineering*, **1990**. 15: p. 137-228.

32. Alexander, S., *Journal of Physics (Paris)*, **1977**. 38: p. 977.

33. Alexander, S., *Journal of Physics (Paris)*, **1977**. 38: p. 983.

34. de Gennes, P.G., Conformations of Polymers Attached to an Interface. *Macromolecules*, **1980**. 13: p. 1069-1075.

35. Cantor, R., Nonionic Diblock Copolymers as Surfactants between Immiscible Solvents. *Macromolecules*, **1981**. 14: p. 1186-1193.

36. Milner, S.T., Witten, T.A., and Cates, M.E., Theory of the Grafted Polymer Brush. *Macromolecules*, **1988**. 21(8): p. 2610-2619.

37. Dolan, A.K. and Edwards, S.F., Theory of the stabilization of colloids by adsorbed polymer. *Proceedings of the Royal Society of London Series A-Mathematical and Physical Sciences*, **1974**. 337: p. 509-516.

38. Cosgrove, T., et al., Configuration of Terminally Attached Chains at the Solid Solvent Interface - Self-Consistent Field-Theory and a Monte-Carlo Model. *Macromolecules*, **1987**. 20(7): p. 1692-1696.

39. Daoud, M. and Cotton, J.P., Star shaped polymers: a model for the conformation and its concentration dependence. *Journal de Physique*, **1982**. 43: p. 531-538.

40. Marques, C., Joanny, J.F., and Leibler, L., Adsorption of Block Copolymers in Selective Solvents. *Macromolecules*, **1988**. 21(4): p. 1051-1059.

41. Dan, N. and Tirrell, M., Self-Assembly of Block-Copolymers with a Strongly Charged and a Hydrophobic Block in a Selective, Polar-Solvent - Micelles and Adsorbed Layers. *Macromolecules*, **1993**. 26(16): p. 4310-4315.

42. Biver, C., et al., Neutral and Charged Polymer Brushes: A Model Unifying Curvature Effects from Micelles to Flat Surfaces. *Macromolecules*, **1997**. 30: p. 1787-1792.

43. Halperin, A., Polymeric Micelles - a Star Model. *Macromolecules*, **1987**. 20(11): p. 2943-2946.

44. Doliveira, J.M.R., et al., Chains Anchored onto Convex Spherical Surfaces - Modification of the Daoud and Cotton Model. *Macromolecules*, **1995**. 28(13): p. 4750-4752.

45. Vagberg, L.J.M., Cogan, K.A., and Gast, A.P., Light-Scattering Study of Starlike Polymeric Micelles. *Macromolecules*, **1991**. 24(7): p. 1670-1677.

46. Farinha, J.P.S., et al., Structure in tethered chains: Polymeric micelles and chains anchored on polystyrene latex spheres. *Langmuir*, **1998**. 14(9): p. 2291-2296.

47. Hedden, R.C. and Bauer, B.J., Structure and dimensions of PAMAM/PEG dendrimer-star polymers. *Macromolecules*, **2003**. 36(6): p. 1829-1835.

48. Roovers, J., et al., Regular Star Polymers with 64 and 128 Arms - Models for Polymeric Micelles. *Macromolecules*, **1993**. 26(16): p. 4324-4331.

49. Johnsson, M., Hansson, P., and Edwards, K., Spherical micelles and other self-assembled structures in dilute aqueous mixtures of poly(ethylene glycol) lipids. *Journal of Physical Chemistry B*, **2001**. 105(35): p. 8420-8430.

50. Lee, A.S., et al., Characterizing the structure of pH dependent polyelectrolyte block copolymer micelles. *Macromolecules*, **1999**. 32(13): p. 4302-4310.

51. Ducker, W.A., Senden, T.J., and Pashley, R.M., Measurement of Forces in Liquids Using a Force Microscope. *Langmuir*, **1992**. 8(7): p. 1831-1836.

52. Israelachvili, J., Intermolecular and Surface Forces. 2nd ed. **1991**, London: Academic Press.

53. Vlassopoulos, D., et al., Multiarm star polymers dynamics. *Journal of Physics-Condensed Matter*, **2001**. 13(41): p. R855-R876.

54. Vlassopoulos, D., Colloidal star polymers: Models for studying dynamically arrested states in soft matter. *Journal of Polymer Science Part B-Polymer Physics*, **2004**. 42(16): p. 2931-2941.

55. Semenov, A.N., et al., Dynamic structure of interacting spherical polymer brushes. *Langmuir*, **1999**. 15(2): p. 358-368.

56. Seghrouchni, R., et al., Controlling the dynamics of soft spheres: From polymeric to colloidal behavior. *Europhysics Letters*, **1998**. 42(3): p. 271-276.

57. Vlassopoulos, D., et al., Ordering and dynamics of soft spheres in melt and solution. *Faraday Discussions*, **1999**: p. 225-235.

58. Lin, E.K. and Gast, A.P., Self consistent field calculations of interactions between chains tethered to spherical interfaces. *Macromolecules*, **1996**. 29(1): p. 390-397.

59. Witten, T.A. and Pincus, P.A., Colloid Stabilization by Long Grafted Polymers. *Macromolecules*, **1986**. 19(10): p. 2509-2513.

60. Likos, C.N., et al., Star polymers viewed as ultrasoft colloidal particles. *Physical Review Letters*, **1998**. 80(20): p. 4450-4453.

61. Jusufi, A., Watzlawek, M., and Lowen, H., Effective interaction between star polymers. *Macromolecules*, **1999**. 32(13): p. 4470-4473.

62. Likos, C.N., Soft matter with soft particles. *Soft Matter*, **2006**. 2(6): p. 478-498.

63. Pinna, N., et al., Magnetite nanocrystals: Nonaqueous synthesis, characterization, and solubility. *Chemistry of Materials*, **2005**. 17(11): p. 3044-3049.

64. Finsy, R., Particle Sizing by Quasi-Elastic Light-Scattering. *Advances in Colloid and Interface Science*, **1994**. 52: p. 79-143.

65. Provencher, S.W., A Contrstrained Regularization Method for Inverting Data Represented by Linear Algebraic or Integral Equations. *Computer Physics Communications*, **1982**. 27: p. 213-227.

66. Provencher, S.W., CONTIN: A General PurposeConstrained Regularization Program for Inverting Noisy Linear Algebraic and Integral Equations. *Computer Physics Communications*, **1982**. 27: p. 229-242.

67. Tanford, C., Physical Chemistry of Macromolecules. **1962**, New York: John Wiley and Sons.

68. Hunter, R.J., Zeta Potential in Colloid Science. **1981**, London: Academic Press.

69. Devanand, K. and Selser, J.C., Asymptotic-Behavior and Long-Range Interactions in Aqueous-Solutions of Poly(Ethylene Oxide). *Macromolecules*, **1991**. 24(22): p. 5943-5947.

70. FitzGerald, P.A., Davey, T.W., and Warr, G.G., Micellar structure in gemini nonionic surfactants from small-angle neutron scattering. *Langmuir*, **2005**. 21(16): p. 7121-7128.

71. Batchelor, F.R.S., Wunsch, C., and Rice, J., Ferrohydrodynamics. **1985**, Cambridge: Cambridge University Press.

72. Plaza, R.C., et al., Stability of dispersions of colloidal nickel ferrite spheres. *Journal of Colloid and Interface Science*, **2001**. 242(2): p. 306-313.

73. Sverjensky, D.A. and Sahai, N., Theoretical prediction of single-site enthalpies of surface protonation for oxides and silicates in water. *Geochimica Et Cosmochimica Acta*, **1998**. 62(23-24): p. 3703-3716.

74. Israelachvili, J., Intermolecular and Surface Forces. 2nd ed. **1992**, London: Academic Press.

75. Huang, Z.B., Tang, F.Q., and Zhang, L., Morphology control and texture of Fe3O4 nanoparticle-coated polystyrene microspheres by ethylene glycol in forced hydrolysis reaction. *Thin Solid Films*, **2005**. 471(1-2): p. 105-112.

76. Bevan, M.A. and Scales, P.J., Solvent quality dependent interactions and phase behavior of polystyrene particles with physisorbed PEO-PPO-PEO. *Langmuir*, **2002**. 18(5): p. 1474-1484.

77. Croll, S., DLVO theory applied to TiO2 pigments and other materials in latex paints. *Progress in Organic Coatings*, **2002**. 44: p. 131-146.

78. Tadmor, R. and Klein, J., Additional Attraction Between Surfactant-Coated Surfaces. *Journal of Colloid and Interface Science*, **2002**. 247: p. 321-326.

79. Prieve, D.C. and Russel, W.B., Simplified Predictions of Hamaker Constants from Lifshitz Theory. *Journal of Colloid and Interface Science*, **1988**. 125(1): p. 1-13.

80. Ashcroft, N.W. and Mermin, N.D., Solid State Physics. **1976**, Fort Worth: Harcourt Brace College Publishers.

81. Beer, F.P. and Johnston, R.J., Vector Mechanics for Engineers: Statics. **1990**, New York: McGraw Hill.

82. Nolan, S.L., et al., Light scattering study on the effect of polymer composition on the structural properties of PEO-PPO-PEO micelles. *Journal of Colloid and Interface Science*, **1997**. 191(2): p. 291-302.

83. Sun, Z.X., et al., Surface characteristics of magnetite in aqueous suspension. *Journal of Colloid and Interface Science*, **1998**. 197(1): p. 151-159.

84. Viota, J.L., et al., Stabilization of magnetorheological suspensions by polyacrylic acid polymers. *Journal of Colloid and Interface Science*, **2005**. 284(2): p. 527-541.

85. Illes, E. and Tombacz, E., The role of variable surface charge and surface complexation in the adsorption of humic acid on magnetite. *Colloids and Surfaces a-Physicochemical and Engineering Aspects*, **2003**. 230(1-3): p. 99-109.

86. Hiemstra, T. and VanRiemsdijk, W.H., A surface structural approach to ion adsorption: The charge distribution (CD) model. *Journal of Colloid and Interface Science*, **1996**. 179(2): p. 488-508.

87. Illes, E. and Tombacz, E., The effect of humic acid adsorption on pH-dependent surface charging and aggregation of magnetite nanoparticles. *Journal of Colloid and Interface Science*, **2006**. 295(1): p. 115-123.

88. Mornet, S., et al., Magnetic nanoparticle design for medical diagnosis and therapy. *Journal of Materials Chemistry*, **2004**. 14(14): p. 2161-2175.

89. Caravan, P., Strategies for increasing the sensitivity of gadolinium based MRI contrast agents. *Chemical Society Reviews*, **2006**. 35(6): p. 512-523.

90. Borodin, O., Bedrov, D., and Smith, G.D., Concentration dependence of water dynamics in poly(ethylene oxide)/water solutions from molecular dynamics simulations. *Journal of Physical Chemistry B*, **2002**. 106(20): p. 5194-5199.

7 EDC-Mediated Crosslinking of Copolymer Micelles

7.1 Abstract

Novel triblock copolymers consisting of two PEO blocks separated by a carboxylic acid-containing urethane center block have been crosslinked by a carbodiimide-mediated amide crosslinking reaction with ethylenediamine. Prior to this, it was determined that addition of dichloromethane, which is a good solvent for the polymers but has very limited water-miscibility, caused the micelles to swell. It was discovered that although the crosslinking scheme did not work on the micelles in aqueous solution alone, addition of this cosolvent to swell the cores allowed the reaction to proceed. The resulting crosslinked micelles were very similar in size to free micelles in water, and the sizes were stable over a wide range of pH conditions. These crosslinked micelles were intended for use as drug carrying vehicles for slow release. To that end, separate attempts were made to encapsulate two drugs, cisplatin and lidocaine. The inability to do so at several conditions may be the result of insufficient free volume and/or carboxylic acid groups in the crosslinked core.

7.2 Keywords

block copolymer; micelle; crosslink; EDC; lidocaine; cisplatin; swelling

7.3 Introduction

The use of polymers for drug delivery[1-11] and gene delivery[12, 13] has been examined by many investigators. PEO-containing polymers are especially desirable, as PEO does not trigger an immune response in vivo and can also make other foreign materials less visible to the immune system. [14] Micelles are also particularly promising, as they self-assemble into a structure capable of encapsulating a drug, whether water-soluble or not.

A primary drawback to using micelles for drug delivery is that upon dilution in the body they can disassemble. One approach to avoiding this problem is by crosslinking the micelles for use as a drug delivery vehicle.

Several groups have approached this by crosslinking the core of a micelle. For instance, Iijima et al. prepared a poly(ethylene glycol)-*b*-polylactide polymer with a methacryloyl group on one end which was then polymerized to crosslink the core.[15] This created a particle that was stable in temperatures to 60°C, sodium dodecyl sulfate concentrations to 20 mg/mL, and in some organic solvents. These micelles were then used to solubilize paclitaxel.[16] Guo et al. made micelles of polystyrene-*b*-poly(2-cinnamoylethyl methacrylate) in organic solvents and used UV irradiation to crosslink the PCEMA core.[17]

The shell of a core-shell micelle may also be crosslinked. Zhang et al. demonstrated crosslinking of poly(ϵ-caprolactone)-b-poly(acrylic acid) micelles by a condensation reaction to form a crosslinked shell.[18] Weaver et al. created a so-called ionically crosslinked shell by addition of an anionic diblock copolymer to a micellar triblock copolymer.[19]

Carbodiimides are commonly used to mediate formation of an amide crosslink between carboxylate and amine groups via condensation.[20] One such carbodiimide is 1-ethyl-3-(3-dimethylaminopropyl)carbodiimide hydrochloride (EDC). It is water-soluble, as are the byproducts of the reaction, making isolation of the product relatively easy. These characteristics have been exploited for crosslinking micelles. For instance, several papers by Bronich et al. [21, 22] describe the use of a divalent metal ion (Ca^{2+}) to cause PEO-b-PMA polymers to form into micelles, despite the charges on the polymethacrylate block. These micelles were subsequently cross-linked to form a drug delivery vessel for cisplatin.

This chapter discusses use of EDC-mediated crosslinking of two unique triblock copolymers comprised of two PEO tail blocks and a central carboxylic acid-containing

urethane block. Due to the partial hydrophobicity of the center block, these copolymers have the potential ability to perform as drug delivery vehicles with the unique advantage that they self-assemble without needing a divalent counter-ion. In addition, they are in a size range (20-30 nm hydrodynamic diameter) that is advantageous for in vivo use. They are large enough (>10 nm) to avoid premature removal via extravasation and renal clearance, yet still small enough (10-70 nm) to pass into capillaries.[1] The general approach is illustrated in Figure 2-6.

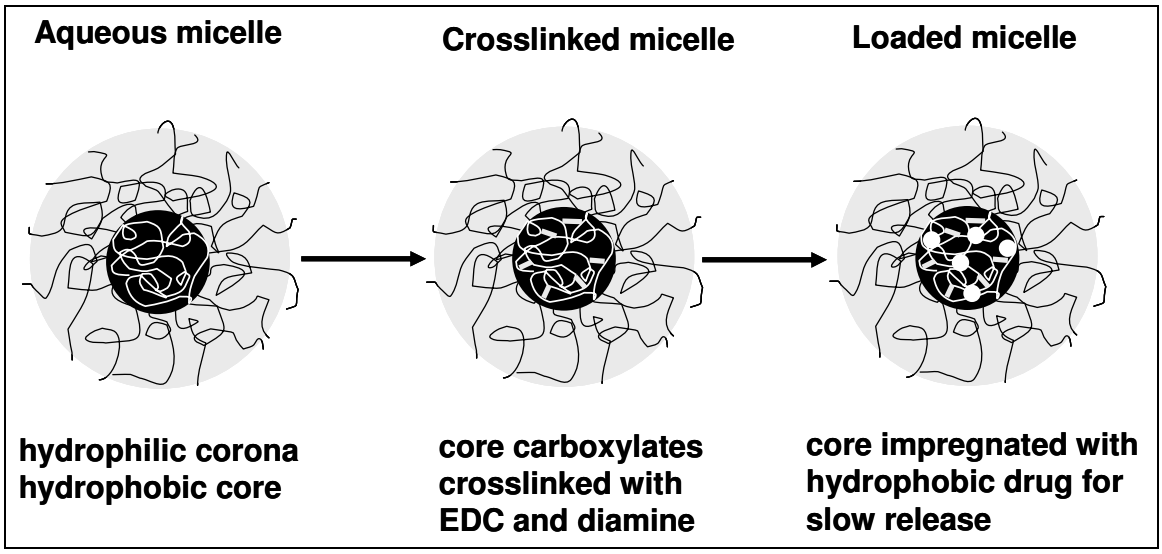

Figure 7-1. Approach to creating crosslinked micelles for drug delivery

7.4 Materials and Methods

7.4.1 Chemicals

All solutions were prepared with deionized water from a NANOpure II ion exchanger (Barnstead) having a resistance above 17 MΩ·cm. ACS reagent grade sodium chloride (Fisher) was used as received to adjust background ionic strength. All pH adjustments were made using sodium hydroxide and hydrochloric acid (Fisher) as received and after dilution with deionized water. N-hydroxysuccinimide (NHS), N-hydroxysulfosuccinimide (sulfo-NHS), 1-ethyl-3-(3-dimethylaminopropyl)carbodiimide hydrochloride (EDC) were purchased from Pierce and used without further purification. NHS and ethylenediamine were stored in the refrigerator with a desiccant. EDC was stored in the freezer with a desiccant. The reactants were allowed to warm to room

temperature before opening the bottles in order to avoid excess condensation of atmospheric water. Ethylenediamine, cisplatin, and lidocaine were purchased from Sigma-Aldrich and used as received.

The polymer used for these experiments were described in a previous paper.[23] The structure of this class of triblocks is shown in Figure 7-2 and the properties are summarized in Table 5-1.

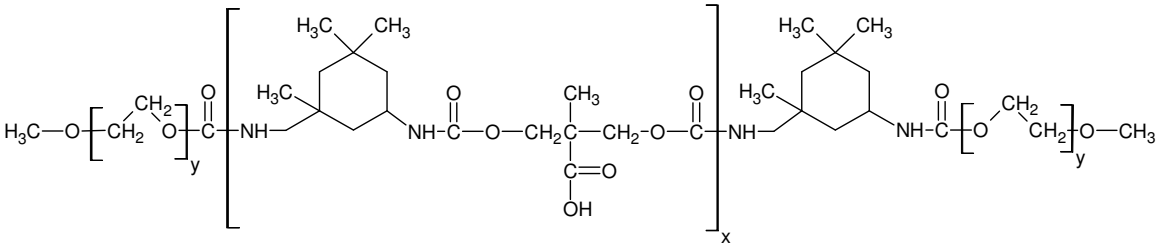

Figure 7-2. Structure of a representative triblock copolymer with PEO tail block and polyurethane center block containing carboxylic acid groups.

Table 7-1. Properties of triblock copolymers.

Copolymer	M_n[a]	DP center [b]	DP tail	Mass fraction PEO
1930-3.1-1930	5160	3.1	44	0.75
4850-4.7-4850	11540	4.7	110	0.84

[a]PEO tail block M_n from ^{1}H NMR. [b]Average number of COOH in the polyurethane center block from ^{13}C NMR.[23]

Phosphate buffered saline (PBS) was prepared using chemicals purchased from Fisher and used as received with deionized water. The proportions are as follows for a 1 L batch.

Table 7-2. Recipe for 1L of PBS.

Material	Amount (g)	Concentration (mM)
Sodium chloride	7.13	122
Sodium bicarbonate	2.10	25
HEPES	2.38	10
Glucose	1.80	10
Potassium chloride	0.22	3
Calcium chloride	0.21	1.4
Magnesium sulfate	0.30	1.2
Potassium sulfate monobasic	0.09	0.4

7.4.2 Separation Methods

When filtration of solutions prior to light scattering is indicated in this chapter, it was accomplished using Anotop alumina syringe filters (Whatman) with a 100 nm pore size. Dialysis steps were performed using either a Spectra/Por 6 membrane made of regenerated cellulose with a MWCO of 25,000 or a Pierce Slide-a-Lyzer dialysis cartridge with a MWCO of 20,000. These are equivalent to a pore size of approximately 4-5 nm which was deemed to be of an appropriate size to prevent escape of crosslinked micelles. The switch was made to the cartridges for their faster dialysis rate and greater ease of sample recovery.

For the step in which the free cisplatin was eliminated from the solution containing cisplatin-loaded micelles, Whatman Anodisc 25 filters were used with a pore size of 20 nm. In this case, the sample was passed gently through the Anodisc filter in a filter casing, then the filter was placed in a known volume of water and sonicated for 30 seconds using a Branson 2200 sonicating bath in order to recover the crosslinked micelles. It had been previously demonstrated that this sonicating step did not damage the alumina filters.

For the corresponding step for the tests involving lidocaine, the separation was accomplished using a Centriplus YM-100 ultrafiltration tube. The samples were spun at 5,000 rpm for 30 minutes in a Marathon 21K (Fisher Scientific). Recovery of the sample was again accomplished by adding a known volume of water and sonicating gently to recover the crosslinked micelles. The switch to these ultrafiltration tubes was motivated by greater ease of handling and sample recovery as compared to the disc filter.

7.4.3 Crosslinking Reaction

EDC is frequently used in bioconjugation reactions for formation of an amide link between a carboxylate and amine group. It has the advantage of being a water-phase reaction that may be performed at physiological pH. The major drawback in working with EDC is that it has a limited effective life in water. In order to crosslink two

caroboxylate groups, a diamine such as ethylene diamine may be used. The crosslinking scheme is shown below in Figure 2-7.

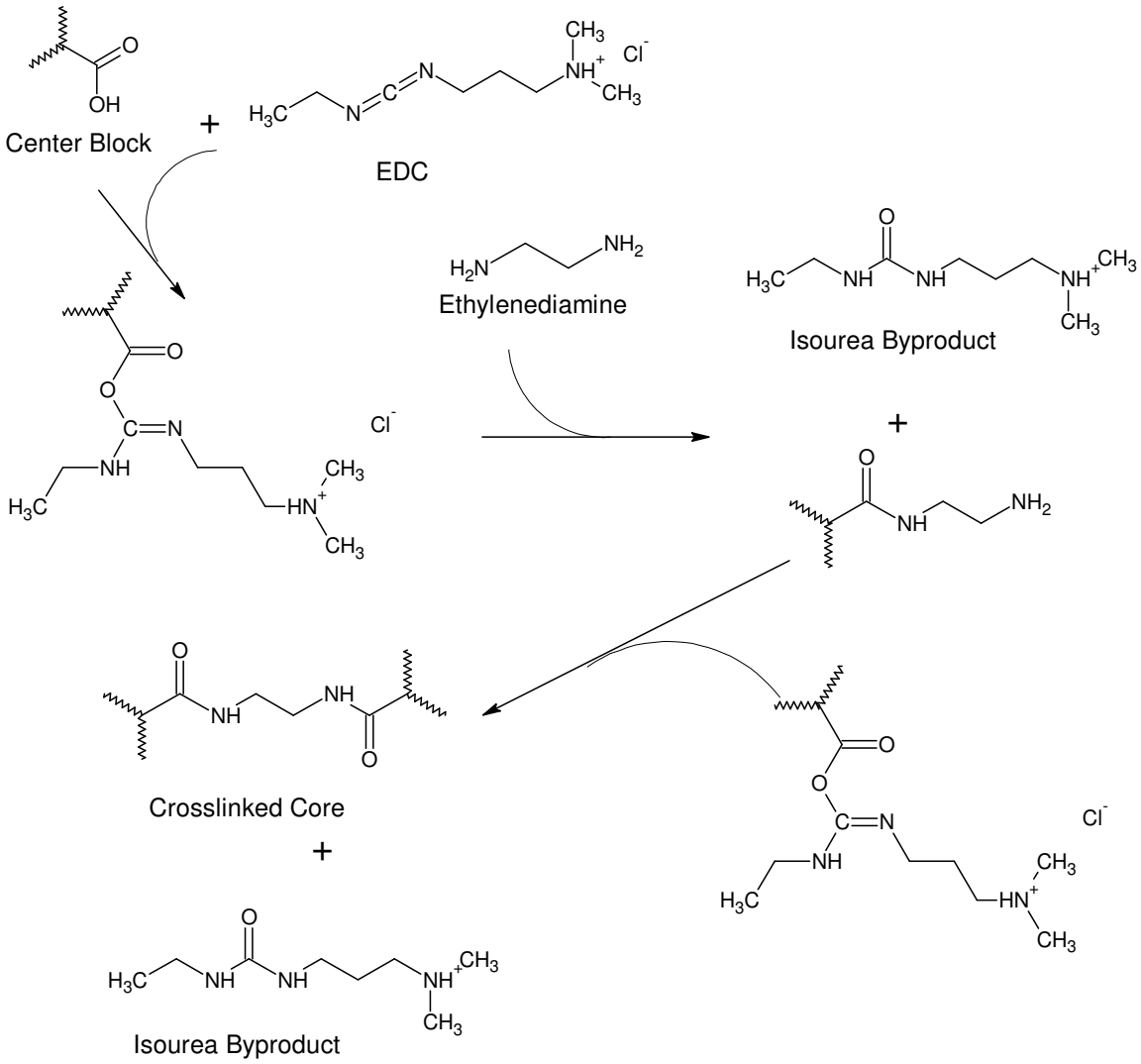

Figure 7-3. EDC crosslinking reaction of two carboxylate groups with ethylenediamine. An isourea by-product is formed.

One common approach to increase the efficiency of the reaction in Figure 2-7 is the addition of either NHS or sulfo-NHS prior to crosslinking. Either may be reacted with a carboxylate in the presence of a carbodiimide such as EDC to form an ester which is more stable than the reactive intermediate in the previous scheme. This may be subsequently reacted with a diamine as before. The choice of NHS or sulfo-NHS alters the property of the resulting ester. NHS decreases water solubility, whereas sulfo-NHS

maintains or increases water-solubility of the species. The scheme using NHS is summarized in Figure 2-8.

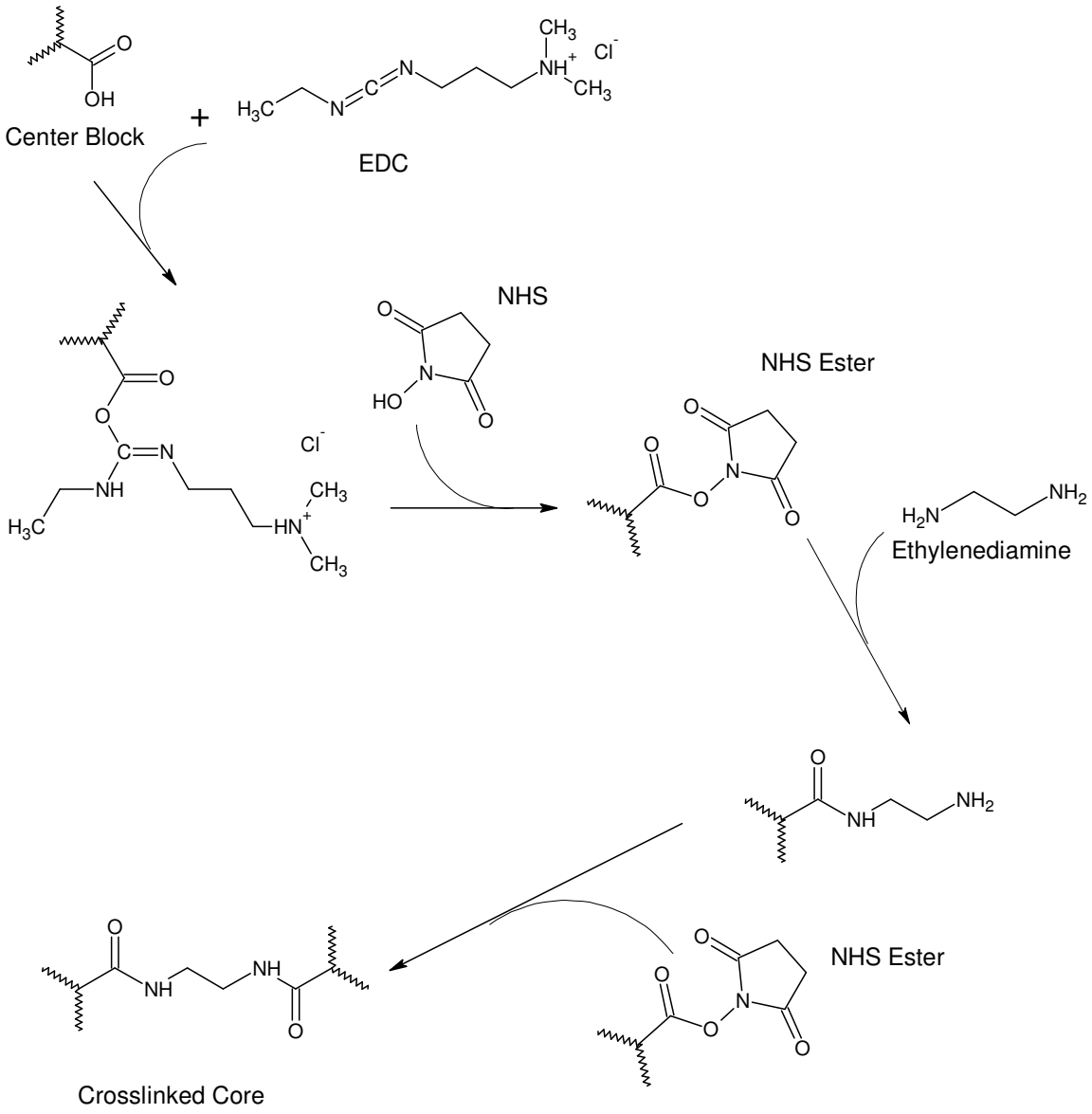

Figure 7-4. EDC-mediated crosslinking reaction of two carboxylate groups with ethylenediamine in the presence of NHS.

One additional change was made to the typical crosslinking procedure, which was the addition of dichloromethane (DCM) as a cosolvent to swell the core of the micelle prior to the crosslinking reaction. This is discussed in detail in a later section.

7.4.4 Cisplatin Encapsulation

Prior to drug loading, the crosslinked particles were dialyzed against PBS and water as described previously. Addition of cisplatin to the crosslinked micelles was accomplished by adding a 1 mg/mL solution of cisplatin in water to a solution of micelles (at pH 9) and incubating for 48 hours at 37°C. These conditions were optimized by Bontha et al.[22] Cisplatin was added in a molar amount equal to half the number of moles of COOH present in the polymer prior to crosslinking. The theoretical amount of excess cisplatin depended on the degree of crosslinking.

Several studies[24-26] have indicated that cisplatin in solution may be degraded over time if exposed to light. The primary degradation product is trichloroammineplatinate(II) (TCAP) due to a substitution of the chloride ligands with water. Zieske et al.[24] found that degradation was less than 1% per week when stored in the dark. Macka et al.[25] demonstrated that the most decomposition occurred at a wavelength of 300, but that some occurred at wavelengths below 500 nm. Sonication at 53°C also caused conversion of cisplatin on the order of several percent after two hours.[25] To minimize degradation, fresh solutions were prepared for each test and sonication to remove the micelles from the filter was kept to a very short period (2 minutes).

7.4.5 Platinum assay for determination of cisplatin concentration

The concentration of platinum in solution was determined using an assay with o-phenylene diamine, which is a ligand for Pt(II). This procedure[27] was adapted from work by Golla and Ayres on Pt(IV).[28] The reaction is shown below:

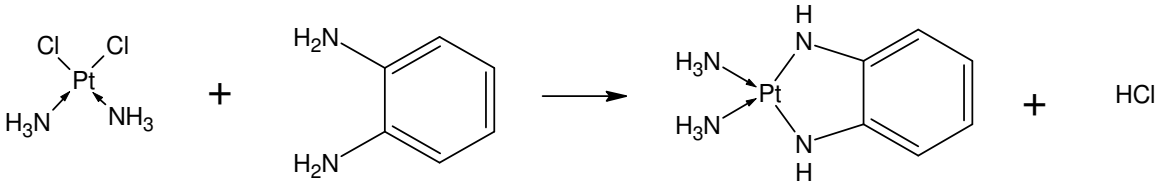

Figure 7-5. Reaction of ODPE with cisplatin to form a light blue solution.

For each of the measurements, 0.6 mL of the platinum-containing solution was combined with 0.6 mL of a 1.2 mg/mL solution of o-phenylene diamine in dimethylformamide (ODPE) in a small plastic tube. These tubes were then placed in a stirred water bath at

100°C for 10 minutes. The resulting blue color was measured using a Milton Roy Spectronic 1201 spectrophotometer at a wavelength of 703 nm. A series of standards was used to calibrate this, as shown in the figure below. This calibration was repeated after a period of one week to demonstrate stability of cisplatin in water.

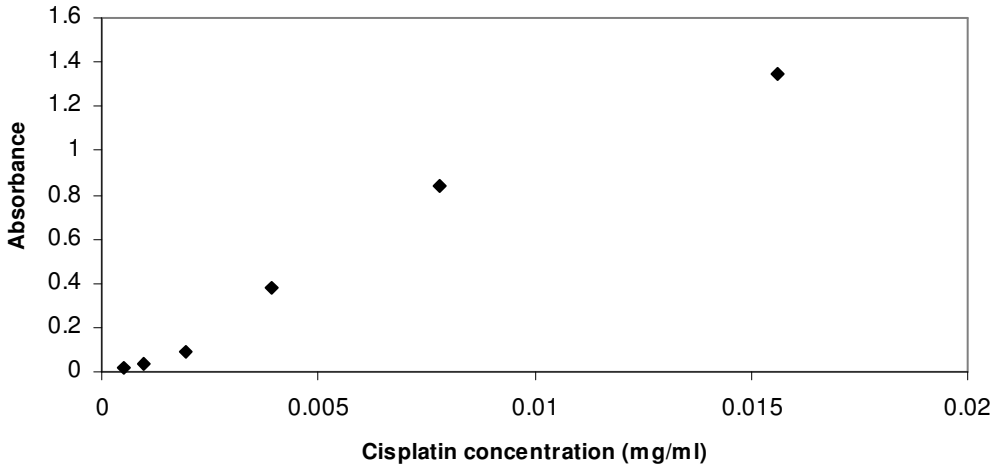

Figure 7-6. Calibration curve for platinum assay. Cisplatin concentration is in the original solution.

7.4.6 Absorbance for determination of lidocaine concentration

The concentration of lidocaine was measured by simple absorbance at 260 nm using a Milton Roy Spectronic 1201 spectrophotometer. This wavelength was chosen as it was in the middle of the range where absorbance was linear with concentration in the concentration range of interest.

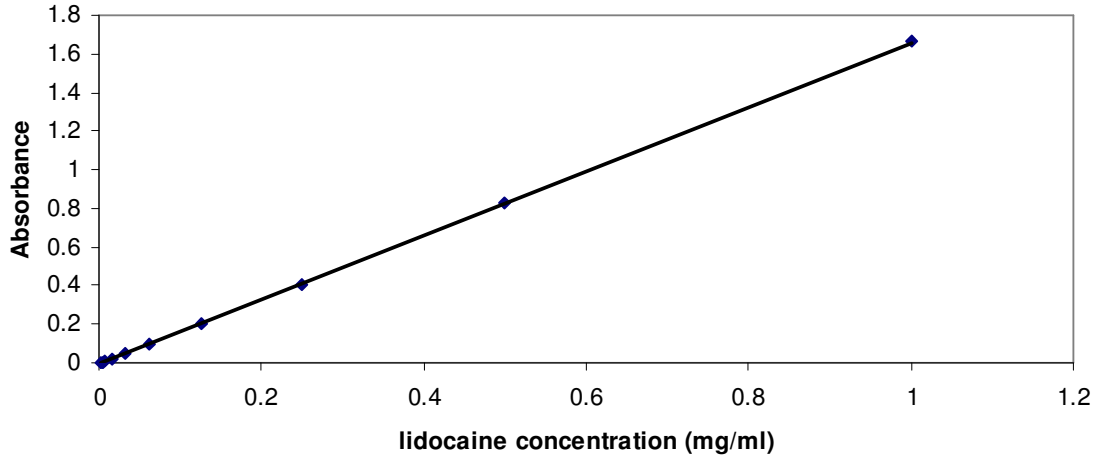

Figure 7-7. Calibration curve for lidocaine in water.

7.4.7 Dynamic Light Scattering

Dynamic light scattering (DLS) is performed by measuring the variation of intensity with time. This is also known as quasi-elastic light scattering and is used to study particle diffusion.[29] Hydrodynamic radii were determined using the Stokes-Einstein relationship, in which k is Boltzmann's constant, T is the temperature, η is the solvent viscosity, D_o is the diffusion coefficient, and R_H is the hydrodynamic radius:

$$R_H = \frac{kT}{6\pi\eta D_o}$$

Eq. 7-1

Dynamic light scattering (DLS) was performed using a Malvern NanoZS operating at a fixed angle of 173° and a wavelength of 633 nm. The DLS data from this device was analyzed using Distribution Technology Software (DTS). This uses an algorithm based on CONTIN, which is a program designed for inversion of noisy equations via a constrained regularization algorithm as described by Provencher.[30, 31] The basic features of CONTIN are prior knowledge (in this case, that the sizes must be non-negative) and parsimony (the solution with the fewest and smoothest peaks is probably best). The CGS-3 also employs a multiple-tau correlation technique, meaning that the Δt value between channels varies; this reduces error due to noise.[32] A detailed description of DLS techniques used is provided in Chapter 3.

7.4.8 Zeta Potential

The zeta potential was measured using a Malvern NanoZS operating at a fixed angle of 173° and a wavelength of 633 nm. The choice of a model for zeta potential depends on the thickness of the Debye layer, κ^{-1}, relative to the radius of the particle, a.

The Debye length, κ^{-1}, can be calculated from the ionic strength, I, in an aqueous system as:

$$\kappa^{-1} = \left(\frac{0.304}{\sqrt{I}} \right)$$

Eq. 7-2

The ionic strength for a solution may be calculated as:

$$I = \frac{\sum c_i z_i^2}{2}$$

Eq. 7-3

in which c_i and z_i are the concentration and charge on a given ion in solution.

For the case of a thin double layer with κa large, the zeta potential, ζ, is related to the electrophoretic mobility, μ, by the viscosity, η, and the electric permittivity of the medium, ε, according to the Smoluchowski approximation:

$$u = \frac{\zeta \varepsilon}{\eta}$$

Eq. 7-4

7.5 Results and Discussion

7.5.1 Self-Assembly in the Absence of Crosslinking

As has been discussed at length in earlier chapters, these triblock copolymers self-assemble in solution at low pH to form micelles. Between pH 6 and 8, these micelles dissociate. An initial attempt was made to form pH-stable micelles by addition of ionic molecules with multiple charges based on the hypothesis that doing so might attract two core chains to the same molecule. This was attempted with both $CaCl_2$ and cisplatin; however, neither was sufficient to stabilize the micelle at physiological pH (7.4). It is likely that even if this had worked, the micelles so formed would have been impractical for drug delivery, as the dilution in vivo would likely have been below the critical micelle concentration.

7.5.2 Crosslinking Reactions

Based on work by Bronich et al.[21] these copolymers were thought to be good candidates for crosslinking with an EDC reaction. The 4845-5-4845 copolymer was chosen for this work in light of its relatively large number of carboxylic acid sites per chain, which seemed likely to make a light crosslinking easier. The 1930-3-1930 copolymer was chosen for its higher aggregation number (32 as compared to 16), which was thought might make the reaction easier by providing more reaction sites in the core.

EDC is labile in the presence of water, and as such, care was taken to store it in cold, dry conditions. Additionally, the bottle was warmed to room temperature in a sealed bag containing desiccant prior to use to avoid excess contact with atmospheric water via condensation. Nonetheless, the useful life of EDC once dissolved in water for the reaction is limited. Therefore, a fresh solution was prepared immediately before addition during each reaction.

The EDC crosslinking reaction is active between pH 4 and at least 7.5 with the optimal range being 4.7-6.[20] The crosslinking reactions were performed without adjustment to the pH of the dissolved polymer, which is about 4.5. In water, the highest pH where micelles are present is less than 6. The objective was to have as many charged COO^- ions available as possible without disrupting the micellization. Trial and error revealed that if the pH was raised to just below the critical point, precipitation of the polymer occurred. It is believed that this is because in this unbuffered system, the crosslinking reagents raised the pH, causing the micelles to disassemble before the crosslinking could take place. The natural pH of the polymer solution provided a sufficient margin of safety.

Initial attempts were made using the reaction scheme outlined in Figure 2-7 with only EDC and diamine. There was great difficulty in getting the reaction to proceed. There are several possible causes for this, including a difficulty in getting the reagents into the core of the micelle, particularly in the timeframe in which the EDC was viable. Two

steps were taken to facilitate the reaction: addition of a cosolvent to swell the micelle core and addition of NHS to improve intermediate stability.

Dichloromethane (DCM) is known to be a good solvent for the copolymer.[23] The reagents in the crosslinking reaction (NHS, EDC, and ethylenediamine) are also soluble in DCM. This solvent was used to swell the core of the micelle as illustrated in Figure 7-8.

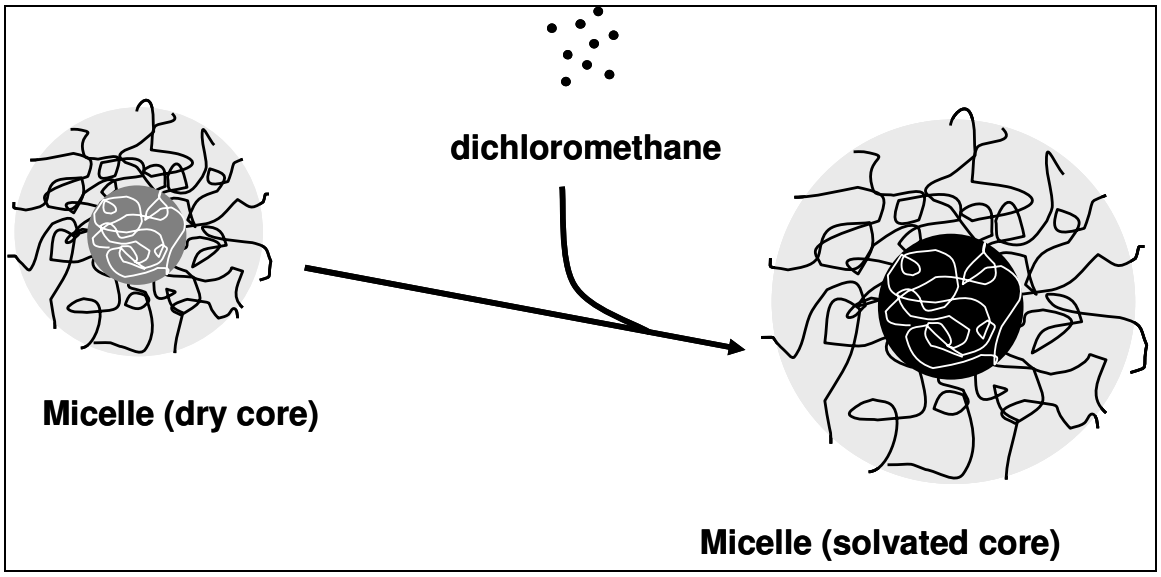

Figure 7-8. Dichloromethane swelling the micelle core.

To examine the effect of solvent addition, various conditions of polymer to DCM and DCM to water ratios were examined. As may be seen in the figure below, increasing the DCM to water ratio at a given polymer to DCM ratio increased the size of the micelle. Since the core of the micelle in a water-only solution is mostly dry based on prior SANS work described in an earlier chapter, it was surmised that the solvent was being incorporated into the core to result in an increase in diameter.

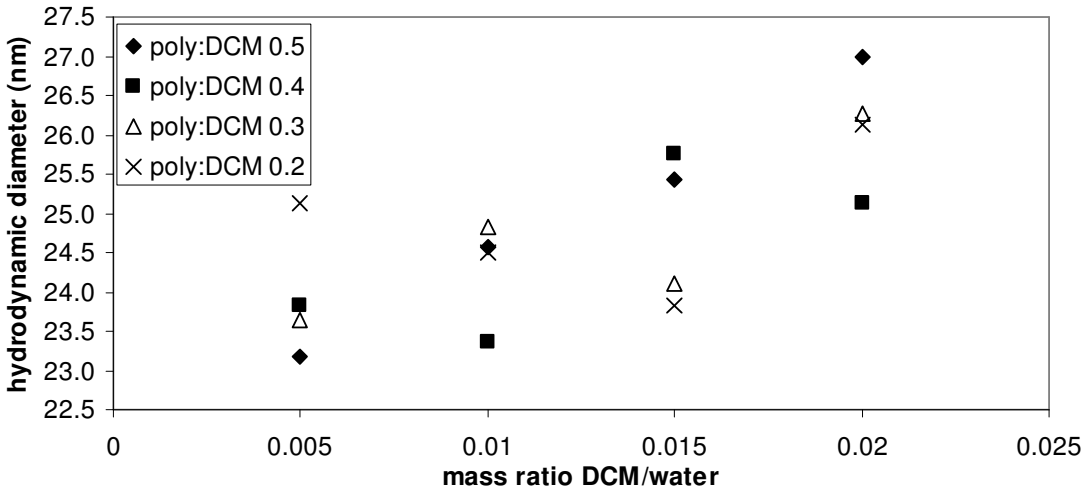

Figure 7-9. Effect of DCM to water ratio on micelle size for 4845-5-4845 polymer in water. The hydrodynamic diameter is an intensity-weighted average.

It was hypothesized that greater swelling of the micelles would lead to a larger volume of the final crosslinked micelle core and, hence, a larger drug-loading capacity. To explore this, increasing amounts of DCM were added to solution containing 7.5 mg/mL 4845-5-4845 polymer in 5 mL of water. The size of the micelle was monitored using DLS. After each DCM addition, the sample was sonicated for several minutes until the solution cleared, then the DLS measurement was made immediately. This worked up to a DCM concentration of 0.06 mg/mg water, after which it became necessary to allow the sealed sample to sit until the turbidity disappeared. The DLS measurement was made as soon as the sample cleared. After making the final (highest DCM concentration measurement), the sample was allowed to sit undisturbed for several days, after which time the size returned to approximately what it had been for the 0.06 mg/mg water sample. This is illustrated in Figure 7-10 The solubility of DCM in water is 13 mg/g, so more than four times the amount that would be soluble in water had been added.[33]

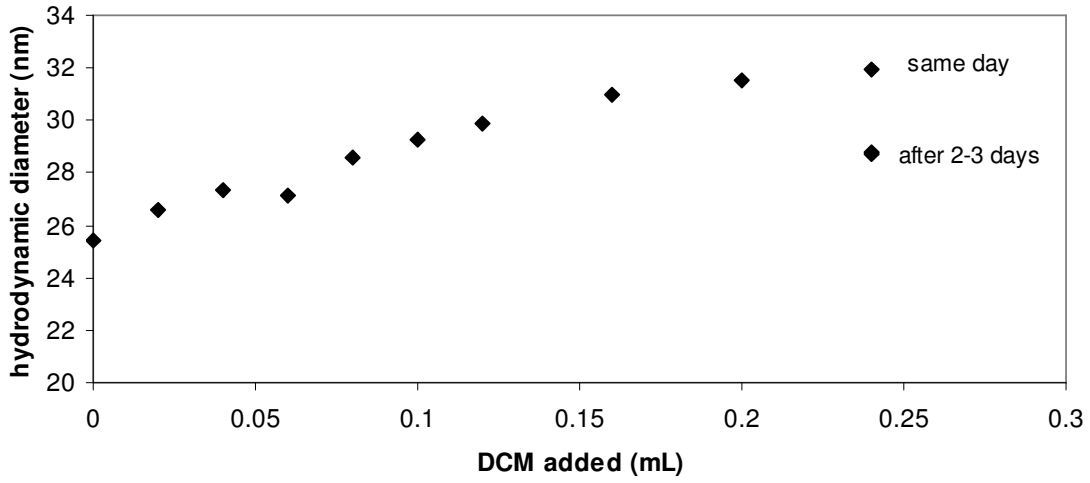

Figure 7-10. Hydrodynamic diameter of a 4845-5-4845 micelle swollen with DCM. The pH was approximately 4 and the initial concentration of polymer was 7.5 mg/mL.

Since it was desirable to swell the micelles as much as possible to create more volume, a simple method was devised for addition of DCM. The polymer was dissolved in water and allowed to equilibrate overnight. DCM was then added in excess (apparent because sonication did not eliminate turbidity). After sonication, the sample was allowed to sit with a loosened cap until the solution cleared, indicating that all remaining DCM was contained in the micelles cores which are too small relative to the wavelength of visible light to cause cloudiness. Immediately after this, the reaction procedure was begun.

NHS increases the stability of the ester intermediate in water. The stability of the NHS-ester is pH-dependent, with a half-life of several hours at physiological pH but only a few minutes at pH 8.6.[34-36] For the NHS-containing reaction, a NHS was added to a concentration of 5 mM. EDC and ethylenediamine were added according to the number of carboxylic acid groups available in the micelle cores based on the mass of polymer added, the molecular weight of the polymer, and the number of COOH groups per chain.

NHS and EDC were added to the swollen polymer solution, then sonicated for two minutes. This mixture was allowed to stir for 15 minutes, then ethylenediamine was added. After sonication for another two minutes, the solution was allowed to stir overnight at room temperature.

The crosslinked micelles were dialyzed against a minimum of 10 changes of solvent, each of about 40X the sample volume over the course of several days. The first three changes were against PBS to screen any electrostatic attraction between excess reagents and the micelle core; the subsequent changes were against water.

Varying degrees of crosslinking were attempted. The desired outcome was a lightly linked core which would still allow site for charged drugs to penetrate. A range of crosslinking degrees was attempted including 20, 50, 70, 90, 100, and 500% of the stoichiometric amount of EDC and ethylenediamine (NHS was always in excess). The stoichiometric ratio was defined as:

$$ratio = \frac{mol\ EDC}{mol\ carboxylic\ acid}$$

Eq. 7-5

and the molar amount of ethylenediamine was always half that of the EDC to account for the two amine groups.

Successful crosslinking, i.e. a micelle that remained at high pH, was only achieved with the stoichiometry at 100% or higher. This is not to say that 100% crosslinking was achieved, as this represents only a maximum amount possible.

The variation in the diameter of the crosslinked micelles with pH was measured using DLS as shown in Figure 7-10. It was expected that if a light crosslinking were achieved, the micelles would increase in size with increasing pH as the charge increased on the remaining un-crosslinked COO^- groups in the core, resulting in a repulsion and expansion in the core. However, none of the crosslinked micelles exhibited a size dependence on pH. This suggests that the micelles may be highly crosslinked, or at least that the charged groups have reacted in some way.

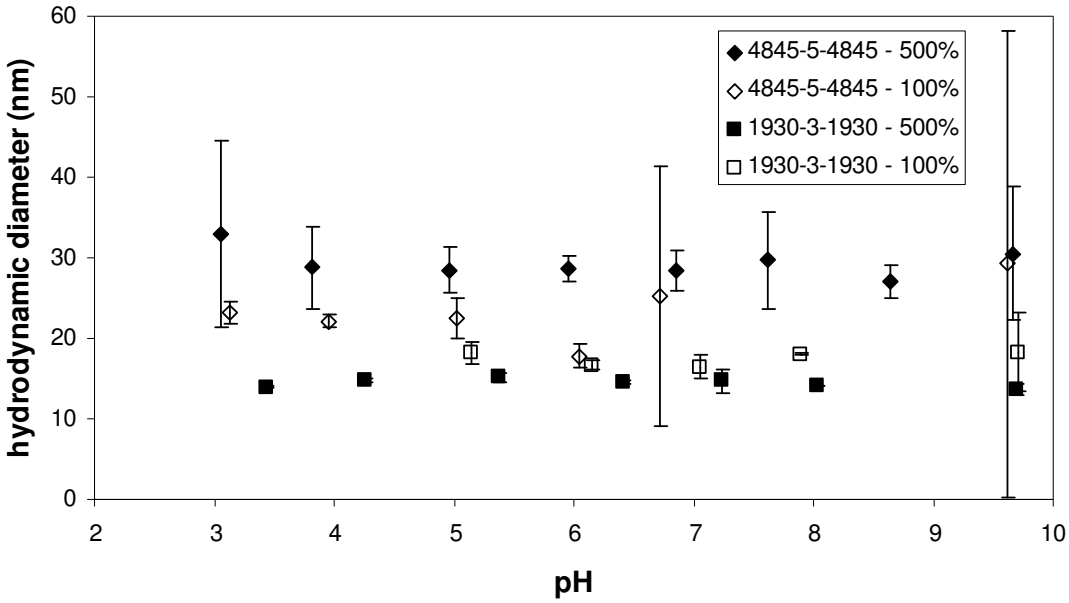

Figure 7-11. pH dependence of hydrodynamic diameter for crosslinked micelles. No electrolyte beyond the titrants was added. The error bars are one standard deviation.

The zeta potentials of the crosslinked micelles were also measured with respect to pH in a titration with 0.1M H_2SO_4 to determine the point of zero charge (PZC). The measured values for PZC were in the range of 3.7-5.1 for the polymers tested as shown in Figure 7-12. The 1930-3-1930 polymer crosslinked at stoichiometric conditions had more charge at high pH than the others. This suggests that some unreacted amine groups remained after dialysis. It is not clear whether these are due to unreacted diamine molecules trapped in the core of the particle after the dialysis or whether these are the result of amine groups which had only reacted on one end. Given both the dialysis procedure and the fact that all of the amine was added at once, the latter is more likely. In order to combat this, one approach might be to add the amine gradually to increase the likelihood of both ends reacting.

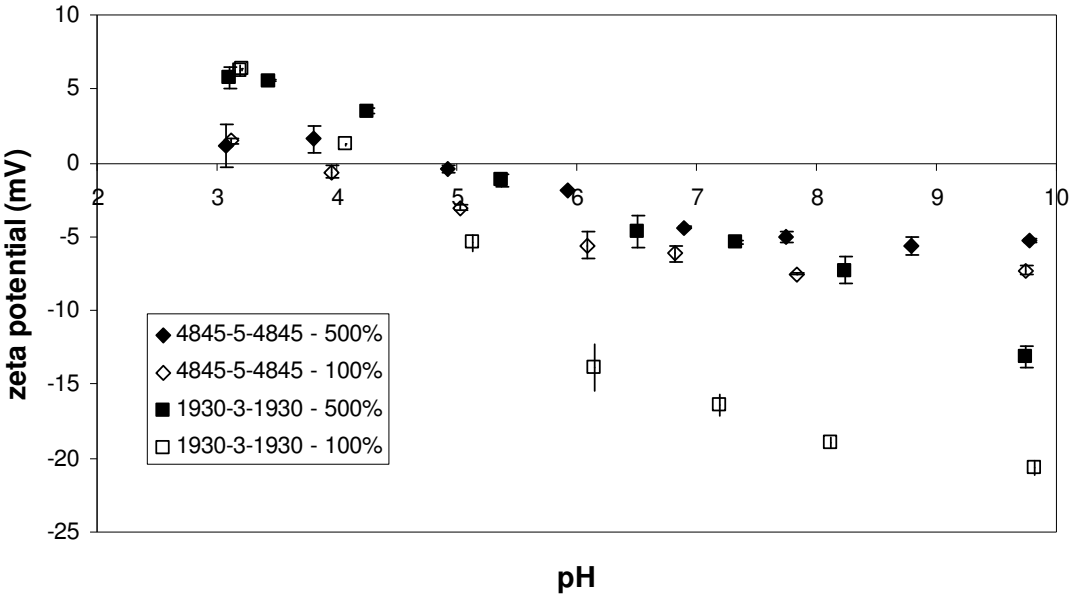

Figure 7-12. Titration of crosslinked micelles with 0.1M H_2SO_4. The error bars are one standard deviation.

7.5.3 Cisplatin encapsulation

Cisplatin was complexed with the micelles by incubation at 37°C for 48 hours. The cisplatin was added in a molar amount equal to half the number of moles of COOH originally present in the polymer. It was anticipated that each cisplatin molecule would be able to bind with two COOH sites. This amount was expected to be an excess, as some of the COOH sites were previously utilized for crosslinking. The pH of the micelle solution was raised to pH 9 prior to addition of cisplatin to maximize available COO^- sites. Provided there is no Cl- background, the exchange of carboxylate ligands for chlorine ligands can proceed.[37]

It has been observed that the presence of chlorine in the system prior to complexation inhibits the interaction, but that after complexation, the addition of NaCl does not cause dissociation.[27] Cisplatin release studies were performed by dialyzing the redispersed micelles against PBS. At each change of the dialyzate, a small portion was retained to measure concentration of cisplatin released. The platinum concentration was measured using the colorimetric assay described previously.

During the first attempt, a curious observation was made. The platinum concentration in the dialyzate rose for several hours, then leveled out and dropped precipitously. As there was no reason to believe that platinum was being removed from the dialyzate, the adequacy of the ODPE and DMF was confirmed by performing another calibration test with known concentrations of cisplatin in water. To rule out degradation of the cisplatin by some component of PBS, a known concentration of cisplatin was dissolved in PBS (from the same stock as the calibration test). This was then divided into vials in four conditions: dark and sealed, dark and open, light and sealed, and light and open. The concentration of cisplatin was measured over a 24 hour period on these four cases. A slight initial drop was observed, but of a much smaller magnitude than observed for the dialyzate. Furthermore, the concentrations remained stable after that initial drop.

It is possible that there is some species left over from the reaction which is perhaps forming an complex with the platinum and thus not being counted. One possibility was leftover unreacted diamine. Since the reactant for the colorimetric test is also a diamine, it seems reasonable that they might be competitive. To test this, identical samples of cisplatin in water were prepared. One was spiked with diamine in a concentration similar to that in the reaction solution. The colorimetric assay revealed an obvious visual difference. The pristine cisplatin solution turned blue, as expected; the one contaminated with diamine turned yellow.

In light of the possible presence of leftover reagents, the purification of the crosslinked micelles before addition of cisplatin was altered. Previously, the solution had been dialyzed against deionized water, as that is the solvent that the micelles would be in for addition of cisplatin. Dialysis was performed against a 40X excess of PBS. The high ionic strength would be expected to screen out electrostatic interactions between the polymer core and the byproducts. In order to monitor this process, samples of the dialyzate were taken at each buffer change. These were then added to a known amount of cisplatin to monitor the presence of an unwanted reactive species by comparing to a control sample containing the same amount of cisplatin in fresh buffer. Over the first few changes, there was a marked increase in the cisplatin reading in the dialyzate indicating

that with each successive dialysis step, less of the unwanted reactive species was present; however, thereafter, no more than 80% of the control amount of cisplatin was registered. It is unclear why the full control amount of cisplatin added was never measured.

In light of the added confusion of the sensitivity of the platinum assay to contamination, it is not clear whether cisplatin was successfully incorporated into the crosslinked micelles.

7.5.4 Lidocaine loading

Lidocaine was chosen as an alternate test drug. It has several advantages over cisplatin. Most notably, it is much safer to handle in the lab, but it also may be readily detected by a simple absorbance measurement. It was expected that lidocaine (Figure 7-13) would be a good candidate for incorporation into the micelle core as it has both a charged amine group and a hydrophobic cyclic structure.

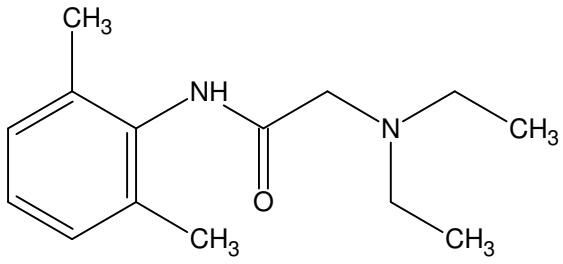

Figure 7-13. Lidocaine was used as a test drug for encorporation into a crosslinked micelle.

Lidocaine and similar compounds are known to move selectively to hydrophobic environments. For instance, Liu et al. used unimolecular micelles (hyperbranched amphiphilic polymers) with a hydrophobic core to entrap lidocaine.[38] Lidocaine so treated had a slower transport across a membrane than free lidocaine. Scherlund et al. solubilized lidocaine and prilocaine in EO-PO-EO and found that the initial release rate was a strong function of pH.[39]

Lidocaine was introduced to aqueous solutions of the four crosslinked micelles described in a previous section at a lidocaine:polymer weight ratio of 1:2, sonicated for one minute, then incubated overnight at 25°C. The samples were subsequently centrifuged through 100,000 MWCO filters. The micelles were eluted from the filter by adding water and

sonicating briefly. The liquid that had passed through the filter was checked by DLS to ensure that the micelles had not gone through. The concentration of lidocaine in this was then measured to determine how much had been taken up by the micelles. Two loading conditions were studied.

The first condition tested was at a pH 6.5 (adjusted with NaOH) and no added salt. The intention was to use electrostatics to drive the attraction between the drug and the crosslinked core. Lidocaine has a pKa of approximately 8,[39] and the micelles had measured values of PZC of 3.7-5.1. Therefore at pH 6.5 it was thought that the negatively charged cores and partially positively charged drug would interact. However, all of the lidocaine passed through the filter during centrifugation. This is counterintuitive, as the zeta potential data indicates that the crosslinked micelles all had a negative charge at pH 6.5

The second condition tested was to be driven by a hydrophobic interaction between the aromatic portion of the lidocaine and the polymer core. To that end, the electrostatics were screened by increasing the ionic strength with 0.15M NaCl at pH 10. In this case also, all of the lidocaine passed through the filter, indicating that none had bound. Hydrophobic interaction was insufficient to attract the lidocaine.

One possible reason for the failure to encapsulate lidocaine at either condition might be that there simply isn't space in the core. Based on earlier unsuccessful attempts to crosslink the core of the micelles without using a cosolvent to expand the micelle, it may be that there isn't sufficient free volume in the core to allow the lidocaine to penetrate. The DCM solvent would have been removed over the course of extensive dialysis prior to introduction of lidocaine. Also, successful crosslinking was only accomplished for those cases with larger amounts of reagents, i.e. 1X or 5X of stoichiometric. In light of that, the core may be too heavily crosslinked to accommodate the addition of the drug molecule.

7.6 Summary

In this chapter, the viability of EDC-mediated crosslinking for carboxylic acid-containing triblock copolymer micelles has been demonstrated. It was found that addition of a cosolvent, dichloromethane, caused the micelles to swell. Dichloromethane readily solubilizes the polymers, but has limited water-miscibility. The addition of this cosolvent allowed crosslinking by improving transport of the reagents (EDC and ethylenediamine) into the core. Two polymers, 1930-3-1930 and 4845-5-4845 have been crosslinked to form micelles that are stable over a broad range of pH conditions. The size of these micelles is not sensitive to pH. This suggests that the micelle cores are heavily crosslinked, as otherwise the increasing charge on the carboxylic acid groups with increased pH would be expected to cause an expansion due to electrostatic repulsion.

Encapsulation of two separate drugs was explored. These were cisplatin, a charged anti-cancer agent, and lidocaine, a charged, hydrophobic analgesic. Cisplatin encapsulation was attempted at a high pH (9) to maximize available COO^- sites in the core. Difficulties in the release study due to interference of reagents with the platinum assay made determination of the outcome difficult. It appeared that most of the cisplatin charged had gone into the micelles, but possible contamination of the platinum assay may have caused a false low reading on concentration of cisplatin in the filtrate. Lidocaine encapsulation was attempted at two conditions, one designed to optimize electrostatic attraction between the core and the drug, the other designed to screen out electrostatic repulsion and allow hydrophobic attraction to play a dominant role. Neither attempt was successful in incorporating the drug into the micelle.

One possible reason for the failure of lidocaine to go into the core of the micelles may be that there was insufficient free volume in the core. In the absence of the cosolvent (dichloromethane), the cores are thought to be mostly dry. A heavily crosslinked core without a swelling cosolvent may not have space to accommodate the lidocaine, which is relatively bulky as compared to cisplatin.

7.7 References

1. Kabanov, A.V. and Alakhov, V., Pluronic (R) block copolymers in drug delivery: From micellar nanocontainers to biological response modifiers. *Critical Reviews in Therapeutic Drug Carrier Systems*, **2002**. 19(1): p. 1-72.

2. Kabanov, A.V., Batrakova, E.V., and Alakhov, V., Pluronic block copolymers as novel polymer therapeutics for drug and gene delivery. *Journal of Controlled Release*, **2002**. 82: p. 189-212.

3. Batrakova, E.V., et al., Effect of Pluronic P85 on ATPase Activity of Drug Efflux Transporters. *Pharmaceutical Research*, **2004**. 21(12): p. 2226-2233.

4. Nakayama, M. and Okano, T., Intelligent thermoresponsive polymeric micelles for targeted drug delivery. *Journal of Drug Delivery Science and Technology*, **2006**. 16(1): p. 35-44.

5. Rangel-Yagui, C.O., Pessoa, A., and Tavares, L.C., Micellar solubilization of drugs. *Journal of Pharmacy and Pharmaceutical Sciences*, **2005**. 8(2): p. 147-163.

6. Torchilin, V.P., Block copolymer micelles as a solution for drug delivery problems. *Expert Opinion on Therapeutic Patents*, **2005**. 15(1): p. 63-75.

7. Kabanov, A.V., Batrakova, E.V., and Miller, D.W., Pluronic((R)) block copolymers as modulators of drug efflux transporter activity in the blood-brain barrier. *Advanced Drug Delivery Reviews*, **2003**. 55(1): p. 151-164.

8. Lavasanifar, A., Samuel, J., and Kwon, G.S., Poly(ethylene oxide)-block-poly(L-amino acid) micelles for drug delivery. *Advanced Drug Delivery Reviews*, **2002**. 54(2): p. 169-190.

9. Rosler, A., Vandermeulen, G.W.M., and Klok, H.A., Advanced drug delivery devices via self-assembly of amphiphilic block copolymers. *Advanced Drug Delivery Reviews*, **2001**. 53(1): p. 95-108.

10. Kwon, G.S. and Kataoka, K., Block-Copolymer Micelles as Long-Circulating Drug Vehicles. *Advanced Drug Delivery Reviews*, **1995**. 16(2-3): p. 295-309.

11. Tobio, M., et al., Stealth PLA-PEG nanoparticles as protein carriers for nasal administration. *Pharmaceutical Research*, **1998**. 15(2): p. 270-275.

12. Park, T.G., Jeong, J.H., and Kim, S.W., Current status of polymeric gene delivery systems. *Advanced Drug Delivery Reviews*, **2006**. 58(4): p. 467-486.

13. Gebhart, C.L., et al., Design and Formulation of Polyplexes Based on Pluronic-Polyethyleneimine Conjugates for Gene Transfer. *Bioconjugate Chemistry*, **2002**. 13: p. 913-944.

14. Vert, M. and Domurado, D., Poly(ethylene glycol): Protein-repulsive or albumin-compatible? *Journal of Biomaterials Science - Polymer Edition*, **2000**. 11(12): p. 1307-1317.

15. Iijima, M., et al., Core-polymerized reactive micelles from heterotelechelic amphiphilic block copolymers. *Macromolecules*, **1999**. 32(4): p. 1140-1146.

16. Kim, J.H., et al., Core-stabilized polymeric micelle as potential drug carrier: Increased solubilization of taxol. *Polymers for Advanced Technologies*, **1999**. 10(11): p. 647-654.

17. Guo, A., Liu, G.J., and Tao, J., Star polymers and nanospheres from cross-linkable diblock copolymers. *Macromolecules*, **1996**. 29(7): p. 2487-2493.

18. Zhang, Q., Remsen, E.E., and Wooley, K.L., Shell cross-linked nanoparticles containing hydrolytically degradable, crystalline core domains. *Journal of the American Chemical Society*, **2000**. 122(15): p. 3642-3651.

19. Weaver, J.V.M., et al., Preparation of shell cross-linked micelles by polyelectrolyte complexation. *Angewandte Chemie-International Edition*, **2004**. 43(11): p. 1389-1392.

20. Hermanson, G.T., Bioconjugate Techniques. **1996**, San Diego: Academic Press.

21. Bronich, T.K., et al., Polymer Micelle with Cross-Linked Ionic Core. *Journal of the American Chemical Society*, **2005**. 127: p. 8236-8237.

22. Bontha, S., Kabanov, A.V., and Bronich, T.K., Polymer micelles with cross-linked ionic cores for delivery of anticancer drugs. *Journal of Controlled Release*, **2006**. 114(2): p. 163-174.

23. Harris, L.A., et al., Magnetite nanoparticle dispersions stabilized with triblock copolymers. *Chemistry of Materials*, **2003**. 15(6): p. 1367-1377.

24. Zieske, P.A., et al., Characterization of cisplatin degradation as affected by pH and light. *American Journal of Hospital Pharmacy*, **1991**. 48: p. 1500-1506.

25. Macka, M., et al., Decomposition of Cisplatin in Aqueous Solutions Containing Chlorides by Ultrasonic Energy and Light. *Journal of Pharmaceutical Sciences*, **1994**. 83(6): p. 815-818.

26. Pujol, M., et al., Kinetics of Cisplatin Photoaquation in Aqueous Solution. *Journal of Chemical Research (S)*, **1991**. 9: p. 258-259.

27. Schechter, B., et al., Cis-platinum(I) Complexes of Carboxylmethyl-Dextran as Potential Antitumor Agents I. Preparation and Characterization. *Cancer Biochemistry and Biophysics*, **1986**. 8: p. 277-287.

28. Golla, E.D. and Ayres, G.H., Spectrophotometric Determination of Platinum with o-Phenylenediamine. *Talanta*, **1973**. 20: p. 199-210.

29. Finsy, R., Particle Sizing by Quasi-Elastic Light-Scattering. *Advances in Colloid and Interface Science*, **1994**. 52: p. 79-143.

30. Provencher, S.W., A Contrstrained Regularization Method for Inverting Data Represented by Linear Algebraic or Integral Equations. *Computer Physics Communications*, **1982**. 27: p. 213-227.

31. Provencher, S.W., CONTIN: A General PurposeConstrained Regularization Program for Inverting Noisy Linear Algebraic and Integral Equations. *Computer Physics Communications*, **1982**. 27: p. 229-242.

32. Peters, R., Noise on photon correlation functions and its effect on data reduction algorithms., in Dynamic Light Scattering: The Method and Some Applications, W. Brown, Editor. **1993**, Clarendon Press: Oxford.

33. Knovel Critical Tables. **2003**; Available from: http://www.knovel.com.

34. Lomant, A.J. and Fairbanks, G., Chemical Probes of Extended Biological Structures - Synthesis and Properties of Cleavable Protein Cross-Linking Reagent [Dithiobis(Succinimidyl-S-35 Propionate). *Journal of Molecular Biology*, **1976**. 104(1): p. 243-261.

35. Staros, J.V., Wright, R.W., and Swingle, D.M., Enhancement by N-Hydroxysulfosuccinimide of Water-Soluble Carbodiimide-Mediated Coupling Reactions. *Analytical Biochemistry*, **1986**. 156(1): p. 220-222.

36. Cuatrecaseas, P. and Parikh, I., Adsorbents for affinity chromatography. Use of N-hydroxysulfosuccinimide esters of agarose. *Biochemistry*, **1972**. 11: p. 2291-2299.

37. Howe-Grant, M.E. and Lippard, S.J., Aqueous Platinum(II) Chemistry; Binding to Biological Molecules, in Metal Ions in Biological Systems, H. Sigel, Editor. **1980**, Marcell Decker: New York. p. 63-125.

38. Liu, H.B., Farrell, S., and Uhrich, K., Drug release characteristics of unimolecular polymeric micelles. *Journal of Controlled Release*, **2000**. 68(2): p. 167-174.

39. Scherlund, M., et al., Thermosetting microemulsions and mixed micellar solutions as drug delivery systems for periodontal anesthesia. *International Journal of Pharmaceutics*, **2000**. 194(1): p. 103-116.

8 Combinatorial Search for Dodecapeptides for Adsorption on Alumina

8.1 Abstract

A thioredoxin random peptide library on *E. coli* was used to search for favorable binding sequences on alumina. Optically isotropic (c-plane) alumina crystals were exposed to the FliTrx™ Random Peptide Display Library, which contained 10^9 dodecapeptides. Loosely bound bacteria were rinsed away; tightly bound bacteria were eluted by shearing. This enrichment process was repeated six times before DNA sequencing. No clear sequence was discovered, indicating that either the primary mechanism for binding was via opposite charges or that insufficient enrichment steps were used. There was a marked preference for neutral or positively charged peptides, which was initially unexpected at pH 7.4, which is below the isoelectric point (IEP) of alumina. However, the phosphate buffer used for growing the bacteria proved to have reversed the charge on the alumina through adsorption. The buffer is necessary for the health of the bacterial library; one future possibility would be the use of a phage display process.

8.2 Keywords

biopanning; alumina; sapphire; adsorption; selectivity; polypeptide; fusion protein

8.3 Introduction

Biopanning techniques have been used in a variety of applications where rapid discovery of optimal sequences is desired. Several groups have devised means of creating peptide libraries.[1-3] The basic premise is that a target (typically an immobilized protein) is exposed to the peptide library, which has been induced to display the polypeptides on the surface of the phage or bacteria. Some polypeptide sequences bind better than either; these remain bound during subsequent rinsing steps. The phages or bacteria having those sequences are then grown to increase their concentration. Ideally, after several rounds of biopanning, a sequence emerges with superior binding ability. This polypeptide may then be isolated and studied further.

Biopanning has also been used to study binding on target inorganic surfaces. In 1992, genetically engineered E. coli were developed that exhibited unique adherence to iron oxide (Fe_3O_4) particles. [4] This was done using a random library inserted into the phage λ receptor. A serial enrichment procedure was used. The iron oxide particles were removed using a magnet, taking the adsorbed bacteria with them. After washing, the iron oxide containing culture was plated, specific colonies were selected, and the procedure was repeated four additional times. After PCR amplification and DNA sequencing, the resulting sequences were compared. In several experiments, the same sequence was identified.

Work has been done by Whaley et al.[5] to develop peptides sequences that selectively bind to semiconductors. Five semi-conductors were studied: GaAs(100), GaAs(111)A, GaAs(111)B, InP(100), and Si(100). Selectivity was found not only for different compounds, but also for different crystallographic faces of GaAs. As is generally done, selection was performed several times, in this case five, to improve selection and reduce the possibility of contamination. The researchers hypothesized that the dodecamers in an extended state were larger than the crystal unit cells, and that as such, the essential sequences were smaller than the full length of the peptide. They subsequently reduced the length of the peptides in the screening library to further isolate the key combinations.

Another application involves use of a polypeptide designed to adsorb with great specificity onto a particularly hazardous metal contaminant in wastewater could be used to remove and recover that metal Some work has been done towards development of specific peptide sequences both with and without combinatorial searching for zinc, [6-9] iron, [4, 6] copper, [6, 9] lead, [6] cerium, [6] nickel, [10] cadmium, [9-11] and mercury. [11, 12]

The objective of this project was to use combinatorial methods to discover an optimal anchor block to be part of a fusion protein for stabilization of alumina particles. The design of the fusion protein is described by Tulpar et al.[13] The combinatorial library employed was the FliTrx™ Random Peptide Display Library from Invitrogen It contains

E. coli bacteria with the capability to display 10^9 dodecapeptides exposed on flagella and constrained by a thioredoxin loop. Due to this forced accessibility, it is possible to select for strongly adsorbing peptide sequences.

8.4 Materials and Methods

8.4.1 Chemicals

The FliTrx™ Random Peptide Display Library was purchased as a kit from Invitrogen (Carlsbad, CA) and used without modification. All solutions were prepared using deionized water from a Labconco Waterpro Plus having a resistance above 17 MΩ·cm, except where the use of bottled sterile water is noted. Plasmid Miniprep kits were purchased from Biorad and used according to the included instructions. Sodium phosphate, potassium phosphate, ammonium chloride, magnesium chloride, sodium hydroxide were purchased from Fisher and used as received. Sodium chloride and ampicillin were purchased from VWR. The ampicillin was filtered with 0.2μm filters also purchased from VWR. Casamino acids, glycerol, and agar were purchased from Sigma and used as received. Glucose, triethanolamine (Tris), ethylenediaminetetracetic acid (EDTA), sodium lauryl sulfate (SDS), phenol chloroform, and ethanol were purchased from vendors and used as received with no further purification.

8.4.2 Substrate

Adsorption experiments were done on crystalline α-alumina (Commercial Crystal Laboratories, Inc. Naples FL). This alumina was cut to the c-face, which is optically isotropic (0001). The root mean surface roughness was measured by N. Nueraji as 1 A using AFM with a cantilever spring constant of 0.26 N/m. This was treated with water plasma to cover the surface with hydroxyl groups and create a hydrophilic surface. The system was purged twice with argon before commencing treatment. The substrate was then placed on a mica slide and treated with water plasma for three minutes at 1.0 Torr and 40-50 watts. This cleaning procedure was done between each round of panning. For transport from the lab containing the plasma chamber to the biochemistry lab, the alumina was immersed in deionized water in a tissue plate and sealed.

Annealing was tried as an alternate method of surface preparation. The sapphire plates were placed in a sample holder that had been previously cleaned with acetone and kimwipes. The furnace was heated to 1450°C over the course of several hours, held at temperature for 14 hours, then left at 400°C until use to prevent organic contamination while waiting. It was then immersed into deionized water, then immediately shifted to IMC media and sealed for transport to the biochemistry lab. Gross surface contamination was found to be a problem, presumably due to other materials having been in the oven previously. Examination by XPS confirmed presence of calcium and sodium. This method was abandoned.

8.4.2.1 10XM9 Salts, 1M $MgCl_2$, and Ampicillin

The 10XM9 salt solution was prepared by combining 30 g sodium phosphate, 15 g monobasic potassium phosphate, 2.5 g sodium chloride, and 5 g of ammonium chloride with deionized water to make 500 mL of solution. This was then adjusted to pH 7.4 with 10 M NaOH. It was autoclaved for 20 minutes at 121°C and stored at room temperature. 1M magnesium chloride solution was prepared by combining 40.7 g of magnesium chloride with 200 mL of deionized water. This was also autoclaved for 20 minutes at 121°C and stored at room temperature. The ampicillin was prepared by passing it through a sterile syringe filter (0.2 μm pore size, VWR).

8.4.2.2 IMC Medium

IMC medium was used for growth of the library prior to induction. The library was ampicillan-resistant. One 1 g of 0.2% of casamino acids was combined with 400 mL of deionized water and autoclaved for 20 minutes at 121°C. To this was then added 40 mL of 10XM9 salt, 0.5 mL of 1 mM $MgCl_2$, and 12.5 mL of 20% glucose. This was stored at 4°C.

8.4.2.3 RM Medium

RM medium was used to grow up larger amounts of the selected plasmids for DNA sequencing. It was prepared by combining 20 g of 2% casamino acids, 10 mL of 100% glycerol, and 890mL of deionized water. This was autoclaved 20 minutes at 121°C.

Subsequently, 100 mL of 10M9 salts, 1mL of 1M MgCl2, and 1 mL of 100 mg/mL ampicillin were added. The medium was stored at 4°C.

8.4.2.4 RMG Plates

RMG plates were used for isolation and growth of colonies of specific clones. 20 g of 2% casamino acids, 15 g of bacteriological agar, and 875 mL of deionized water were combined and autoclaved 20 minutes at 121°C. 100 mL of 10XM9 salts, 25 mL of 20% glucose, and 1 mL of 100 mg/mL ampicillin were mixed in. The mixture was poured into Petri plates and stored at 4°C.

8.4.3 Biopanning

8.4.3.1 Overview

The FliTrx™ Random Peptide Display Library, marketed by Invitrogen, uses *E. Coli* to display a library of peptides. The dodecapeptides are displayed at the ends of flagellar filaments. This system makes use of a thioredoxin loop to constrain the peptide in order that it may best adsorb to the surface.[14] The FliTrx™ system was an innovation by Lu et al.[15] based on previous work to display surface fusion proteins. The technique makes use of a dispension region of the gene for flagellin (fliC) in E. coli. The researchers replaced this section with a sequence coding for thioredoxin (trxA). The intention was to create a strain of bacteria that would display the thioredoxin loop on the surface as part of the flagellae. This is very useful for observing surface interactions. The authors developed a panning method wherein the library was grown in a medium containing casamino acids, glucose, salts, and ampicillin. A sample of sufficient size to ensure that it contained 100 times the diversity of the library was grown in media containing tryptophan in order to induce the growth of fringe-like fimbriae. The authors used protein-antibody interactions as the basis for their study. They coated plates with antibody and added a blocking solution to prevent undesirable interactions before exposing the plate to the culture. They allowed the interaction to occur for one hour. They then washed the plates five times and then used mechanical agitation to shear off the remaining tightly-bound bacteria. This procedure was repeated several times. The resulting elutions from the final selection were plated onto ampicillin-containing plates, and individual colonies were selected. DNA was isolated from each. Three antibodies were studied (HIL8-NR7, HM7/7.7.10,

and C11.5.14). The DNA from each colony was sequenced. For each antibody, a sequence could be identified that typically occurred (with some variations). The researchers performed separate confirmatory tests and concluded that the FliTrx system could be used to determine binding sequences for antibodies.

Three rounds of biopanning were done in total. The first round had problems with the cleaning procedures for the alumina plate. The second round appeared to have biological contamination. The results reported herein are from the third and final round. The biopanning steps were repeated a total of 6 times in the third round. The flowchart below outlines in broad view the procedure followed for the third round of biopanning.

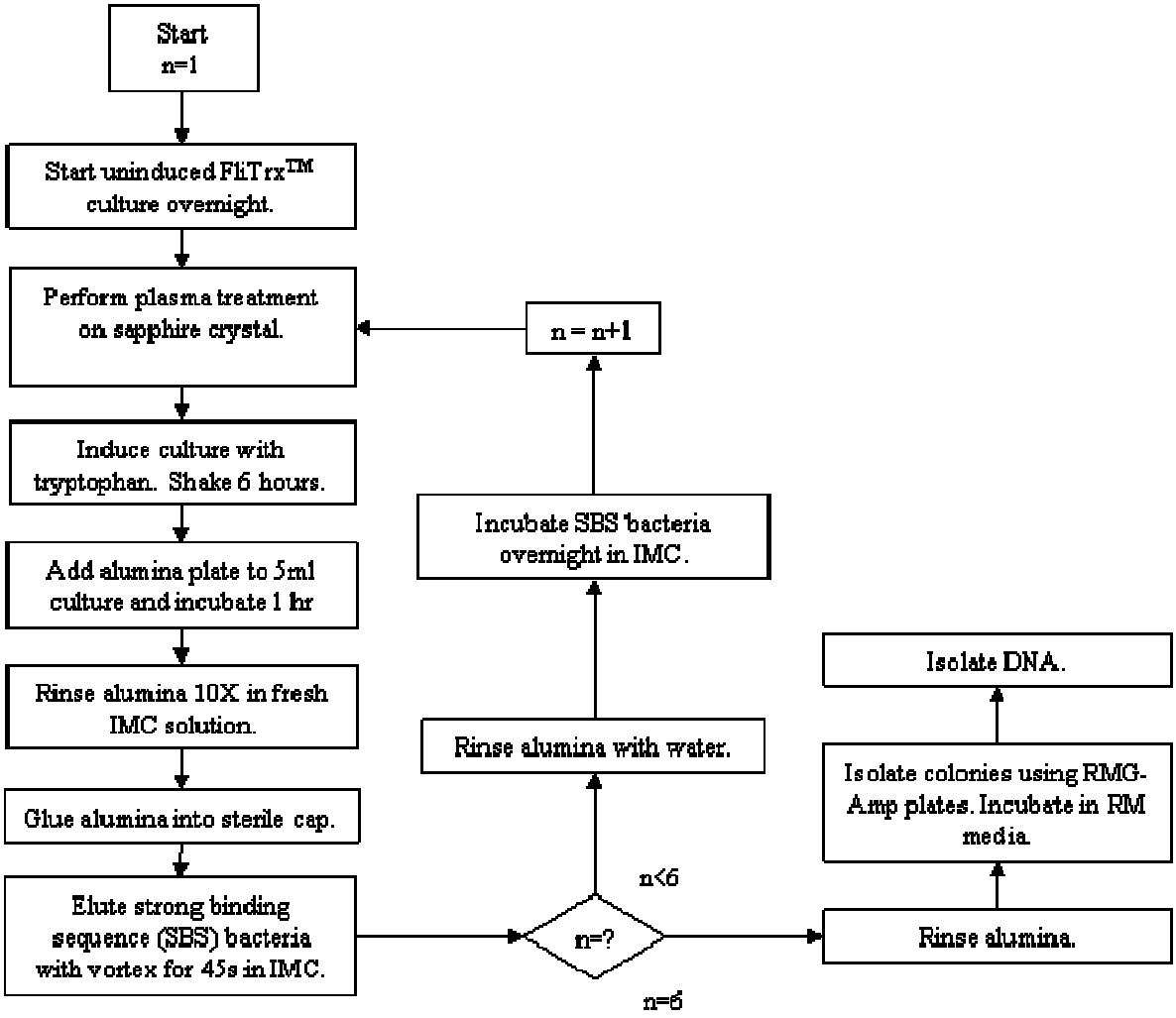

Figure 8-1. Flowchart for third round of biopanning. Six panning steps were performed.

8.4.3.2 Growth

The FliTrx library contained $1.77X10^8$ primary clones. A fresh aliquot of this was used at the start of each round of biopanning. To start the experiment, the bacteria was thawed by immersing the tube in a beaker of room temperature water. A sterile pipette was used to transfer 50 mL of IMC medium into an autoclaved flask. The aliquot was then added to the flask, which was closed with an autoclaved foam stopper. This was placed into an Enviro-shaker 3597X (Lab-line Instruments, Inc. Melrose Park, Illinois) and allowed to shake at approximately 300 rpm for 15 hours at 25°C.

In some cases, the growth overnight was inadequate and the samples were allowed to grow a second day. This determination was generally made by visual inspection of turbidity. Although the procedure called for checking the OD_{600} on the sample to determine necessary dilution, it was generally obvious when the culture hadn't grown sufficiently overnight. A blank sample of IMC media was placed into the shaker alongside the cultures each night in order to make sure that the growth was not due to contamination.

At the beginning of the next day, two samples (0.75 mL each) were removed with a sterile pipette. To one of these, 3 drops of glycerol was added. Both were stored in the -80° freezer in case of the need to repeat a panning step (due to poor growth or suspected contamination). The concentration of the sample was then determined using a Milton Roy Spectronic 1201 UV spectrophotometer (Ivyland, PA) by measuring the optical density at a wavelength of 160 nm (OD_{600}). 1 OD_{600} is approximately 10^9 cells. The volume of sample which would contain 10^{10} cells was determined and was added to 50 mL of fresh IMC medium in an autoclaved flask.

Tryptophan was then added (0.5 mL of 10 mg/mL stock) to yield a concentration of 100 μg/mL. The tryptophan was added to induce expression of the protein. This was placed back on the shaker for 6 hours at 25°. The bacteria containing expressed proteins were then ready for application to the alumina substrate.

8.4.3.3 Adsorption and Selection

In order to selectively adsorb bacteria, the deionized water was removed from the small tissue plate containing the freshly cleaned alumina plate and 5 mL of sample culture was added by sterile pipette. Based on the dilution to 10^{10} cells per 50 mL prior to induction, this exposed the substrate to approximately 10^{9} cells. The tissue plate was then gently agitated by rotating in small circles on the benchtop by hand for one minute at about 50 rpm. After this, the sealed container was left immobile on the benchtop for one hour to allow adsorption.

The loosely bound bacteria were then removed by submerging the alumina plate into 10 individual sequential tubes each containing 10 mL of IMC media. The tweezers were rinsed with deionized water each time. After this, the plate was immobilized in the cap of a centrifuge tube containing IMC media and placed against a mechanical vortexer for 45 seconds in order to shear off the strongly bound bacteria. This strongly bound bacteria was then added to 50 mL of IMC and placed on the shaker for 15 hours to grow, thereby beginning the next panning step. For a time, the 10 tubes of IMC used for washing off the loosely bound bacteria were also grown overnight. It was consistently found that although early washing steps had growth, the 10^{th} step did not, suggesting that the procedure had successfully rinsed away those bacteria which were not strongly bound to the substrate.

It was determined that a standard low-melt hot glue gun was a good tool for immobilizing the alumina pieces such that only the desired face (0001) was available for elution of the bound bacteria. The bond was sufficiently strong to immobilize the pieces for the vortexing, yet was simple to remove afterwards without damage to the alumina plate. Immersing the cap in water as hot as comfortable to the touch for a short time allowed the slide to be gently pried loose with a spatula. Any remaining glue was easy to remove after immersion in cold water to make the glue brittle.

After the elution step, the alumina slide was well-rinsed with deionized water and set aside to be plasma treated before the next panning session.

8.4.3.4 Isolation

After 6 successive biopanning steps, colonies of individual bacteria were grown. From the final panning step, the elusions were grown up overnight in IMC media as usual. Samples were aliquoted and placed into the freezer. Previously prepared RMG-Amp plates were removed from the cold room and placed in a Precision Economy Incubator (Jouan, Inc, Newington, NH) at 30°C with the lids ajar to allow evaporation of moisture. They were left in the incubator until the clear lid no longer showed moisture. They were then removed and placed upside down until use. One µL of culture was combined with 1 mL of blank IMC media. One µL of this dilution was then added to 1mL of blank IMC media to make the final dilution. Two µL of this dilution and 20 µL of blank IMC were spread onto an RMG plate. This was placed right side up in the incubator with the top ajar to evaporate moisture. After 10 minutes, the top was placed on and the plates were turned upside down. They were incubated overnight until colonies appeared.

Individual colonies were selected by dragging a sterile loop across the colony and dipping it into 20 mL of RM media (containing ampicillin). Ten individual colonies were selected. The culture plates were wrapped with parafilm and placed into the cold room for safekeeping. The individual colonies were grown overnight in the shaker at 25°C. The next morning, 1.5 mL of each culture was placed into a microcentrifuge tube and spun for 30 seconds at 13,000 rpm (12,000 g) in a Beckman Microfuge Light microcentrifuge in the cold room (4°C). The supernatant was decanted and 1.5 mL more of each culture was added. The centrifugation step was repeated. The resulting pellets were frozen at -20°C. Stock solutions were prepared of the remaining cultures, each containing 0.75 mL of culture and 3 drops of glycerol. These were frozen at -80°C.

8.4.3.5 Plasmid Isolation

Two methods were used for DNA isolation. The first was a BioRad Plasmid Miniprep Kit, which had the advantage of being simple and effective, but was expensive in the quantities used. The second was a phenol chloride extraction, which was more difficult

to perform, but quite inexpensive. Both procedures are described here. Ultimately, the phenol chloride extraction was used.

For plasmid isolation using the BioRad Miniprep kit, the neutralizer (provided in the kit) was placed in the freezer before beginning. To each pellet, 200 µL of resuspension agent from the kit and 1µL of Ribonuclease A was added. The pellets were vortexed until completely suspended. 250µL of lysis solution was added to each pellet, and the tubes were gently inverted 10 times to yield a clear solution. 250µL of cold neutralizer was added, and the tubes were inverted 10 times to yield a visible white precipitate. The samples were centrifuged at 13,200 rpm for 5 minutes. For each sample, a miniprep column was placed into a centrifuge tube and the supernatant from the centrifuged sample was placed into the column. The sediment was discarded. 200 µL of well-shaken matrix resin was added to each tube. Each tube was mixed by pipetting twice with a sterile pipette. The column-tube assemblies were centrifuged for 30 seconds at 13,200 rpm. The liquid that had passed into the tube was discarded, and the column was replaced. 500 mL of wash solution was added to each tube, being sure to wash down any material on the upper rim of the column. The assembly was centrifuged one minute. The liquid that passed into the tube was discarded, and this step was repeated. The column was placed atop a new tube. The assembly was centrifuged for one minute to dry the columns. The columns were placed into new tubes, 50 µL of bottled sterile water was added to each column, and the assembly was allowed to sit for one minute. The assembly was centrifuged for one minute. The columns were removed and discarded, then the material which had passed into the tube underneath was collected and stored in the freezer at -20°C.

The phenol chloride extraction also used pellets condensed from 3 mL total of culture. Each pellet was resuspended in 100 µL of GTE solution with 1 µL of RNAase, vortexed, and allowed to sit for 5 minutes. During this waiting period, fresh lysis solution was prepared of 19.6 mL of deionized water, 0.4 mL of 10N NaOH, and 200 mg of sodium lauryl sulfate. 200 µL of lysis solution was added to each tube. The tubes were placed on ice for 15 minutes. 150 µL of cold 5M potassium acetate (pH 4.8) solution was added

to each tube. They were vortexed and placed back on ice, then centrifuged 3 at 13,200 rpm for minutes. The supernatant was removed by pipette and placed into fresh centrifuge tubes to which 800 µL of 95% ethanol at ambient temperature was added. After two minutes, this was centrifuged for one minute. The ethanol was decanted, and 1 mL of 70% ethanol was added. After two minutes, this was centrifuged for one minute and the ethanol was decanted. Any remaining ethanol was dried under vacuum. The contents of each tube were resuspended by tapping gently in 50 µL of 1X TE buffer. Four tubes of identical content were combined to make a total of 200 µL of solution. A 1:1 volume ratio of phenol chloroform was added and the mixture was vortexed for 10 seconds. The mixture was centrifuged for 15 seconds, leaving the DNA in the top aqueous layer, which was removed to a fresh tube. The remaining bottom layer had 200 µL of 1X TE buffer added and the extraction was repeated to increase the yield. The two top layers were combined.

An extra salt precipitation step was used to further purify the aqueous DNA layer, as follows. The DNA solution was dried down in the speedvac and resuspended in 100 µL of sterile water plus 10 µL of 3M sodium acetate. 330µL of 95-100% freezer-cold ethanol was added and mixed gently by hand. The combination was placed in the -80°C freezer for one hour. After this the sample was centrifuged at 13,200 rpm in the cold room (4°C) for 15 minutes. The liquid was carefully decanted. 0.5 mL of room-temperature 70% ethanol was added, and the sample was centrifuged for an additional 5-10 minutes. The liquid was decanted and the resulting DNA was dried in the speedvac to remove any ethanol, then resuspended in sterile water.

8.4.3.6 Sequencing

DNA samples were sequenced by Cleveland Genomics (Cleveland, OH) using a Perkin-Elmer ABI Prism model 377 DNA Sequencer. A FliTrx forward sequencing primer (5'ATTCACCTGACTGACGAC-3') was provided. 40 uL Samples were submitted in sterile water at an approximate concentration of 500-1000 ug/mL.

8.4.4 Zeta potential

The zeta potential was measured using a ZetaSizer 3000 (Malvern Instruments, Ltd, Worcestershire, UK). Each zeta potential reported was the average of 5 measurements. In the case of a thin electric double layer, electrophoretic mobility measurements may be used to determine zeta potential using the Smoluchowski equation, in which μ particle mobility, ε is the permittivity, η is the viscosity, and ζ is the zeta potential:

$$\mu = \frac{\varepsilon\zeta}{\eta}$$

Eq. 8-1

For a thick double layer, Huckel's equation applies:

$$\mu = \frac{2\varepsilon\zeta}{3\eta}$$

Eq. 8-2

For measurements made using the Smoluchowski assumption, a correction is necessary to account for electrophoretic retardation. Zeta potentials in this chapter from both instruments were measured using the Smoluchowski approximation, then reported using the Henry correction factor as described by Hunter.[16] The correction takes the following form, in which a is the radius of the particle and κ^{-1} is the Debye length:

$$\zeta_{corrected} = \frac{\zeta_{measured}}{\frac{2}{3} f_1(a\kappa)}$$

Eq. 8-3

The correction factor, f_1, is given by the following two equations:

$for\ \kappa a < 1,$

$$f_1(\kappa a) = 1 + \frac{(\kappa a)^2}{16} - \frac{5(\kappa a)^3}{48} - \frac{(\kappa a)^4}{96} + \frac{(\kappa a)^5}{96} - \left[\frac{(\kappa a)^4}{8} - \frac{(\kappa a)^6}{96}\right] e^{\kappa a} \int_{\infty}^{\kappa a} \frac{e^{-t}}{t} dt$$

Eq. 8-4

$for\ \kappa a > 1$

$$f(\kappa a) = \frac{3}{2} - \frac{9}{2\kappa a} + \frac{75}{2\kappa^2 a^2} - \frac{330}{\kappa^3 a^3}$$

Eq. 8-5

8.5 Results and Discussion

8.5.1 Round 3 results

Table 8-1. Bound sequences.

ID	Sequence	
3	Cys-Arg-Arg-Val-Trp-Arg-Thr-Leu-Leu-Trp-Gly-Ser	CRRVWRTLLWGS
1-1	Asp-Ser-Asn-Asp-Gly-Leu-His-Lys-Val-Gln-Arg-Leu	DSNDGLHKVQRL
1-2	Arg-Leu-Arg-???-Ala-Leu-Trp-Val-Gly-Gly-Gly-Leu	RLRXALWVGGGL
2-1	Gly-Arg-Thr-Lys-Val-Val-Arg-Leu-Gly-Ser-Val-Gly	GRTKVVRLGSVG
2-2	Val-Val-Gln-Thr-Thr-Lys-Gly-Leu-Thr-Arg-Gly-Arg	VVQTTKGLTRGR
1-4*	Arg-Gln-Arg-Arg-Ser-Val-Gly-Gly-Val-Asn-Asp-Thr	RQRRSVGGVNDT
1-5*	Arg-???-Arg-???-Ser-Val-Gly-Gly-Val-Asn-Asp-Thr	RXRXSVXGVNDT
1-6	Arg-Thr-Val-Lys-Gln-Ala-Arg-Arg-Lys-Gly-Gly-Arg	RTVKQARRKGGR
1-7	Pro-Leu-Gln-Gly-Pro-Arg-Arg-Pro-Gly-Gly-Arg-Arg	PLQGPRRPGGRR

Note: 1-4 and 1-5 are duplicates.

Table 8-2. Classification of bound sequences.

Class	Name	Abbreviation	Number of Occurrences
Hydrophobic	Alanine	Ala	2
	Valine	Val	13
	Leucine	Leu	10
	Isoleucine	Ile	0
	Methionine	Met	0
	Phenylalanine	Phe	0
	Proline	Pro	3
	Tyrosine	Tyr	0
	Tryptophan	Trp	3
Hydrophilic, Acidic	Aspartate	Asp	4
	Glutamate	Glu	0
Hydrophilic, Basic	Arginine	Arg	23
	Histidine	His	1
	Lysine	Lys	5
Hydrophilic, Neutral	Asparagine	Asn	3
	Cysteine	Cys	1
	Glutamine	Gln	5
	Glycine	Gly	19
	Serine	Ser	5
	Threonine	Thr	8

There is a marked preference for amino acids which are either neutral or positively charged at physiological pH. This was contrary to expectation, as alumina is net positive at pH 7.4. However, the buffer in which the bacteria were grown had not been taken into account.

In the buffer, the charge was completely reversed on the alumina surface. It is believed that this is due to the presence of phosphate, which is divalent. Due to the necessity of using this buffer for viability of the bacterial library, the program was halted until such a time as use of a phage library would be feasible.[5]

8.5.2 Selectivity

One question raised by these results is how selectivity for this sort of experiment compares to the original intent of the combinatorial library. The instructions by the manufacturer indicate that five rounds should be sufficient.[14] However, this kit was designed for antibody-antigen recognition. In this experiment, it is expected that there would be rather unique selectivity based on the chemical characteristics and confirmations of the amino acid sequence. For instance, the quality control procedure by Invitrogen involves performing 5 successive biopanning steps using the antibody HIL-8-NR7. Ten clones are sequenced, and all ten contain a known epitope.[14] However, the results for adsorption on alumina do not highlight a particular sequence. Instead, they favor cationic amino acids. There are no specific sequences which appear multiple times. This indicates that selectivity was not so high as that typically seen. The table below illustrates the relationship between selectivity (defined as the % of bacteria washed away during the gentle rinsing steps), the number of panning steps, and the number of dodecamers remaining.

Table 8-3. Relationship between selectivity, number of panning steps, and number of unique sequences remaining.

# of panning steps	Selectivity	95%	90%	75%	50%	Unique sequences remaining
	0	1.77E+08	1.77E+08	1.77E+08	1.77E+08	
	1	8.85E+06	1.77E+07	4.43E+07	8.85E+07	
	2	4.43E+05	1.77E+06	1.11E+07	4.43E+07	
	3	2.21E+04	1.77E+05	2.77E+06	2.21E+07	
	4	1.11E+03	1.77E+04	6.91E+05	1.11E+07	
	5	5.53E+01	1.77E+03	1.73E+05	5.53E+06	
	6	2.77E+00	1.77E+02	4.32E+04	2.77E+06	

One possibility is that the surface does not have features that lend themselves well to a unique mating of substrate and adsorbate. If indeed, the primary reason for adsorption is electrostatic, then there are many combinations which are net negative and so should work.

Another possibility is that the procedure did not do an adequate job of isolating the most strongly bound bacteria. Measures were taken to ensure that the weakly bound bacteria, once washed off, stayed off. To do this, the slides were rinsed in 10 separate containers, then these wash containers were incubated to make sure that the later ones were clean. Pains were also taken with the equipment and handling to prevent re-introduction of bacteria that had been washed away. However, it is possible that the rinsing steps were too gentle to wash away sufficient bacteria, leaving a range of adsorbates.

8.5.3 Ionic strength of the IMC Media and Resulting Debye Length

For solutions in water at 25°C, κ^{-1} is given by [17]

$$\kappa^{-1}(nm) = \frac{0.3}{I^{½}}$$

Eq. 8-6

Ionic strength may be calculated by the following, in which c_i is the concentration of species i and z_i is the number of electronic charges:

$$I = \frac{1}{2}\sum_i c_i z_i^2$$

Eq. 8-7

The ionic strength of IMC media was 0.42M. This corresponds to κ^{-1} of 0.46 nm.

8.5.4 Effect of IMC buffer on Substrate

Alumina is an amphoteric oxide. The point of zero charge of alumina has been measured by a variety of methods to be between 7 and 10 in various electrolytes. [18] The IMC medium is a mixture of several salts: magnesium chloride, sodium phosphate, potassium phosphate, sodium chloride, and ammonium chloride. Sodium chloride is documented as an indifferent electrolyte for alumina, [19] as is potassium nitrate. [20] However, literature data indicate that the presence of phosphate can reverse the charge of an alumina surface at pH values below the IEP of alumina in an indifferent electrolyte. Phosphate is a competitive anion, having a high affinity for the surface. [21] A study of adsorption of alkyl phosphate surfactants on alumina, for instance, zeta potential reversal occurred at sufficiently high surfactant concentrations. At concentrations between 1-100 ppm, the zeta potential was negative across the entire pH range studied (3-10). Adsorption density as measured by ATR was higher at lower pH and higher surfactant concentration, but adsorption occurred in all cases. [22]

XPS performed by N. Nueraji on the alumina before and after biopanning revealed the presence of phosphate, calcium, magnesium, and silicon on the surface. The initial sample was new as received from the vendor with only a rinsing of deionized water to clean away dust. The final sample had undergone 6 panning steps with plasma cleaning between each. It had been rinsed with deionized water at the end, but no additional plasma cleaning had been done. Therefore, it was representative of the surface used in the final biopanning step. The large quantity of phosphorus present on the sample strongly supports the supposition that this may have reversed the charge of the alumina.

Table 8-4. XPS performed by N. Nueraji on alumina plate (c-plane) before beginning experiment and after 6 panning steps. In each instance, the plate had been rinsed with deionized water before the measurement. Surface contamination by the growth medium is evident.

	Concentration (%)	
Element	Before	After
C1s	52.72	41.14
O1s	26.57	35.39
N1s	0.17	16.08
Al2p	20.29	1.21
Mg2s	0.00	0.28
Na1s	0.00	0.00
Cl2p	0.00	1.35
P2p	0.00	3.70
F1s	0.26	0.87

It is also interesting to note that magnesium was present on the substrate after the tests. Magnesium is a divalent cation which adsorbs more with increased ionic strength and increased pH (as compared to monovalent cations also present, such as sodium and potassium.) [23]

Zeta potential measurements of alumina nanoparticles in IMC media confirmed that the charge is indeed negative. The zeta potential was measured on an alumina suspension made up to a concentration such that the ratio of alumina surface area to salt concentration was approximately the same as what would have been encountered under experimental conditions during biopanning. The zeta potential was around -25mV. In light of this, the preference for positively charged amino acids is reasonable; however, the results do not reflect the intentions of the study.

8.6 Summary

The FliTrx™ Random Peptide Display Library was used to search for a sequence of peptides that would anchor strongly on alumina. The expectation was that this search would locate either a favored sequence for binding or a marked preference for negatively charged peptides, given that the work was at pH 7.4, below the IEP of alumina. Conversely, a preference for positively charged amino acids was found. This was due to the phosphate buffer, a necessary component of the bacteria-based system. The

phosphate buffer reversed the charge on the alumina. One possibility would be to repeat this study using a phage display process; however, at present the necessary facilities for this work are not available. This work was included in a paper by Tulpar et al. [13]

8.7 References

1. Smith, G.P., Filamentous Fusion Phage: Novel Expression Vectors that Display Cloned Antigens on the Virion Surface. *Science*, **1985**. 228: p. 1315-1317.

2. Parmley, S.F. and Smith, G.S., Antibody-selectable filamentous fd phage vectors: affinity purification of target genes. *Gene*, **1988**. 73: p. 305-318.

3. Scott, J.K. and Craig, L., Random Peptide Libraries. *Current Opinion in Biotechnology*, **1994**. 5: p. 40-48.

4. Brown, S., Engineered iron oxide-adhesion mutants of the Escherichia coli phage lambda receptor. *Proc. Natl. Acad. Sci. USA*, **1992**. 89: p. 8651-8655.

5. Whaley, S.R., et al., Selection of peptides with semiconductor binding specificity for directed nanocrystal assembly. *Nature*, **2000**. 405: p. 665-668.

6. Barbas, C.F., Rosenblum, J.S., and Lerner, R.A., Direct selection of antibodies that coordinate metals from semisynthetic combinatorial libraries. *Proc. Natl. Acad. Sci. USA*, **1993**. 90: p. 6385-6389.

7. Kjaegaard, K., et al., Sequestration of zinc oxide by fimbrial designer chelators. *Applied and Environmental Microbiology*, **2000**. 66: p. 10-14.

8. Kjaegaard, K., Schembri, M.A., and Klemm, P., Novel Zn2+ -chelating peptides selected from a fimbria-displayed random peptide library. *Applied and Environmental Microbiology*, **2001**. 67: p. 5467-5473.

9. Kotrba, P., et al., Enhanced Bioaccumulation of heavy metal ions by bacterial cells due to surface display of short metal binding peptides. *Appl. Environ. Microbiol.*, **1999**. 65: p. 1092-1098.

10. Sousa, C., Cebolla, A., and de Lorenzo, V., Enhanced metalloadsorption of bacterial cells displaying poly-His peptides. *Nature Biotechnology*, **1996**. 14: p. 1017-1020.

11. Pazirandeh, M., Wells, B.M., and Ryan, R.L., Development of bacterium-based heavy metal biosorbents: enhanced uptake of cadmium and mercury by Escherichia coli expressing a metal binding motif. *Applied and Environmental Microbiology*, **1998**. 64: p. 4068-4072.

12. Chen, S. and Wilson, D.B., Construction and characterization of escherichia coli genetically engineered for bioremediation of Hg2+ -contaminated environments. *Appl. Environ. Microbiol.*, **1997**. 63: p. 2442-2445.

13. Tulpar, A., et al., Unnatural Proteins for the Control of Surface Forces. *Langmuir*, **2005**. 21: p. 1497-1506.

14. Invitrogen Life Technologies FliTrx(TM) Random Peptide Display Library Version G. **2002**.

15. Lu, Z., et al., Expression of thioredoxin random peptide libraries on the Escherichia coli cell surface as functional fusions to flagellin: a system designed for exploring protein-protein interactions. *Bio/Technology*, **1995**. 13: p. 366-372.

16. Hunter, R.J., Foundations of Colloid Science. **1987**, Oxford: Clarendon Press.

17. Evans, D.F. and Wennerstrom, H., The Colloidal Domain. 2 ed. **1999**, New York: Wiley-VCH.

18. Kosmulski, M., pH-dependent surface charging and points of zero charge III. Update. *Journal of Colloid and Interface Science*, **2006**. 298: p. 730-741.

19. Heimstra, T., Yong, H., and Van Riemsdijk, W.H., Interfacial Charging Phenomena of Aluminum (Hydr)oxides. *Langmuir*, **1999**. 15: p. 5942-5955.

20. Rao, A.S., Electrophoretic Mobility of Alumina, Titania and their Mixtures in Aqueous Dispersions. *Ceramics International*, **1988**. 14: p. 71-76.

21. Kasprzyk-Hordern, B., Chemistry of alumina, reactions in aqueous solution and its application in water treatment. *Advances in Colloid and Interface Science*, **2004**. 110: p. 19-48.

22. Jeon, J.S., et al., In situ analysis of alkyl phosphate surfactant adsorption at the alumina/aqueous solution interface. *Colloids and Surface A: Physicochemical and Engineering Aspects*, **1996**. 111: p. 29-38.

23. Huang, C.-P. and Stumm, W., Specific Adsorption ofCations on Hydrous g-Al2O3. *Journal of Colloid and Interface Science*, **1973**. 43: p. 409-420.

9 Summary

9.1 Conclusions

The overall objective of this research was to develop an approach to deliberately designing polymer-particle complexes that would be of an appropriate size, stable in vivo, and would possess the necessary structure for the application (such as for MRI contrast or drug delivery). In order to accomplish this task, two models for star polymers (one for structure, one for interaction) were applied first to a series of micelles in water. The size and structure was examined in light of the star polymer model for brush extension, and the model for interaction was used to develop a means of predicting the second virial coefficient, A_2. A comparison of experimental and predicted A_2 validated the models. Subsequently, the same principles were used to predict size and stability of polymer-magnetite complexes in water and phosphate buffered saline. This methodology may be applied to any polymer-nanoparticle complex.

Using dynamic light scattering, the hydrodynamic size of the micelles was characterized as a function of temperature, pH, and composition. In addition, static light scattering was used to determine the aggregation numbers of the micelles and the second virial coefficients. This was described in **Chapter 3**. The pH had a large effect on the micellization behavior of the copolymers. At low pH, micellization occurred due to protonation of the carboxylic acid groups present in the polyurethane core. As the pH increased, a transition to unimers occurred between pH 6 and 8. This occurred for all polymers studied except the one with the largest PEO blocks, which did not micellize at all due to the overwhelming solubility of the PEO chains in water. Upon increasing the temperature through the range of 25-65°C, the two polymers with moderate length PEO chains (4845-2.5-4845 and 4845-2.7-4845) exhibited little change in aggregation number and a steady decrease in hydrodynamic radius due to temperature-induced disruption of hydrogen bonding in the PEO corona. The polymer with the shortest PEO block (1930-3.1-1930) had a much larger aggregation number than the others, and the aggregation number increased with increasing temperature. This may have been caused by increased

hydrophobic interactions in the core due to a decrease in hydrogen bonding. A star polymer model[1] was used to predict the size of the polymer micelles. The predicted size was less (~20%) than the measured hydrodynamic radius based on an intensity average, but the predicted size trend with changing polymer composition was observed experimentally.

Chapter 4 described an extension of this work using small angle neutron scattering (SANS). By using a modified SANS model[2-4] consisting of a homogeneous polyurethane core and a non-interacting Gaussian corona, good fits were obtained for scattering data on three species of triblock copolymer micelles. The triblock model was a better fit for the data from samples with a higher aggregation number. The polymer with the smallest aggregation number (4845-2.5-4845) was best fit as by a star polymer model. The cores of all three micelles were predominantly composed of PU with the addition of PEO for the micelles with lower aggregation numbers, indicating that interpenetration of PEO into the core was more prevalent for sparser micelles.

Another portion of the work focused on interactions between micelles in solution. In **Chapter 5**, an extension of the star polymer model allowed development of a mathematical means of predicting the second virial coefficient. Comparison of this method with experimental A_2 data a calculated value for A_2 of a hard sphere for both the novel triblock copolymers and four literature examples (PEO-PPO-PEO in water, PEO-PS in cyclopentane, and polybutadiene and polyisoprene star polymers in good solvents) demonstrated that the new model was a good match. The star model was better able to predict A_2 as compared to a hard sphere prediction, particularly for micelles with lower aggregation numbers and hence less dense coronas.

The characterization of the micelles in solution laid the foundation for a study of the utility of these polymers in stabilizing paramagnetic magnetite nanoparticles, which was described in **Chapter 6**. The star polymer model was applied to a magnetite core with polymer chains anchored on the surface, then further extended to describe a surface layer attributed to the anchor block. The predicted sizes for the magnetite-polymer complexes

were compared to experimentally measured values from DLS with good agreement. An extended version of the DLVO theory was applied to predict stability of various magnetite complexes in both water and phosphate buffered saline. According to the prediction, all of the complexes were expected to be stable in both water and PBS, despite electrostatic screening from the higher ionic strength. This is because the amount of polymer adsorbed on the particles should have been sufficient for steric interactions to cause stabilization. However, the experimental observation was that although all of the complexes were stable in water, the two complexes containing carboxylic acid as the anchor block aggregated in PBS. It is likely that the PZC of the magnetite was shifted to a lower pH in the presence of adsorbing electrolytes from the PBS.

Chapter 7 was concerned with demonstration of an EDC-mediated crosslinking reaction to stabilize the triblock copolymer micelles against changes in pH. Such crosslinked micelles have potential as drug carriers, as they would not disassemble at physiological pH and under dilution. In addition, the outer PEO layer would not be expected to trigger an immune response. It was discovered that addition of dichloromethane as a cosolvent caused the micelles to swell and improved crosslinking. Encapsulation of two separate drugs (cisplatin and lidocaine) was explored, although neither was successfully incorporated into the crosslinked micelles. Zeta potential studies revealed the presence of free amine groups in the micelle. This suggested that some portion of the diamine was reacted on only one end, leaving charged amine groups to repel the cisplatin. There was also a potential problem with free volume in the small micelle core, particularly in the case of the relatively bulky lidocaine molecule. In order to examine this, a size vs. pH study was performed. The micelle sizes were constant across the range of pH, suggesting that the crosslinking was too extensive to allow the micelles to expand as the cores became more protonated.

A body of work largely unrelated to the rest of the dissertation was described in **Chapter 8**. A biopanning technique with a combinatorial library of *E. coli* was used to search for dodecapeptide sequences that would bind selectively to alumina at pH 7.4. It was expected that either a unique favored binding sequence would be found or that a

preponderance of negative peptides would be observed. Conversely, a preference for positively charged amino acids was found. The phosphate in the growth medium for the combinatorial library had reversed the charge on the alumina surface.

9.2 Future Work

9.2.1 Micelles

The most immediate future work in characterizing solution behavior of the triblock copolymers is to use deuterated PEO tailblocks for SANS experiments. This would allow for much greater contrast, which would be a boon in examining brush structure and corroborating it with the predictions from the Vagberg model. The degree of hydration of the brush is expected to have an impact on performance as an MRI contrast agent.

In addition, deuteration of the PEO corona would make it much easier to see how much interpenetration of the corona into the core is occurring. It may also be possible to do true contrast matching between the solvent and the PEO corona, thus determining a true core size, which is important for structure and stability predictions.

9.2.2 Magnetite-polymer complexes

One important study in going forward with the magnetite stabilization project will be to fully understand the effect of the various components in PBS on the surface chemistry of magnetite. Phosphate is not an indifferent electrolyte and is likely having a profound effect on the magnetite surface. These magnetite-polymer complexes are intended for use in vivo, so this must be understood for the particles to work effectively. A better understanding of the surface chemistry of magnetite could lead to new ideas for anchor blocks.

For a given polymer, a study which varied the graft density (magnetite:polymer ratio) would be very useful. This would allow elegant modeling of the brush extension of the polymer on the surface of the magnetite. It would also allow testing of the method of calculating A_2 described in Chapter 5, as the "hardness" of the interaction should increase

with a higher graft density. Varying the graft density would also provide very useful information relative to the relaxivity studies being undertaken at UWA.

Once the effect of polymer brush thickness and/or segment density profile on magnetic resonance imaging (MRI) relaxivity was well established, it would then be possible to use that knowledge in combination with stability predictions from DLVO to engineer improvements into future polymer synthesis. This could be done by varying the anchor:tail ratio to provide the optimal brush density and thickness for both relaxivity and stability.

An additional open question is whether a PEO brush anchored with a cationic PEI block will be sufficient to prevent an immune response due to the PEI. This can be tested directly with cell studies, and preliminary work suggests that this may not be a problem.

Another in vitro study that would be helpful would investigate the question of how thick the PEO brush layer must be on a particle with specified diameter to prevent nonspecific adsorption onto cell membranes. This can be investigated using a quartz crystal microbalance (QCMD) in one of two configurations. Either a layer of adsorbed PEI-PEO block copolymer can be adsorbed onto the crystal while a suspension of cells is allowed to pass over the surface, or a lipid bilayer can be adsorbed on the QCM crystal while a suspension of stabilized nanoparticles is allowed to pass over it.

As design of these complexes becomes increasingly sophisticated, one possibility would be to bury a bioactive peptide selectively within the PEO brush to control access of the peptide to the liquid phase outside the brush. In such a way, the peptide (or antibody) could be hidden from the immune system until it reached its intended target. This could allow identification of specific tissues, such as tumors. For this reason, a study of the dynamics of terminally attached polymer chains (especially close to the terminal end) would be important. Dynamics within the brush are not particularly well understood and may very well require machine simulations to probe in detail. The chain dynamics could

affect how easily the antibody or the peptide could be presented to the liquid phase and thus have access to a cell membrane.

Finally chain dynamics of the brush layer will be important in understanding the rheology and structure of concentrated dispersions of sterically stabilized nanoparticles, an area of great interest both scientifically as well as technologically.[5]

9.2.3 Crosslinked micelles for drug delivery

A means must be found to crosslink the carboxylic acid groups without leaving amine groups free on one end of the diamine molecules so as to avoid reversing the charge in the micelle core. One means of doing this may be by adding the diamine gradually, so as to keep the concentration of available amine groups low. A better understanding of the reaction kinetics will be required. It may also be that in light of the relatively small number of acid groups available for crosslinking, some sort of multi-functional crosslinker would be desirable.

The demonstration of swelling of the micelle by addition of a cosolvent could be useful in creating crosslinked micelles with sufficient volume in the core for inclusion of drug molecules. This swelling process might be modeled. For instance, Nagarajan developed a model describing solubilization of hydrocarbons in the hydrophobic core of PEO-PPO-PEO triblock copolymers based on minimization of free energy.[6-8]

9.2.4 Combinatorial search for custom anchor blocks

A good approach for this project might be the use of a phage display library in place of the bacterial one described in Chapter 8. This could be used to eliminate the need for elaborately buffered salt mediums which complicate the surface chemistry of adsorption.

9.3 References

1. Vagberg, L.J.M., Cogan, K.A., and Gast, A.P., Light-Scattering Study of Starlike Polymeric Micelles. *Macromolecules*, **1991**. 24(7): p. 1670-1677.

2. Pedersen, J.S. and Gerstenberg, M.C., Scattering Form Factor of Block Copolymer Micelles. *Macromolecules*, **1996**. 29: p. 1363-1365.

3. Pedersen, J.S. and Gerstenberg, M.C., The structure of P85 Pluronic block copolymer micelles determined by small-angle neutron scattering. *Colloids and Surfaces a-Physicochemical and Engineering Aspects*, **2003**. 213(2-3): p. 175-187.

4. Pedersen, J.S., et al., A Small-Angle Neutron and X-ray Contrast Variation Scattering Study of the Structure of Block Copolymer Micelles: Corona Shape and Excluded Volume Interactions. *Macromolecules*, **2003**. 36: p. 416-433.

5. Vlassopoulos, D., et al., Multiarm star polymers dynamics. *Journal of Physics-Condensed Matter*, **2001**. 13(41): p. R855-R876.

6. Nagarajan, R., Solubilization in aqueous solutions of amphiphiles. *Current Opinion in Colloid & Interface Science*, **1996**. 1(3): p. 391-401.

7. Nagarajan, R., Solubilization of hydrocarbons and resulting aggregate shape transitions in aqueous solutions of Pluronic (R) (PEO-PPO-PEO) block copolymers. *Colloids and Surfaces B-Biointerfaces*, **1999**. 16(1-4): p. 55-72.

8. Nagarajan, R. and Ganesh, K., Solubilization in Spherical Block Copolymer Micelles - Scaling Analysis Based on Star Model. *Journal of Chemical Physics*, **1993**. 98(9): p. 7440-7450.

Appendix: Propagation of Errors

This is a derivation of the standard deviation of the aggregation number, N_{agg}, and the second virial coefficient, A_2. These values are based on the propagation of errors from the measured standard deviation of the slope and intercept of a Debye plot having described by y = a + bx.

In general, if a variable, x, may be described as a function of u and v,

$$x = f(u, v)$$

Then the standard deviation, σ, is defined by:

$$\sigma_x^2 = \sigma_u^2 \left(\frac{dx}{du} \right)^2 + \sigma_v^2 \left(\frac{dx}{dv} \right)^2$$

The aggregation number is calculated from the Debye plot as follows:

$$N_{agg} = \left(\frac{1}{MW_{unimer}} \right) \left(\frac{1}{a} \right)$$

The derivative with respect to a is:

$$\frac{dN_{agg}}{da} = \left(-\frac{1}{MW_{unimer}} \right) a^{-2}$$

After several algebraic manipulations,

$$\sigma_{N_{agg}}^2 = \sigma_a^2 \left(\frac{dN_{agg}}{da} \right)^2$$

$$\sigma_{N_{agg}}^2 = \sigma_a^2 \left[\left(-\frac{1}{MW_{unimer}} \right) a^{-2} \right]^2$$

$$\sigma_{N_{agg}}^2 = \sigma_a^2 \left(\frac{1}{MW_{unimer}} \right)^2 a^{-4}$$

an expression for the standard deviation of N_{agg} is reached.

$$\sigma_{N_{agg}} = \sigma_a \left(\frac{1}{MW_{unimer}} \right) \left(\frac{1}{a} \right)^2$$

Similarly, the expression for A_2 is given by:

$$A_2 = \frac{b}{2}$$

The algebraic manipulations are as follows:

$$\frac{dA_2}{db} = \frac{1}{2}$$

$$\sigma_{A_2}^2 = \sigma_b^2 \left(\frac{dA_2}{db} \right)^2$$

$$\sigma_{A_2}^2 = \sigma_b^2 \left(\frac{1}{2} \right)^2$$

The resulting expression for the standard deviation of A_2 is therefore:

$$\sigma_{A_2} = \frac{\sigma_b}{2}$$